A METHODOLOGY FOR THE INTEGRATED DESIGN OF SMALL SATELLITE CONSTELLATION DEPLOYMENT

A thesis submitted to the University of Manchester
for the degree of Doctor of Philosophy
in the Faculty of Engineering and Physical Sciences

2016

By

Nicholas Husayn Crisp

School of Mechanical, Aerospace and Civil Engineering

Contents

Word Count: 57149

List of Tables

List of Figures

Acronyms and Abbreviations

A-PICOMO Aerospace Picosatellite Cost Model.

ADCS Attitude Determination and Control System.

AFRL Air Force Research Laboratory.

AFSPC Air Force Space Command.

AIS Automatic Identification System.

ALASA Airborne Launch Assist Space Access.

ALSET Air Launched System Enabling Technology.

AoP Argument of Perigee.

BLISS Bi-level Integrated System Synthesis.

CCD Central Composite Design.

CDC Concept Design Center.

CER Cost Estimating Relationship.

CGT Cold Gas Thruster.

CO Collaborative Optimisation.

COTS Commercial Off-The-Shelf.

CRS Commercial Resupply Services.

CSLI CubeSat Launch Initiative.

DARPA Defense Advanced Research Projects Agency.

DEMETER Detection of Electromagnetic Emissions Transmitted from Earthquake Regions.

DMC Disaster Monitoring Constellation.

DoD Department of Defense.

DoE Design of Experiments.

DSM Design Structure Matrix.

DSS Distributed Satellite System.

DSST Draper Semianalytic Satellite Theory.

EA Evolutionary Algorithm.

ECEF Earth-Centred, Earth Fixed.

ECI Earth-Centred Inertial.

EELV Evolved Expendable Launch Vehicle.

ELaNa Educational Launch of Nanosatellites.

EML-1 Earth-Moon L_1 Lagrange Point.

ESA European Space Agency.

ESPA EELV Secondary Payload Adapter.

EUV Extreme Ultraviolet.

FEEP Field-Emission Electric Propulsion.

FORMOSAT-3/COSMIC FORMOSA Satellite Series No.3/Constellation Observing System for Meteorology, Ionosphere and Climate.

FPI Fixed Point Iteration.

GA Genetic Algorithm.

GAST Greenwich Apparent Sidereal Time.

GINA Generalised Information Network Analysis.

GNB Generic Nanosatellite Bus.

GPS-RO GPS Radio Occultation.

GSD Ground Sample Distance.

HANDE Hoots Analytic Dynamic Ephemeris Theory.

HCW Hill-Clohessy-Wiltshire.

ICBM Intercontinental Ballistic Missile.

ICE Integrated Concurrent Engineering.

ISS International Space Station.

JPL Jet Propulsion Laboratory.

LCROSS Lunar Crater Observation and Sensing Satellite.

LEO Low Earth Orbit.

LHS Latin Hypercube Sampling.

MATE Multi-Attribute Tradespace Exploration.

MATE-CON Multi-Attribute Tradespace Exploration with Concurrent Design.

MDO Multidisciplinary Design Optimisation.

MEMS Microelectromechanical Systems.

MOEA Multiple-Objective Evolutionary Algorithm.

MSIS Mass Spectrometer and Incoherent Scatter Radar.

NASA National Aeronautics and Space Administration.

NEAR Near Earth Asteroid Rendezvous.

NEMO Nanosatellite for Earth Monitoring and Observation.

NGDC National Geophysical Data Center.

NGSA-II Non-dominated Sorting Genetic Algorithm II.

NLS Nanosatellite Launch Service.

NOAA US National Oceanic and Atmospheric Administration.

NRLMSISE-00 2001 Naval Research Laboratory Mass Spectrometer and Incoherent Scatter Radar Exosphere.

ODE Ordinary Differential Equation.

OEC Overall Evaluation Criterion.

P-POD Poly-Picosatellite Orbital Deployer.

PAES Pareto Archived Evolution Strategy.

PCB Printed Circuit Board.

PDFLAP Prediction of Flux and A_p.

PRNG Pseudo-Random Number Generator.

PSA Pareto Simulated Annealing.

PSLV Polar Satellite Launch Vehicle.

PSO Particle Swarm Optimisation.

QRNG Quasi-Random Number Generator.

RAAN Right Ascension of the Ascending Node.

RSE Response Surface Equation.

RSM Response Surface Methodology.

S3TV Surrey Small-Satellite Transfer Vehicle.

SA Simulated Annealing.

SALT Semi-Analytical Liu Theory.

SCOUT Spacecraft Concept Optimization and Utility Tool.

SFL Space Flight Laboratory.

SoC System on a Chip.

SPEA-2 Strength Pareto Evolutionary Algorithm 2.

SSA System Sensitivity Analysis.

SSCM Small Satellite Cost Model.

SSO Sun Synchronous Orbit.

SSPS Spaceflight Secondary Payload System.

SSTO Single-Stage-to-Orbit.

START Strategic Arms Reduction Treaty.

SWORDS Soldier-Warfighter Operationally Responsive Deployer for Space.

SWPC Space Weather Prediction Center.

THEMIS Time History of Events and Macroscale Interactions during Substorms.

TLE Two-Line Element.

TRL Technology Readiness Level.

ULA United Launch Alliance.

USAF US Air Force.

USCM Unmanned Space Vehicle Cost Model.

UTIAS University of Toronto Institute of Aerospace Studies.

List of Symbols

Greek Symbols

ΔV	Delta-V
η	Mass Margin
μ_E	Earth Standard Gravitational Parameter
$\nu_{p,g}$	Propellant/Pressurant Specific Volume
Ω	Right Ascension of the Ascending Node (RAAN)
ω	Argument of Perigee (AoP)
ω_a	Atmospheric Rotational Speed
ρ	Atmospheric Density
ρ_p	Propellant/Pressurant Density
ρ_{tank}	Tank Construction Material Density
σ_{yield}	Material Yield Strength
θ	Plane Change Angle

Roman Symbols

A	Cross-sectional Area
a	Semi-major Axis
$\vec{a}$	Acceleration

B	Ballistic Coefficient
C_D	Coefficient of Drag
e	Eccentricity
f	True Anomaly
g_0	Earth Standard Acceleration due to Gravity
I_{sp}	Specific Impulse
i	Inclination
J_2	Second-degree Earth Zonal Harmonic
M	Mean Anomaly
M_p	Propellant/Pressurant Molar Mass
m	Mass
m_0	Spacecraft Mass before Manoeuvre
m_1	Spacecraft Mass after Manoeuvre
m_p	Propellant Mass
m_{PS}	Propulsion System Mass
$m_{PS,d}$	Propulsion System Dry Mass
m_{tank}	Tank Mass
n	Mean Motion
p	Power
P	Propellant/Pressurant Pressure
R	Ideal Gas Constant
R_E	Earth Radius
R_{tank}	Tank External Radius

r	Magnitude of Position Vector
r_{tank}	Tank Internal Radius
SF	Tank Safety Factor
T	Temperature
t_{wall}	Tank Wall Thickness
V	Orbital Velocity
V_e	Exhaust Velocity
V_p	Propellant/Pressurant Volume
V_{tank}	Tank Volume
$\vec{\mathrm{v}}_{\mathrm{rel}}$	Velocity Relative to the Atmosphere

ABSTRACT OF THESIS submitted by **Nicholas Husayn Crisp** for the degree of Doctor of Philosophy at The University of Manchester, entitled "**A Methodology for the Integrated Design of Small Satellite Constellation Deployment**".

Submitted June 2016

A growing interest in distributed systems of small satellites has recently emerged due to their ability to perform a variety of new mission types, increasing technical capability, and reduced time and cost for development. However, the lack of available and dedicated small launch services currently restricts the establishment of these systems in orbit. Secondary payload launch opportunities and alternative deployment strategies can address the issue of access-to-orbit and support the delivery of the constellation to the correct orbit configuration following launch. Of these deployment strategies, the method of indirect plane separation, which utilises the natural precession of Earth orbits, is particularly applicable to the deployment of small satellite constellations due to the potential to significantly reduce propulsive requirements, albeit at the cost of increased deployment time.

A review of satellite constellation design revealed that existing methods and tools are not suitable for the analysis of small satellite constellations and are not equipped to investigate alternative deployment strategies, despite the potential benefits of improved access-to-orbit, reduced system complexity, and reduced cost. To address the identified gaps in the design process, a methodology in which the analysis of small satellite constellation deployment is integrated into the system design framework is presented in this thesis. The corresponding system design-space is subsequently explored using a numerical optimisation method, which aids the identification of effective system designs and promotes the understanding of relationships between the design variables and output objectives. The primary objectives of this methodology are to ensure that the different opportunities for deployment of small satellite constellations are thoroughly examined during the design process and to support the development of improved mission and system designs.

The presented methodology is demonstrated using a reduced order framework comprised of an analysis for the deployment of small satellite constellations, preliminary vehicle and propulsion system sizing processes, and system cost estimating relationships. Using this simplified mission design framework, the design space-exploration of three small satellite constellation mission case-studies is performed by application of a multiobjective genetic algorithm. Objectives of time-to-deploy, system mass, and system cost are used to direct the optimisation process and search for the most effective solutions in the system design-space. In order to perform the analysis of constellation deployment by the process of indirect plane separation, a simulation method using a semi-analytical propagation technique and time-varying atmospheric density model was developed and verified by comparison to the actual deployment of the FORMOSAT-3/COSMIC mission.

The results of the case-studies presented illustrate the ability of the developed methodology to support the design process for satellite constellations and enable the identification of promising and improved system architectures for further development. Moreover, through the enumeration and quantification of the system design-space and tradespace, the methodology is shown to support the identification of relationships and trends between the design variables and selected output objectives, increasing the knowledge available to the system design team during the design process.

Declaration

No portion of the work referred to in this thesis has been submitted in support of an application for another degree or qualification of this or any other university or other institute of learning.

Copyright

Acknowledgements

I would first like to thank my supervisors Dr Kate Smith and Dr Peter Hollingsworth, initially for encouraging me to begin this journey and then guiding me throughout the process of completing this thesis. You have made the past three or so years interesting and challenging, but ultimately very rewarding and successful. I am grateful for all your advice and support.

I would also like to extend my deepest gratitude to my father, William Crisp, and uncle, Shiraz Pradhan, for their valuable time and generous advice whilst I was deciding whether to venture down this path. Here's to the future!

To the friends I have made here at the University of Manchester, I can't express how grateful I am to you for making this such a positive experience. From the frequent coffee breaks and after-work pub trips to our weekly football games, I have you all to thank for keeping me sane during this endeavour. To my friends from school and earlier, thanks for having faith in me and providing distraction from these studies when it was needed most.

To all my family, extended and acquired, I'm always thankful for you! Without your care and support this journey would have been so much more difficult. Thank you for being there for me. I can only hope that I can do the same for all of you. To my brother, Rehman, I must express a special thanks for providing the constant motivation to complete this thesis. And yes, I have finished my PhD now!

To my parents, Tazmina and William Crisp, I am eternally grateful for the opportunities which you have provided, and the encouragement to make the best of these chances. Your enduring love and support have made all of this possible.

Finally, I would like to thank Elizabeth for her unwavering belief in me throughout this process. Thank you for your tireless love, patience, and positivity. But most of all, thank you for being my best friend.

Chapter 1

Introduction

Small satellite constellations have been identified as an enabling architecture for a variety of new mission types of commercial, scientific, and military significance. Small satellites, due primarily to their smaller cost per unit, can be launched in larger numbers than traditional satellites, and in constellations can perform many simultaneous and distributed measurements or observations of interesting dynamic or global phenomena [1, 2]. Constellations of small satellites can be also used to augment or replace traditional satellite missions, benefiting from shorter possible revisit times due to their greater numbers, therefore able to achieve a greater temporal resolution of data.

However, the launch of constellations of small satellites is impacted by the availability of suitably sized and accessible launch vehicles. Whilst secondary payload opportunities can be used, the lack of control on launch schedule and destination orbit prohibits the use of multiple secondary launch opportunities by constellations which require accurately coordinated orbits. This issue is further compounded by restrictions on propulsion system capability to maintain the low cost of development and manufacture, particularly for nanosatellites and picosatellites. A review of current and future launch vehicles and opportunities for small satellites was published during the course of this research in Crisp et al. [3].

Traditionally, the deployment of constellations of large satellites is achieved by launching each payload individually into the required orbital plane, or by launching small clusters of satellites to orbit and using propulsive manoeuvres to achieve the correct orbits. However, with an increasing number of payloads of smaller mass requiring launch and the issues of availability

of access-to-orbit, reduced propulsive capability, and lower development and launch budget, the traditional method of constellation deployment is not suitable for small satellites.

In order to enable the cost-effective realisation of small satellite constellations with multiple orbital planes a number of deployment strategies have been proposed which enable the launch of these systems on a single vehicle or using appropriate secondary payload opportunities. Whilst these methods of deployment are not able to eliminate the need for propulsion systems entirely, the propulsive requirements for deployment can be significantly reduced in comparison to the use of direct orbital manoeuvres to populate the constellation. For the deployment of small satellite constellations in Low Earth Orbit (LEO), the method of indirect plane separation is the most promising of these alternative strategies due to the lower vehicle requirements and system complexity, as discussed in Crisp et al. [4]. Aside from lower propulsion system complexity and cost other aspects of the design process may also be economised such as power system and Attitude Determination and Control System (ADCS) requirements. Thus far, the FORMOSAT-3/COSMIC mission is the only example of a multi-plane small satellite constellation to be completely deployed from a single launch vehicle.

1.1 Design of Small Satellite Constellations

The design of traditional satellite systems is a multidisciplinary process generally consisting of analyses considering the configuration of the constellation, design of the individual spacecraft, the launch and deployment procedure, and the cost of the system. For traditional satellite constellations, these contributing analyses and the approaches to design of these systems are well established [5, 6, 7]. However, these methods are generally not suitable for application to small-satellite missions which often have different mission priorities, utilise secondary payload opportunities, and require the use of alternative deployment strategies. Furthermore, the corresponding analyses for small satellite constellation design are less mature. In particular the analysis of alternative deployment strategies for small satellite constellations are yet to be developed, despite the potential benefits of increased opportunities for access-to-orbit, reduced spacecraft complexity, and reduced system cost. As a result, the design of small satellite constellation deployment is currently either selected a priori or performed on an ad hoc basis without complete analysis.

1.2 Thesis Aims and Objectives

Given the motivating factors discussed previously, the ultimate aim of this research is to improve the development of small satellite constellations by considering the deployment strategies for such systems during the early design stages. To achieve this aim, this research focuses on the development of a methodology for the integration of deployment analysis into the design process for small satellite constellations. The resulting design-space is also explored using a numerical optimisation approach to enable the effective search for optimal or Pareto-efficient system solutions in the presence of multiple objective criteria.

Development of a methodology for the integrated design of satellite constellation deployment ensures that this aspect of the mission is examined during the design process. For small satellite constellations in particular, this supports the consideration of methods which can utilise secondary payload launch opportunities and reduce the required propulsive capability. Exploration of the corresponding design-space aids the understanding of relationships which exist between the design variables and the chosen objectives, increasing the knowledge available to the system design team. Furthermore, through enumeration of the tradespace, the most effective solutions can be identified and used to develop improved overall mission and system designs.

The development of this proposed methodology is fulfilled through the following objectives, forming the individual contributions of this research.

1. To *develop a methodology* which supports the consideration of satellite constellation deployment during the conceptual design phase for such systems. The methodology uses a numerical optimisation-based approach to effectively explore the design-space and resulting system tradespace to aid the identification of the best available solutions. The results of the exploration process can also be used to increase knowledge of the trades and relationships which exist in the design-space, supporting the ongoing design process.

2. To *support the integration* of satellite constellation deployment design into the wider design process for these systems. Using an analysis framework approach, the design of satellite constellation deployment is integrated into the design process for these systems. This integration ensures that this aspect of the mission design is considered during the system design process and supports a more complete exploration of the design-space for satellite constellation missions.

3. To *develop and implement a verified analysis method* for the deployment process of small satellite constellations. To demonstrate the proposed methodology, a design and analysis method for satellite constellation deployment is required. A simulation process for deployment using the method of indirect plane separation is developed as part of this work, the details of which were first presented in Crisp et al. [4]. This method of analysis is further developed and verified for use in this thesis.

4. To *use the methodology and framework with an integral method of constellation deployment design* developed in this research to perform the design-space exploration of small satellite constellation deployment to *identify improved designs or system architectures.* Using a reduced-order design framework and the developed method of constellation deployment analysis, the proposed methodology is demonstrated using a series of three mission case-studies. The known point-designs of the FORMOSAT-3/COSMIC and ORBCOMM missions are compared to the solutions generated. The design-space and output tradespace are also examined for relationships and trends which can be used to inform the system design team and ongoing design process.

1.3 Thesis Overview

The remainder of this document describes the development and implementation of the proposed methodology for integrated design-space exploration of small satellite constellation deployment. Chapter 2 provides a review of small satellite constellations and their design. A discussion of the different methods for the deployment of small satellite constellations is also provided. In Chapter 3 the methodology forming the crux of this research is developed from motivating research questions and stated hypotheses. A means of demonstrating the methodology is also presented. Chapter 4 provides an introduction to design-space exploration and presents a review of methods applied to space systems. The application of a method of numerical optimisation to the problem of small satellite constellation design is then described. In Chapter 5 the development of a reduced-order analysis framework for demonstration of the methodology is described. This consists of the satellite constellation deployment simulation method, preliminary satellite vehicle and propulsion system sizing processes, and a corresponding system cost model. In Chapter 6 the implementation of the developed methodology is presented, and the results of

three mission case-studies are analysed and discussed. In closing, Chapter 7 states the conclusions from the methodology development and presents recommendations for improvements and future work. Finally, concluding remarks on this research are provided.

1.4 Publications

Some of the work presented in this thesis has previously been published in conference proceedings and as journal articles.

A review of existing and in-development launch vehicles was presented at the 29th International Symposium on Space Science and Technology in Nagoya-Aichi, Japan [8], and subsequently published in Transactions of the Japan Society for Aeronautical and Space Sciences, Aerospace Technology, Japan [3]. In this paper, the payload capability and cost of existing launch vehicles and secondary-payload opportunities was analysed and the potential benefits of small launch vehicles in development were discussed. It was concluded that the introduction of these vehicles would not result in an cost reduction in comparison to existing secondary-payload opportunities. However, the accessibility of selected orbits and schedules to individual or systems of small payloads would be improved through the provision of available dedicated or cluster launch opportunities.

An analysis and comparison of small satellite constellation deployment using different strategies was presented at the 65th International Astronautical Congress [9], and subsequently published in Acta Astronautica [4]. In this paper, the initial development of the analysis method for constellation deployment by the method of indirect plane separation, presented in Section 5.1, was described. Deployment using Earth-Moon L_1 Lagrange Point (EML-1) as a staging point for return to Earth orbit was also considered. By analysis of a series of three example missions, it was shown that the method of nodal precession was capable of achieving a significant reduction in required propulsive capability, but at the expense of time to perform the deployment of the constellation. For low Earth orbits, it was also shown that the method could be be sensitive to effects of orbital decay due to the extended drift periods involved.

1.4.1 List of Publications

[3] Nicholas H. Crisp, Katharine L. Smith, and Peter M. Hollingsworth. Small Satellite Launch to LEO: A Review of Current and Future Launch Systems. *Transactions of the Japan Society for Aeronautical and Space Sciences, Aerospace Technology Japan*, 12 (ists29), 2014. ISSN 1884-0485. doi:10.2322/tastj.12.Tf_39.

[4] Nicholas H. Crisp, Katharine L. Smith, and Peter M. Hollingsworth. Launch and deployment of distributed small satellite systems. *Acta Astronautica*, 114:6578, 2015. ISSN 00945765. doi:10.1016/j.actaastro.2015.04.015.

[8] Nicholas H. Crisp, Katharine L. Smith, and Peter M. Hollingsworth. Small Satellite Launch to LEO: a Review of Current and Future Launch Systems. In *29th International Symposium on Space Technology and Science*, Nagoya-Aichi, Japan, 2013. Japan Society for Aeronautical and Space Sciences (JSASS).

[9] Nicholas H. Crisp, Katharine L. Smith, and Peter M. Hollingsworth. Launch and Deploy- ment of Distributed Small Satellite Systems. In *65th International Astronautical Congress*, pages 115, Toronto, Canada, 2014. International Astronautical Federation (IAF).

Chapter 2

A Review of Small Satellites and Constellations

The recent rise in interest in small satellite missions has been described as potentially disruptive to traditional satellite missions, particularly with reference to CubeSats [10]. The reason for this characterisation is primarily due to the differences in design, manufacture, and operational philosophies which can be achieved through the use of cheaper and smaller satellites with much shorter development cycles. As a result of these fundamental differences, it is necessary to understand the reasons for the growth of interest and use of small satellites and the benefits that these vehicles can provide to different mission types. This chapter begins with a brief review of small satellites and their current state of development and operation.

The use of small satellites collaboratively in constellations has also recently experienced significant interest and development, primarily driven by the successes of small satellites in performing increasingly productive and valuable missions previously served by larger, more complex, and more expensive satellites. However, whilst the existing launch paradigm supports the launch of individual small satellites through secondary payload opportunities, the launch of constellations of small satellites has additional requirements which are currently poorly served. This chapter includes a review of small satellite constellations and the methods by which these systems can be launched into orbit, concluding with a summary of the possible approaches for the deployment of these systems.

2.1 Development of Small Satellites

Since their initial use in the early days of the space age, the capabilities of small satellites have increased significantly beyond their initial simple technology demonstration and store-and-forward communication missions. Early examples of small satellites included the Strela-1M Soviet military communication microsatellites and initial OSCAR amateur radio satellites [11].

The evolution of these small satellites since their beginnings is primarily attributed to the advancement and miniaturisation of enabling technologies and electronic components, eg microprocessors, solid-state electronics, and Microelectromechanical Systems (MEMS) sensors [11], and the introduction of general-purpose, standardized, or modular bus designs, resulting in dramatically reduced time and costs for development and manufacture in comparison to larger satellites [12, 13]. These advancements have enabled small satellites to perform a number of missions previously served exclusively by larger satellites. In particular, the miniaturisation of 3-axis attitude determination and control system technologies has enabled the use of small satellites for Earth observation and space imaging applications [11].

In recent years, the successful launch and operation of small satellites in a range of missions has demonstrated the value and increasing capability of this class of spacecraft in a range of different applications. For example, the CanX-6/NTS 20 cm cubic satellite has demonstrated the ability to perform Automatic Identification System (AIS) detection from a space-borne asset [14]. Similarly, the O/OREOS [15] and GeneSat-1 [16] satellites have demonstrated the capability to perform in-situ biological experimentation on small satellite systems.

2.1.1 Classification and Standardisation of Small Satellites

The increased capability of small satellites has also been accompanied by a trend of increasing miniaturisation of the satellites themselves. This trend, beginning with the re-emergence of sub-10 kg payloads in the 1990s, has resulted in the generation of a system of classification to identify small satellites by their mass, shown in Table 2.1.

The emergence of the picosatellite-class of payloads is somewhat attributable to the introduction of small satellite development projects in engineering courses at educational establishments [12]. In order to reduce the cost of manufacture and launch further, payloads in the nanosatellite and picosatellite class were chosen for development by these institutions and the use of Commercial Off-The-Shelf (COTS) components was embraced. The first satellites developed

Table 2.1: Small satellite classification by mass [12].

Class	**Mass [kg]**
Minisatellite	100-1000
Microsatellite	10-100
Nanosatellite	1-10
Picosatellite	0.1-1
Femtosatellite	0.01-0.1

by these institutions were typically of educational consequence only, often referred to as 'Beep-Sats' due to their transmission of simple signals and relatively low functionality. However, the follow-on attempts have in many cases addressed useful and real mission objectives [17].

A key development in the use of small satellites for education purposes has been the CubeSat, a standardised form of picosatellite or nanosatellite, where a single unit, referred to as 1U, is a $100 \times 100 \times 100$ mm cube with a maximum mass of 1.33 kg. The CubeSat specification was developed in 1999 at Stanford University and the California Polytechnic State University, San Luis Obispo [18], to address issues with the cost, time, and expertise required to develop a University-class satellite [19]. Subsequently, the specification has evolved to include larger 2U $100 \times 100 \times 200$ mm and 2.66 kg, and 3U $100 \times 100 \times 300$ mm and 4 kg nanosatellites based on the original 1U specification.

The Space Flight Laboratory (SFL) at the University of Toronto Institute of Aerospace Studies (UTIAS) has also developed the Generic Nanosatellite Bus (GNB) in the form of a 200 mm cube with a mass of up to 7.5 kg. The GNB was developed to increase cost efficiency through the use of standardised and commercial components and the design of a single bus to perform a variety of different missions. Responsiveness is also increased through the mitigation of platform redevelopment and testing for new missions [20]. The GNB has since been developed into the larger Nanosatellite for Earth Monitoring and Observation (NEMO) bus with increased power generation and payload efficiency. The NEMO bus has a mass of up to 15 kg and measures 200 mm $\times$ 200 mm $\times$ 400 mm, enabling higher performance missions [21].

The standardisation in form and electrical function of CubeSats and similar satellite buses has enabled the use of standardised ejection or deployment mechanisms. The Poly-Picosatellite Orbital Deployer (P-POD) was the first of these deployment mechanisms and utilises a spring to eject the three contained payloads. The P-POD also serves to isolate the satellites from the launch vehicle and other payloads to minimise any potentially damaging interactions [11]. As a result, there is typically no power or other services available to the payloads once manifested

in the deployment mechanism. Figure 2.1 shows three 1U CubeSats with a 3U P-POD. The P-POD and similar deployment mechanisms, eg Japanese T-POD and UTIAS/SFL X-POD, have increased the number of launch opportunities available to these payloads [19]. For example, the GNB and NEMO bus are designed to be compatible with the XPOD separation system to facilitate piggyback and cluster launch opportunities through ongoing UTIAS/SFL Nanosatellite Launch Service (NLS) program.

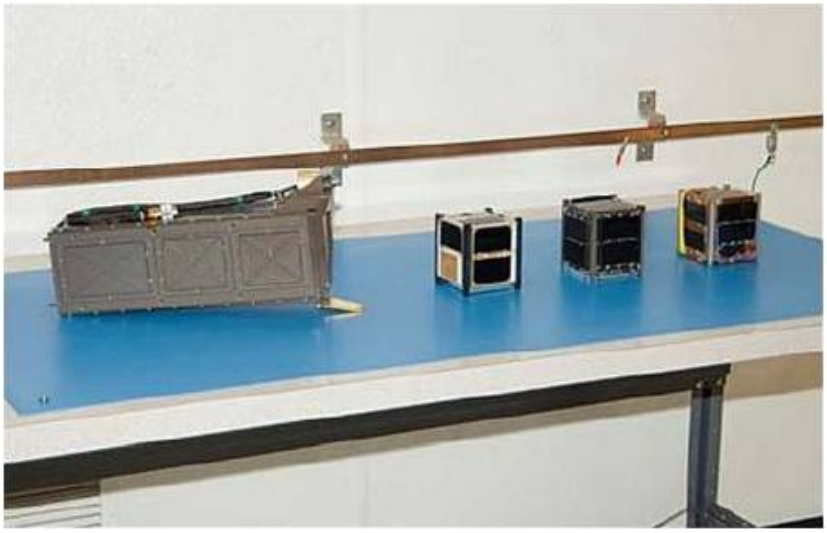

Figure 2.1: P-POD with CP6, HawkSat-1, and AeroCube 3 CubeSats [22].

2.1.2 Launch of Small Satellites

The advantages that can be offered by small satellites, primarily reduced cost and time of development, are diminished when the access-to-orbit of these systems is considered.

Primarily, the absence of sufficiently small or inexpensive launch vehicles for the dedicated delivery of small satellites to orbit represents a significant obstacle to such missions given their typically smaller budgets and the relative cost of launch to their hardware development. This issue is somewhat addressed by secondary payload launch opportunities, where satellite operators can either share launch vehicle capacity through clustering or rideshare agreements, or utilise excess capacity on a commissioned launch of a larger satellite, a practise termed piggybacking [23, 24]. However, unless arranged through a sponsored launch programme, for example the NASA CubeSat Launch Initiative (CSLI) and Educational Launch of Nanosatellites (ELaNa), with provided or subsidised launch, the price of these secondary payload opportunities is typically much greater than the specific cost, $ per kg, of the launch vehicle itself [3]. Whilst

the cost of launch of small satellites may be disproportionate in comparison to larger payloads, the use of secondary payload opportunities enables small payloads to achieve access-to-orbit at a significantly lower total expense than a dedicated commissioned launch. A more complete analysis of the current state of small satellite launch is presented in Appendix A.

Further issues with secondary payload opportunities include the lack of control on the destination orbit of the vehicle and launch schedule, both controlled by the requirements of the primary payload or as a compromise between the payload operators in the case of a rideshare launch [25]. As a result, satellites launched as secondary payloads must therefore either be agnostic to the destination orbit, flexible enough in design to operate in a variety of LEO environments, or have the capability to individually manoeuvre into their required orbit. For some missions, this flexibility or capability may not be feasible or may be too costly to embed in the system design.

Additional restrictions on the launch of small satellites utilising secondary payload opportunities can include the requirement to be compatible with a certain class of deployment mechanism, for example the P-POD, to reduce the level of certification required by the launch provider. This can further constrain the mass and volume of the satellite and any provision for deployable surfaces such as solar arrays or wireless communication antennae. Constraints on volumes and pressures of stored propellant, nominally to protect the primary launch payload [26], can also limit the capability of on-board propulsion systems, further restricting the ability of the secondary payloads to manoeuvre into more suitable mission orbits. The use of these standardised deployment mechanisms has however resulted in an increase in the number of available secondary launch opportunities and therefore more timely access-to-orbit for these payloads [27, 12, 19].

A number of new launch vehicles aiming to address the microsatellite and nanosatellite launch capability gap are currently in varying stages of development. The payload capability of these vehicles ranges from 12 kg to 300 kg with specific launch costs in the range of current secondary payload opportunities. These vehicles will support the dedicated launch of microsatellites and nanosatellites, avoiding the potentially mission critical issues related to secondary payload launch opportunities. The development of these vehicles is explored further in Appendix A.

2.2 Small Satellite Constellations

Constellations of satellites, on-orbit systems consisting of multiple spacecraft working together, can be used to perform missions which could not be realised using a single satellite alone. The primary advantages of these multi-satellite systems are enhanced coverage capability, multi-point sensing, or decreased revisit time. Additional benefits can include more gradual degradation of system performance on the occasion of individual satellite failures and survivability due to the presence of a multitude of spread or dispersed on-orbit assets [28, 29].

Satellite constellations can be designed with a number of different configurations in order to achieve specific coverage, revisit, or diversity requirements to perform different mission types. Single-plane constellations, often termed *string-of-pearls* systems comprising of a number of satellites orbiting in a common orbital plane, can achieve daily revisit times and are therefore often specified for Earth observation missions.

Satellite constellations consisting of multiple orbital planes of satellites can be used to further improve the revisit time of the system, provide a continuous level of coverage, or enable different mission types which might require higher diversity, the number of satellites simultaneously visible from a given target area, or the the collection of distributed measurements or observations. The most commonly used multi-plane constellations can be broadly categorised as either star or delta configurations, both comprising of commonly inclined orbital planes and coordinated placement of satellites within the planes. Various approaches to the design of these constellations were developed, most notably using the *streets-of-coverage* approach first demonstrated by Luders [30] and subsequently by Rider [31, 32] and the sub-satellite separation formulation by Walker [33] and Ballard [34] leading to the terms *Walker delta*, *Walker star*, and *Ballard rosette*. Additional configurations consisting of mutually-perpendicular orbital planes or planes with differing inclinations may also be considered to satisfy particular mission requirements [28].

The emergence of small satellite constellations began with the deployment of the Iridium, Globalstar, and ORBCOMM commercial LEO communications systems during the 1990s and 2000s. Details of the mass and constellation configuration of these systems is presented in Table 2.2. Constellations of small satellites have since also been successfully demonstrated in remote sensing roles, for example the RapidEye, Disaster Monitoring Constellation (DMC), and FORMOSAT-3/COSMIC missions.

Table 2.2: Example small satellite constellations

Constellation	Mass per Satellite [kg]	Orbit and Configuration
Iridium [35]	667	66 satellites, 6 planes, Walker star configuration Alt: 780 km, Inc: 86.4°
Globalstar [36, 37]	450	48 satellites, 8 planes, Walker delta configuration Alt: 1414 km, Inc: 52°
ORBCOMM [38, 39, 40]	40–45	35 satellites total Planes A–C: 8 satellites ea, Alt: 815 km, Inc: 45° Plane D: 7 satellites, Alt: 815 km, Inc: 45° Plane F: 2 satellites, Alt: 740 km, Inc: 70° Plane G: 2 satellites, Alt: 875 km, Inc: 108°
RapidEye [41]	150	5 satellites Single plane string-of-pearls configuration 620 km SSO
DMC [42]	1G: 98–166 2G: 87–270	1G: 5 satellites, single plane configuration 2G: 4 satellites, single plane configuration 660 km to 710 km SSO
FORMOSAT-3/COSMIC [43]	61	6 satellites, 6 planes Modified walker delta (180° spread in RAAN) Alt: 800 km, Inc: 72°

This demonstration of capability by small satellite constellations has recently resulted in the proposition and development of larger constellations of smaller satellites, enabled primarily due to the typically lower cost of satellite development and manufacture. With increased numbers of satellites on-orbit, these systems can enable missions which require many simultaneous and distributed measurements, allowing the study of dynamic physical phenomena [44, 45]. Other benefits of these larger constellations can include increased temporal resolution or further reduced revisit times, increased diversity, and reduced impact on operations on the occasion of individual satellite failures.

Two such examples of this new generation of constellations are the Earth imaging systems of Planet Labs [46], ∼5 kg satellites, and Skybox Imaging [47], ∼120 kg satellites, which are currently being developed and launched. A variety of novel missions demonstrating the capability and flexibility of constellations of small satellites have also been proposed, for example in

meteorology; climate-science; atmospheric, magnetospheric, and ionospheric measurement and observation; and gravity and other Earth science [48, 2, 49, 44, 1, 50, 51].

Distributed systems or constellations of small satellites systems have also been proposed as a direct alternative or replacement for constellations of larger satellites. A greater number of smaller satellites, given a different distribution, may be able to achieve a shorter revisit time than fewer large satellites thereby producing data of potentially higher value. An example study by Tsitas and Kingston [52] proposes a constellation of 35 8 kg satellites distributed between 7 orbital planes to replace the five ∼150 kg satellite RapidEye constellation. By comparison of the cost per bit of data downlinked, the authors conclude that for approximately the same total mission cost, including launch, and similar image resolution, the proposed nanosatellite constellation could achieve a higher temporal resolution of data than the existing RapidEye constellation.

A specific area of current development within the US Department of Defense (DoD) is the use of multiple small satellites to perform highly responsive communications and Earth observation operations for ground based military forces. The SMDC-ONE [53, 54] beyond-line-of-sight communications system and Kestrel Eye [55] and SeeMe [56] space-based imagery satellites are currently in development with a view to demonstrating the capability of small satellites in these roles.

Looking further forward, studies investigating the longer-term development and evolution of small satellites have identified new roles and mission concepts for these systems beyond Earth orbit [57, 58]. Example applications include communication and observation systems to support exploration of celestial bodies, constellations to observe heliophysics phenomena, and formations or systems for investigating or observing deep-space astrophysics.

Further miniaturisation of small satellites has also been predicted, exemplified by the specification of PocketQubes (5 cm cubes) [57] and the development of even smaller satellite-on-a-PCB and satellite-on-a-chip systems, payloads in the picosatellite or femtosatellite classes based on a single Printed Circuit Board (PCB) or System on a Chip (SoC) architecture [44, 49, 59]. These systems have the potential to enable missions requiring hundreds to thousands of real-time and distributed measurements or observations, but will be significantly constrained by technical limitations such as power capability, attitude determination and control, and maximum antenna or sensor size, for example aperture size for Earth imaging. [44]. An appreciation of the impact of the presence of such large numbers of uncontrolled objects on the space environment is also

required to mitigate issues with orbital debris. The lifetime and operation of these systems, particularly in well-used and valuable Earth orbits must therefore be carefully considered.

2.2.1 Launch of Small Satellite Constellations

Traditionally, constellations of large satellites are typically populated through many launches, one or more per orbital plane, or even one per satellite. However, due to the prohibitive cost of launch in comparison to the development cost of smaller satellites, launch in this manner is generally not economically viable for small satellite constellations.

During the development of the first minisatellite and microsatellite communications constellations in LEO, multiple-manifesting of the satellites became critical in order to reduce the total cost of launch. A notable example was the Iridium constellation which used 3 different launch vehicles to deliver the payloads to orbit: 5 satellites on each Delta II launch, 7 satellites on each Proton launch, and 2 satellites on each Long March 2C/SD launch [35]. Similarly, up to 8 satellites were manifested on each launch of a Pegasus-XL HAPS vehicle to deploy each plane of the ORBCOMM constellation [39]. Following delivery of the payloads to initial parking orbits by the launch vehicle, propulsive manoeuvres were performed in order to compensate for any insertion error and to transfer the individual satellites into their required mission orbits.

The launch of the complete set of payloads comprising a constellation as a cluster on a single launch vehicle can provide the most affordable access-to-orbit for constellations for small satellites. For example, the RapidEye constellation of five 150 kg satellites was launched on a single Dnepr launch vehicle in 2008 [45, 60] and the FORMOSAT-3/COSMIC mission consisting of five 61 kg satellites was launched on an Orbital Sciences' Minotaur I vehicle in 2006 [43].

For smaller systems however, the lack of sufficiently small launch vehicles currently presents a significant financial obstacle to their launch using single or multiple dedicated cluster launches. The emergence of new small launch vehicles, explored in detail in Appendix A, may provide new support for the cluster launch of small satellite constellations, primarily in the nanosatellite and picosatellite classes.

Currently, the use of a single or multiple secondary payload opportunities can present the most economical means of launch for nanosatellites and picosatellite constellations. However, the destination orbits of multiple available launch opportunities are unlikely to coincide with the required orbits for the constellation mission, thus requiring propulsive manoeuvres to achieve the correct deployment. This lack of control of the schedule of multiple secondary payload

launches may also be detrimental to the set-up of constellation, particularly for constellations operating in the low-altitude, high-drag regimes, presenting significant risks to the potential success of the mission. These issues may be further compounded by the necessity to comply with secondary payload launch regulations, discussed previously in Section 2.1.2, and requirements to maintain the low cost of platform development and manufacture. As a result, payloads in the nanosatellite and picosatellite classes generally have limited capability to manoeuvre into coordinated mission orbits.

The launch of a very small satellite constellation, the Planet Labs Flock constellation, has achieved orbit by both manifestation on Commercial Resupply Services (CRS) launches to the International Space Station (ISS) and subsequent deployment from the Kibo module and deployment as secondary payloads from a Dnepr launch into a higher altitude orbit [46]. Thus far, the satellites launched have not been coordinated into a fixed constellation beyond simple in-plane phasing using differential drag techniques. This is primarily due to the launch cadence of the CRS missions and the short lifetime in orbit of satellites deployed from the ISS due to atmospheric drag such that the constellation is unable to be built up.

2.2.2 Deployment Methods for Small Satellite Constellations

Whilst the use of cluster or secondary payload launch methods can support the more economical delivery of small satellite constellations to orbit, the transfer of the individual payloads from the injection orbit to their planned mission orbits must then also be considered.

For some swarm or cluster systems the basic requirement of deployment may only be the establishment of a stable collision-free formation. In these cases, payloads without any individual propulsion system can be deployed by a manoeuvring or rotating launch vehicle upper-stage equipped with a multi-payload dispenser. Planned separation schemes can be used to ensure collision-free deployments and generate initial satellite separation distances [61]. For other formation flying or fractionated systems of satellites the payloads may require the ability to perform on-orbit reconfigurations or maintenance of relative inter-satellite positioning or distances. Individual propulsion systems may therefore be required to perform the necessary station-keeping or reconfiguration manoeuvres [49].

In the case of more traditional constellations, where orbital planes with significantly different RAAN or inclination are required, the deployment of the satellites is typically achieved using multiple launch vehicles and propulsive manoeuvres. For example, the bulk of the first

ORBCOMM constellation was launched using Pegasus-XL vehicles, each used to deliver up to eight satellites into one of the prescribed orbital planes [40]. Alternative deployment strategies which can enable the use of fewer launches or significantly reduce the propulsive requirements of the individual satellites have also been developed and are reviewed in the following sections.

Direct Orbital Transfer

The method of direct orbital transfer involves the use of propulsive manoeuvres to transfer the payloads from the launcher injection orbit into the required mission orbits. In-plane transfers may be required to correct for launch vehicle insertion errors or to perform orbit raising manoeuvres to enter the correct mission orbit. Furthermore, if transfer to planes of different RAAN or inclination is required, significant propulsive capability is needed to provide the ΔV for out-of-plane manoeuvres. The ΔV for such manoeuvres can be determined by calculating the difference between the initial and final orbital velocity vectors at their point(s) of intersection. For the case where the magnitude of velocity is equal in the initial and final orbits, ie two orbits of similar size, the ΔV can be expressed by Eqn. (2.1), where V_1 is the velocity in the initial orbit and θ is the required plane change.

$$\Delta V = 2V_1 \sin\frac{\theta}{2} \tag{2.1}$$

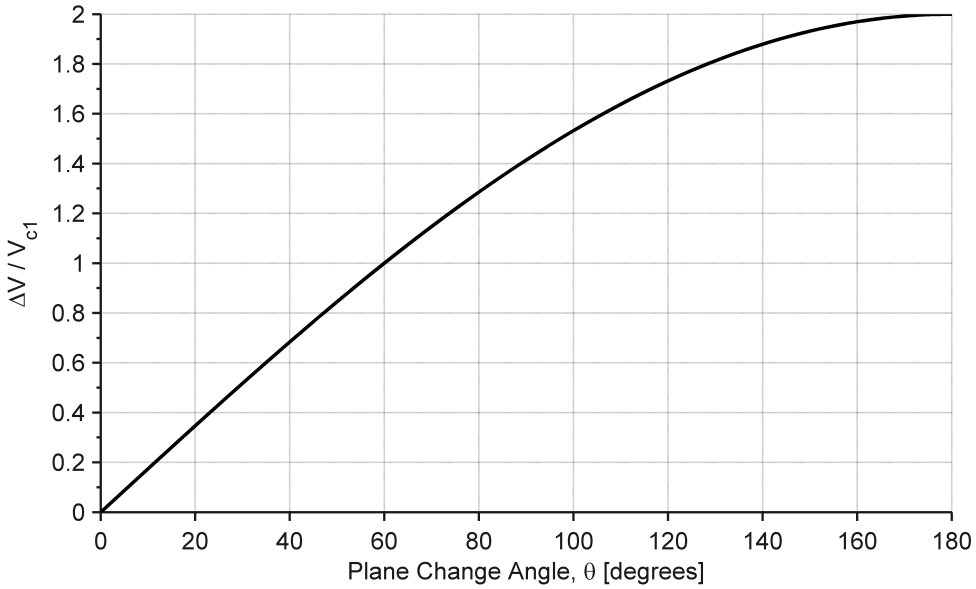

Figure 2.2: Variation of ΔV with rotation angle for direct orbital plane change.

As indicated in Figure 2.2, the ΔV required for direct plane changes manoeuvres is significant, resulting in high propellant expenditure [62]. For a circular orbit, a direct plane-change of 60° requires a ΔV equal to the magnitude of the orbital velocity itself.

The use of a manoeuvring launch vehicle upper-stage or one or more orbital transfer vehicles can be used to transport the satellites to the correct orbits. However, the total ΔV required to perform the deployment cannot be mitigated in these cases as the same number or more propulsive manoeuvres are required of the transfer vehicle. The benefit of transfer vehicle use is the elimination or minimisation of individual propulsion systems on each spacecraft platform, allowing for reduced mass and complexity. The transfer vehicle itself may also benefit from economies of scale as a common propulsion system serving a number of satellites is less constrained by mass and volume. Some propulsion technologies which are not suitable for individual small satellite platforms may also become viable due to the larger mass, volume, and power of the system.

The proposed Surrey Small-Satellite Transfer Vehicle (S3TV) is an example vehicle of this type, utilising a restartable hybrid rocket motor to deploy groups of nanosatellites into their required orbits [63, 64]. The design of these vehicles is complex, either requiring bespoke specification for each mission or flexibility to accommodate various launch vehicles and payloads. The necessity for highly capable and restartable propulsion is also challenging whilst minimising mass to reduce launch costs. As a result, the development of multi-payload transfer vehicles has been limited with no such systems demonstrated in orbit thus far.

Indirect Plane Separation

A method of constellation deployment using natural orbital perturbations to separate orbits in RAAN was patented in 1993 by King and Beidleman [65]. The method, rather than using costly direct out-of-plane manoeuvres, utilises coplanar manoeuvres to leverage the natural effect of nodal precession caused by the non-spherical geopotential of the Earth. Earth orbits with different size, shape, or orientation precess at different rates, allowing plane separations in RAAN to be achieved without direct out-of-plane manoeuvring. Equation (2.2) [28] expresses the rate of nodal precession of an Earth orbit as a function of semi-major axis a, eccentricity e, and inclination i:

$$\dot{\Omega}_{J_2} = -\frac{3}{2} J_2 \frac{{R_E}^2}{(a(1-e^2))^2} n \cos i \tag{2.2}$$

where R_E is the radius of the Earth, J_2 the second degree Earth zonal harmonic, and n the mean motion of the orbit.

The use of this method for the deployment of a constellation from a common insertion orbit initially requires an in-plane manoeuvre of a satellite into an orbit which has a different rate of nodal precession. A drift period is then required whilst the orbital planes precess at different rates until the correct angular separation is achieved. The satellite can then be returned to the initial orbit, again using an in-plane manoeuvre, fixing the developed angle of plane separation. This process can then be repeated by the remaining satellites in the initial orbit for all required planes in the constellation.

The drift time required for such a deployment, Eqn. (2.3) is dependent on the required angular separation between the two planes θ_{sep} and the differential drift rate between the initial and modified orbits, described by Eqn. (2.4).

$$t_{drift} = \frac{\theta_{sep}}{\Delta\dot{\Omega}_{J_2}} \tag{2.3}$$

$$\begin{aligned}\left(\Delta\dot{\Omega}_{J_2}\right)_{1\to 2} &= \left(\dot{\Omega}_{J_2}\right)_1 - \left(\dot{\Omega}_{J_2}\right)_2 \\ &= -\frac{3}{2}J_2\frac{{R_E}^2}{(a_1(1-e_1^2))^2}n_1\cos i_1 + \frac{3}{2}J_2\frac{{R_E}^2}{(a_2(1-e_2^2))^2}n_2\cos i_2\end{aligned} \tag{2.4}$$

Due to the requirement of a difference in semi-major axis, eccentricity, or inclination between the two orbits, the drift time is limited by the propulsive capability of the transferring satellite. The relationship between time for a fixed plane separation or 60° and propulsive capability (ΔV) required to perform a simple in-plane transfer is shown in Figure 2.3. For modest ΔV expenditures, drift periods for the deployment of a complete constellation can be expected to be on the order of several months to years.

The deployment of multiple-satellites into each orbital plane can be facilitated by manifesting the payloads on carrier vehicles, termed pallets by King and Beidleman [65]. These carrier vehicles, each equipped with a centralised propulsion system, can perform the required coplanar manoeuvres and drift procedure to enter the correct orbital plane before releasing the individual satellites. Finally, the satellites on each pallet can be distributed about the orbit in each plane. This can be achieved using in-plane deployment strategies discussed later in Section 2.2.2.

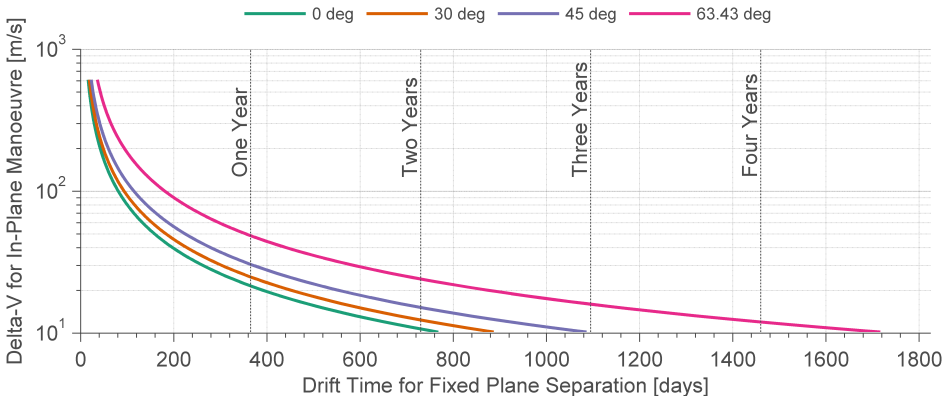

Figure 2.3: ΔV with drift time for a required plane separation of 60° at varying inclinations.

Thus far, the FORMOSAT-3/COSMIC mission [43, 66] is the best example of constellation deployment using nodal precession to separate planes in RAAN. The mission consisted of six satellites each be separated into a different plane spaced at intervals 30° (initially designed for 24° separation). The satellites were initially launched together into a near-circular orbit of 6893 km, before being sequentially raised into their mission orbit with a final semi-major axis of 7178 km. An estimated ΔV of 147 m s^{-1} was required by each satellite, provided by multiple thrust-burns of the Hydrazine monopropellant propulsion subsystem. This resulted in a estimated propellant mass of 4.6 kg per satellite [43]. This is significantly less than the propulsive requirements which can be calculated for a direct plane change of 30° at a semi-major axis of 7178 km. For a similar propulsion system with a specific impulse of 200 s, a propellant mass of 46.8 kg is required to produce the necessary ΔV of 3.86 km s^{-1} for a direct plane change manoeuvre. As a result, a much smaller propulsion subsystem and less complex attitude control system could be specified on each FORMOSAT-3/COSMIC spacecraft. Further more, due to the reduction in required propellant and propulsion system mass, the use of this deployment procedure enabled the launch of all six satellites on a single Orbital Sciences Minotaur I launch vehicle.

Whilst this method can eliminate the necessity for out-of-plane manoeuvres, a tradeoff between drift time and magnitude of in-plane manoeuvres must be considered. For large separation angles and low ΔV systems, the drift time for full deployment may be on the order of years. For the deployment of small satellite constellations in LEO, especially with very low mission altitudes, orbital drag may cause decay of one or more satellites before the constellation can be fully deployed.

The use of deployment strategies utilising differential nodal precession has also been proposed for the deployment of novel constellation types such as a moderately elliptical flower constellation, the FLORAD mission [67].

Lunar L1

An alternative method for the deployment of a complete satellite constellation, utilising the Earth-Moon L_1 Lagrange Point (EML-1), was hypothesised by Chase et al. [68], and subsequently developed by Nadoushan and Novinzadeh [69].

EML-1 is the point in space directly between the Earth and Moon at which the gravitational pull of the two bodies is in equilibrium. About this point a halo or Lissajous orbit requiring minimal station-keeping manoeuvres can be maintained, requiring on the order of $10\,\mathrm{m\,s^{-1}}$ to $200\,\mathrm{m\,s^{-1}}$ ΔV per year [70, 71]. In this method of constellation deployment, the satellites destined for each orbital plane in the constellation are manifested on a series of carrier vehicles and launched together to EML-1. The carrier vehicles are then inserted into orbit about EML-1 and individually returned to Earth orbit on prescribed trajectories to achieve the required inclination (up to 60°) and ascending node. The use of an aerocapture or aerobraking manoeuvre is also proposed by Chase et al. [68] in order to reduce the propulsive requirement of reinsertion of the carrier-vehicles into Earth orbit. The individual satellites can then deployed in each plane from the carrier-vehicles using individual propulsion systems or other phasing methods discussed in Section 2.2.2.

The propulsive requirements of this method initially involve either direct launch to EML-1 (Characteristic Energy, $C_3 = -2.4\,\mathrm{km^2\,s^{-2}}$) or transfer from LEO to EML-1, requiring a ΔV of approximately $3.77\,\mathrm{km\,s^{-1}}$. The subsequent manoeuvres of the carrier vehicles are transfer into and ejection from the halo orbit at EML-1, each in the range of $600\,\mathrm{m\,s^{-1}}$ to $800\,\mathrm{m\,s^{-1}}$, and recircularisation of the Earth orbit following aerocapture, between $100\,\mathrm{m\,s^{-1}}$ to $200\,\mathrm{m\,s^{-1}}$ [68, 69].

The preliminary feasibility and systems analysis performed by Chase et al. [68] indicates that significant savings on launch cost can be made through the use of this mission architecture over traditional deployment methods. These savings are primarily achieved through fewer launches of larger and more cost-efficient launch vehicles. Furthermore, Nadoushan and Novinzadeh [69] demonstrate that the deployment of a constellation by this method is can be performed in a

significantly shorter period of time in comparison to the indirect method of deployment utilising nodal precession.

However, whilst the basic feasibility of this method has been established, further development of the Halo or Lissajous orbit dynamics, LEO return trajectories, and aerocapture manoeuvre is required. The development of suitable carrier vehicles to enable this method is also a significant challenge due to the capability of propulsion system needed and requirement to protect the payloads from atmospheric heating when performing the aerocapture manoeuvre. The uncertainty in the cost of the development and production of the satellites and carrier vehicles is therefore high. A more detailed system analysis is required in order to evaluate the true benefit of this launch and deployment strategy.

In-Plane Separation

In many constellation systems, payload deployment in the form of spacing of satellites in a single orbital plane is required, creating either a string-of-pearls formation or equispacing of the payloads about the orbital plane. Classically, to achieve these distributions the satellites are released from the launch vehicle and perform simple phasing manoeuvres to reach the correct orbital position. However, for satellites with lower ΔV capabilities, alternative strategies have been developed. A method presented by Sorensen et al. [72] proposes the use of a carrier vehicle which transfers in and out of a phasing orbit, deploying the individual satellites into the mission orbit as the required separations are achieved. The benefits of using these carrier vehicles are broadly the same as those identified for orbital transfer vehicles discussed previously, though the scaling of propulsion systems required may be less due to reduced ΔV requirements for only in-plane manoeuvring.

Puig-Suari et al. [73] discuss the deployment of CubeSats about a single plane using differential spring energy deployment from a P-POD style dispenser. Whilst the analysis demonstrates that the required separations can be achieved using only spring deployment, minor propulsive manoeuvres are required by each satellite in order to freeze the in-plane drift between payloads and prevent degradation of the separation pattern. The time to achieve an evenly distributed separation of satellites in this manner is dependent on the orbital altitude and the differential spring energies. For typical CubeSat deployment mechanisms the velocity provided by the separation springs is typically in the range $0.1\,\mathrm{m\,s^{-1}}$ to $2\,\mathrm{m\,s^{-1}}$ [73, 74, 18, 75] resulting in a deployment time on the order of weeks to months.

Differential drag can also be used in order to distribute the satellites out within a plane, as demonstrated by the AeroCube-4 mission [76] and Planet Labs Flock 1 constellation [46] and proposed for use on the NASA CYGNSS mission due for launch in 2016 [77]. These systems use attitude control techniques and deployable surfaces to alter the drag area of the satellites and therefore the rate of orbital decay to achieve minor alterations in semi-major axis. As the affected orbits will have slightly different periods, the satellites will drift apart and achieve in-track angular separations over time. These separations can then be fixed by bringing all the satellites to a common orbit with the same semi-major axis and period.

Whilst in-track separations can be achieved using this method, the use of increased drag configurations required to perform the manoeuvres results in faster decay of the satellites in the orbit. The use of these manoeuvres and their effect on the lifetime of the constellation in orbit therefore requires management [78]. Furthermore, to enable the correct control of drag configuration and separation between the satellites, accurate orbital position and attitude determination and control subsystems are needed which may contribute to the already constrained mass, volume, and power requirements.

Table 2.3: Summary of constellation deployment strategies.

Method	**No of Launches**	**Propulsive Requirements**	**Deployment Time**	**Additional (Optional) System Requirements**
Direct launch	One per Satellite	Insertion error correction	Launch schedule	None
Cluster launch (per plane)	One per Plane	Insertion error correction; phasing manoeuvre	Launch schedule	Payload dispenser; (Multi-satellite phasing carrier-vehicles)
Cluster launch (single vehicle)	One	Insertion error correction; Plane change manoeuvre; phasing manoeuvre	Short	Payload dispenser; (Multi-satellite plane change and phasing carrier-vehicles)
Nodal Precession	One	In-plane manoeuvres; phasing manoeuvres	Months to years	Payload dispenser; (Multi-satellite in-plane and phasing carrier-vehicles)
Lunar L_1	One	Transfer into and from halo orbit at EML-1; re-circularisation following Earth aerocapture; phasing manoeuvres	Weeks to months	Launch vehicle capability to EML-1; Payload dispenser; (Halo orbit insertion and ejection, and Earth orbit re-circularisation carrier-vehicles); Aerocapture device and heat-shielding

2.3 Design of Small Satellite Constellations

The conceptual design of modern aerospace vehicles or systems is typically described as a complex and multidisciplinary problem. To enable the system designer to to make informed design decisions in this complex environment, analysis tools and methodologies are used which allow the designer to quickly and effectively explore the design-space for appropriate solutions. This process can be either applied to a singular contributing analysis or in the case of an integrated or distributed design environment, a complete multidisciplinary system.

The system design of constellations or distributed systems of satellites is an example of a complex aerospace system, characterised by the involvement of mutually-dependant variables and multiple, often conflicting design objectives. A simplified representation of the traditional satellite constellation design problem, presented by Budianto and Olds [5], is shown in Figure 2.4. The Design Structure Matrix (DSM) shown indicates the interdependency of system variables on the different disciplinary design analyses, represented by the lines and nodes on the diagram. Due to the presence of both upstream and downstream variables tradeoffs between the different design analyses may be required, possibly requiring an iterative design procedure.

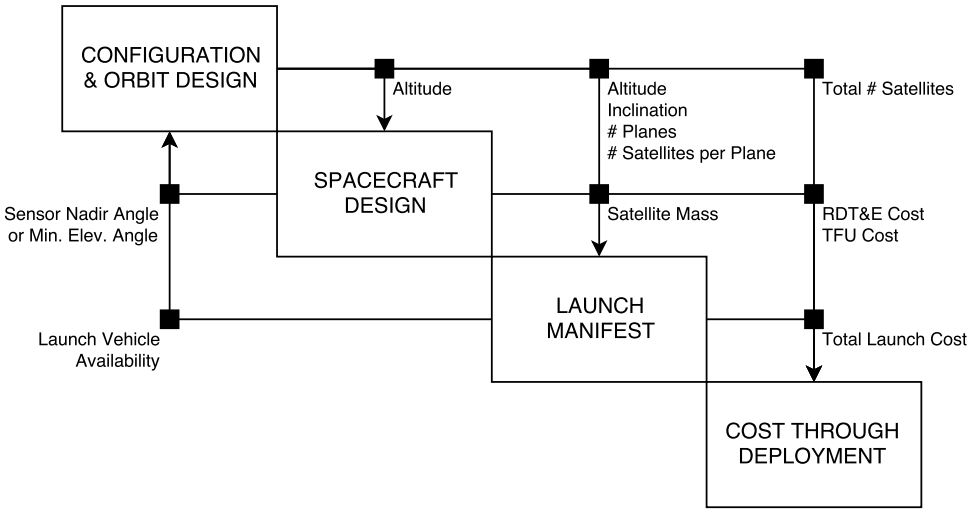

Figure 2.4: Simplified DSM of the traditional satellite constellation design process [5].

To solve this multidisciplinary problem of satellite constellation or distributed system design, a number of different methods which address the process of system-level design have been developed, of which the launch, deployment, and set-up strategy typically forms one of the contributing analyses. Due to the specific requirements of small satellites, methods which are

specifically designed for analysis of the deployment of constellations of these payloads have also been developed. In the following sections, a review of these methods and approaches is presented.

2.3.1 System-Level Design of Satellite Constellations

Initial attempts at system level design for constellations of satellites were implemented at the Jet Propulsion Laboratory (JPL) Project Design Center [79] and Aerospace Corporation's Concept Design Center (CDC) [80] where relevant disciplinary experts are brought together to work collaboratively through a real-time iterative process coordinated by a system-level designer. Whilst these processes, generally termed Integrated Concurrent Engineering (ICE), have demonstrated significant cost and time savings during the conceptual design phase, due to the lack of organised search method there is no guarantee that the design-space will be properly explored, or that improved or optimal solutions will be found [81].

The design optimisation of space systems has been investigated by a number of authors, and a variety of different techniques applied. The design process of these systems is typically multidisciplinary, requiring a number of disciplinary analyses which may share common design variables. In the case of multidisciplinary problems an optimisation framework or architecture is used in order to coordinate the interactions between the individual disciplinary analyses.

Jilla and Miller [6] developed and applied a multiobjective Multidisciplinary Design Optimisation (MDO) methodology to the conceptual design of a Distributed Satellite System (DSS). This method utilises the Generalised Information Network Analysis (GINA) model, based on previous work by Shaw et al. [82], in which satellite systems can be represented as information transfer networks rather than physical systems, allowing different architectures to be compared using a common set of quantitative metrics. The MDO methodology, proposed by Jilla and Miller [6], enables the exploration of very large design-spaces using a system-level heuristic optimisation technique to identify better system architectures. A range of different analysis modules were developed and implemented using the GINA method based on the specifics of the DSS type being investigated. In the example provided by Jilla [83] of a broadband communications system, the analysis modules included were: orbital dynamics, market analysis; link budget; payload and spacecraft bus; launch and operations; and the systems analysis.

The GINA methodology has also been developed into the Multi-Attribute Tradespace Exploration with Concurrent Design (MATE-CON) framework by Diller [84] and Ross [85], which

incorporates design-space exploration of system architectures, the use of multi-attribute utility theory to measure the system performance and capture the preferences of decision makers, and methods based on ICE to perform design-level analysis of the system. The Multi-Attribute Tradespace Exploration (MATE) methodology has since been applied to the design of a system consisting of 1 to 2 independent space vehicles (X-TOS mission) [7] and a swarm of satellites consisting of a central 'mother' spacecraft and many 'daughter' satellites (B-TOS mission) [86].

An alternative method, presented by Budianto and Olds [5], utilises a Collaborative Optimisation (CO) approach to coordinate a distributed system analysis architecture. In this method, a system level optimiser is used to direct the optimisation processes at the disciplinary analysis level. In the implemented method, three sub-analysis modules are considered: configuration and orbit design; spacecraft design; and launch manifest. Simplifications of the analysis modules included the consideration of walker constellations only, such that orbital perturbations could be neglected and the limited appreciation for deployment of the system where the satellites are launched directly into their designated plane thus neglecting other deployment methods. In each subspace, different optimisation techniques were used based on the variables present and the analysis required.

However, whilst each of these approaches has demonstrated some success in improving the problem of constellation or distributed satellite system design, in each case the deployment of constellations has been limited to only the traditional consideration of cluster or individual launch of satellites and is constrained to the manifesting of the payloads on a set of available launch vehicles. As discussed previously in Section 2.2.2, the design of a launch and deployment strategy for small satellite constellations requires consideration of the alternative methods of deployment, the required propulsive manoeuvres, orbital decay, and the time required to perform the deployment procedure. Thus far, the development of an analysis method which is capable of considering these small satellite specific characteristics has yet to be studied and integrated with the other aspects of the mission and system design process.

2.3.2 Analysis of Small Satellite Constellation Deployment

The Orion or *focuscn* software tool [87], developed by GMV and ESA, is a life-cycle constellation mission analysis tool. The tool comprises of a number of analysis modules: initial constellation design, optimisation, and performance; constellation launch and set-up; replacement and spare strategy; and end-of-life strategy. The constellation launch and set-up module contains a launch

vehicle and site selection algorithm, and evaluation of constellation set-up through satellite injection and transfer strategies, including consideration for both direct impulsive and indirect orbital transfer strategies [88]. The deployment analysis however, is limited to satellites with individual propulsion systems and the consideration of atmospheric drag effects is neglected during the drift segment of the indirect plane-change manoeuvre. Thus, the tool is unable to perform the analysis of small satellite deployment using carrier vehicles or for individual small satellites with low propulsive capability in very LEO environments. Furthermore, whilst optimisation for minimum transfer ΔV can be performed, the tool does not provide the capability to integrate this information with the wider design process or perform the exploration of the different system design options. Investigation of different deployment strategies and their effect on the system-level design of the constellation is therefore not supported.

A tool for the visualisation and analysis of multiple small satellite deployment from a single launch vehicle has been developed by Bridges et al. [61]. SatLauncher utilises the Hill-Clohessy-Wiltshire (HCW) and polar-relative equations of motion to propagate a set of satellites following deployment from a launch vehicle. The calculated motion can then be analysed for collisions and separation of the satellites over time. The tool is of particular interest for the deployment of stable formations, clusters, or swarms of small and non-manoeuvring satellites. However, due to the absence of orbital perturbations, primarily atmospheric drag and geopotential effects, the tool is limited to the accurate analysis of the motion of a satellite formation whilst separation distances remain small, and is thus inappropriate for the analysis of globally distributed constellation missions.

The analysis of staged communication constellation build-up is considered by de Weck et al. [89]. The progressive deployment of a constellation is proposed to reduce the economic risk of large systems whilst enabling the system capability to be increased when required. In order to plan the staged deployment, feasible paths of constellation architectures are identified which have increasing levels of system capacity and can be achieved by the launch of additional satellites and reconfiguration of the existing in-orbit assets. Whilst suitable for large communication constellations which can have system-capacity requirements which grow with the number of service users, the use of staged-deployment is less suitable for small satellite constellations which may have short lifetimes in LEO and are typically launched together using secondary launch opportunities.

The assembly of constellations of small satellites using multiple rideshare or piggyback launch opportunities is investigated by Marinan et al. [90] and Gangestad et al. [91]. The launch of these *ad hoc* constellations is approached by launching one or two satellites on each available rideshare opportunity, comparing the global and US only (with and without ISS re-supply mission) manifests. The results of the study by Marinan et al. [90] indicate that deployment using global rideshare launch opportunities can produce constellations with competitive revisit properties to similarly sized Walker constellations, but for percent coverage and response time were found to be inferior. An evolutionary algorithm was also implemented by Gangestad et al. [91] to explore the benefit of selecting different combinations of rideshare opportunities. In each case, the maximum, 95-percentile, and average global revisit time of the constellation and number of satellites launched was used to indicate the performance of the constellation. The results of this study indicated that rideshare-initiated constellations can be used to achieve competitive revisit metrics, but at the expense of a greater number of satellites than would be required for a comparable symmetric Walker-type constellation.

Methods for achieving required in-plane deployment and separations of satellites were discussed previously in Section 2.2.2. However, whilst the mechanisms for achieving these separations using host carrier vehicles, differential spring energies, and differential drag are described by Sorensen et al. [72], Puig-Suari et al. [73], and Li and Mason [78] respectively, corresponding methods for exploring these different strategies have not yet been developed. A means of establishing the effect on the system design and performance of these methods and their varying implementation has therefore not yet been studied.

Chapter 3

Research Aim and Methodology

Significant advancements in small satellites and enabling technologies have recently been made, enabling these systems to perform a variety of new and valuable missions previously served exclusively by larger satellites. Whilst interest in the use of small satellites in constellations has also grown, particularly to realise multi-point sensing and responsive Earth observation needs, the establishment of these systems in LEO is currently restricted by the availability of affordable and dedicated launch opportunities for small satellites. Furthermore, due to mass, volume, and complexity constraints to maintain low development costs and time, small satellites are also limited in their capability to perform high-ΔV manoeuvres, restricting their ability to transfer into a required orbit following launch. The use of more economical cluster launch or secondary payload opportunities for delivery of constellations of small satellites to orbit is therefore limited by the orbital configuration of the system and the ability of the payloads to perform the more costly plane-change manoeuvres.

A number of strategies for the deployment of small satellite constellations have been proposed which can facilitate the establishment of these systems in orbit. A brief summary of these methods and their key characteristics was presented in Table 2.3. The use of nodal precession and indirect plane separation currently appears to be the most feasible method for the deployment of a complete small satellite constellation, particularly for very small payloads in the nanosatellite and picosatellite classes. Deployment of a constellation using this method has the capability to significantly reduce the propulsive requirements of the individual satellites, but at the expense of the time needed to implement the strategy.

The examination of existing literature presented in Section 2.3 indicates that little attention has yet been given to the analysis of small satellite constellation deployment, particularly the novel methods identified in Section 2.2.2, capable of deploying constellations using fewer launches. Furthermore, design methodologies are not equipped to consider these alternative strategies and the effect that their use may have on the overall system design. Currently, the development of a deployment strategy for small satellite constellations is performed on an ad hoc basis and often a priori without complete analysis. The deficiencies in current design methods and the need to develop a means by which the deployment of small satellite constellations can be suitably considered during the design process have lead to the research aim presented in this thesis.

In this chapter the overall aim of this research is presented and broken down into a set of research questions and corresponding hypotheses which form key steps in the development of the proposed methodology. Finally, the proposed methodology and a means of demonstration by implementation are presented.

3.1 Research Aim

The primary goal of this research is the development of a methodology to improve the current practice of small satellite constellation deployment design during the system-level conceptual design phase. In order to achieve this aim, integration of an analysis method for deployment strategy design into the system design process for satellite constellation missions is required. In addition, a means of using such an integrated design process to inform the system design team about the trades between different deployment strategy implementations is required, thereby enabling the identification of more effective design architectures or overall better system designs.

Finally, in order to support the demonstration of the developed methodology, a means of performing the system-level analysis of satellite constellation deployment is required. In particular, methods of deployment strategy analysis for small satellite constellations in LEO using a single launch event or secondary payload launch opportunities were found to be poorly addressed in the literature review.

3.2 Research Questions

In order to achieve the overall research aim it is useful to ask a series of research questions. Each research question posed addresses a specific area of interest requiring development which was identified in the background and literature review. The solutions to the research questions form key steps in the development of the overall methodology.

Research Question I: *How can the consideration of deployment strategies be integrated into the design process for satellite constellation missions?*

As identified in the literature review, current design methods for satellite constellations do not include adequate analysis of the deployment of these systems. Critically, due to the use of secondary payload launch opportunities and the lower propulsive capability of small satellites, the selection of deployment strategy for these constellations can have a significant effect on the overall system design, requiring a greater level of attention than that of traditional constellations. Improvement to the design process therefore requires a means of considering the deployment of the constellation concurrently with these other aspects of the mission during the design process, especially for constellations of small satellites.

This question therefore addresses the integration of deployment strategy design and analysis for these systems with the other contributing analyses in the design process. In order to perform this integration, the input and output information required by each contributing analysis must be considered. An analysis framework is typically used to provide structure for the different elements of the design process and define a network for information exchange to take place. Through an organised design process of this type, the contributing analyses can interact with each other, enabling the development of a system-level design.

Research Question II: *Can an analysis method be created for the deployment of small satellite constellations?*

In order to enable the design of small satellite constellation missions the development of an analysis method for the deployment of such systems is required. For traditional satellite constellations deployment is typically performed using multiple launch vehicles and direct orbital transfers. Contrastingly, constellations of small satellites are generally launched using a single vehicle or secondary payload opportunities. However, due to reduced propulsive capability the use of direct plane change manoeuvres for deployment of these systems is not generally feasible.

Thus, an understanding and assessment of the alternative methods for launch and deployment of small satellite constellations is required before a suitable analysis method can be developed.

The primary requirement of such an analysis method is to establish the feasibility of design points of interest and to enable assessment of the system performance and output objectives. Additional system parameters may also need to be considered and used as inputs to other contributing analyses, possibly in an iterative process, to ensure that a system-level design can be generated and is feasible. Consideration of the orbital environment in which the satellite constellation will be operated will also be required to ensure that the correct behaviour of the system can be represented. Finally, due to the rate of technology development which can be associated with small satellites, any developed method should consider the capability to integrate new subsystem technologies which may have a significant effect on the output objective space.

If such an analysis method can be developed, the effects of a deployment strategy on the system level design of a satellite constellation can be examined quantitatively with respect to the chosen objective parameters. Moreover, such an analysis can enable the investigation and comparison of different designs for the deployment of small satellite constellations, thus enabling more informed decision making and the selection of better deployment strategies.

Research Question III: *Can the integration of an analysis method for deployment be used to generate improved designs or improve the design process for small satellite constellations?*

In order to enable an improvement the process for small satellite constellation mission design, the implementation of different constellation deployment strategies and their effect on other aspects of the system design or overall system performance must be explored in a structured manner. This process, typically termed design-space exploration, can increase the information and knowledge available to the system design team and enable the identification of more effective design architectures or support the selection of better overall system designs.

Using a system model or analysis method, design-space exploration enables either the full enumeration of a design-space or the intelligent searching of the design-space for an optimal solution or set of equally optimal solutions. This information can then be used to influence other aspects of the system design.

The selection of a suitable design-space exploration method is required in order to enable the effective search of different design variable combinations for an optimal solution or set of solutions reflecting the best deployment strategy design. Due to the possible number of

contributing factors to the deployment analysis method, the design-space may be large, possibly too big to perform a full enumeration of all design vectors. The method of exploration must therefore also be able to efficiently search the full extent of the design-space.

Selection of an appropriate design-space exploration method also requires an understanding of the output space of the analysis method. If multiple conflicting objectives are present then either a priori preference information is required to generate an single Overall Evaluation Criterion (OEC) or a multiobjective method of design-space exploration is required. If multiple conflicting objectives are present the design-space exploration will result in the generation of a set of equally optimal solutions, a Pareto set, rather than a single optimal solution.

3.3 Hypotheses

The following hypotheses are posed in response to the above research questions, forming the basis of the proposed methodology for the analysis of small satellite constellation deployment.

Hypothesis I: *The deployment of small satellite constellations can be integrated as an individual contributing analysis in a framework for small satellite constellation design.*

Consideration of the deployment of small satellite constellations during their design is required due to the particular constraints of small satellite design and the current paradigm of their launch to orbit. However, in order to aid the selection of improved system designs, the analysis of deployment should be integrated with the other aspects of the small satellite constellation. Thus, it is proposed that the analysis of deployment is presented as an contributing analysis in the design process for small satellite constellation design.

The integration of this analysis module into a design framework provides a more complete exploration of the components of the constellation mission which contribute to the development of the overall system design, and thus enables the identification and selection of better system solutions.

An example of the resulting framework for small satellite constellation design, incorporating an analysis for the deployment of the constellation, is presented in Figure 3.1 as a Design Structure Matrix (DSM). The other modules present in this example indicate the the major contributing analyses which are typically considered during the design of satellite constellations. However, additional analysis modules may be required to evaluate mission specific parameters or to enable the evaluation of additional output objectives which are of interest to the system

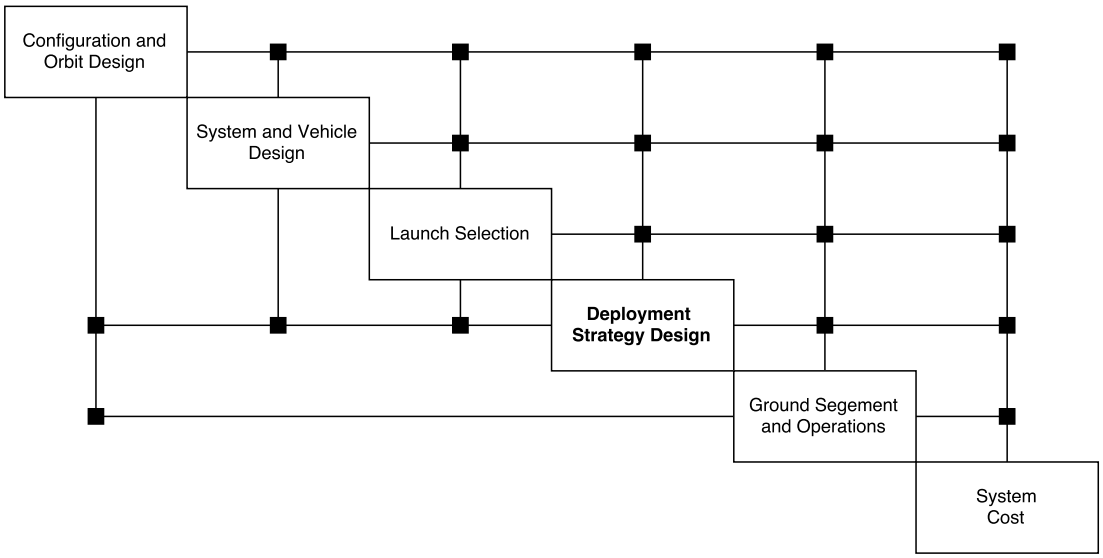

Figure 3.1: Design Structure Matrix (DSM) representation of an example analysis framework for the mission design of small satellite constellations including consideration of deployment strategy design.

designer. For example, the revisit time or time to 100% coverage of the system through deployment could be investigated for an Earth imaging constellation, similar to that of the study of Gangestad et al. [91] on rideshare-initiated constellations, enabling a measure of the system utility or value during the system set-up phase. Similarly, for a communications constellation, the level of service provided during the set-up and deployment phase can be considered. Alternatively, extensive attributes of the system design could be investigated, for example reliability, risk, or robustness.

In the example analysis framework presented, the deployment module is able to take inputs from the configuration and orbit design, vehicle design, and launch vehicle selection analyses. The deployment analysis is also able to directly contribute to the operations and cost modelling modules. Through feedback mechanisms, displayed below the diagonal of the DSM, the deployment analysis is also able to influence the upstream analysis modules, for example providing propulsive capability requirements to the vehicle design process. However, if the feedback relationships are to be used an iterative procedure may be required to ensure that convergence in the design is achieved.

Hypothesis II: *The analysis of small satellite constellation deployment by indirect plane separation can be performed by simulation using a method of orbit propagation.*

In the review of the constellation deployment methods presented previously in Section 2.2.2, it was identified that the method of indirect plane separation represents the most viable opportunity for enabling the establishment of these systems in LEO. Due to the use of only in-plane orbital manoeuvres the propulsive requirements of the satellites comprising the constellation can be reduced significantly in comparison to direct plane transfer strategies. However, due to the use of plane separation using the natural nodal precession of Earth orbits, the time required to perform the deployment of a constellation using this method can be significant. This hypothesis seeks to demonstrate that an analysis method for constellation deployment by indirect plane separation can be developed and can be shown to be a potentially useful means for investigating the deployment of small satellite constellations.

Constellations of traditional satellites in LEO are generally operated in higher altitude orbits than small satellite constellations, reducing the number required to achieve a given coverage and to increase their lifetime in orbit. Due to their low relative development cost, small satellites can be manufactured and launched in greater numbers and into lower orbits with shorter mission lifetimes, increasing both spatial and temporal resolution. An appreciation of atmospheric drag during the deployment of these constellations is therefore critical due to their lower operational altitude and high rate of orbital decay. To enable the integration of atmospheric drag effects, the use of an an orbit propagation method coupled with an atmospheric density model is proposed. Furthermore, due to the length of time which deployment by indirect plane separation can take and the variability of atmospheric density with time, a complex time-varying atmospheric density model based on forecast space weather data is considered.

The development of an analysis of this type enables the assessment of constellation deployment feasibility and performance for small satellite systems in LEO, and therefore provides a means of considering the deployment of these systems in the wider design process.

Hypothesis III: *An integrated design framework with analysis of deployment can be utilised by a numerical optimisation method to effectively explore the design-space for small satellite constellation missions.*

To enable the identification of better system-level designs and support the decision making process of the system design team, increased knowledge of the design-space for small satellite constellation missions is required. In this hypothesis it is proposed that the use of the extended

design framework with an integrated analysis method for the deployment of satellite constellations can be used to support and improve the design process for these systems using a method of design-space exploration.

To support the selection of an appropriate method of design-space exploration, the characteristics of the design-space must first be understood. The set of variables comprising the complete design-space for satellite constellation missions can be nominally characterised as mixed discrete-continuous due to the presence of both categorical or discrete and continuous real-numbered variables. Furthermore, the number of design variables and their range of possible values or options may be considerable, resulting in a very large design-space. For individual studies, the design-space may be simplified due to known constraints, mission parameters, or a priori decisions.

In the output space for such a design-space exploration the preferences of the system design team may not be known a priori. Multiple conflicting objectives may therefore exist which cannot be simply combined to form a single criterion. In addition, due to the nature of the contributing analyses contained in the design framework, gradient information of the output objectives may not be readily available, and may therefore require the use of finite-differencing methods.

An a posteriori, population-based optimisation method is therefore proposed as the method of design-space exploration, primarily for its ability to handle multiple objective functions and search globally across a large and multivariate design-space for a set of Pareto-optimal solutions. Furthermore, these methods typically support the range of expected input variable types and do not require the calculation of objective function gradients, simplifying the implementation of this design-space exploration method and reducing the number of supplementary function calls.

3.4 Methodology Outline

To test the hypotheses presented previously the following methodology, summarised in Figure 3.2, is proposed. The aim of this methodology is to provide a means of integrating the analysis of deployment into the overall design process of small satellite constellations and enable exploration of the corresponding design-space. The results of this design-space exploration

can then be used to inform the system designer of the tradeoffs involved during design and support the identification of effective solutions or improved overall designs.

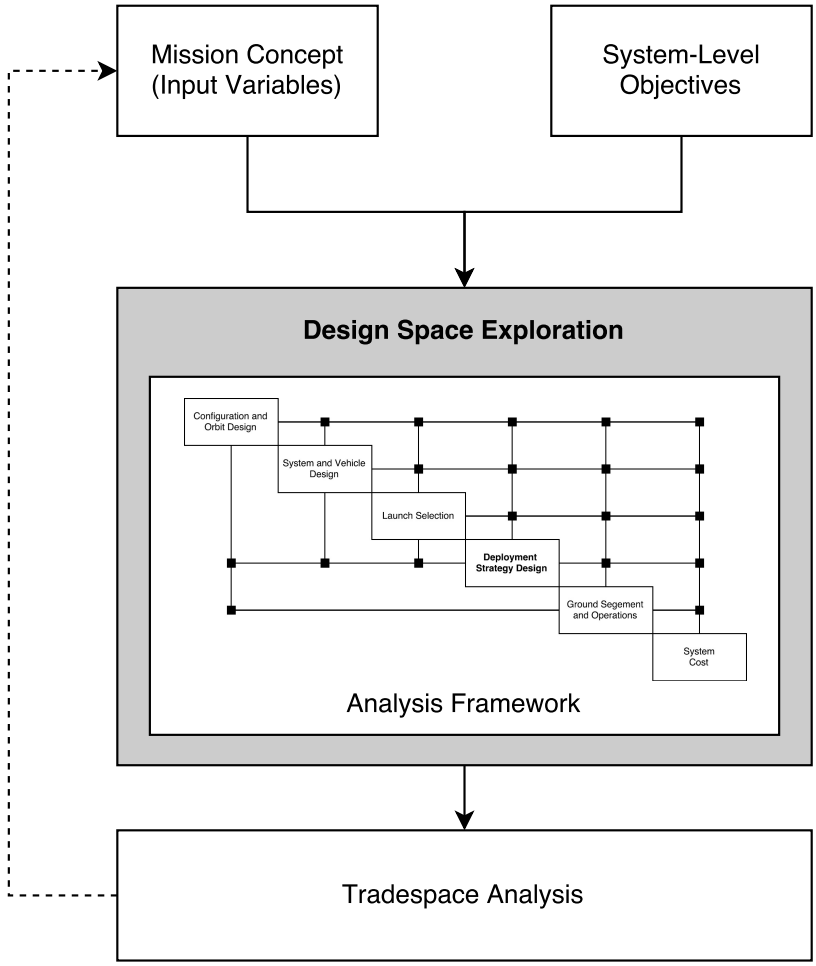

Figure 3.2: Overview of the proposed methodology for the design-space exploration of small satellite constellation deployment. The framework for small satellite constellation design features an integrated method of analysis for the deployment of these systems.

The methodology first requires a definition of the mission concept, including the variables which are required to perform the system analysis and design process. The set of system-level objective functions by which generated solutions can be assessed and compared are also required to direct the design-space exploration method and perform the subsequent tradespace analysis.

A design framework, described in Hypothesis I, is used to organise the qualitative analysis of different system design vectors. The contributing analysis modules which comprise the design framework can encompass the complete life-cycle of a satellite constellation mission, for example factors such as launch vehicle selection and end-of-life compliance. The development of an appropriate design framework is dependant on the analysis modules which are available

and required to enumerate the objective functions of interest to the system design team. Simplification of the design process may be achieved by decomposition approaches in which the analysis modules can be re-ordered or combined together, reducing the number of feedback loops and iterative processes required. The total set of variables used in the analysis framework can subsequently be identified, and through a process of parametrisation be reduced to the set of input variables which comprise the design-space for exploration. This set of input variables is dependant on the modules contained in the analysis framework and may be specific to the mission to be performed by the system or the chosen objective functions.

The proposed method of design-space exploration utilises a population-based approach, and therefore requires the simultaneous solution of multiple design vectors during each iteration. To initialise the design-space exploration process a number of initial design vectors are required, often generated probabilistically from set bounds on each design variable. The mission design and analysis process, structured using the analysis framework, is then used to determine the feasibility and output performance of each design vector. These solutions are then ranked using the input system-level objectives and Pareto-dominance methods, the results of which can be used to generate the next set of input design vectors if required.

The design and solution spaces generated by the design-space exploration method can then be investigated to identify trends and tradeoffs which exist between the design variables and the system-level output objective functions. Finally, the results of this tradespace analysis can be used iteratively to influence or redefine the initial set of system requirements, variables, and parameter ranges. Alternatively, an individual or subset of the most promising designs can be taken forward for further design analysis and development.

The developed methodology is also applicable to design-studies which utilise a reduced form of the overall analysis framework for the system. These cases may arise when design decisions have already been made, reducing the necessity for some elements of the analysis framework. Alternatively, for some contributing analyses, insufficient information is available to perform other contributing analyses assumed behaviour may need to be considered. Whilst the resulting tradespace analysis will not be representative of the complete system design-space, knowledge of any identified trends can be used to focus subsequent iterations of the design process or reduce the design-space for future design studies.

3.5 Methodology Demonstration and Verification

Due to the complexity of the complete design process for a small satellite constellation, comprised of a number of different analysis modules for which limited information may be available, eg Figure 3.1, a reduced-order framework which focuses on the deployment of the constellation can be used to demonstrate the principals of the proposed methodology.

In this implementation, shown in Figure 3.3, the contributing analyses are limited to the constellation deployment simulation, preliminary vehicle and propulsion system sizing procedures, and a model for estimating the resultant cost of the system. These analysis modules were selected to demonstrate the primary tradeoffs associated with the deployment of a small satellite constellation in a simple and mission agnostic manner.

To perform this implementation, a design of the constellation mission orbit and configuration will be assumed a priori and will be provided as an input to the reduced analysis framework. This input consists of parameters describing the constellation configuration, mission orbit properties, the launch epoch, and payload mass or initial spacecraft dry-mass. Delivery of the complete constellation to the initial orbit by a single launch vehicle will also be assumed, eliminating the requirement for an additional analysis module to perform the selection and cost estimation of available launch opportunities. The analysis of operations costs are similarly neglected due to the lack of available information and complexity of developing such a model. Following a parametrisation of the design-space to generate the set of design variables, an initial population of designs can then be produced and evaluated using the simplified analysis framework.

Simulation of the deployment of the constellation is performed using propagation of the satellite orbits and transfers required to achieve the mission configuration using the method of indirect plane separation. The use of an atmospheric density model is also required to capture the effects of drag in the LEO environment. The process of preliminary vehicle sizing is performed using heuristic methods and is supported by a set of representative propulsion system models. Interaction between the vehicle sizing and constellation deployment analyses is required due to the interdependence of the vehicle configuration, system mass and the required ΔV for manoeuvres. Finally, a measure of the spacecraft cost is evaluated by application of system-level cost-estimating relationships. An additional analysis module which checks the feasibility of input design vectors is also used as a screening process to reduce wasted computational effort.

Exploration of the design-space is achieved by the use of an optimisation scheme which operates by varying the available design variables whilst seeking to minimise the values of the selected output objectives. After a given number of function calls or otherwise defined stopping criteria, the design-space exploration process can be halted and the resulting tradespace analysed. Comparison of the output objectives and their corresponding design vector can be performed and any present trends, tradeoffs, or limits of feasibility identified.

If useful results can be generated using this simplified representation of the constellation design process, considering primarily the deployment of the constellation, then the integration of further analysis modules which cover different aspects of the mission life-cycle should provide additional information which can be used to aid the identification and selection of improved overall system designs.

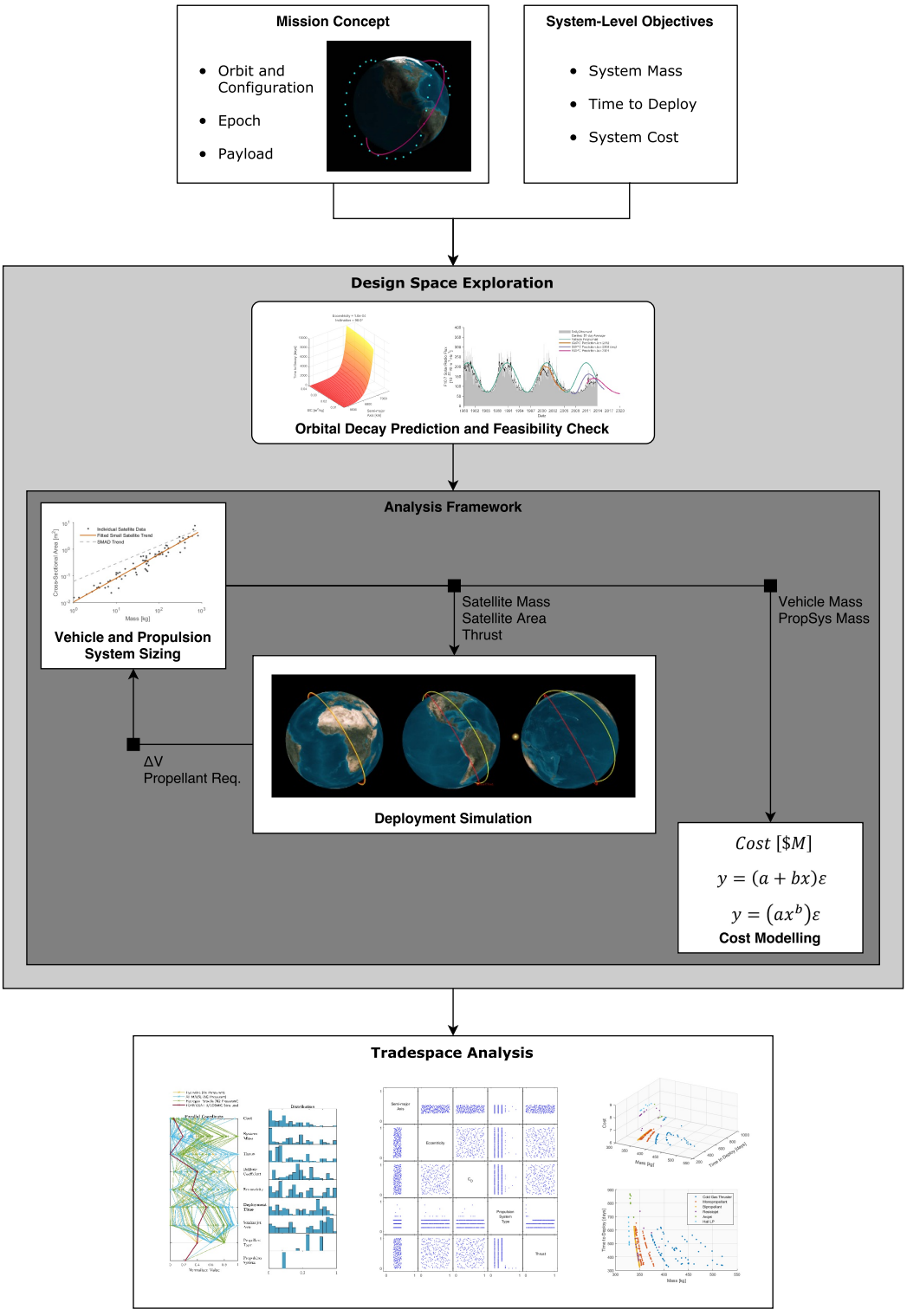

Figure 3.3: Overview of the designed implementation to demonstrate the proposed methodology. A reduced-order analysis framework and fundamental system-level objectives are featured, focusing the design-space exploration on the system-level effects of constellation deployment design.

Chapter 4

Design-Space Exploration

During the design process methods of design-space exploration can be used to search the design-space and investigate different design alternatives or vectors before decisions are made. These methods can help to increase the knowledge and understanding of the system design team of interdependencies or tradeoffs between the design variables or output system characteristics. Design-space exploration methods can also be used to search for feasible system solutions which are are comprised of multiple components or analyses and have system-level constraints or requirements [92].

At the system level, increased knowledge of the tradeoffs between the system objectives and the effects of variations in a decision space can be used to influence other aspects of the system design. Utilisation of the knowledge obtained using the design-space exploration can support better and more informed decision making in the ongoing design process and therefore development of improved system designs.

In this chapter, an introduction to design-space exploration and a review of design-space exploration and optimisation methods is presented. The problem formulation for the design-space exploration of small satellite constellation deployment is then discussed. Finally, the application of a numerical optimisation method to this problem is described.

4.1 Introduction to Design-Space Exploration

During the conceptual design phase the freedom of design is typically high as the number and range of design variables is large. This results in a significant number of possible design vectors which can be generated and a large design-space which requires exploration. The exploration of a parametric design-space or tradespace is used to enhance understanding of the design problem and aid the identification of feasible design solutions. Exploration of a design-space can either be performed by full factorial enumeration or using optimisation algorithms to search for optimal solutions given an individual or set of objective functions. Further efficiency gains in design-space exploration can be achieved using approximations to complex analysis procedures in the form of surrogate or meta-models [93].

If multiple objectives are present in the design problem, a number of equally optimal solutions may exist which form the set of nondominated solutions or the Pareto-optimal set. A solution is described as nondominated if its value for a single objective cannot be improved on by another known solution without suffering a decline with respect to another objective [94]. This principle is demonstrated in Figure 4.1 where minimisation of the two objectives is sought. When a design-space has been completely enumerated, the Pareto-optimal set is represented by the set of nondominated solutions [95]. For a partially explored design-space, the nondominated set is often considered to approximate the Pareto-optimal set.

Alternatively, if sufficient information about the priorities or preferences of the decision makers is available a priori, scalarisation of the objectives can be performed. An OEC, or combined objective or utility function can then be utilised to search the design-space for a single optimal solution. Using a basic weighted-sum method, demonstrated in Eqn. (4.1), the three discrete objectives $f(x)_i$ can be collapsed into a single function $f(x)_{OEC}$, using a series of weightings λ_i, based on known or chosen preferences [94].

$$f(x)_{OEC} = \lambda_1 f(x)_1 + \lambda_2 f(x)_2 + \lambda_3 f(x)_3 + \cdots + \lambda_k f(x)_k \tag{4.1}$$

$$\sum_{i=1}^{k} \lambda_i = 1$$

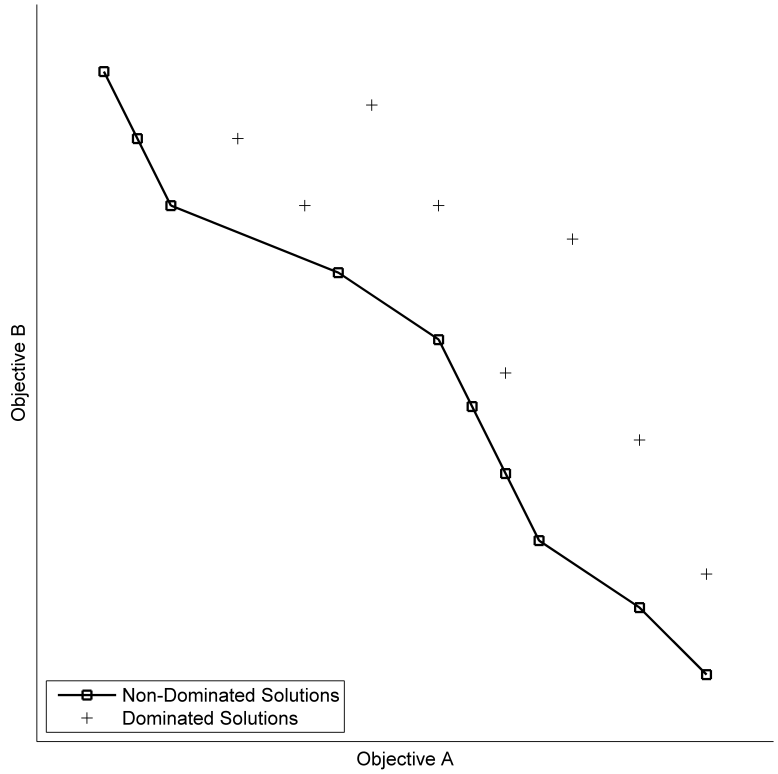

Figure 4.1: Example of a multiobjective minimisation problem indicating dominated solutions and the nondominated Pareto set.

However, whilst this formulation can simplify the problem of multiple objectives, the weighted-sum method cannot be used to explore concave regions of a design-space. Furthermore, normalisation of the objectives in the design-space is required if the different objectives are not of similar magnitudes. Alternative scalarisation methods exist, such as the ϵ-constraint method, Tchebycheff Function, and non-linear methods, which can overcome these issues and explore non-convex regions of the Pareto set [96]. However, with each of these methods a priori information is required to define the relative priorities or weightings of the objectives and can lead to search of a limited region of the design-space or cause the analysis to miss solutions which may be more acceptable. In addition, use of normalisation methods a priori, especially the use of unbounded minimum or maximum values, can introduce a preference structure which is not explicitly known by the decision maker [97].

Scalarised formulations can be also used to generate Pareto-set approximations for multiple objective problems. The selection of different weightings can be used to find different Pareto-optimal solutions. Alternatively, a scalarised objective function can be implemented a posteriori

by application of a weighted formulation to the set of solutions enumerated by a prior design-space exploration, allowing the identification of a single optimal solution.

The full enumeration of a design-space by definition guarantees optimality. In addition, knowledge of the complete design-space enables system designers to select the most appropriate solution rather than the use of a priori or locally optimum solutions [7]. However, whilst appropriate for smaller design studies with few variables, the use of full design-space enumeration, or brute-force searching, can become inappropriate for larger design-spaces due to the number of analysis evaluations and therefore computational expense required [98]. To address these issues, a number of different optimisation algorithms and routines which perform a more computationally efficient search of the design-space have therefore been developed.

4.1.1 Methods of Design-Space Exploration

Optimisation methods for design-space exploration can be generally categorised as either deterministic methods or probabilistic methods, each exhibiting suitability to different applications. Deterministic methods, eg gradient or calculus based methods, utilise the analytical properties of a problem to converge towards optimal solutions in the design-space. On the other hand, probabilistic or stochastic optimisation methods utilise randomness during the search process to explore the design-space for improved solutions.

The characteristics of the design-space and method of analysis for small satellite constellation deployment make the design-space exploration of this problem challenging and affect the selection of a method of optimisation. First, due to the absence of a priori information or preference from the system designer regarding the tradeoffs between the different objectives, the design-space exploration method must be able to identify different feasible system designs which are effective across the range of the multiple output objectives. Methods of design-space exploration or optimisation which satisfy this criteria are generally termed a posteriori, referring to the role of the decision maker which begins after a set of Pareto optimal solutions has been generated. Methods of a priori design-space exploration can be adapted to explore multiobjective design-spaces in this manner by converting the problem to many single-objective optimisation problems by varying a scalarisation formulation [96]. However, whilst these methods can ensure the Pareto optimality of developed solutions, selection of the appropriate objective function weightings to effectively explore the full range of the Pareto set can be challenging, particularly if this process is to be automated.

Secondly, due to the analysis methods utilised, the objectives in the output space are not readily differentiable. This is due to the method by which the objectives are calculated using a number of different analysis techniques including orbit propagation. Furthermore, the problem of small satellite constellation deployment is of mixed continuous-discrete nature. The presence of discrete variables in the design-space can result in a discrete objective space or islands of feasibility and discontinuities in the objective space. Derivative approximation using finite-differencing cannot therefore be applied as this typically requires the objective space to be smooth. The additional computational requirement of derivative approximation can also be significant, requiring many additional function calls depending on the optimisation method used. Gradient-based design-space exploration or optimisation methods are therefore unsuitable for a problem of this type.

Finally, analysis for the deployment of small satellite constellations utilises a method of simulation by orbit propagation and has a significant computational expense. The number of function calls required by the optimisation method to effectively explore the design-space is therefore of significance.

A number of suitable gradient-free design-space exploration and optimisation methods can considered for this problem, including evolutionary or genetic algorithms, particle swarm optimisation methods, and simulated annealing. These methods are each described herein.

Evolutionary and Genetic Algorithms

Evolutionary Algorithm (EA) is the term for a number of metaheuristic, problem-independent, optimisation methods which are inspired by the processes of evolution and natural selection observed in nature. These methods use a population based approach to search the design-space for optimal solutions to the problem at hand. As the population can cover a large range of the design-space, an EA is less likely to converge on local minima than conventional single-point or derivative-based optimisation methods and is thus classed as a global optimisation method. Furthermore, due to the evaluation of a population a single EA implementation can be used to effectively explore a design-space for a Pareto-optimal set and identify the tradeoffs between different objectives [95].

A Genetic Algorithm (GA), a subset of EA methods, operates by successively modifying populations of individuals over a number of generations such that the population evolves towards the optimal solutions. The typical composition of a Genetic Algorithm (GA) is described by

Coley [99] to include a population of individual candidate solutions, a method of determining the fitness or performance of the solutions within the population, a method of selecting and combining the good or best individuals in the population with the aim to form new and improved individuals, often termed crossover or mating, and a mutation operator to maintain or introduce diversity to the population. Elitism, preservation of the best population members between generations, can also be implemented to ensure that the best solutions are maintained and not corrupted by crossover or mutation operations. Finally, to ensure that the diversity of successive populations is preserved, individuals which result in solutions in less crowded regions of the design-space can be preferentially selected over other individuals of comparable fitness. This environmental selection can ensure that the full range of the Pareto-set is represented and explored.

Further modifications can be made to the basic GA methodology. Sub-populations and island models, between which migration of individuals can occur, can result in better search of the solution space for certain problems, particularly when increasing population size does not provide improved solutions [100]. Similarly, adaptive GA methods, in which the probability or rate of mutation and crossover operations can change with the fitness of the population in a given generation, can affect the convergence properties of the algorithm and the diversity of generated populations [101].

A number of different GA methods have been developed specifically for application to multiobjective optimisation problems. Whilst each of these Multiple-Objective Evolutionary Algorithm (MOEA) methods follows the same basic principals of a GA, their specific implementations of evolutionary and environmental selection, crossover, mutation, and elitism can differ, leading to varying performance for different problems and applications. A key objective of MOEA methods is the preservation of diversity within the population such that a good spread of solutions is obtained and the entire range of the Pareto-set can be explored. Popular MOEA implementations include NGSA-II [102], Strength Pareto Evolutionary Algorithm 2 (SPEA-2) [103], Pareto Archived Evolution Strategy (PAES) [104], and ParEGO [105].

Particle Swarm Optimisation

Particle Swarm Optimisation (PSO) methods are a class of population-based metaheuristic optimisation methods first proposed by Kennedy and Eberhart [106], which take inspiration from the social behaviour of flocks of birds or schools of fish. In traditional PSO methods a

population of individuals, typically referred to as particles, explore the design-space through movement influenced by their current velocity, the best solution previously known to each individual, and the best global solution. Through a process of iteration, the velocity of each particle can be updated based on the best known solutions and the position in the subsequent generation determined. Over a number of generations, the population is likely to move towards the best solution in the search space [107].

Modifications to traditional PSO theory can include the use of different social structures, population topologies, or local neighbourhoods to help avoid premature convergence to local minima [108] and mutation operators which can improve the exploratory capability of the algorithm and enable it to escape local minima by reintroducing diversity to the population [109].

Whilst the basic PSO theory is designed for the identification of a single optimal solution within a design-space, the concept of Pareto-dominance can be introduced to allow for the identification of a Pareto-set of solutions for multiobjective problems. For example, the method of Coello Coello et al. [110] utilises both mutation operators and a concept of elitism by which each particle records any nondominated solutions generated in the past. Over successive generations the archive of nondominated solutions approximates the Pareto-set. Exploration of the full Pareto-set is emphasised by considering the spatial density of the returned solutions and preferentially selecting new leaders of the swarm which exist in less crowded regions of the objective space.

Whilst initially designed for use with only continuous variables, methods for adapting PSO techniques for use with discrete variable classes have been developed. Most commonly, integer variables are obtained by simply rounding-off of the continuous variables. However, this process can result in the return of designs with lower fitness or infeasibility, particularly if the objective space is non-smooth or discontinuous. Alternatively, a penalty-based approach can be used, whereby individuals which have non-integer variables are assigned a lower fitness value. However, this method can produce an objective space with high modality and thus many local minima which may trap the algorithm. Significant additional computation may also be required in order to implement the penalty function [111, 112].

Simulated Annealing

Simulated Annealing (SA) is a method of metaheuristic optimisation which imitates the process

of annealing in metallurgy to locate a global optimal solution within a large design-space [113]. Annealing in metallurgy involves the heating and controlled cooling of a material to alter the size and organisation of its crystals to achieve a lower energy state, increasing the ductility and reducing hardness and brittleness.

Simulated Annealing (SA) methods operate in a probabilistic and iterative fashion, starting with an initially random design for which the objective or cost is then calculated. In subsequent iterations, new designs are proposed in the neighbourhood of the previous design by successively varying the individual design variables using a random process. SA approaches to optimisation utilise the notion of controlled cooling of a material by implementing an annealing or cooling schedule by which the probability of the algorithm to select a less optimal solution reduces over time. This control parameter of probability is often referred to in the literature as the *temperature* of the optimisation process [113]. The use of an initially high *temperature* or probability at the beginning of a run allows the algorithm to accept worse solutions and therefore escape from local minima, aiding the search for the best global solution. At the beginning of an optimisation run, it is advantageous to explore the whole design-space. However, as the algorithm progresses, the cooling schedule can limit the distance of new proposed solutions from the current accepted solution and focus the search for the optimal solution to an increasingly smaller region of the design-space.

The selection of appropriate internal tuning parameters to determine a suitable cooling schedule for SA can be problematic and time-consuming. If the initial *temperature* is too hot, the method can approximate that of a random search until the *temperature* has cooled sufficiently. As the *temperature* reduces an increasing number of iterations may be required such that the local optima can be fully explored. However, a tradeoff therefore exists between rate of cooling and the computational-time required [114]. Adaptive cooling schedules can be used to change the *temperature* or rate of *temperature* reduction based on the solutions which are found by the algorithm.

Extension of SA methods to multiobjective optimisation problems can be considered by utilising a population of solutions at each iteration of the algorithm, for example, the method of Pareto Simulated Annealing (PSA) by Czyzak and Jaszkiewicz [115]. However, in order to develop a population of solutions which can approximate the full range of the Pareto-optimal set, these methods use scalarisation of the objectives, potentially limiting their ability to fully explore the Pareto-set. Alternatively, the method of Suppapitnarm et al. [116], and later

Bandyopadhyay et al. [117], utilise Pareto-dominance based measures and thus do not require the use of composite objective functions.

4.2 Design-Space Exploration of Aerospace Systems

Methods of design-space exploration and optimisation have been applied to a range of different problems in the field of aerospace systems design. In the following sections, application of design-space exploration methods to the design of space systems and in particular satellite constellations is reviewed.

Design of Satellite Constellations

In the past a number of methods of design-space exploration and optimisation have been applied to the design of satellite constellations. Initially, these studies focused primarily on the configuration of the constellation. However, other aspects and multidisciplinary approaches to the design of satellite constellations have since been investigated.

A study by George [118] utilises a single-objective GA to investigate the design of sparse constellations for non-continuous global coverage. Optimising the constellation for minimum maximum revisit time, the study results in the identification of constellations which can provide significant performance advantages over Walker constellations of the same number of satellites.

A similar study was performed by Crossley and Williams [119] in which GA and SA approaches to the optimisation of satellite constellations with discontinuous coverage requirements for minimum maximum revisit time are compared. The authors found the SA approach to be most efficient at finding the best design for each problem examined, requiring fewer function evaluations to achieve the minimum result. However, the GA approach was found to explore the design-space more thoroughly due to its population based approach, returning multiple different designs with the same minimum revisit time during each run.

A multiobjective GA optimisation method was applied by Ely et al. [120] to the design-space exploration of constellations requiring zonal coverage between two latitudes, often specified by LEO communications systems. Due to the inclusion of both elliptical and inclined orbits, a semi-analytical streets-of-coverage approach to the design of the constellation was developed by the authors. In each example case studied, the constellation design was optimised simultaneously for minimum number of satellites and minimum altitude to provide the required coverage. Ely

et al. [120] conclude that the approach using a GA is useful in identifying constellations which utilise elliptical orbits and required fewer launches or less expensive orbital manoeuvres.

Other multiobjective approaches to the design of satellite constellation configuration are investigated by Mason et al. [121], Ferringer and Spencer [122]. In these studies, the development of Pareto optimal sets of designs are generated using GA. Mason et al. [121] focus on optimisation of the constellations based on coverage and number of satellites, whilst the study by Ferringer and Spencer [122] investigated the tradeoff between temporal and spatial resolution for constellations of different sizes. In a follow-up study, Ferringer et al. [123] investigate the performance of two different parallel computing implementations of NGSA-II, master-slave architecture against an island-based model with migration of individuals, on the design of constellations optimised for both minimum average revisit time and minimum maximum revisit time. The authors conclude that both approaches are capable of approximating the true Pareto frontier using a single seed and are able to almost completely represent the true Pareto frontier when the results of multiple seed trials are combined.

The design-space for LEO communications constellations is also considered by de Weck and Chang [124], using a developed method for predicting the system capacity and lifecycle cost to determine the system performance. Due to the restricted design-space considered and the relatively fast solution time of the analysis, a full enumeration of the design vectors was performed. The analysis method was validated using simulated and actual point designs of the Iridium and Globalstar communication constellations. The results of the design-space exploration suggest that the design of the Globalstar and Iridium systems are not Pareto efficient with respect to system lifetime capacity and system lifecycle cost indicating that significant improvements to their system design could have been made.

Design of Other Space Vehicles and Systems

An integrated design solution for the conceptual design of a fully reusable manned launch system was attempted by Stanley et al. [125]. Analysis tools for the trajectory, weights and sizing, geometry, aerodynamics, and aeroheating were used to produce designs for a rocket-powered, two-stage fully reusable launch vehicle. However, the trade studies performed using the analysis tools were only completed for point vehicle designs created for each variation in a design variable.

In the conceptual design of an advanced rocket-based combined-cycle Single-Stage-to-Orbit (SSTO) vehicle by Olds [126], analysis tools for the aerodynamics, performance, aeroheating, weights and sizing, structures, and propulsion disciplines were integrated in an analysis cycle to simulate the process of a typical design team. The implementation of the integrated environment however required significant computational time for each iteration of the analysis cycle and gave no guarantee of a converged solution. Olds [126] used a variety of MDO techniques in order to evaluate their usefulness for aerospace vehicle conceptual design, specifically Taguchi methods, Central Composite Design (CCD), and Response Surface Methodology (RSM).

A further study by Olds [127] investigated the use of the System Sensitivity Analysis (SSA) optimisation method for the conceptual design of a space transportation vehicle. The study, the conceptual design of a SSTO launch vehicle, utilised three standalone analysis codes for the propulsion, performance, and weights and sizing disciplines. However, In the application of the SSA method, the three disciplinary analyses were not integrated into an automated framework, rather the derivative and gradient information was passed between the codes manually. Olds [127] identifies this manual method of applying SSA as an advantage of the technique, allowing for geographically distributed analyses to be performed by different disciplinary experts, whilst eliminating the time required to integrate the different analyses. In parallel, a study by Braun et al. [128] generated a single monolithic design code, integrating the three disciplinary analyses. The results of the two different implementations to the conceptual design of a SSTO launch vehicle were shown to compare well by Rowell et al. [129].

In the study of a single disciplinary analysis, Cage et al. [130] compared the performance of a GA to a grid-search method for the optimisation of interplanetary trajectories. The authors concluded that the GA was superior due to the multi-modal and discontinuous nature of the design-space. Furthermore, as the dimensionality of the design-space was increased, the performance advantage of the GA was shown to increase.

The process of spacecraft conceptual design was addressed by Mosher [98] using a GA optimisation scheme. The conceptual design problem presented was based on the Near Earth Asteroid Rendezvous (NEAR) spacecraft, in which six discrete design variables each with a small and limited number of options were traded. A GA was chosen due to the combinatorial aspect of the spacecraft design process and the compatibility of the method with the cost-estimating Spacecraft Concept Optimization and Utility Tool (SCOUT). The performance of the GA approach was found to require on average less than half the number of analysis calls

than a comparable full enumeration study. The GA was also able to reach the optimum solution in the design-space in 60 % of the performed iterations whilst failing to find a feasible solution only 4 % of the time.

Bayley et al. [131] used a GA for the design optimisation of a solid propellant launch vehicle for minimal mass and therefore reduced system cost. In the study, four disciplinary analyses were used to determine the overall performance of the vehicle: propulsion, mass, aerodynamics and flight dynamics simulation. The authors concluded that the GA was able to generate solutions which improved on existing designs.

The MDO of the design and operation of an individual small satellite to investigate atmospheric density is considered by Hwang et al. [132]. A number of different coupled analyses were considered encompassing the orbital dynamics, vehicle design, and operation of the satellite. The optimisation of the system was performed using a gradient-based method for the objective of highest average data-downloaded over the six analysed 12 hour time periods, spaced at intervals of 2 months. Optimisation was performed on three different problems with an increasing amount of design freedom enabled by increasing the scope of the design variables to include geometry and attitude in successive studies. The authors found that the overall objective function was improved when the optimisation method had greater authority over the design of the system.

The interdisciplinary and multiobjective conceptual design of CubeSat missions is considered by Lowe and Macdonald [133]. The authors use reduced-order models to quickly evaluate the different objectives of interest. Thus the exploration of a large number of different design candidates can be performed using the implemented GA method and the Pareto-efficient set identified. A variety of integrated models were developed including propagation and decay prediction, conceptual CubeSat design, ground-segment design, and mission cost analysis. Two example missions were analysed, the first an Earth observation optimised for minimum Ground Sample Distance (GSD) and revisit time in which only orbital altitude was varied, and the second a notional scientific mission for which downlinked-data was maximised and cost minimised for different orbital altitude, inclination, and ground station latitude. Lowe and Macdonald [133] conclude that the developed method is useful for rapidly exploring the tradespace and identifying designs which may not have been considered using a traditional point-design approach.

A consideration of the different disciplinary analyses, multidisciplinary optimisation techniques, and integration frameworks for the conceptual design of space transportation systems is presented by Rowell et al. [129]. The authors identify that the development of new analysis tools in the disciplines of sizing and weights, cost, reliability, maintainability, and operations is required in order to enable the integrated conceptual design of vehicles which represent a departure from existing developments or technologies. Previously, these analyses would have utilised empirical databases of information gathered from existing vehicles in order to provide a response by extrapolation. A review of different MDO techniques is also presented by Brown and Olds [134]. In the study performed, Bi-level Integrated System Synthesis (BLISS), CO and modified CO, are compared both qualitatively and quantitatively to each other and the traditional method of Fixed Point Iteration (FPI) of the individual disciplinary analyses. The design of a reusable launch vehicle was used as the example test problem. Whilst each MDO technique showed some improvement over the use of FPI, the authors were unable to categorically indicate the best architecture without further studies on different test problems. A comprehensive review of MDO architectures has recently been presented by Martins and Lambe [135], a number of which have been previously applied to complex aerospace engineering and in particular space system design problems.

The development of a generic design process for space systems is approached by Ross et al. [7] using the Multi-Attribute Tradespace Exploration (MATE) framework. The MATE process integrates the interests and requirements of various stakeholders by generating a combined objective or utility function from individual attribute objective functions. Full enumeration of the design-space is enabled by reduction of the number of design variables to only those which are strongly linked to the generated utility function. The complete evaluation of the design-space in this manner is proposed by Ross and Hastings [136] to benefit system designers in the early phases of the design process by allowing an understanding of the full design-space rather than optimising against a dynamic or ill-defined objective function. The framework is also able to respond to changes in stakeholder preference, requiring only modification of the individual and common utility functions by which each design vector is assessed. However, no comment is made regarding the effects of eliminating design variables to enable the full enumeration of the design-space. Furthermore, the time taken to perform the full enumeration of the design-space compared to an optimisation method is not explored.

Design of Other Aerospace Systems

A methodology for the integration of aircraft conceptual design and environmental performance was developed by Antoine and Kroo [137]. The method utilises a multiobjective GA optimisation scheme to explore the design-space for conceptual aircraft design for minimum operating cost, fuel consumption, nitrous oxides emissions, and aircraft noise. The results presented by Antoine and Kroo [137] demonstrate the tradeoffs present between the different, conflicting objectives. The authors however do conclude that a trend towards "slower, lower, greener" aircraft can be identified from the results if greater emphasis is placed on reduced noise, fuel consumption, and nitrous oxides emissions during design.

The combined optimisation of commercial aircraft configuration and departure trajectory to reduce environmental impact was studied by March et al. [138]. The developed method utilised two contributing analyses, a low-speed aerodynamics model and a departure trajectory simulation, and optimisation using a GA. Sequential quadratic programming, Nelder-Mead direct search, and particle swarm optimisation methods were also considered, but were either not able to find global minima or not suited to the mixed discrete-continuous nature of the problem. The results of the optimisation indicate that opportunities to reduce environmental impact and operational cost exist, particularly if the design of aircraft configuration and operation are considered together.

A hybrid optimisation method was applied by Drack and Zadeh [139] to two aerospace design problems. The two-stage method presented initially uses a SA algorithm to search the design-space for a good solution. The second optimisation method utilises a gradient-based method to obtain the optimum solution in the region of the accepted good solution. The SA optimiser was chosen due to its efficiency at searching high-dimensional and discontinuous design-spaces with many local minima. A two-stage approach was therefore chosen to enable the efficient identification of the true optimum whilst avoiding convergence on a non-global minima. The method presented by Drack and Zadeh [139] was applied to the design of quiet and efficient propellers and the design of a manoeuvre controller for a satellite.

Summary of the Literature Review

The review of existing literature related to the design of space systems and other relevant studies demonstrates the benefits which design-space exploration methods can have, primarily through the generation of increased knowledge of the tradespace and identification of system

designs which may have not been found by traditional design methods. Furthermore, the use of optimisation methods, in particular the use of GAs, have been demonstrated for a range of different space system design problems and have generally been shown to be more efficient than full-factorial analyses for complex design-spaces.

The application of an optimisation based approach in the proposed methodology for the design of satellite constellation deployment is therefore supported by these studies, enabling the exploration of the design-space and identification of new effective solutions or previously unconsidered design architectures.

4.3 Design-Space Exploration of Constellation Deployment

The first step in the application of design-space exploration to the problem of interest is the selection of an appropriate method or technique. A key aspect of this selection is the trade between the computational efficiency and effectiveness. For a single-objective problem, the effectiveness of a design-space exploration or optimisation method is a measure of the ability of the method to find the best or optimal solution. However, when solutions to multiobjective problems are considered, effectiveness may refer to the total number of Pareto-efficient solutions found, the amount of the total Pareto-efficient set identified, the spread of the Pareto-efficient solutions, or a combination of these properties. These measures of efficiency are termed cardinality, coverage, and uniformity or spacing by Sayn [140] and Faulkenberg and Wiecek [141] respectively. The efficiency of a design-space exploration method on the other hand, balances these measures of effectiveness with the number of function calls or total computational load required to achieve a given result. Limiting the number of function calls required to perform the exploration of a design-space can be advantageous, especially when complex and time-consuming analysis modules are involved.

In order to perform the exploration of a design-space, selection of a single or set of objective functions is required. In the case of small satellite constellation deployment the ultimate objective or value function of the deployment strategy is highly mission specific, requiring knowledge of the relative priorities of system aspects such as the deployment period, propulsive capability, total system mass, system complexity, launch vehicle and payload compatibility, and cost. Due

to the tradeoffs which exist in this design-space a single objective is incapable of characterising the design-space without significant a priori information, thus requiring a multiobjective analysis. Consequently, the design-space exploration method must support the consideration of multiple objective functions, some of which may be in direct conflict with each other.

Parametrisation of the Design-Space

Finally, the identification and selection of the set of input design variables which comprise the design-space is required. The selection of these design variables can be obtained by parametrisation with the aim to characterise the deployment strategy and corresponding vehicle design using as few variables as possible.

For the deployment of small satellite constellations in LEO using the method of indirect orbital plane transfers, the strategy of deployment is primarily controlled by the insertion orbit properties of the satellites. The differences in semi-major axis, inclination, and eccentricity of the insertion orbit compared to the required mission orbit control the time-required to achieve the required deployment and the propulsive requirements of the spacecraft comprising the constellation.

With respect to the vehicle-design for the constellation, both individual satellite and carrier-vehicle/sub-satellite architectures should be considered. The capability of these vehicles to execute the planned deployment strategy is dependent on the characteristics of the specified propulsion system, namely the thrust and specific impulse of the systems. In addition to the system type and propellant type, these propulsion system characteristics also drive the mass of propellant required and the dry-mass of the spacecraft. If carrier-vehicles are used, the use of sub-satellite deployment mechanisms with different energies can affect the propulsive requirements of the individual satellites.

The feasibility of the deployment of the constellation is also dependent on the atmospheric drag experienced by the spacecraft whilst in orbit. The drag caused by interaction between the spacecraft body and the atmospheric particles causes degradation of the spacecraft's orbit, requiring additional propellant to counteract the effects of drag, or ultimately cause the spacecraft to re-enter. The ballistic coefficient of the spacecraft can also have a significant affect on the amount of drag experienced in orbit and should therefore be considered in the exploration of the design-space.

Table 4.1: Summary of design variables for small satellite constellation deployment analysis.

	Variable	Type	Feasible Range
Insertion Orbit	Semi-major Axis [km]	Continuous	$R_E < a$
	Eccentricity	Continuous	$0 < e < 1$
	Inclination [°]	Continuous	$0 < i < 180$
Satellite Design	Coefficient of Drag	Continuous	2 to 4 (viable [142])
	Propulsion System Type	Categorical	-
	Propellant	Categorical	-
	Thrust Scalar	Continuous	0 to 1
Carrier Vehicle	Carrier Vehicle Use	Binary	0 or 1
	Coefficient of Drag	Continuous	2 to 4 (viable [142])
	Propulsion System Type	Categorical	-
	Propellant	Categorical	-
	Thrust Scalar	Continuous	0 to 1
	Separation Velocity [$\mathrm{m\,s^{-1}}$]	Continuous	0 to 2

The resulting set of input design variables comprising the design-space is summarised in Table 4.1. Variables described as categorical have a finite number of different options which may exist in the design-space and can be selected from, for example different propulsion system types. These variables can be treated as discrete variables, but cannot be considered to be ordered or have any intermediate values.

4.3.1 Application of Genetic Algorithm Optimisation

In this study, the GA method Non-dominated Sorting Genetic Algorithm II (NGSA-II) of Deb et al. [102] was chosen to perform the design-space exploration for small satellite constellation deployment. A GA method was chosen primarily for the ability of the method to effectively explore a design-space for a set of solutions which demonstrate the tradeoffs between the different objectives of interest without utilisation of any a priori information or scalarisation formulae. Whilst the stochastic nature of GAs means that there is no certainty that any solutions found are truly optimal in the global design-space, the aim of this design-space exploration is to increase the knowledge available to the system designer in the conceptual design process through characterisation of these tradeoffs and the effects of employing different deployment strategies. Furthermore, GA methods are particularly suitable for problems which consist of both discrete and continuous design variables and do not require the computation of objective-function derivatives, which may not be directly available from the analysis method.

NGSA-II is a popular GA optimisation method, often considered due to its ability to generate a better spread of solutions than other popular GA methods such as SPEA-2 and PAES [102]. This is primarily due to the use of a crowding-comparison measure which preserves diversity. The use of real-value design variable encoding rather than use of binary-strings can also be advantageous when considering variables of continuous nature. The MATLAB implementation of NGSA-II, *gamultiobj* was used to simplify the integration of the optimisation method with the analysis method developed. Parallel processing of the individual population members within each generation of the algorithm is also supported in MATLAB, a characteristic which can significantly reduce the total time required to perform the exploration of the design-space.

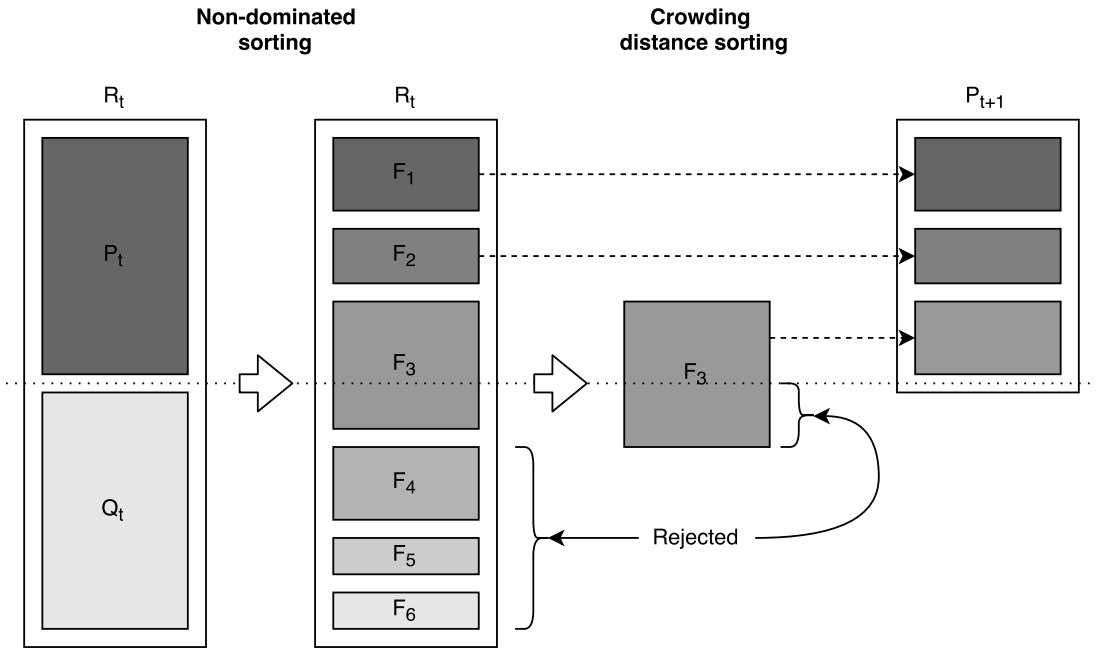

Figure 4.2: Sorting procedure of NGSA-II. P_t, the parent population, and Q_t, the offspring population, are combined to produce population R_t, which is sorted first by non-domination and then by crowding-distance to produce the new parent population for crossover and mutation, P_{t+1}. Adapted from Deb et al. [102].

NGSA-II is an elitist GA method for multiobjective problems which utilises a fast nondominated sorting approach and crowding-distance estimation and comparison to preserve the diversity of the population [102]. In this method, elitism is implemented by combining the current parent and offspring populations before selection of the individuals comprising the subsequent population is performed. By sorting using non-domination rank, the best individuals in this combined population can be retained for the next generation. To emphasise the preservation of diversity in the population, a crowding-distance operator is used to sort the individuals within

each non-domination rank. The crowding-distance measure for an individual is calculated by considering the average side-length of the hyperrectangle, an n-dimensional rectangle, defined using the nearest-neighbours of the individual as vertices. The selection of the subsequent parent population is performed by first selecting in rank order the nondominated sets until a set cannot be wholly accommodated due to the chosen population size. The remaining space in the population is then selected from the last nondominated set using ranking based on the calculated crowding-distance of each individual. These features of NGSA-II are demonstrated in the sorting procedure shown in Figure 4.2.

Representing a Solution

The design variables or chromosome for application using the *gamultiobj* function are represented using a vector with real-value encoding. The summary of design variables comprising the complete chromosome for the problem of deployment of small satellite constellations is presented in Table 4.1. The use of real-value encoding ensures support for continuous input variables. Binary encoding requires some element of discretisation, which can become significant if small changes in the decision space can result in significant changes in the objective space [122].

For compatibility with the MATLAB implementation of the multiobjective NGSA-II algorithm, each design variable is represented by a real number generated within the allowed bounds. The binary variable indicating carrier-vehicle use for multiple-satellite-per-plane constellations is handled by performing a rounding operation on the real-number bound between 0 to 1. The categorical variable indicating the propellant type is dependent on the propulsion system type. These two system-parameters can therefore be combined into a single real-value input-variable for use with the genetic algorithm. The integer component of the real-value number is used to determine the propulsion system type and the decimal component used to select the propulsion system type from the available number of options for the selected propulsion system type. Mapping of the propulsion system type and propellant type variable to the range 0 to 1 can also support a varying number of options for each of the categorical variables. This supports flexibility in the propulsion system model and allows for integration of new propulsion system types and propellant combinations. In addition, this variable mapping ensures that the probability of each propulsion system type and corresponding options of propellant type have an equal probability of selection.

The input design vector can be described by the eleven variables shown in Eqn. (4.2), derived from the design variables identified in Table 4.1. However, if the constellation configuration only calls for a single satellite in each orbital plane, or a design does not utilise carrier vehicles to aid the deployment, the design vector required is limited to only the first six variables.

$$x_{input} = \left\{ \begin{array}{c} x_1 \\ x_2 \\ x_3 \\ x_4 \\ x_5 \\ x_6 \\ \left\{ \begin{array}{c} x_7 \\ x_8 \\ x_9 \\ x_{10} \\ x_{11} \end{array} \right\} \end{array} \right\} = \left\{ \begin{array}{cc} \text{Semi-major Axis} & [\text{km}] \\ \text{Eccentricity} & [-] \\ \text{Inclination} & [^\circ] \\ \text{Coefficient of Drag} & [-] \\ \text{Propulsion System} & [-] \\ \text{Thrust Scalar} & [-] \\ \left\{ \begin{array}{c} \text{Carrier Vehicle Use} \\ \text{CV Coefficient of Drag} \\ \text{CV Propulsion System} \\ \text{CV Thrust Scalar} \\ \text{Separation Velocity} \end{array} \right\} & \begin{array}{c} [-] \\ [-] \\ [-] \\ [-] \\ [\text{m}\,\text{s}^{-1}] \end{array} \end{array} \right\} \tag{4.2}$$

Initial Population Generation

The population used to initiate a GA is generated by the creation of a number of individuals with design characteristics, genes, selected from within the set bounds. Commonly, these initial candidate designs are produced using Pseudo-Random Number Generators (PRNGs) and the bounds provided for each design variable [143]. However, a number of alternative methods of population initiation have been utilised to promote uniformity in coverage of the search space or accelerate convergence and improve the final solution. For example, the use of Quasi-Random Number Generators (QRNGs) was investigated by Maaranen et al. [144] to generate more a uniform sampling distribution than achieved through the use of PRNGs. Stratified-sampling and Latin Hypercube Sampling (LHS) methods have also been used to improve upon the simple random selection of design points by ensuring that selection is performed across the whole search space [145, 146]. In these methods the range of each design variable is discretised into intervals and random selection subsequently performed within these intervals. A relatively uniform distribution over each variable can be thus be ensured due to the partitioning of the search space.

Example populations of 100 individuals with 3 variables generated using these different methods of initialisation are shown in Figure 4.3, demonstrating the differences between the PRNG, QRNG, and LHS population initialisation methods. By qualitative observation, the QRNG method can be seen to demonstrate the most uniform coverage of the space, a result of the use of low-discrepancy sequencing. A pattern can also be observed in the output population of the QRNG method, indicating the true non-random nature of this method. In comparison, the PRNG and LHS result in less uniform distributions, but do not appear to have any identifiable pattern. The PRNG method demonstrates more clumping of points, resulting in reduced uniformity of coverage and more areas of unexplored space compared to the LHS and QRNG methods.

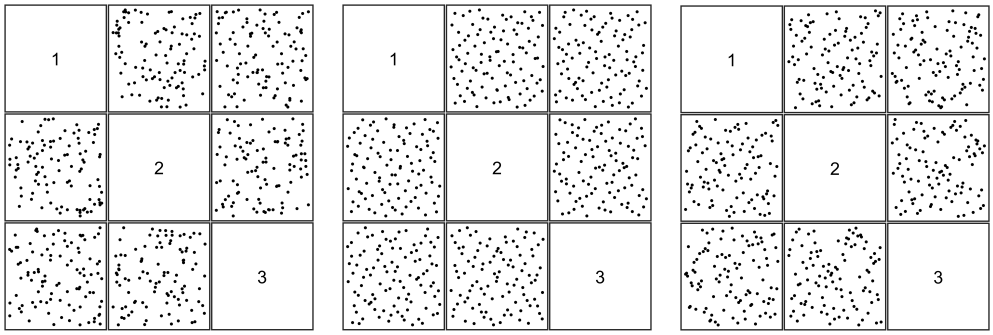

(a) Pseudo-random number generation. **(b)** Quasi-random number generation. **(c)** Latin-hypercube sampling.

Figure 4.3: Comparison of different methods of population initialisation. A sample population of 100 individuals with 3 variables is used.

Application specific population initialisation can also be performed when information about the design-space is known a priori. This can include excluding areas of the design-space which are known to be inefficient, thus avoiding unnecessary computation expense and increasing convergence speed [143]. Seeding of the initial population with genetic information from known good designs or using heuristic methods has also been shown to improve GA performance [147], but at the risk of reducing the exploratory capability of the algorithm [148].

To ensure that enough feasible solutions are present in the initial population to maintain diversity during the subsequent crossover and mutation processes a screening procedure can be used. In this process, reduced order analysis models are used to iteratively assess the feasibility of the randomly generated individuals and replace infeasible solutions with newly generated individuals. The initial assessment of feasibility for a given deployment strategy is performed

by considering the time required by the satellites to perform the necessary drift manoeuvres and the projected lifetime of the satellites in their initial orbit. If the lifetime of the satellite in its initial orbit is shorter than the required drift time, the deployment strategy is infeasible. The sizing of the spacecraft with the specific propulsion system types can also also be considered to ensure that the vehicle design required to perform the necessary orbital transfers is also feasible.

The size of the initial population can also have a significant effect on the progression of the algorithm and the performance of the design-space exploration. For multiobjective problems, the number of nondominated solutions in a given population increases with the number of objectives [95]. Thus, to fully characterise a high-dimensional Pareto-set a large population may be required. However, if the population size is too large, the computational expense can be high and the progress of the algorithm can be slow. To provide the algorithm with sufficient initial diversity, the population size chosen is typically related to the complexity of the problem, ie the number of design variables [94]. A common rule of thumb is to consider a population of 15 to 20 times the number of design variables [149].

Selection

Selection in a GA is used to pick individuals from the current population for use during the mating or crossover process. The method of selection utilised can control the selection pressure, the probability that only the best individuals are selected for crossover, and consequently affect the genetic diversity of the following population.

The tournament selection procedure is used in NGSA-II. Tournament selection involves the random selection of a number of individuals from the population, determined by the tournament size, from which the best individual is selected and entered into the crossover and mutation pool. Competition between individuals is first determined by non-domination rank, and then by crowding-comparison, thus promoting diversity. By conducting a number of separate tournaments, the pool for crossover and mutation can be filled.

Mutation

The primary task of the mutation operator is to maintain or generate diversity in the working population used by the GA and allow the method to avoid or escape from locally optimal points. Use of the chosen mutation operator is typically controlled using a mutation rate or probability parameter. If the rate of mutation is set too high, too much random variation will be introduced to the population and the algorithm will approximate that of a random search

method. Conversely, if the mutation rate is set very low, the algorithm may be susceptible to becoming trapped in local minima.

A number of different mutation operators are implemented in the MATLAB *gamultiobj* function. The most common mutation operator functions by randomly selecting a fraction of the available variables in the chromosome, determined by the mutation rate. The value of each selected variable is then replaced with a new value randomly determined from the allowable range. Alternatively, a Gaussian-based mutation operator can be used, which varies the probability and range from which the new mutated value is selected from. Furthermore, the standard-deviation used in Gaussian distribution can be set to grow or shrink with increasing generations to alter the behaviour of the mutation operator as the algorithm progresses.

Crossover

In EA methods, genetic or evolutionary operators are used to create new individuals in the population through modification of the existing population members. The crossover and mutation operators are responsible for performing the search within the design-space for better solutions [94].

Crossover operations are typically performed using pairs of individuals from the mating pool to produce offspring by exchanging information between the parents. The NGSA-II method nominally specifies the use of single-point crossover. Single-point crossover for real-number encoded chromosomes first involves the random selection of a single crossover point between 1 and the number of elements in the chromosome. The genetic information beyond this selected point is then swapped between the two chosen parents, generating two offspring as demonstrated by Eqn. (4.3).

$$
\begin{aligned}
Parent_1 &= \left[\begin{array}{cccc:cccc} a & b & c & d & e & f & g & h \end{array}\right] \\
Parent_2 &= \left[\begin{array}{cccc:cccc} 1 & 2 & 3 & 4 & 5 & 6 & 7 & 8 \end{array}\right] \\
&\qquad\qquad\qquad\qquad \uparrow \text{crossover point} \\
Child_1 &= \left[\begin{array}{cccc:cccc} a & b & c & 4 & 5 & 6 & 7 & 8 \end{array}\right] \\
Child_2 &= \left[\begin{array}{cccc:cccc} 1 & 2 & 3 & d & e & f & g & h \end{array}\right]
\end{aligned}
\tag{4.3}
$$

However, the use of only a single point for breaking of the chromosomes can introduce a positional bias, in that variables which are further apart in the chromosomal vector are more likely to be disrupted by crossover than variables which are close or adjacent to each other [150].

In the *gamultiobj* implementation of NGSA-II a number of alternative crossover methods are available including two-point and scattered crossover methods. Two-point crossover is implemented in much the same manner as the single-point method, but two breaking points are randomly selected. The genetic information between these two points is then swapped between the parents to produce the offspring. In the scattered crossover method a random binary vector is created with the same length as the chromosomal vector. The binary vector is then used to determine which variables are swapped between the two parents to generate the offspring. This method is also known as uniform crossover.

Finally, to produce the correct number of offspring individuals to complete the new population, the ratio of offspring created by crossover to mutation is required. This value is often known as the crossover fraction. If this value is set too high, mutation will be severely restricted and new genetic information cannot be introduced to the population. The algorithm may therefore converge prematurely in the vicinity of a local rather than globally optimal point. On the other hand, if crossover operations are not performed, the algorithm may be unable to converge at all, as the genetic information of the best-performing individuals cannot be combined [99]. A balance between crossover and mutation is therefore required in order to control the exploration of the design-space. Selection of the ratio of crossover to mutation is typically problem-specific and dependent on the diversity present in the population, and cannot therefore be determined a priori [151]. However, values in the range of 0.7 to 0.8 are generally accepted as good initial parameters [152].

Chapter 5

Analysis Framework Development

In order to demonstrate the proposed methodology for design-space exploration of satellite constellation deployment, a method to assess the feasibility and performance characteristics of a given design vector is required. The planned implementation of the methodology, shown previously in Figure 3.3 utilises a simplified analysis framework, focusing on the direct effects of the constellation deployment strategy whilst remaining agnostic to the mission type. The objectives of interest have therefore been reduced to the following system-level characteristics.

Time to achieve deployment

The time taken to obtain the desired constellation configuration from the initial insertion orbits of the satellites is of interest to the system designer as this may affect the execution of the mission to be performed or may drive the required lifetime of the satellite subsystems or individual components. However, reduction of the time to perform the deployment of a small satellite constellation may require additional propulsive capability affecting the requirements of the satellite design. The selection of different initial orbit parameters can also affect the range of suitable launch vehicles and may have an impact on the viability of the mission.

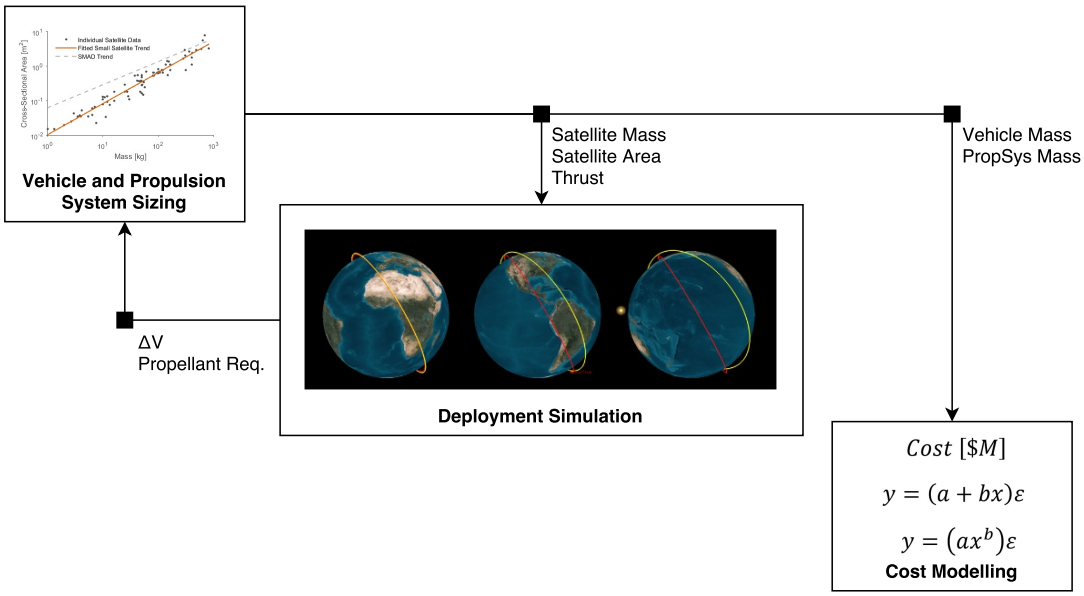

Figure 5.1: Flow of information between the different contributing modules in the implemented analysis framework for the deployment of small satellite constellations.

Total system mass

The total mass of the system is a key factor in determining the launch systems or opportunities which can be used deliver the satellites to their initial orbits. The total mass of the system is tightly coupled to the propulsive capability of the vehicles required to perform the necessary manoeuvres and the propulsion system type and propellant specified. However, minimisation of the mass of the system is typically in opposition to minimisation of the time required to perform the deployment due to their dependency on propulsion system capability and performance.

System cost

As a key value proposition of small satellites compared to larger traditional satellites, the cost of the satellite constellation is an important indicator of system performance. Whilst the true cost of the mission cannot be determined without performing detailed design studies, estimated costs can be used to investigate the relative effects of different design choices on system cost to be explored.

To evaluate these output characteristics the analysis framework presented in Figure 5.1 is proposed. A method of simulation using an orbit propagation technique is used to analyse the feasibility of the deployment strategy and the required propulsive capability. A vehicle design module including propulsion system sizing processes is also required to generate input

information required by the deployment simulation method. Finally, a cost model based on Cost Estimating Relationships (CERs) is used to determine the system cost of the constellation. These three analysis modules are presented in the following sections.

5.1 Constellation Deployment Analysis

To evaluate the feasibility and performance of constellation deployment, an analysis method which simulates the motion of the vehicles which comprise the constellation can be performed. The required input parameters for such an analysis are described as follows:

Epoch

The date and time defined at the start of the analysis period. The primary effect of changing the epoch is different space weather conditions resulting in different orbital decay profiles.

Constellation Mission Configuration

The configuration of the constellation consists of the number of satellites which comprise the constellation, the configuration of these satellites in the constellation, and the orbital parameters which describe each plane of the constellation. These parameters effectively define the desired end-state of the constellation which the algorithm will attempt to achieve using the deployment strategy.

Initial Orbit Properties

The initial orbit properties of the satellites define the starting conditions for the constellation deployment strategy. In many cases, the initial orbit properties may be the insertion orbit of the satellites following their launch.

Spacecraft Configuration

The configuration of the spacecraft to be deployed can have a significant effect on the feasibility and performance of the deployment strategy. The significant parameters in this group include the propulsion system characteristics of the vehicles, primarily thrust and specific impulse, and the physical characteristics of the spacecraft, principally the initial mass, cross-sectional area, and coefficient of drag required to calculate the ballistic coefficient.

Deployment Strategy Parameters

A number of additional parameters are required in order to fully define and direct the implementation of the constellation deployment strategy. For constellation configurations which specify multiple satellites in each orbital plane, the algorithm must be instructed whether to use carrier vehicles or perform the deployment using satellites with individual propulsion systems. A deadline for the deployment of the constellation is also implemented to limit the length of analyses which would provide solutions with very long deployment times. The basis for this deadline may be mission specific, required in order that the constellation is complete before a specified date, or related to the expected lifetime of the satellite components.

Due to the effects of atmospheric drag in LEO and the potentially lengthy drift periods associated with deployment by the method of indirect plane separation a purely analytical method is not viable. Thus, a numerical process based on a method of orbit propagation and supported by additional functions to calculate and simulate the necessary orbital transfer manoeuvres to perform the deployment is proposed. The operation of this constellation deployment algorithm is described in Figure 5.2.

The deployment algorithm operates by first considering any inclination plane changes which need to be made by the individual satellites or carrier spacecraft. The first vehicle is then transferred to the mission orbit by in-plane transfer and the time required for each subsequent vehicle to separate by differential nodal drift is calculated analytically using Eqns.(2.3) and (2.4). Given these calculated drift-times, the complete system is propagated to the next transfer opportunity time. However, due to the absence of drag-terms in the analytical calculation for differential drift, the developed plane-separation may differ from that calculated. Furthermore, the use of low-thrust and non-impulsive manoeuvres can result in significant orbit transfer times and may contribute to increased drift-times and therefore greater separation angles. A backwards search is therefore performed from the calculated transfer opportunity to determine if a true transfer opportunity resulting in the correct final plane-separation exists. In this manner, both the actual orbital conditions including drag effects and the specified propulsion system and spacecraft configuration can be considered during the drift and in-plane manoeuvre. If the search finds a valid solution, the orbit transfer and in-plane separation of satellites, if required, is executed by simulation and the algorithm moves on to the next vehicle transfer opportunity. If no solution

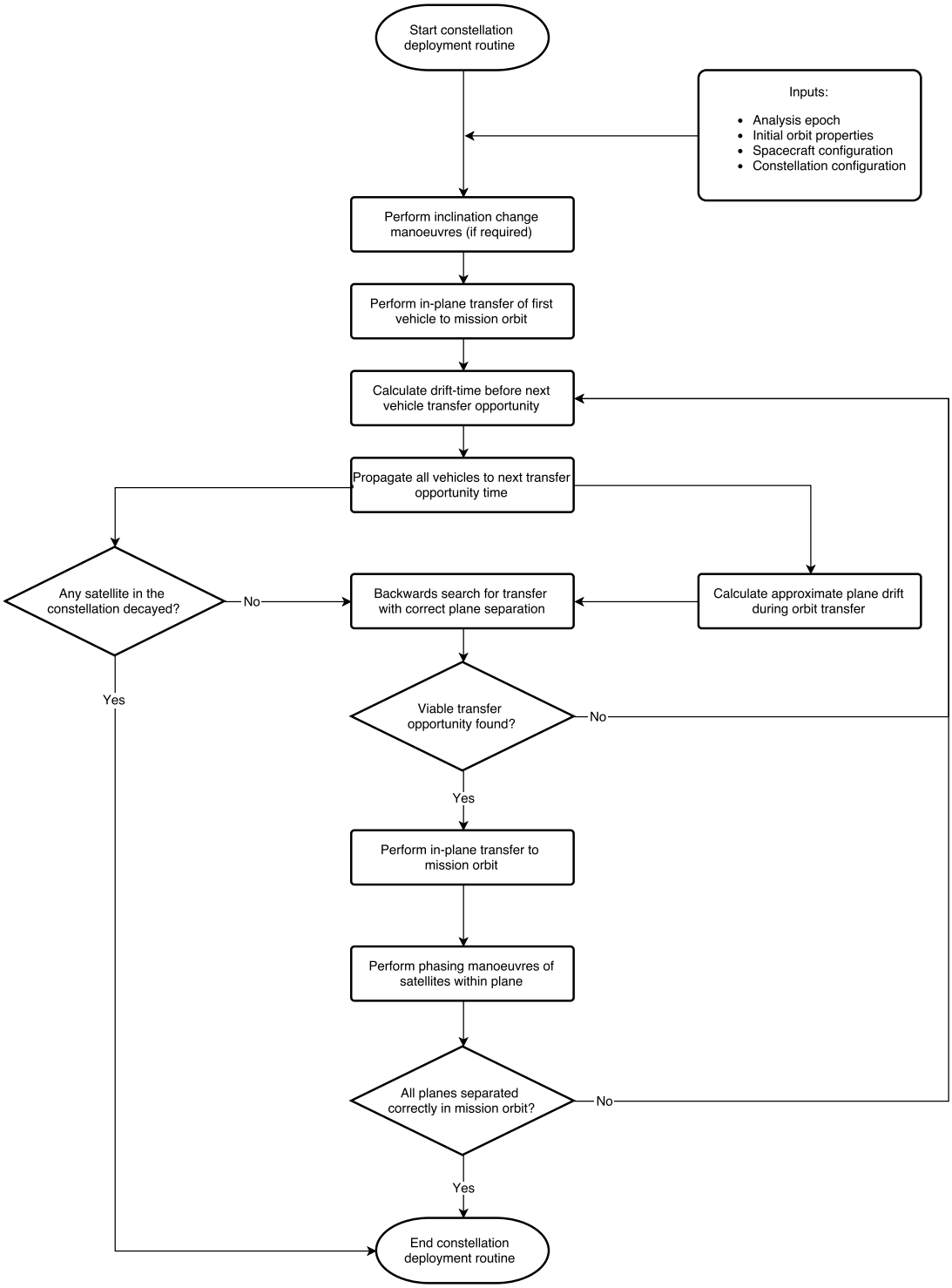

Figure 5.2: Constellation deployment algorithm flow diagram.

is found, the transfer time is re-estimated analytically and the system is propagated forward again. This process is then repeated until the desired constellation configuration is achieved.

In order to generate the logic for the deployment method described, a number of assumptions and limitations are introduced. First, any necessary inclination manoeuvres are performed prior to the deployment of the constellation. This prevents the rate of nodal precession being adversely affected by any difference in inclination between the satellites as they separate, see Eqn. (2.4), and also ensures that the satellites are presented with similar atmospheric drag environments, and thus have orbits which evolve and decay in a similar manner. Furthermore, it is assumed that the inclination change is performed by either the carrier vehicles or individual satellites rather than a launch vehicle upper-stage or additional propulsive system. Second, the deployment process does not consider strategies in which satellites perform opposite in-plane manoeuvres to increase the rate of planar separation. These limitations to the method reduce the complexity of the analysis by eliminating additional design variables which would be required to describe the strategy. However, correspondingly the extent of the true design space which can be explored using the analysis is also reduced.

The contributing components to this simulation method are presented in the following sections. The overall behaviour of the developed analysis method is subsequently verified by comparison to the actual deployment of the FORMOSAT-3/COSMIC mission.

5.1.1 Orbit Propagation Method

In the study of satellite motion, the consideration of perturbing accelerations or forces requires a departure from the classic two-body analysis. The solution to this perturbed motion can be determined through the use of two contrasting techniques. Methods which use numerical integration of the perturbed equations of motion of the satellite are known as special perturbation techniques, whilst analytical methods which use approximate expressions for the perturbed motion of the satellite are referred to as general perturbation techniques. The choice between these methods is typically determined by the application or problem to be investigated. Special perturbation techniques can provide high levels of accuracy, but may require lengthy computational time, whilst general perturbation techniques can be computed quickly, but are less accurate by virtue of their use of approximate expressions for the perturbations examined.

To support the modelling of satellite constellation deployment strategies, an appropriate set of perturbations must be considered. Perturbations due to a non-spherical geopotential are

important due to the use of nodal precession to separate orbital planes of different size or shape. The effect of atmospheric drag is also significant due to the typical operation space of projected small satellite constellation missions in LEO and the time period over which deployment and operation will be analysed. In LEO, perturbations due to higher order geopotential effects, third-body gravity, solar-radiation pressure, solid and ocean tides, and Earth albedo are of much lower magnitude than the primary geopotential perturbations and atmospheric drag and therefore have a significantly smaller effect on the motion of Earth orbiting bodies [153].

For the study of satellite constellations where the period of analysis may be lengthy and the number of satellites is potentially high, a purely numerical propagation method would be computationally impractical. Conversely, in order to accurately investigate the effects of drag on satellites in low Earth orbits over these time periods, models which capture the significant variability of the atmospheric density are required. Analytical models for atmospheric density are currently incomplete and not capable of capturing these complex and time-varying effects [153]. The accuracy of numerical integration of the disturbing accelerations and the speed of analytical propagation methods can be combined through the use of a semi-analytical approach. In these methods the long-period and secular effects are evaluated numerically with a large step size, whilst the short period motion (2π periodic in true or mean anomaly) is treated analytically. For the analysis of satellite constellation deployment, accuracy of the short-period motion is less critical than the long-period and secular motion of the satellites which controls the rate at which the vehicles will separate due to differences in semi-major axis, eccentricity, and inclination.

Semi-Analytical Liu Theory

The semi-analytical technique developed by Liu and Alford [154], Semi-Analytical Liu Theory (SALT), was chosen for use as the propagation method for implementation and is described in the following paragraphs. A number of alternative semi-analytical propagation methods were also considered for use including the Draper Semianalytic Satellite Theory (DSST) of Cefola [155] and the Hoots Analytic Dynamic Ephemeris Theory (HANDE) of Hoots and France [156]. Whilst each of these techniques is capable of supporting the proposed analysis method, providing the capability to propagate Earth orbits with non-spherical geopotential and integration of a time-varying atmospheric density model with similar accuracy, SALT and HANDE are particularly suitable for the propagation of satellites in low-altitude orbits [153]. Ultimately, SALT

was chosen primarily for the simplicity of its implementation in MATLAB, the programming framework of choice.

SALT utilises a combination of special and general perturbation techniques to capture the effects of atmospheric drag and the gravitational field of an oblate Earth. A major assumption of the theory is that the perturbations due to solar and lunar gravitational effects, solar radiation pressure, and high order geopotential functions are dominated by the uncertainty present in the estimation of atmospheric density and ballistic coefficient (primarily the uncertainty in drag coefficient) and can therefore be neglected [154].

In SALT, the effects of short-periodic motion of the satellite are removed by propagation of a mean orbital element set. The method of averaging is used to transform the set equations of motion for the osculating state into a system which is propagated using only the mean element set [157]. If required, the initial osculating orbital elements are transformed to a mean orbital element set. The averaged system of equations is then solved using the time-rate of change of the mean elements. The effects of drag are evaluated numerically using a Gauss-Legendre Quadrature, whilst the effects of Earth oblateness are calculated analytically [154].

Equations of Motion

The equations of motion in terms of the osculating orbital elements for a satellite in Earth orbit are given by Eqn. (5.1), in which the subscripts G and D refer to the perturbations by non-spherical geopotential and atmospheric drag respectively.

$$\dot{x}_j = \dot{x}_{j_G} + \dot{x}_{j_D} \tag{5.1}$$

$$\text{where } \{x_j\} = \{a, e, i, \omega, \Omega, M\}$$

In order to remove the short-periodic motion in each orbital element $x_{j,sp}$, the transformation from osculating orbital elements to the averaged or mean orbital elements $x_{j,m}$ is introduced, demonstrated by Eqn. (5.2). The first-order transformation is obtained under the assumption that the drag-effects are second order and can therefore be neglected.

$$x_j = x_{j,m} + x_{j,sp}\left(a_m, e_m, i_m, \omega_m, \Omega_m, M_m\right) \tag{5.2}$$

In order to recover the averaged orbital elements from the above set of equations an iterative procedure is employed in which the values for the osculating elements are used as the starting conditions. The expressions for the short-period variation in each orbital element are given in Eqns. (B.2a) and (B.2f). In each case, the variation is a function of only the averaged orbital elements. Following the transformation, the dynamic system can be expressed as in Eqn. (5.3), where $\langle x_j \rangle$ indicates the averaged value of x_j over the range of the mean anomaly (0 to 2π):

$$\dot{x}_{j,m} = \langle \dot{x_j} \rangle_G + \langle \dot{x_j} \rangle_D \tag{5.3}$$

Given that the effects of Earth oblateness do not have a secular effect on the semi-major axis of the orbit, and that the primary perturbations due to atmospheric drag act on the semi-major axis and eccentricity, the following assumptions can be made.

$$\langle \dot{a} \rangle_G = 0 \tag{5.4a}$$

$$\langle \dot{i} \rangle_D = \langle \dot{\omega} \rangle_D = \langle \dot{\Omega} \rangle_D = \langle \dot{M} \rangle_D = 0 \tag{5.4b}$$

As a result, the transformed equations of motions can be simplified and expressed as shown by Eqn. (5.5).

$$\begin{aligned}
\dot{a}_m &= \langle \dot{a} \rangle_D \\
\dot{e}_m &= \langle \dot{e} \rangle_G + \langle \dot{e} \rangle_D \\
\dot{i}_m &= \langle \dot{i} \rangle_G \\
\dot{\omega}_m &= \langle \dot{\omega} \rangle_G \\
\dot{\Omega}_m &= \langle \dot{\Omega} \rangle_G \\
\dot{M}_m &= \langle \dot{M} \rangle_G
\end{aligned} \tag{5.5}$$

In the following paragraphs, the expressions required to solve these equations of motion are described for the orbital perturbations due to non-spherical geopotential and atmospheric drag in the LEO environment.

Perturbations due to the Non-Spherical Geopotential

Whilst often assumed to be spherical for simplicity, the Earth is in fact an aspherical body characterised by a bulge at the equator and flattening at the poles, often termed an oblate spheroid. This aspherical nature and non-uniform mass distribution of the Earth results in a non-uniform gravitational potential which causes perturbing accelerations in the orbit of satellites in Earth orbit. The force due to the geopotential is conservative in nature meaning that the the total energy in the system remains constant. A potential function can therefore be used to characterise the accelerations due to the central-body force in Earth orbit [153].

The geopotential function of the Earth can be expressed using a set of spherical harmonics, which are described by empirically determined models. The accuracy of these models is set by the number of coefficients, known as degree and order, which are defined. The spherical harmonics are divided into zonal (order = 0), sectoral (degree = 0) and tesseral harmonics (order = m and degree = l) which describe the spatial variation in the geopotential function.

The even zonal harmonics are responsible for the secular perturbations from geopotential effects, whilst all the spherical harmonics contribute to periodic variations in all Keplerian orbital elements [29]. The zonal harmonic coefficient of degree 2 and order 0, known as J_2, or Earth dynamic oblateness, is principally responsible for the secular perturbations in RAAN and AoP of a satellite in Earth orbit. In comparison, the higher order zonal coefficients and sectoral and tesseral harmonics are orders of magnitude smaller and therefore have a much smaller effect on the variation in the orbit of the satellite.

Analytical expressions for the averaged variation of the mean Keplerian elements due to the zonal Earth harmonics, J_2, J_3, and J_4, are presented in Appendix B, Eqns. (B.1a) and (B.1f) [154].

Perturbations due to Atmospheric Drag

In low Earth orbits, the interaction between the surfaces of a satellite and atmospheric molecules and atoms produces a force, namely drag, which acts in the direction opposite and tangential to that of the velocity vector of the satellite. The net effect of this retarding force is non-conservative, reducing the energy of the orbit, resulting in a reduction of the semi-major axis of the orbit. As the semi-major axis of a low Earth orbit is reduced, the atmospheric density will generally increase and the satellite will experience significant orbital decay and eventually experience re-entry. The acceleration due to atmospheric drag on a satellite can be expressed

as a function of the physical characteristics of the satellite, atmospheric density ρ, and velocity relative to the co-rotating atmosphere $\vec{\mathrm{v}}$, as in Eqn. (5.6) [153].

$$\vec{a}_{\mathrm{drag}} = -\frac{1}{2}\rho\frac{C_D A}{m}\mathrm{v}_{\mathrm{rel}}^2\frac{\vec{\mathrm{v}}_{\mathrm{rel}}}{|\vec{\mathrm{v}}_{\mathrm{rel}}|} \tag{5.6}$$

For eccentric orbits, the force due to atmospheric drag is typically greatest where the atmospheric density is highest, usually at the lowest altitude in the orbit, the perigee. As a result, the altitude of the apogee decreases more rapidly than the altitude of the perigee. The eccentricity of the orbit therefore also tends to zero as the semi-major axis decreases [158].

The co-rotation of the atmosphere with the surface of the Earth can have a secular effect on the inclination of a non-equatorial satellite orbit due to the presence of an out-of-plane force [159]. However, as discussed by King-Hele [160], the maximum magnitude of this variation over the lifetime of a satellite is small, approximately 0.5° for an initial perigee height of 300 km. In addition, small variations in the inclination of the satellite orbit can also be produced by the angle formed between the orbital plane and upper atmospheric winds, however, over long time periods the effect of meridional wind components on inclination cancel out [161]. Similarly, when the orbital perigee is located away from the equator, the effect of zonal wind components approximate to zero. However, as the perigee approaches the equator, the effect of zonal winds can accumulate, resulting in a secular decrease in inclination. The consideration of atmospheric wind effects is difficult and complex as they are typically either unknown or unpredictable, and as a result is poorly modelled [153, 162]. Furthermore, the magnitude of these perturbations due to atmospheric winds are small, Δi of the range 0.01° to 0.05° per year [163]. Due to the small magnitude of these perturbations due to atmospheric co-rotation and winds, these effects are neglected in this analysis.

The perturbations due to atmospheric drag on the semi-major axis and eccentricity are given in Eqns. (5.7a) and (5.7b) respectively [154], where the expression for V gives the magnitude of velocity of the satellite relative to the co-rotating atmosphere.

$$\dot{a}_D = -B\rho V\frac{a}{1-e^2}\left\{1 + e^2 + 2e\cos f - \omega_a\cos i\sqrt{\frac{a^3\left(1-e^2\right)^3}{\mu_E}}\right\} \tag{5.7a}$$

$$\dot{e}_D = -B\rho V\left\{e + \cos f - \frac{r^2\omega_a\cos i}{2\sqrt{\mu_E a\left(1-e^2\right)}}\left[2\left(e+\cos f\right) - e\sin^2 f\right]\right\} \tag{5.7b}$$

$$V = \left[\frac{\mu_E}{p}\left(1 + e^2 + 2e\cos f\right)\right]^{\frac{1}{2}} \left[1 - \frac{\left(1-e^2\right)^{\frac{3}{2}}}{1 + e^2 + 2e\cos f}\frac{\omega_a}{n}\cos i\right]$$

$$B = \frac{C_D A}{m}$$

In order to evaluate the perturbations due to atmospheric drag, the effects are integrated over a single orbital revolution ($M = 0 \rightarrow 2\pi$), demonstrated by Eqns. (5.8a) and (5.8b).

$$\langle \dot{a} \rangle_D = -\frac{1}{2\pi}\int_0^{2\pi} B\rho V \frac{a}{1-e^2}\left\{1 + e^2 + 2e\cos f - \omega_a \cos i\sqrt{\frac{a^3\left(1-e^2\right)^3}{\mu_E}}\right\} dM \tag{5.8a}$$

$$\langle \dot{e} \rangle_D = -\frac{1}{2\pi}\int_0^{2\pi} B\rho V \left\{e + \cos f - \frac{r^2\omega_a \cos i}{2\sqrt{\mu_E a\left(1-e^2\right)}}\left[2\left(e + \cos f\right) - e\sin^2 f\right]\right\} dM \tag{5.8b}$$

$$\text{where} \quad dM = \left(\frac{r}{a}^2\right)\left(1-e^2\right)^{-\frac{1}{2}} df$$

Numerical Evaluation of Drag Effects

In order to incorporate complex atmospheric density models, a numerical approach to the evaluation of the effects of drag on semi-major axis and eccentricity is employed. A quadrature of the Gauss-Legendre formulation, shown in Eqn. (5.9), is used to specify the nodes and weights at which the integrands are evaluated.

$$\int_{-1}^{1} f(x)dx \approx \sum_{i=1}^{n} w_i f(x_i) \tag{5.9}$$

The quadrature evaluation is implemented as per the method of Liu and Alford [157]. For orbits with low perigee altitude ($90 \leq r_p \leq 300$ km) and large eccentricities (e ≥ 0.001) two quadratures are used. One quadrature is centred about the perigee and the second covers the remaining part of the orbit, demonstrated by Eqn. (5.10). The angular range of the quadratures (θ) is varied with the perigee radius, orbital eccentricity, and rate of change of density at the perigee.

$$\int_{-\pi}^{pi} f(x)dx = \int_{-\theta}^{\theta} f(x)dx + \int_{\theta}^{2\pi-\theta} f(x)dx \tag{5.10}$$

5.1.2 Atmospheric Density Modelling

The density of the atmosphere of the Earth is governed by the interaction between the gaseous molecules of which it is comprised, and the dynamic environment in which they exist. The

simplest models of atmospheric density are static in time and utilise the ideal gas law and hydrostatic equation to relate temperature, pressure, and density to altitude.

However, the accurate evaluation of density is complicated by the varying distribution and mixing of the different chemical constituents of the atmosphere at different latitudes, longitudes, and altitudes. Furthermore, variation in the magnitude of incident radiation from the Sun, interactions between charged energetic particles and the gases constituting the atmosphere, the rotation of the Earth, high-altitude winds, and tidal effects also affect the global and local atmospheric density [162].

As a result, complex upper-atmospheric models have been developed specifically for the purpose of density calculation for determining atmospheric drag. Examples of atmospheric models in this class include the Jacchia [164] and Mass Spectrometer and Incoherent Scatter Radar (MSIS) [165] series of models which utilise empirical data from sources such as measured spacecraft drag data, and mass spectrometer and incoherent radar scatter respectively [153]. These time-varying models typically take inputs of $F_{10.7}$ Solar radio flux, A_p or K_p geomagnetic index, satellite position (altitude, latitude, longitude) and the date and time in order to evaluate the total density of the atmosphere or molecular atmospheric components in the proximity of a spacecraft of interest.

It is important to appreciate that whilst the development of complex atmospheric models can improve the accuracy of density evaluation, many assumptions are made in order to simplify the atmosphere for modelling. The specific assumptions made and their validity given the available data is specific to each atmospheric model and may result in errors in the density output by the model [162]. The error in density evaluation by these models is typically in the range of 10 % to 20 %, but can be significantly greater during periods of exceptionally high or low solar activity [166].

The 2001 Naval Research Laboratory Mass Spectrometer and Incoherent Scatter Radar Exosphere (NRLMSISE-00) model was selected for use in this analysis for the evaluation of atmospheric density in the orbit propagation environment due to slightly improved performance in comparison to earlier MSIS and Jacchia models, measured by Akins et al. [167]. NRLMSISE-00 is a global and time-varying model of Earth atmosphere is valid from the ground to 1000 km altitude [165]. The required inputs to the model include: geodetic altitude and latitude; longitude; date and time; A_p geomagnetic index; and daily and 81-day centred average $F_{10.7}$ solar radio flux.

5.1.3 Space Weather Indices

The prediction of future satellite motion or lifetime and decay analyses presents further complications to the evaluation of atmospheric density as measured values of solar flux and geomagnetic index are not available and forecast data must be used. However, these values are difficult to predict due to the high variability and unpredictability of the Sun. The error or uncertainty associated with these predictions or forecasts can be high, therefore resulting in potentially significant errors in drag force evaluation, lifetime calculations, or other analyses.

Solar Flux

Solar flux incident on the Earth affects density by heating of the upper atmosphere, primarily by Extreme Ultraviolet (EUV) radiation. Variation in the level of solar flux can therefore have a significant effect on the amount of drag experienced by a satellite in Earth orbit.

For atmospheric density modelling, the level of solar flux with a wavelength of 10.7 cm ($F_{10.7}$), measured in Solar Flux Units ($1\,\text{SFU} = 1 \times 10^{-22}\ \text{W}\,\text{m}^{-2}\,\text{Hz}$), is used to approximate the solar output of EUV radiation. EUV and $F_{10.7}$ radiation originate in the same layers of the Sun and are therefore output with similar strength. However, $F_{10.7}$ is not absorbed by Earth atmosphere and ground based measurements of these radio waves can therefore be used as a surrogate for the level of incident F_{EUV} radiation on the upper atmosphere [153]. A delay in the response of atmospheric density with the incident $F_{10.7}$ solar flux is present, generally agreed to be approximately 1 day [168, 169, 170]. The NRLMSISE-00 model therefore uses the measured $F_{10.7}$ magnitude of the previous day in conjunction with the 81-day centred average value to calculate the output atmospheric density.

The magnitude of $F_{10.7}$ incident on the Earth exhibits both a number of periodic trends and significant random variation as shown in Figure 5.3, which shows historical measured values of $F_{10.7}$ from October 1957 to the present, obtained from archived US National Oceanic and Atmospheric Administration (NOAA) data (available from `www.celestrak.com`). The apparent 11-year periodicity in $F_{10.7}$ is attributable to the solar cycle which gives rise to the two extreme periods of solar heating known as solar maxima and minima. In addition to this long-period cycle there is significant short-term variability in solar flux, demonstrated by the difference between the daily and centred 81-day averaged values of measured $F_{10.7}$. This additional variability can be attributed to a variety of different influences, primarily the 27-day rotation of the Sun which causes any transient areas of high or low local activity to turn to or away

from the Earth, seasonal variations related to the eccentricity of the orbit of the Earth about the Sun, and the day-to-night variation caused by the axial rotation of the Earth [153, 160]. Finally, the variability in solar flux is shown to be significantly higher during periods of solar maximum. This is demonstrated by the increased differences that can be seen between the daily and the centred 81-day average measurements during solar maximum in Figure 5.3.

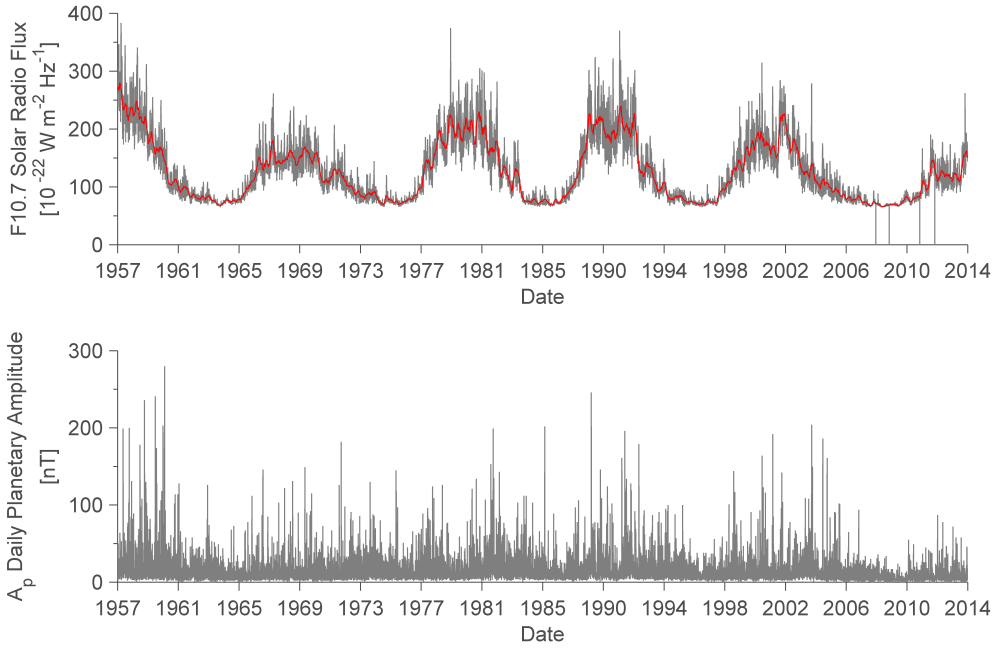

Figure 5.3: Measured daily and 81-day centred average $F_{10.7}$ Solar radio flux and A_p daily planetary amplitude.

Geomagnetic Activity

Variation in the magnetic field of the Earth, primarily caused by the magnetic influence of the Sun, also has an effect on the atmospheric density. The collision of energetic charged particles from the Sun with the atmospheric molecules causes ionisation and a heating effect, which in turn affects the atmospheric density [153]. However, the magnitude of this variation in geomagnetic activity on atmospheric density is significantly less than that of incident solar flux discussed previously.

Geomagnetic activity is typically expressed using either the quasi-logarithmic planetary index, K_p (0 to 9), or linear equivalent planetary amplitude, a_p (0 to 400) in units of nano-Tesla, nT. These global values are obtained through measurement every 3-hours at a variety of

locations. The daily planetary amplitude A_p, is subsequently generated through the averaging of the eight 3-hourly amplitude measurements in a day.

Due in part to the coupling with influences from the Sun, high variability exists in geomagnetic activity, demonstrated by the historic measurements of A_p shown in Figure 5.3. Whilst some relationship to the solar cycle can be seen, most prominently increased activity and variability during periods of solar maxima, the overall behaviour of the geomagnetic environment is highly changeable.

Similarly to solar flux, a delay in the response of atmospheric density with the measured geomagnetic index exists [162]. Values for this delay between observed K_p or a_p index and response in atmospheric density are stated by Jacchia [171] to average about 6.7 hours and by Forbes et al. [172] to be between 1–5 hours depending on the time of day and latitude of interest. The NRLMSISE-00 model accommodates this lag by utilising the input of the 3-hourly a_p and daily A_p observations covering the previous 57 hours [173].

Space Weather Forecasting

For the deployment of satellite constellations in LEO, the use of forecast solar flux and geomagnetic activity data is required in order to evaluate the effects of drag on the constellation deployment process. A number of approaches for the prediction of these indices are examined by Vallado and Finkleman [162] and Vallado and Kelso [174, 175]. The long-term prediction of space weather is of interest in the context of satellite constellation deployment, as it is envisaged that the analysis will be performed during the conceptual and preliminary design process, far in advance of the launch of the satellites.

The prediction of solar flux and geomagnetic index over long time periods, particularly over more than a single solar cycle, presents a significant challenge. Figure 5.4 shows the variability and recent performance of a series of long-term predictions of $F_{10.7}$ from the NOAA/Space Weather Prediction Center (SWPC). Comparison of these forecasts with the available measured data indicates a capability of matching the trend in solar flux through the remainder of the current solar cycle, but also demonstrates that these forecasts are usually unable to predict both the timing and magnitude of the following cycle. The behaviour of predicted Schatten solar cycle data was also shown to demonstrate a similar performance by Vallado and Kelso [175].

In Figure 5.4 a simple polynomial predictor developed by Vallado [153] is also shown. The form of this polynomial is described by the following equation where t is the number of days from 1 January 1981.

$$F_{10.7} = 145 + 75\cos(0.001696t + 0.35\sin(0.00001695t)) \tag{5.11}$$

The trend is generated to best match the preceding few solar cycles and provide a forecast of solar flux on the basis that the following cycle(s) are not significantly different in both timing and magnitude. However, the performance of this trend in forecasting the latest solar cycle shows significant errors in comparison to the available measured values due to the lower and later solar maximum of the current cycle.

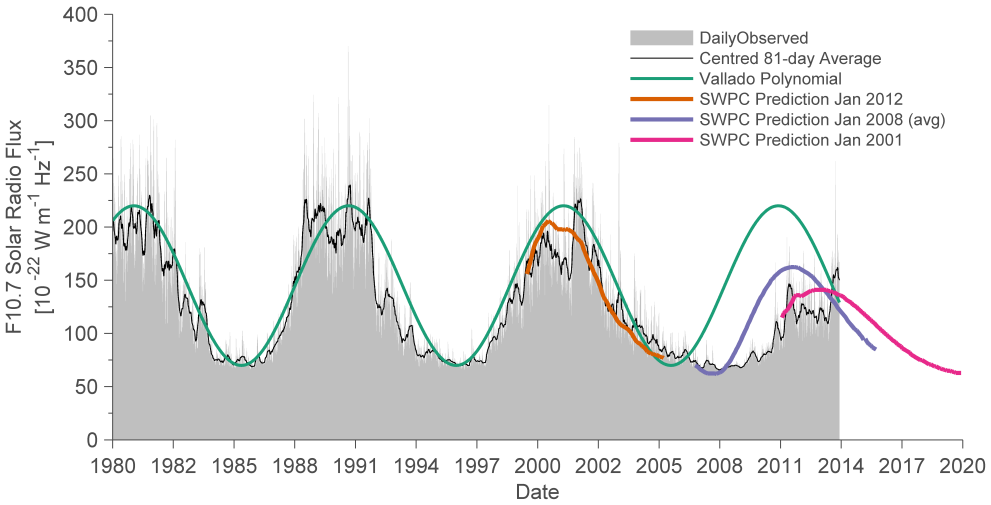

Figure 5.4: Comparison of measured and predicted $F_{10.7}$ Solar radio flux.

A number of other methods and sources of prediction for $F_{10.7}$ and A_p are also available. These include Schatten predictions, European Space Agency (ESA) Prediction of Flux and A_p (PDFLAP) and SOLMAG forecast programs, and a method developed by Oltrogge and Chao [176] which utilises a Monte Carlo random draw approach to generate a future solar cycle of an average length from measured values of the previous five complete solar cycles.

The accuracy and confidence of solar flux and geomagnetic index prediction have significant implications on mission and spacecraft design. In the short term, inaccuracies in forecasted data leads to positional differences which increase with the period of analysis due to error propagation. For spacecraft lifetime analyses, the difference between predicted and actual

space weather indices results in different estimations of rate and time of decay. Significantly, the overestimation of $F_{10.7}$ and A_p results in a reduced predicted spacecraft lifetime, a conservative estimation, which can ensure that the mission does not fail due to early spacecraft decay.

5.1.4 Physical Satellite Characteristics

The physical properties of a spacecraft, nominally the coefficient of drag C_D, area A, and mass m contribute to the drag force which is experienced whilst in orbit. These three parameters are typically combined to create the ballistic coefficient B for the spacecraft, shown in Eqn. (5.12). This expression is often also seen in its reciprocal form.

$$B = \frac{C_D A}{m} \tag{5.12}$$

In the context of the basic drag equation, Eqn. (5.6), a higher ballistic coefficient results in greater acceleration due to drag and therefore faster orbital decay. Due to the significance of ballistic coefficient in the drag equation, the accuracy of calculation or estimation of satellite ballistic coefficient is critical in the estimation of satellite drag effects and lifetime analysis. The calculation or estimation of the three components of ballistic coefficient are each discussed individually herein.

Coefficient of Drag

Coefficient of drag is dependent on both the shape of the spacecraft and the molecular interaction between the gas particles in the atmosphere and the surfaces of the spacecraft. Classically a value of 2.2 has been used for the coefficient of drag [177]. However, the coefficient of drag can vary considerably with altitude due to varying atmospheric pressure and adsorption of atmospheric molecules, primarily atomic oxygen, onto the surfaces of the spacecraft, affecting the momentum transfer between incident atmospheric particles and the satellite [142]. For long duration analyses of satellite lifetime, the ISO standardised approach [178] suggests that the value of 2.2 for coefficient of drag can be adopted as the errors will be averaged out over the lifetime of the satellite.

Area

For the calculation of ballistic coefficient, the cross-sectional area of the satellite normal to the velocity vector is required. For some satellites which have spin-stabilised, fixed, or controlled

attitude, the cross-sectional area can be calculated as required. However, for many satellites the precise attitude may not be known a priori. In these cases, the mean cross-sectional area for these satellites can be calculated by integrating the cross-sectional area over the complete range of different spacecraft attitudes.

Alternatively, the simpler method of Oltrogge and Leveque [179], utilising a composite flat-plate model can also be used to approximate the cross-sectional area for simple geometries such as parallel-piped spacecraft. Equation (5.13) demonstrates the calculation of a cuboid spacecraft with side-panel areas of S_i with optional additional surfaces.

$$A = \frac{1}{2}[S_1 + S_2 + S_3 + (S_4 + \cdots)] \tag{5.13}$$

However, for a tumbling cuboid spacecraft, this method can overestimate the average cross-sectional area. If additional surfaces are included as flat-plate areas, eg deployable solar arrays, this method of estimation can become systematically biased towards a greater area as occultation or self-shadowing of the spacecraft body surfaces is not accounted for. Furthermore, the thickness or aspect-ratio of these additional surfaces with respect to the velocity vector may also require consideration.

These effects result in a conservative effect on the evaluation of drag effects, as the orbital lifetime is decreased by increased area. The use of a masking-reduction factor can be introduced to maintain accuracy for cases which include additional surfaces [179].

Satellite Mass

For the purposes of ballistic coefficient determination the mass of the satellite can be assumed to be constant unless propulsive manoeuvres are performed which result in reduced fuel mass. The rocket equation, Eqn. (5.14), under the assumptions of constant specific impulse I_{sp} can be used to equate the change in velocity ΔV of a vehicle to the required ratio of mass before (m_0) and after (m_1) the change in velocity.

$$\Delta V = V_e \ln \frac{m_0}{m_1} = I_{sp} g_0 \ln \frac{m_0}{m_1} \tag{5.14}$$

This equation is independent of the burn time, but assumes that there are no additional atmospheric or gravitational losses during the manoeuvre. For orbital transfers, impulsive thrust manoeuvres are therefore generally assumed for which the burn duration is assumed to be

very small in comparison to the coast-arc or orbit period [62]. Approaches for low-thrust or continuous-thrust propulsion systems, for which this assumption cannot be made, are discussed later in Section 5.1.7.

Alternatively, the rearranged rocket equation, Eqn. (5.15), can be used to determine the mass of propellant m_p required to perform a manoeuvre of velocity change ΔV, where m_0 is the mass before the manoeuvre.

$$m_p = m_o \left[1 - e^{-\frac{\Delta V}{I_{sp} g_0}}\right] \tag{5.15}$$

As a result of the assumptions made when applying these equations, the returned ΔV or propellant mass to perform a given orbital manoeuvre is the minimum requirement, and will be subject to some losses due to the finite period of burn.

5.1.5 Orbit Propagation Implementation

The method of semi-analytical orbit propagation described in the previous sections was implemented in the MATLAB programming environment. This decision was made due to the availability of a range of different built-in functions including atmosphere models (particularly the NRLMSISE-00 model) and the author's familiarity with MATLAB as a programming language.

The flow-diagram in Figure 5.5 demonstrates the process by which the orbit propagation method is implemented. The process can be crudely divided into two sections, an initialisation stage and the orbit propagation procedure.

During the initialisation process information required by the orbit propagation procedure are organised for input or calculated from the relevant models or databases. These inputs include the necessary initial conditions for the propagation, satellite physical characteristics, and space weather index data.

The orbit propagation process is set up as an iterative procedure which runs until the requested analysis period is addressed or satellite decay occurs. The main routine within the orbit propagation process involves the calculation of the orbit perturbations due to non-spherical geopotential and atmospheric drag and the subsequent solution of the orbital equations of motion using an Ordinary Differential Equation (ODE) solver. A number of sub-procedures

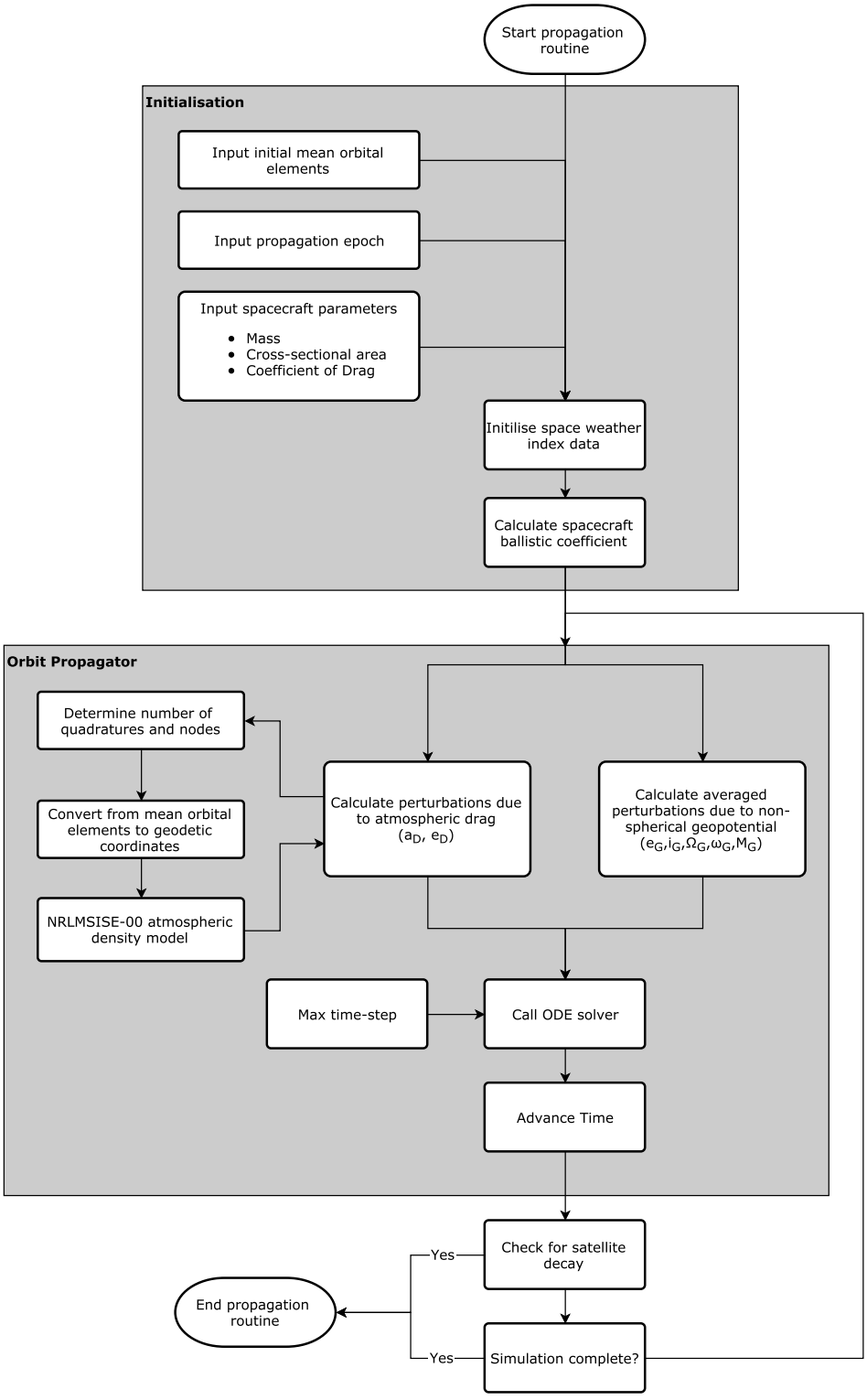

Figure 5.5: MATLAB propagation flow diagram.

are performed within the orbit propagation process to facilitate the calculation of the orbit perturbations, including coordinate transformations and evaluation of atmospheric density.

Integration of the Orbital Equations of Motion

The SALT equations of motion, Eqn. (5.5), are propagated using the *ode45* function, the MATLAB implementation of the Dormand-Price Runge-Kutta (4,5) method for solution of ODEs with adaptive step-size control. The differential equations are separated into the perturbations due to central-body-gravity, which are calculated analytically using Eqns. (B.1a) and (B.1f) and the perturbations due to atmospheric drag, Eqns. (5.8a) and (5.8b), which are calculated numerically using the Gauss-Legendre quadrature formulation. In order to correctly perform the numerical evaluation of drag effects, the quadrature evaluation must be performed about a whole orbit, mandating a minimum step-size of a single orbital period.

Variable step-size control is utilised by the *ode45* integrator in order to realise greater computational efficiency. Due to the varying dynamics of orbit propagation with atmospheric drag effects, shorter time-steps are required when lower orbital altitudes are present and the satellite experiences more rapid changes in semi-major axis and eccentricity. However, for higher orbits which are less affected by atmospheric drag the step-size can be allowed to increase, shortening the time required for simulation. For simplification of the results, the output of the *ode45* function is set to return the state of the orbital parameters at every revolution of the orbit. In order to ensure the accuracy of the developed solution, the variable step-size is controlled by specified relative and absolute error tolerances. These tolerances are set to provide a compromise between the computation speed of the solver and accuracy of the solution.

NRLMSISE-00 Implementation

The implementation of the NRLMSISE-00 atmosphere model requires inputs of the longitude, geodetic altitude and latitude, date and time, A_p geomagnetic index, and daily and 81-day centred average $F_{10.7}$ solar radio flux in order to provide the output of local atmospheric density.

Several coordinate transformations are required in order to convert the mean Keplerian orbital elements used in the propagation method to the longitude, latitude, and altitude values required by the atmosphere model. The mean Keplerian elements are first transformed to osculating orbital elements by adding the absent short-periodic variations as described in Eqn. (5.2). The expressions for short-period variations as described by Liu and Alford [154] are shown in Appendix B, Eqns. (B.2a) and (B.2f). These osculating Keplerian orbital elements

are then converted first to the Earth-Centred Inertial (ECI) and then the Earth-Centred, Earth Fixed (ECEF) coordinate systems before the longitude and geodetic latitude and altitude can be calculated.

Conversion to ECI coordinates is achieved by first transforming the Keplerian elements to position and velocity in the perifocal coordinate system (PQW) using Eqns. (B.3a) and (B.3b). The perifocal coordinate system is centred at the focus of the orbit and defined using the plane of the orbit with unit vector $\hat{p}$ directed towards the periapsis, $\hat{q}$ with a true-anomaly of 90°, and the angular momentum vector $\hat{w}$, orthogonal to the orbital plane. The transformation matrix, Eqn. (B.4), can then be used to obtain the position and velocity of the spacecraft in the ECI coordinate frame.

The position and velocity coordinates in the non-rotating J2000 ECI frame are then transformed to the ECEF frame which is fixed with respect to the surface of the Earth. This conversion is performed using Eqns. (B.5a) and (B.5b) and the rotation matrix, Eqn. (B.5c), and its derivative, Eqn. (B.5d). Calculation of the Greenwich Apparent Sidereal Time (GAST) is required in order to perform this transformation from celestial to terrestrial coordinates.

The position of the satellite in ECEF coordinates is finally transformed to longitude and geodetic latitude and altitude. Due to the complex and non-spherical shape of the Earth geoid, a simplified spheroid shape is used. Geodetic latitude and altitude, as opposed to geocentric coordinates, are calculated using the vector from the equator and normal to the surface of this spheroid rather than the vector which passes directly through the centre of the spheroid. A flatness factor or eccentricity of the central body is used to define the variation of the reference spheroid from a a true sphere. The calculation of geodetic coordinates is performed using the method of Borkowski [180] as implemented by Vallado [153], using the WGS 84 datum surface and flattening factor.

Space Weather Index Data

An aggregated set of historical and forecast space weather data released by the SWPC and National Geophysical Data Center (NGDC) departments of the NOAA is freely available from CelesTrak website (`http://celestrak.com/SpaceData`). The data file is split into 4 sections: historic observed data; 45-day forecast values, approximately 2-years of monthly forecast data for $F_{10.7}$, and further monthly fit data for $F_{10.7}$ using the polynomial trend shown in Eqn. (5.11)

[174]. This data set was chosen due to the completeness and availability of up-to-date measured and forecast data.

The daily and 81-day centred average $F_{10.7}$ solar radio flux and A_p geomagnetic index values required by the NRLMSISE-00 atmosphere model are extracted from the data file as required. Unlike $F_{10.7}$, for which monthly predicted and monthly fit data is available, predicted A_p geomagnetic index is not available beyond 45-days. An average value of 15 nT is therefore suggested by Vallado [153] in these cases. Similarly, when missing values for daily or average $F_{10.7}$ solar radio flux are present in the data file an average value of 150 SFU is used.

5.1.6 Orbit Propagator Validation

The objective of the validation of the developed propagator is to demonstrate the accuracy of the semi-analytical orbit propagation method combined with NRLMSISE-00 atmospheric density model over long-term propagation periods. For the purpose of constellation deployment, the propagation method is required to accurately capture the secular variations in the orbital elements such that the effects of nodal precession, perigee rotation, and orbital decay can be appreciated.

The developed method of propagation is validated against the observed orbital ephemerides of a number small satellite missions with different physical characteristics, in orbits of different semi-major axis, eccentricity, and inclination, and at different epochs. The range of test cases, shown in Table 5.2, was chosen to ensure that the propagation method performed as expected with a suitable level of accuracy and was validated over the range of its intended use. The sets of observed ephemerides were obtained from the public-access US Air Force Space Command (AFSPC) managed Space-Track website (`www.spacetrack.org`), where historical satellite position data is available in Two-Line Element (TLE) form.

The epoch for each test satellite was chosen such that any identifiable propulsive manoeuvres or significant changes in spacecraft configuration were performed prior to the analysis period. The state of the satellite was then extracted from the TLE at the chosen epoch and used as the initial state for the propagator.

Due to the lack of information available regarding the physical characteristics of some of the propagated satellites, assumptions about the mass, cross-sectional area, and coefficient of drag had to be made in order to provide the propagator with the necessary input of ballistic coefficient. For satellites with propulsion systems, the reported dry mass of the vehicle was used

in the absence of actual fuel-use data. This was based on the assumption that all the planned orbital manoeuvres had been performed and that the majority of the loaded propellant, save for a small amount of leftover unusable propellant, known as ullage, had been expended. The averaged cross-sectional area of the satellite was used when no fixed attitude control was known to be applied to the satellite. Finally, the classical value of drag coefficient ($C_D = 2.2$), was used when no actual drag coefficient was reported.

In each test case, the satellite was propagated to the date of the last available TLE set or until it experienced orbital decay and atmospheric re-entry, whichever occurred first. The generated ephemerides produced by the propagator were then be compared to the observed orbital data extracted from the TLE sets. Both osculating orbital elements and mean orbital elements (without short-period perturbations as per Kozai [181]) were used for comparison. Whilst the computation of Kozai mean orbital elements and mean orbital elements using SALT are not strictly the same, the two methods were noted by Liu [182] to be in almost exact agreement, and can therefore be used for comparison at the scale of this investigation.

In order to perform a quantitative assessment of the performance of the propagator, the difference in time between the propagated and actual re-entry time was calculated for satellites which experienced decay. Otherwise, the difference in mean orbital elements at the end of the analysis period was compared.

Whilst these validation cases have been performed using measured space weather data, the inherent error in density evaluation by the NRLMSISE-00 atmosphere model and uncertainty associated with the value of ballistic coefficient used will result in errors in the propagation of a satellite from an initial state. Furthermore, due to the compounding effect of atmospheric drag, even small errors in density estimation and ballistic coefficient can result in significant differences in orbital parameters over longer propagation periods. Thus, for the long-term or lifetime propagation of satellites, the expected error of the propagation method is expected to be of the same order as the atmospheric density model and ballistic coefficient, 10 % to 20 %.

For the missions tested in which the satellite decayed from orbit during the analysis period, the error in time of decay is shown in Table 5.1. As a percentage of the analysis period, the absolute error was found to vary in the range of 0.83 % to 14.90 %, with an average percentage error of 4.67 %. Additionally, of the 19 satellites investigated which experienced atmospheric re-entry within the analysis period, only two missions indicated an error of greater than 10% in the time of decay from epoch.

Table 5.1: Actual and estimated lifetime of satellites used for propagator validation.

Satellite	**True Lifetime from Epoch [Days]**	**Estimated Lifetime from Epoch [Days]**	**Error [Days]**	**Error [%]**
Calsphere-3	2481.0	2533.7	52.7	2.12
Calsphere-5	2563.5	2644.3	80.8	3.15
Calsphere-4	2089.5	2106.9	17.4	0.83
GFZ-1	1516.4	1642.9	126.5	8.34
TubSat-N	1362.0	1299.2	-62.8	-4.61
TubSat-N1	812.0	825.6	13.6	1.67
MightySat-1	340.6	327.5	-13.1	-3.85
Starshine-1	258.9	246.2	-12.7	-4.89
Starshine-3	477.0	470.0	-7.0	-1.47
Starshine-2	130.2	124.7	-5.5	-4.22
MIMOSA	3086.0	3050.0	-36.0	-1.17
CUTE-1.7 APD	1304.0	1109.7	-194.3	-14.90
GeneSat-1	1327.4	1152.1	-175.3	-13.20
AnuSat	1093.3	1045.9	-47.4	-4.33
PharmaSat	1182.4	1197.8	15.4	1.31
HawkSat I	703.7	736.7	33.0	4.69
QbX1	24.1	23.0	-1.1	-4.58
Tiantuo 1	906.9	885.0	-21.9	-2.42
TechEdSat	209.0	206.9	-2.1	-1.02
Mean Error (Absolute)				**4.79**
Standard Deviation of Error				**3.91**

Table 5.2: Orbit and physical properties of satellites used for propagator validation.

Name	**Form**	**Semi-major Axis [km]**	**Ecc**	**Inc [°]**	**Ballistic Coefficient [$m^2\ kg^{-1}$]**	**Epoch**
GFZ-1	Sphere	6767	0.0016	51.6	0.004	01-05-1995
TubSat-N	Cuboid	6963	0.0276	78.9	0.020	01-07-1998
TubSat-N1	Cuboid	6960	0.0272	78.9	0.030	01-07-1998
MightySat-1	Hexagonal Prism	6768	0.0003	51.6	0.009	17-12-1998
Starshine-1 [183, 184, 185]	Sphere	6767	0.0010	51.6	0.010	05-06-1999
Starshine-3 [185]	Sphere	6848	0.0008	67.1	0.010	01-10-2001
Starshine-2 [185]	Sphere	6754	0.0024	51.6	0.015	18-12-2001
MIMOSA [186]	26-sided Prism	6957	0.0373	96.8	0.009	01-07-2003
AAU CubeSat	1U CubeSat	7199	0.0017	98.7	0.033	30-10-2003
CUTE-1.7+APD [187]	2U CubeSat	6877	0.0297	98.2	0.015	01-04-2006
GeneSat-1 [16, 12]	3U CubeSat	6797	0.0010	40.1	0.019	16-12-2006
Formosat3A (FM-6) [43, 188]	Hexagonal Prism	7178	0.0057	72.0	0.040	01-12-2007
AAUSat II	1U CubeSat	7000	0.0007	98.0	0.033	30-04-2008
CUTE-1.7+APD II [189]	Cube	7000	0.0005	98.0	0.031	01-05-2008
AnuSat [190]	Cube	6858	0.0112	41.2	0.042	18-04-2009
PharmaSat [191]	3U CubeSat	6828	0.0025	40.5	0.017	20-05-2009
HawkSat I	1U CubeSat	6824	0.0021	40.4	0.033	01-10-2009
QBX1 [179]	3U CubeSat	6672	0.0016	34.6	0.032	15-12-2010
Tiantuo 1	Cuboid	6845	0.0011	97.2	0.019	10-05-2012
TechEdSat	1U CubeSat	6791	0.0021	51.6	0.033	09-10-2012

These errors are of the same order as the uncertainty in drag evaluation, comprised of the error in atmospheric density estimation (from measured solar flux and geomagnetic values) and uncertainty or assumptions made with respect to the mass, coefficient of drag, and cross-sectional area of the satellite.

When the percentage error is plotted against the lifetime of the satellite from epoch, as in Figure 5.6, the results indicate that the length of the analysis period has little effect on the accuracy of the propagation method. However, the satellites analysed over the longest propagation periods (the MIMOSA and Calsphere missions) have more accurately known ballistic coefficient values due to the information available about these systems. Furthermore, due to the spherical or near-spherical form of these satellites, the coefficient of drag is shown by Moe and Moe [142] to vary less with altitude than other forms, and therefore also contributes to the reduced error in estimation of decay date. The distribution of the results showing both positive and negative errors in lifetime from epoch in Figure 5.6 also suggests that there is no inherent bias towards underestimation or overestimation of satellite lifetime when historical observed values for the space weather indices are used.

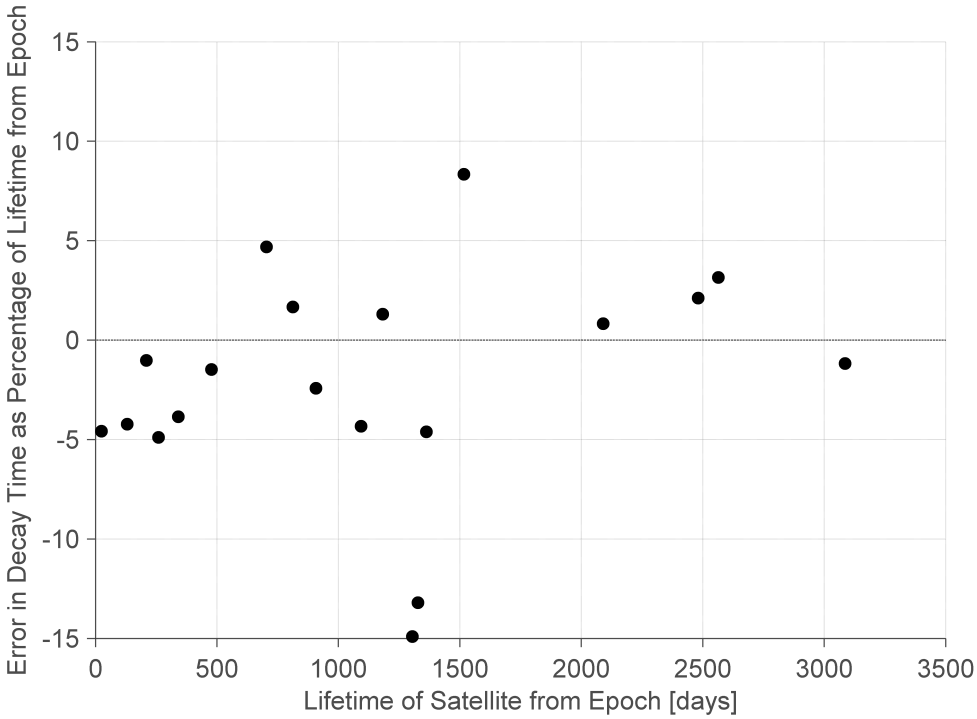

Figure 5.6: Variation of error in decay time with satellite lifetime from epoch.

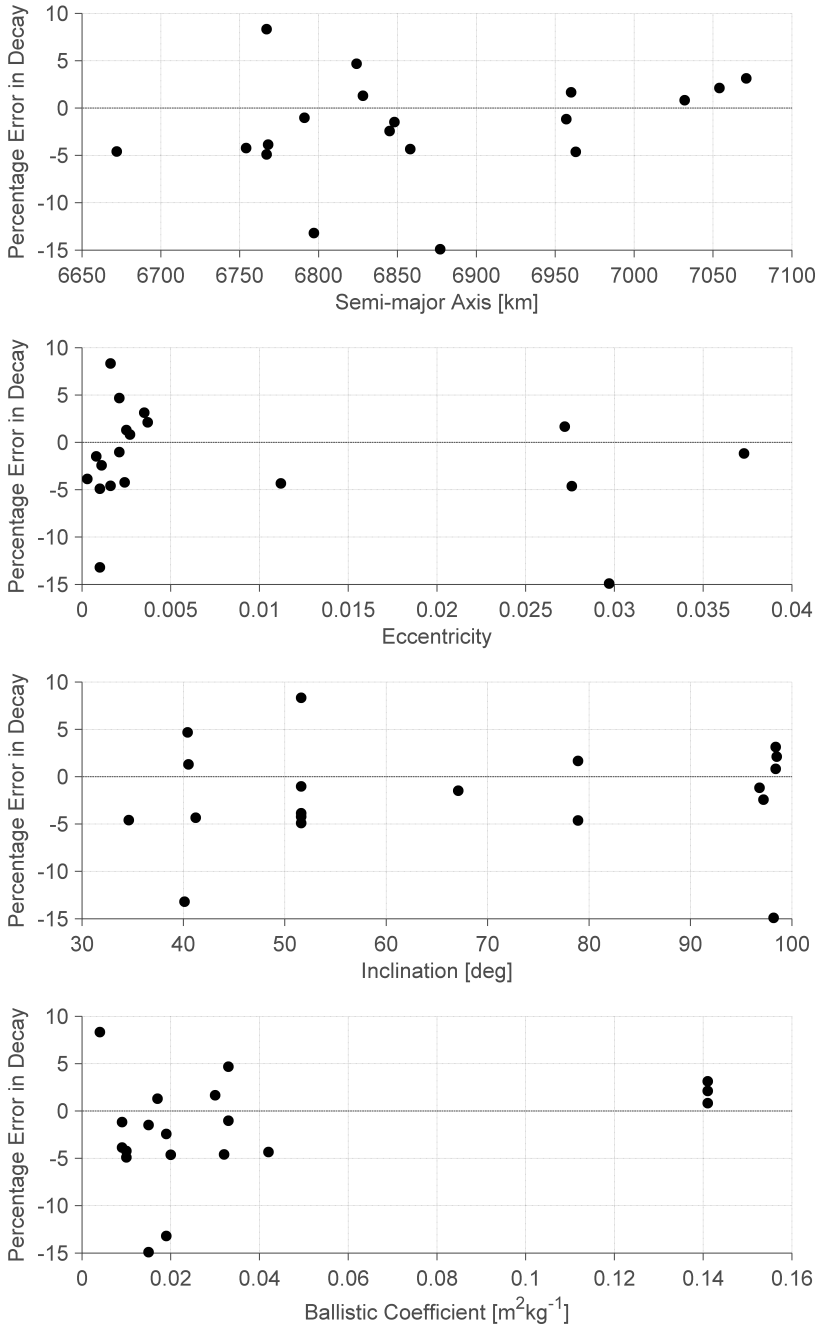

Figure 5.7: Variation of error in decay time with initial semi-major axis, eccentricity, inclination, and ballistic coefficient.

The sensitivity of the error in lifetime from epoch to other factors, such as the initial orbital parameters and physical characteristics of the satellites is also shown in Figure 5.7. The distribution of the points about the x-axis and lack of identifiable trend indicates that the propagation method itself not sensitive to satellites of different type or in different orbits. This supports the idea that the primary source of error in the lifetime estimation of the propagated satellites results from errors in the input parameters provided for each mission.

Individual investigations of three of the cases presented in Table 5.2, GeneSat-1, CUTE-1.7+APD-II, and PharmaSat, are presented in the following sections. These cases were chosen to demonstrate the range of accuracy in position and lifetime estimation achieved using the propagation method. Additionally, in the third case, PharmaSat, the use of forecast space weather data is compared to observed data and the effect on the propagated solution and estimated lifetime analysed.

GeneSat-1

Observed and propagated orbital parameters of the GeneSat-1 satellite from epoch 17 December 1999 are presented in Figure 5.8 against the time from epoch in days. GeneSat-1 was a 3U CubeSat with body-mounted solar cells launched as a secondary payload on 16 December 2006 to demonstrate nanosatellite capability to perform in-situ biological research and processing [16]. The satellite decayed from orbit on 04 August 2010.

The error in lifetime from epoch of the propagation method compared to the actual mission, reported in Table 5.1 to be -175.3 days, is shown in Figure 5.8 to be due to the more rapid decay in semi-major axis of the propagated satellite, resulting in an earlier re-entry date. This decay in semi-major axis is not constant over time, primarily due to the increasing atmospheric density and therefore drag force as the size of the orbit decreases. The effect of varying solar flux and geomagnetic index on atmospheric density can also be seen in the development of the semi-major axis as changes in the rate of decay.

The cause of the increased rate of decay and ultimate difference in predicted lifetime by the propagated solution is overestimation of the effect of atmospheric drag on the satellite. This may be caused by a combination of any error in the estimation of atmospheric density by the NRLMSISE-00 model and the assumptions made in order to generate the ballistic coefficient of the satellite. Overestimation of the cross-sectional area of the satellite may be a factor, as in the absence of attitude information it was assumed that the satellite was tumbling and the

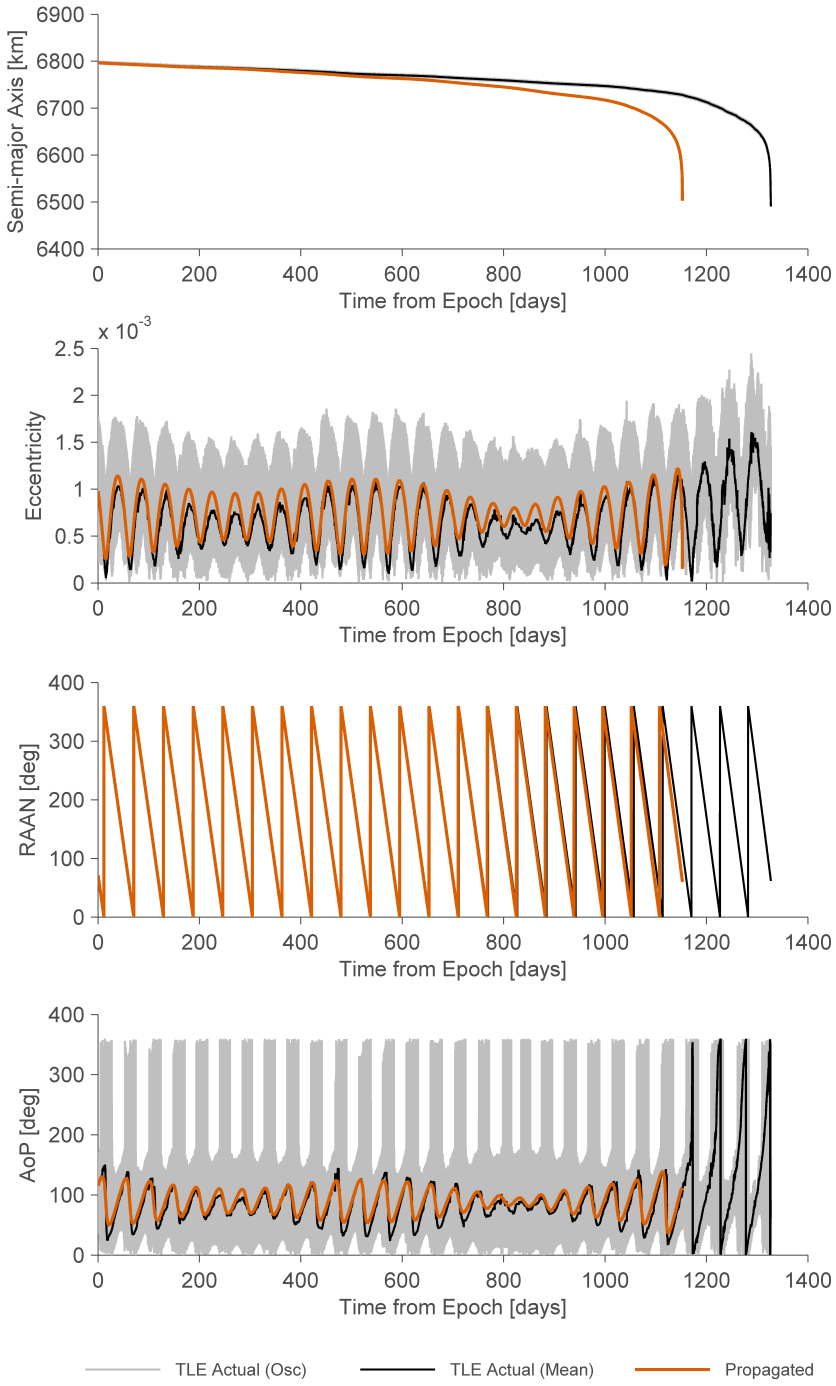

Figure 5.8: Observed and propagated orbital parameters of GeneSat-1 satellite.

average cross-sectional area of the satellite body was used. However, if travelling with a fixed attitude, the cross-sectional area of the 3U CubeSat could be as little as 0.01 m, compared to the calculated average of 0.039 m. Similarly, as the coefficient of drag of the satellite was unknown, the standard value of 2.2 was used.

This error in semi-major axis development over time also causes errors in the development of the other propagated orbital parameters, most visibly in RAAN, which becomes out of phase with the true orbital data as the semi-major axis diverges. This effect is due to the dependence of the secular rate of nodal drift on semi-major axis, described simply in Eqn. (2.2) or by the first-order terms in Eqn. (B.1e). A similar, but less visible effect is also present in the drift of AoP.

Comparison of the propagated result and mean observed orbital data in Figure 5.8 indicates that the propagation method is capable of capturing the long-periodic motion of the satellite, classed by Vallado [153] as motion which is one to two orders of magnitude greater than the orbital period. However, the short-periodic motion, indicated by the true osculating dataset is not addressed.

CUTE-1.7+APD-II

The orbital elements of the CUTE-1.7+APD-II satellite generated from observed data and the use of the developed propagation method are presented in Figure 5.8 from epoch 01 May 2008 to 01 December 2014. CUTE-1.7+APD-II is a technology-demonstration nanosatellite developed by the Tokyo Institute of Technology, launched as a secondary payload on 28 April 2008. In June 2015, the satellite was still reported to be in-orbit and operational.

The evolved error in the mean semi-major axis of the CUTE-1.7+APD-II satellite over the propagation period of 2405 days to 01 December 2014 is 3.96 km, corresponding to an absolute percentage error of 0.057 %. Similarly to the previous example, the error in development of the semi-major axis is attributable to either errors in the estimated atmospheric density or the ballistic coefficient used.

However, whilst the maximum error in semi-major axis is relatively small, significant errors in the other orbital parameters developed by the end of the analysis period as a result of this discrepancy. At the end of the 2405 day period the angular errors in RAAN and AoP are 47.5° and 24.8° respectively. Similarly, the largest error in eccentricity is 2.9×10^{-4}. The growth of

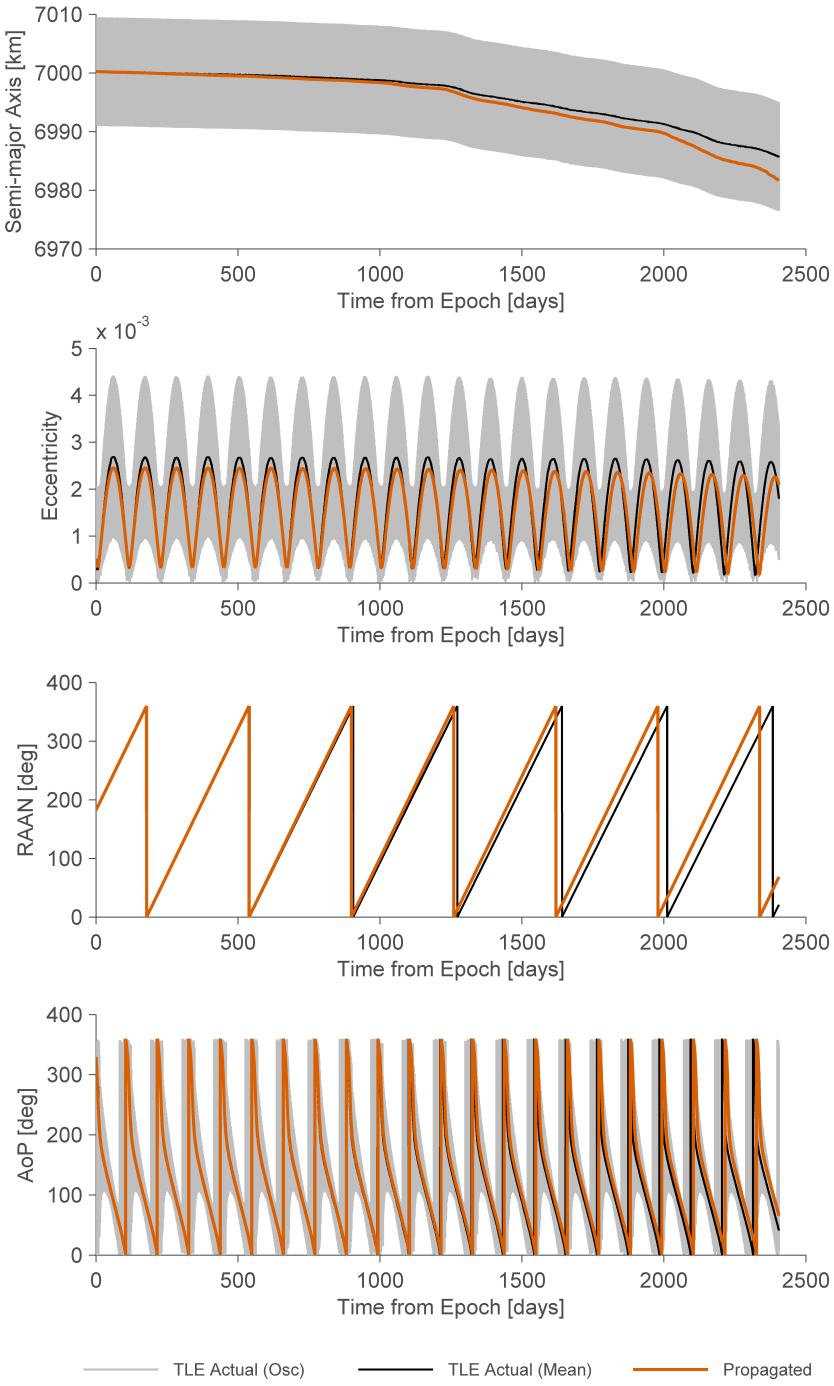

Figure 5.9: Observed and propagated orbital parameters of CUTE-1.7+APD-II satellite.

these errors can be seen in Figure 5.9, demonstrating the effect that even small errors in the evaluation of drag on semi-major axis can have when propagated over a long analysis period.

PharmaSat with Forecast Space Weather Indices

The true orbital parameters of the PharmaSat satellite from epoch 20 May 2009 are compared to those generated using the developed propagation method with both observed and forecast space weather index data ($F_{10.7}$ solar flux and A_p geomagnetic index) in Figure 5.11. PharmaSat was a 3U CubeSat with body-mounted solar cells launched as a secondary payload on 19 May 2009 to perform a biological investigation of anti-fungal agent efficacy in the microgravity environment [191]. The satellite decayed from orbit on 14 August 2012.

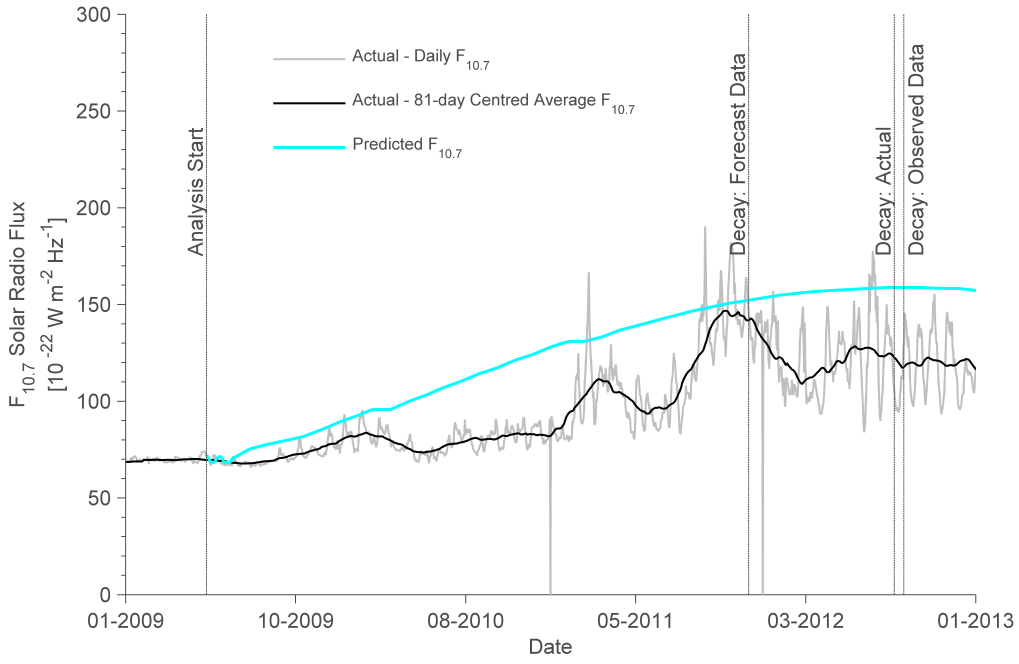

Figure 5.10: Forecast and observed $F_{10.7}$ solar radio flux over analysis period of PharmaSat satellite.

The propagated data shows a very close prediction of the decay date of the satellite when historic observed $F_{10.7}$ solar flux and A_p is used, reflected in the low percentage lifetime error of 1.31% from Table 5.1. As a result of this close match in the evolution of the semi-major axis, the induced errors in other orbital elements remain very small throughout the lifetime of the satellite to re-entry.

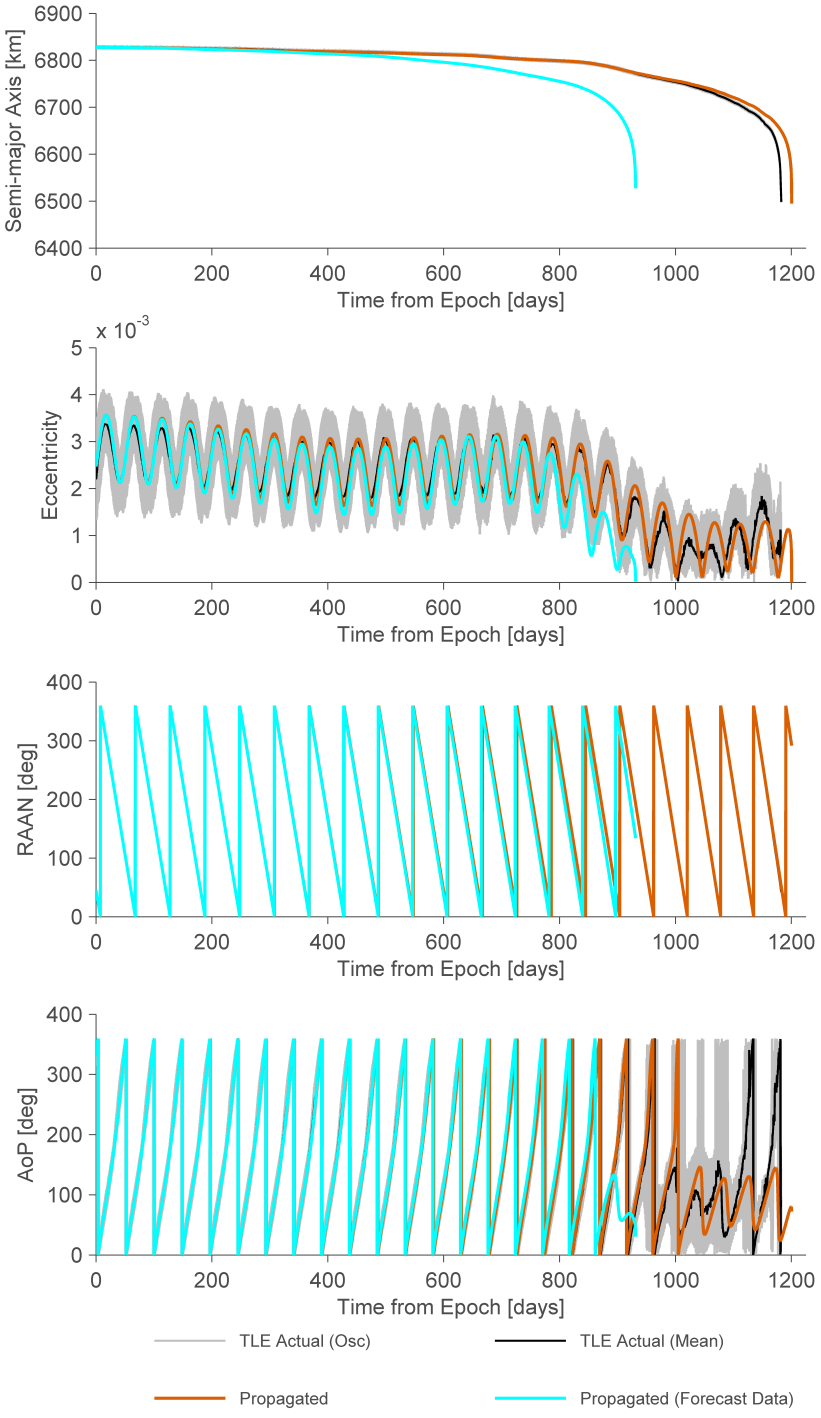

Figure 5.11: Observed and propagated orbital parameters of PharmaSat satellite with forecast space weather indices.

The propagation of the satellite using the predicted space weather data, forecast from the date of the launch of the satellite, however shows a significantly different result from the propagation performed using observed data. The earlier decay date (251 days before the actual satellite) of this propagation result indicates that the forecast space weather data over-predicts the $F_{10.7}$ solar flux and A_p geomagnetic index during the analysis period. This is supported by Figure 5.10, which shows that the forecast $F_{10.7}$ solar flux was consistently higher than the observed 81-day centred average and higher than the majority of the observed daily solar flux measurements throughout the analysis period.

Propagator Validation Summary

Investigation of the performance of the orbit propagation technique has demonstrated the behaviour of the method for the long-term trajectory prediction of orbiting bodies under the effects of Earth oblateness and atmospheric drag.

The average percentage error in time to decay from Epoch of less than 5 % demonstrates the accuracy of this method of propagation combined with the use of the NRLMSISE-00 atmosphere model for orbital lifetime prediction. Furthermore, analysis of these errors has also indicated that the method is not inherently biased towards under-prediction or over-prediction of the satellite lifetime when historical measured space weather index data is used, and is not sensitive to spacecraft of different mass or area, or orbits of different size, shape, and inclination.

Comparison of the predicted to actual satellite trajectory data has indicates that the propagation method is capable of capturing both long-term periodic and secular variations in the semi-major axis, eccentricity, RAAN, and AoP. However, uncertainties in the estimation of atmospheric drag result in errors in the semi-major axis which can subsequently cause significant errors in the other orbital elements to develop, particularly over long orbital lifetimes. The use of predicted space weather index data introduces further uncertainty and can result in even greater absolute errors in both lifetime and orbital position.

However, for the analysis of satellite constellation deployment by indirect plane separation, the primary requirement is the capability to evaluate the differential orbital decay and drift in RAAN between satellites in different orbits. For a given set of input information, including space weather index data, the correct behaviour of the propagation method and the relative error between different orbit trajectories is key. The absolute error of the orbit propagation method and corresponding orbital elements, especially for the simulation of future scenarios

which include the significant uncertainty of predicted space weather data, is therefore of less significance.

5.1.7 Orbital Manoeuvres

Modelling of orbital manoeuvres is required to capture the correct behaviour of the spacecraft whilst performing the orbit transfers required to effect the orbital deployment strategy. For the purpose of performing the analysis of satellite constellation deployment strategies, calculation of the propellant expenditure and trajectory of the vehicle during the manoeuvre is required.

In-plane orbital transfers are required to develop the differential drift-rates in RAAN necessary to perform the deployment of a satellite constellation using the method of indirect plane separation. If multiple satellites are required in each orbital plane, phasing manoeuvres may also be required to produce the desired separation by true anomaly about each orbital plane. Finally, inclination change manoeuvres may also be required to transfer the spacecraft from an initial orbital inclination to the mission orbit inclination.

The analysis of low-thrust or constant-thrust propulsion systems presents somewhat of a challenge when modelling orbit transfers, as the assumption of instantaneous velocity change used in impulsive transfer models may not be valid. As the duration of the thrust-burn becomes significant with respect to the coast-arc, gravity losses increase. This is due to the application of impulse away from the optimal thrusting points, typically orbital nodes or apses [192], or at an angle to the velocity direction [158]. The common solution for this problem involves the use of numerical propagation techniques in which thrust is modelled as an additional perturbing acceleration to the system [29].

Alternatively, the equivalence between an infinite series of consecutive Hohmann transfers and a continuous-thrust spiral transfer can be utilised to model continuous-thrust propulsion systems. Bettinger and Black [193] demonstrate this relationship, indicating that the percentage error in ΔV calculated using this method is less than 1% when 20 consecutive Hohmann transfers are performed and that the errors approach zero as the number of Hohmann transfers tends to infinity. Thus, due to the low-thrust capability of the continuous-thrust propulsion systems, the manoeuvre can be approximated by simulating many consecutive Hohmann transfers.

For low-thrust, but non-continuous thrust propulsion systems the analyses operate by simulating multiple finite-duration thrust-burns at the appropriate location (typically nodes or

apses) during the orbit. For a fixed, non-vectored thruster, when the duration of the thrust-burn is finite, gravity losses are encountered due to the misalignment of the thrust vector and the flight-path angle of the vehicle. By limiting the duration of each thrust-burn the gravity loss can be limited. Thus, by performing short-duration finite thrust-burns over many revolutions the required orbital transfer can be completed.

5.1.8 Carrier Vehicles

To enable the investigation of deployment strategy architectures using host-carrier vehicles additional input parameters are required by the deployment algorithm. In addition to a flag which indicates that a carrier vehicle is to be used to perform the deployment, the physical characteristics and propulsion system information of the host vehicle is required. An additional parameter which specifies the separation velocity capability of the vehicle can also be passed to the deployment algorithm. Typical linear deployment velocities for a CubeSat from P-POD or similar deployment mechanisms are of the order $0.3\,\mathrm{m\,s^{-1}}$ to $1.5\,\mathrm{m\,s^{-1}}$ [18, 73].

The deployment of the sub-satellites from the host-carrier vehicle is not analysed in detail. It is assumed that the separations result in a collision-free and stable deployment with only small separation distances between the satellites. Thus, the deployed satellites can be considered to have the same orbital parameters and will experience the same orbital perturbations. Specific strategies and mechanisms for deployments of this type are discussed by Bridges et al. [61] and Puig-Suari et al. [73].

5.1.9 Constellation Deployment Validation

To validate the developed method of constellation deployment the FORMOSAT-3/COSMIC mission was used. This mission is currently the only constellation to have been deployed using the method of indirect plane separation proposed by King and Beidleman [65] described previously in Section 2.2.2. Whilst a single point of validation is less than ideal in demonstrating the legitimacy and capability of the developed analysis method, the validation of the individual components comprising the analysis method can compensate for the lack of additional validation cases. The underlying method of semi-analytical propagation was individually validated in Section 5.1.6. Similarly, the validation of the spacecraft sizing module is presented later in Section 5.2.4.

The FORMOSAT-3/COSMIC Mission

The FORMOSA Satellite Series No.3/Constellation Observing System for Meteorology, Ionosphere and Climate (FORMOSAT-3/COSMIC) is a mission designed to perform GPS Radio Occultation (GPS-RO) of the atmosphere and ionosphere in order to provide near-real-time information for operational global numerical weather prediction, climate-change monitoring, ionospheric phenomena, and space weather research [43]. The constellation of six microsatellites was launched in April 2006 into a parking orbit and subsequently deployed into the configuration required to perform the GPS-RO mission.

Table 5.3: FORMOSAT-3/COSMIC mission specifications.

Property	**Value**
Number of Satellites	6
Number of Orbital Planes	6
Satellite Dry Mass [kg]	54
Satellite Fuel Mass [kg]	6.65
Thrust Force, BoL to EoL [N]	1.1 to 0.2
Specific Impulse [s]	217 to 194
Satellite Area [m^2]	$\frac{1}{2}(\pi \times 0.52^2 + 2(1.04 \times 0.165) = 0.5963$
Satellite Coefficient of Drag	2.2
Insertion Semi-major Axis, a [km]	6893
Insertion Eccentricity, e	0.003 23
Insertion Inclination, i [°]	71.992
Insertion RAAN, Ω [°]	301.158
Mission Semi-major Axis, a_i [km]	7178
Mission Eccentricity, e_i	< 0.014
Mission Inclination, i_i [°]	71.992
Mission RAAN, Ω_i [°]	Ω_1, $(\Omega_1 - 30)$, $(\Omega_1 - 60)$, $(\Omega_1 - 90)$, $(\Omega_1 - 120)$, $(\Omega_1 - 150)$ ± 5
Mean Anomaly Phasing, M_i [°]	M_1, $(M_1 - 52.5)$, $(M_1 - 105)$, $(M_1 - 157.5)$, $(M_1 - 210)$, $(M_1 - 262.5)$ ± 8

The primary requirement of the constellation configuration was separation of the six satellites into six different orbital planes spaced at 30°. Relative phasing of the satellites in adjacent planes by 52.5° was also specified in order to maximise the downlink of mission data to the groundstation. The constellation was deployed using the method of indirect plane separation using nodal precession over a period of 20 months. The initial satellite insertion orbit, constellation mission orbit and satellite properties of the mission are defined in Table 5.3. The deployment of the constellation was performed using individual blowdown monopropellant Hydrazine propulsion systems with gaseous Helium pressurant on each satellite.

During the deployment of the constellation a number of operational issues were encountered. The first of these issues was the result of a change in the constellation configuration from an inter-plane spacing of 24° to 30° at the request of the mission science team. To accomplish the deployment of this new configuration, the orbit-raising manoeuvre of FORMOSAT-3F was interrupted in order to achieve the increased plane separation. The consequence of this change in configuration was an increase in the total constellation deployment time of approximately six months [66].

The second major deployment issue was a propulsion system malfunction which occurred during the orbit-raising manoeuvre of FORMOSAT-3D, resulting in the incomplete deployment of the constellation. The satellite was unable to reach its intended mission orbit and therefore has a different orbital period to the remaining satellites [43, 66].

Other slight issues in the deployment of the constellation, documented by Fong et al. [43]. include discontinuities and flaws in the orbit-raising manoeuvres for the satellites. These differences are due to numerous thrust-burn failures and an issue with attitude control of the satellites whilst thrusting during sunlight-periods. In addition to wait-periods such that the thrust-burns could be performed during periods of eclipse, the success-rate of the propulsion system use ranged from 49.8 % to 86.2 %. As a result, the orbit-raising profiles of the satellites are not continuous and smooth.

Simulation of FORMOSAT-3/COSMIC Constellation Deployment

The input variables for the deployment analysis of the FORMOSAT-3/COSMIC constellation are detailed in Table 5.3, derived from the mission requirements of the constellation and satellite information provided by Fong et al. [43, 66].

The result of the simulated deployment of the FORMOSAT-3/COSMIC constellation mission is presented in Figure 5.12 alongside the actual deployment profile of the satellites. Comparison of these two datasets immediately indicates the discrepancies between the intended deployment procedure of the constellation and the actual execution. This is shown most clearly by the interrupted deployment profile of FORMOSAT-3F and the incomplete orbit-raising of FORMOSAT-3C, resulting in a final semi-major axis of approximately 7100 km. Aside from these operational discrepancies, the orbit-raising traces of the simulated deployment appear to

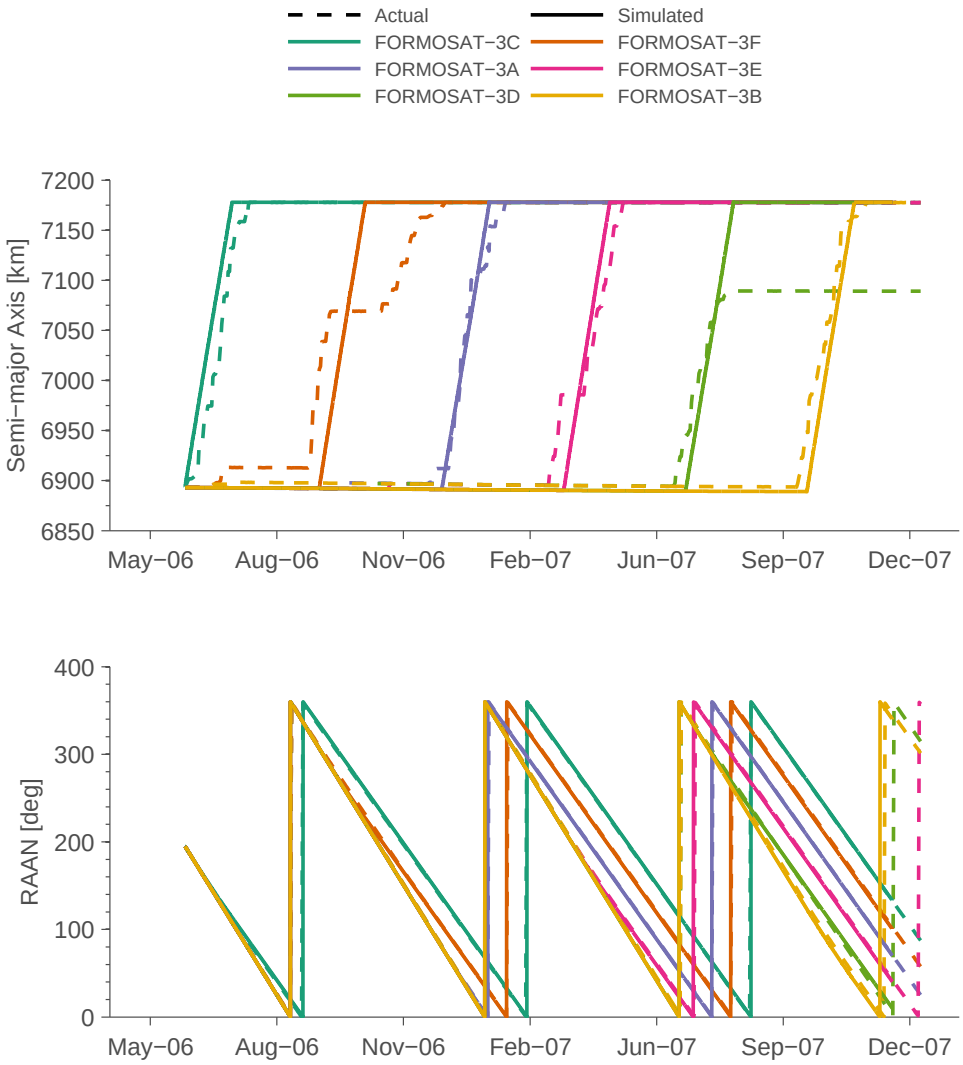

Figure 5.12: Semi-major axis and RAAN of simulated and actual FORMOSAT-3/COSMIC mission deployment.

Table 5.4: Calculated ΔV requirement for FORMOSAT-3/COSMIC deployment.

Satellite	**Simulated ΔV [m s^{-1}]**	**Actual ΔV [m s^{-1}]**	**Error [%]**
3C (FM5)	152.2	153.1	0.59
3F (FM2)	152.6	154.0	0.91
3A (FM6)	153.0	153.0	0.00
3E (FM4)	153.7	154.0	0.19
3D (FM3)	154.1	107.9[a]	42.82
3B (FM1)	154.5	129.8[b]	19.03

[a] Propulsion system failure
[b] Minimum ΔV for transfer is 152.1 m s^{-1}

match the average gradient of the actual orbit-raising procedures in semi-major axis. Similarly, the separation of the satellites in RAAN is well characterised by the simulation method, resulting in the desired angular separations at the end of the deployment period.

Small levels of underestimation of the gradient at the beginning and overestimation at the end of each orbit-raising segment can be attributed to the use of a single nominal value for the thrust of each satellite. A varying magnitude of thrust from beginning to end of life is more characteristic of a blowdown cold-gas thruster propulsion system. However, due to the increased complexity of modelling the thrust and specific impulse blowdown curves as functions of remaining tank pressure, average values for these parameters were chosen to approximate the effect of blowdown.

The simulated and actual ΔV required by each satellite to perform the necessary orbit-raising manoeuvre to achieve the deployment is presented in Table 5.4. For the actual deployment, the useful ΔV for each satellite was calculated from the average increase in semi-major axis per thrust-burn and the number of thrust-burn events recorded for each satellite as reported by Fong et al. [43]. The small differences in ΔV between the satellites are due to the orbital decay experienced by the satellites. The satellites which remained in the lower altitude initial orbit for longer experienced drag effects over an extended period and therefore required slightly larger orbit-raising manoeuvres in order to achieve the final mission orbit. This supports the hypothesis that consideration of the orbital decay which satellites will experience during the deployment procedure is critical, requiring the use of a complex atmospheric density model.

The ΔV calculated during the simulation can also be compared to the actual ΔV utilised by each satellite during the deployment of the constellation. For FORMOSAT-3C, FORMOSAT-3F, FORMOSAT-3A, and FORMOSAT-3E, the error in simulated ΔV is less than 1 %, indicating that the simulation method is capable of modelling the deployment of the constellation and

the propulsive capability which is required. However, for FORMOSAT-3D and FORMOSAT-3B significant errors in ΔV are present. The error between the actual and simulated ΔV for FORMOSAT-3D can be attributed to the propulsion system failure that the satellite experienced, thus preventing the satellite from completing the intended manoeuvre. With regards to the error in ΔV calculated for FORMOSAT-3B, it appears that the published data for the thrust-burn performance for the satellite is incorrect as a minimum ΔV of $152.1\,\mathrm{m\,s^{-1}}$ is required to perform the orbit transfer from the initial orbit with a semi-major axis 6893 km to the mission orbit of 7178 km.

5.2 Spacecraft and Propulsion System Sizing

During the conceptual and early preliminary design phases of a constellation mission the design of the individual spacecraft comprising the constellation may not have been initiated or any early designs may be associated with high uncertainty due to the coupling between the different elements of the design.

In the absence of the necessary vehicle design information, the parameters required by the constellation deployment procedure can be replaced with suitable estimated values. In order to perform the analysis of constellation deployment, the propulsion system characteristics and physical parameters of the spacecraft should be approximated.

In order to generate a set of representative characteristics for a spacecraft prior to the actual design of the vehicle, a spacecraft sizing procedure can be used. The use of such a method enables the calculation of approximate physical characteristics of the spacecraft given an initial dry mass, propulsion system parameters, and the required capability of the propulsion system. A set of representative models which estimate the characteristics of different propulsion systems is also necessary to support the spacecraft sizing method and ensure the feasibility of the approximated spacecraft design.

5.2.1 Spacecraft Sizing

The design of the individual vehicles comprising a constellation typically forms a discrete discipline within the overall system design process for a satellite constellation. However, in the absence of detailed design information, an estimated dry-mass of the satellite can be used in conjunction with a method of weight budgeting and top-down subsystem allocation to perform

the preliminary sizing of the vehicle, for example the method presented by Wertz and Larson [28]. In this method, the payload of the spacecraft is used to determine the initial spacecraft configuration and an estimate of the dry-mass of the spacecraft based on ratio of dry-mass to payload mass in the empirically determined range of 2:1 to 7:1. Subsystem mass budgets can then be allocated in a top-down fashion before individual subsystem design analyses are performed to determine individual subsystem performance and compliance with the design requirements and constraints. An iterative process can then used to perform system-level trades between the individual subsystems and update the top-level allocation to generate an acceptable system design.

To perform the sizing of satellites comprising a constellation requiring deployment, the procedure shown in Figure 5.13, based on the sizing process of Wertz and Larson [28], was implemented. For the design-space exploration of constellation deployment, the effect of different propulsion system type and propulsive capability will determine the amount of propellant required and therefore the total wet-mass of each satellite. The fraction of the satellite mass allocated to the required propulsion system, including tank mass and additional power system requirements, is also of interest as less mass may be reserved for the remaining subsystems. Finally, the cross-sectional area of the satellite plays a key role in the interaction of the satellite body with the atmosphere, affecting the magnitude of drag experienced, and must therefore also be considered.

Propulsion System Mass

To calculate estimated values of the total mass and cross-sectional area of these spacecraft from the known dry-mass, the mass of fuel required to perform the necessary manoeuvres is required. The mass of the propulsion system can then be estimated by considering the propulsion system type, propellant type and volume, and required thrust. Finally, the cross-sectional area of the satellite can be estimated heuristically from the total wet mass of the spacecraft.

First, to calculate the mass of propellant needed by the satellite, the propulsive requirement of the deployment strategy must be understood. The total ΔV requirement of each vehicle can be estimated by considering the propulsive manoeuvres which will be required in order to perform the constellation deployment. Simple reduced order models for the required orbital manoeuvres can be used to generate the estimates for the necessary ΔV contributions. Given

Figure 5.13: Vehicle and propulsion system sizing procedure.

an initial guess of wet mass, the required propellant mass can be found by iteration of the modified rocket equation, Eqn. (5.15).

Following calculation of the required propellant mass and the corresponding wet-mass of the spacecraft, the representative mass of the propulsion system, m_{PS} can be calculated using Eqn. (5.16), in which the mass of the thrusters, total propellant, pressurant if used, and tank masses are summed. An additional mass contribution related to the power system requirement of the propulsion system can also be included. System mass margins η_i, are also incorporated to account for uncertainty in the calculated propellant requirement, tank ullage, and propulsion system dry mass, thus providing a conservative mass estimate for the wet propulsion system mass.

$$m_{PS} = (m_{tank} + m_{thruster} + m_{power})\,\eta_1 + m_p\eta_2 \tag{5.16}$$

The dry-mass fraction of the propulsion system $f_{PS,d}$ and the total propulsion-system-mass fraction of the spacecraft f_{PS} can then be calculated from the propellant mass m_p, propulsion system dry mass $m_{PS,d}$, and satellite dry mass m_{dry} using Eqns. (5.17a) and (5.17b).

$$f_{ps,d} = \frac{m_{PS,d}}{m_{PS}} \tag{5.17a}$$

$$f_{PS} = \frac{m_{PS}}{m_{dry} + m_p} \tag{5.17b}$$

Calculation of Tank Mass

Given the calculated propellant mass required in order to perform the necessary orbital manoeuvres, the mass of the tanks used to store the propellant and pressurant can be estimated. To simplify the estimation of tank mass it is assumed that the tanks are spherical. The mass of the tank can then be calculated using Eqn. (5.18) by considering the volume required by the propellant V_p, the wall-thickness t_{wall} that is necessary to support the pressure of the contained volume, and the density of the material ρ_{tank} used for the tank construction. A safety factor, SF is also included during the calculation of required wall-thickness.

$$m_{tank} = \frac{4}{3}\pi\left(R_{tank}^3 - r_{tank}^3\right)\rho_{tank} = \frac{4}{3}\pi\left[\left(r_{tank} + t_{wall}\right)^3 - r_{tank}^3\right]\rho_{tank} \tag{5.18}$$

Table 5.5: Propulsion system tank materials. Adapted from Humble et al. [194]

Material	**Density, ρ [kg m^{-2}]**	**Yield Strength, σ [MPa]**	**Propellant Compatibility**
Aluminium	2800	413	Hydrazine Hydrogen Peroxide Hydrogen
Titanium	4460	1230	Nitrogen Helium Water Ammonia Xenon Argon Sulphur Hexafluoride Butane R-134a Carbon Dioxide AF-M315E Nitrogen Dioxide

.

where the tank radius and wall-thickness can be calculated:

$$r_{tank} = \sqrt[3]{\frac{V_p}{\frac{4}{3}\pi}} \tag{5.19a}$$

$$t_{wall} = SF\frac{P_{max}r_{tank}}{2\sigma_{yield}} \tag{5.19b}$$

Whilst the tank material with the highest yield-strength for the lowest mass would be the obvious choice, compatibility of the tank material with the chemical properties of the propellant must be ensured. The properties and compatibilities of common spacecraft propellant tank materials is shown in Table 5.5.

For gaseous propellants in blowdown mode, a volume of propellant will remain in the tank after the minimum feed-pressure has been reached. The mass of this leftover propellant can be calculated under the assumption that the propellant behaves as an ideal gas which fills the volume of the tank. The maximum pressure of the tank is calculated by considering the initial mass of propellant. An optimisation scheme used by Chiasson and Lozano [195], composed using Eqns. (5.18) and (5.20a) to (5.20c) can be used to find the minimum combined mass of the tank and leftover propellant.

$$m_{p,leftover} = m_{p,total} - m_{p,required} \tag{5.20a}$$

$$V_{tank} = \frac{m_{p,leftover} RT}{P_{min} M_p} \tag{5.20b}$$

$$P_{max} = \frac{m_{p,total} RT}{V_{tank} M_p} \tag{5.20c}$$

For self-pressurizing liquid propellants (eg Carbon Dioxide, Ammonia), the high-vapour pressure of the propellant can be used to force the liquid phase propellant out of the tank. Under these conditions, the mass of leftover propellant can be calculated by considering the mass of saturated vapour which would remain in the tank. By iteration of Eqns. (5.21a) to (5.21c), assuming in the first case that there is no leftover propellant, the total propellant mass can be calculated. The iterative procedure can be controlled by imposing convergence criteria on the value of calculated leftover propellant mass.

$$m_{p,total} = m_{p,required} + m_{p,leftover} \tag{5.21a}$$

$$V_{tank} = \frac{m_{p,total}}{\rho_p} \tag{5.21b}$$

$$m_{p,leftover} = \frac{V_{tank}}{\nu_{p,g}} \tag{5.21c}$$

Liquid propellants can also be maintained at a constant feed-pressure by using an additional pressurant at high pressure. The mass of pressurant required to provide the system-feed pressure can be calculated using the ideal gas equation, the combined volume of the propellant and pressurant tanks, and the minimum required feed pressure of the system, as in Eqn. (5.22a). The initial volume of pressurant required can then be calculated using the initial pressurant pressure and mass of pressurant required, as in Eqn. (5.22b). The total tank volume can then be calculated using Eqn. (5.22c). Iteration of these equations with an initial condition of no pressurant mass can then be used to find the total combined tank volume and subsequently the total tank mass including pressurant mass.

$$m_{pressurant} = \frac{\left(V_{propellant\_tank} + V_{pressurant\_tank}\right) P_{min} M_{pressurant}}{RT} \tag{5.22a}$$

$$V_{pressurant} = \frac{m_{pressurant} RT}{M_{pressurant} P_{pressurant}} \tag{5.22b}$$

$$V_{total} = V_{pressurant} + V_{propellant} \tag{5.22c}$$

For bipropellant propulsion systems requiring separate fuel and oxidiser tanks, the above method for sizing of liquid propellant tanks with a pressurizing gas can be performed for both the fuel and oxidizer individually assuming that the nominal mixture ratio, or oxidiser-to-fuel ratio, of the system is defined. The mass of the fuel and oxidiser given the total required propellant can be calculated from the nominal mixture ratio r_{mix} using Eqns. (5.23a) and (5.23b).

$$m_{fuel} = \frac{m_{propellant}}{1 + r_{mix}} \tag{5.23a}$$

$$m_{ox} = \frac{m_{propellant}}{1 + \frac{1}{r_{mix}}} \tag{5.23b}$$

Power System Mass

A key trade off between different propulsion system types is the amount of power required for their operation. For example, for development of thrust along a single axis, a cold gas thruster system may only require enough power to actuate a single valve, whereas the power requirement for an electrostatic propulsion system may be three or more orders of magnitude greater. In order to capture this effect the power requirement of different propulsion system types can be transformed into an equivalent mass using a measure of power density. In this way, the contribution of the propulsion system to the mass required by the power-subsystem of the spacecraft can be estimated and used to more effectively explore the trade between different propulsion system types.

The value of power density used to define the mass contribution of the propulsion system is reflective of the type of power subsystem used by the spacecraft. Chiasson and Lozano [195] use a power density of $0.015\,\mathrm{kg\,W^{-1}}$, assuming that solar arrays are used as the power source and that power-processing hardware is included in the estimate. Humble et al. [194] indicate power densities in the range of $0.0072\,\mathrm{kg\,W^{-1}}$ to $0.0250\,\mathrm{kg\,W^{-1}}$ for planar solar arrays at beginning-of-life, whilst Wertz and Larson [28] suggest a nominal value of $0.04\,\mathrm{kg\,W^{-1}}$ at end-of-life. Current COTS solar arrays for nanosatellites have characteristic power-densities in the range $0.012\,\mathrm{kg\,W^{-1}}$ to $0.025\,\mathrm{kg\,W^{-1}}$ [196, 197].

Ongoing development and improvement in solar cell and power management technology may be able to improve the power density of the systems available to small satellites, affecting the trade between different propulsion system types.

Estimating Cross-sectional Area

Given the total mass of a satellite, the volume and area can be estimated using trends fitted through the data of historical satellites. Rules for estimating the volume V and average cross-sectional body area A from satellites of mass m over the range of 35 kg to 3625 kg are shown in Eqns. (5.24a) and (5.24b), given by Wertz and Larson [28].

$$Vol = 0.01m \tag{5.24a}$$

$$A = \left(0.25m^{1/3}\right)^2 \tag{5.24b}$$

However, for smaller nanosatellites and picosatellites, these rules appear to systematically overestimate the volume and area. For example, use of the full 1.33 kg mass allocation allowed for a 1U CubeSat results in a density of 1330 $\mathrm{kg\,m^{-3}}$ rather than the 100 $\mathrm{kg\,m^{-3}}$ predicted by these relationships. The poor fit of this trend for small satellites is demonstrated by Figure 5.14, which shows the described area-mass relationship significantly diverge from the actual data with decreasing satellite mass.

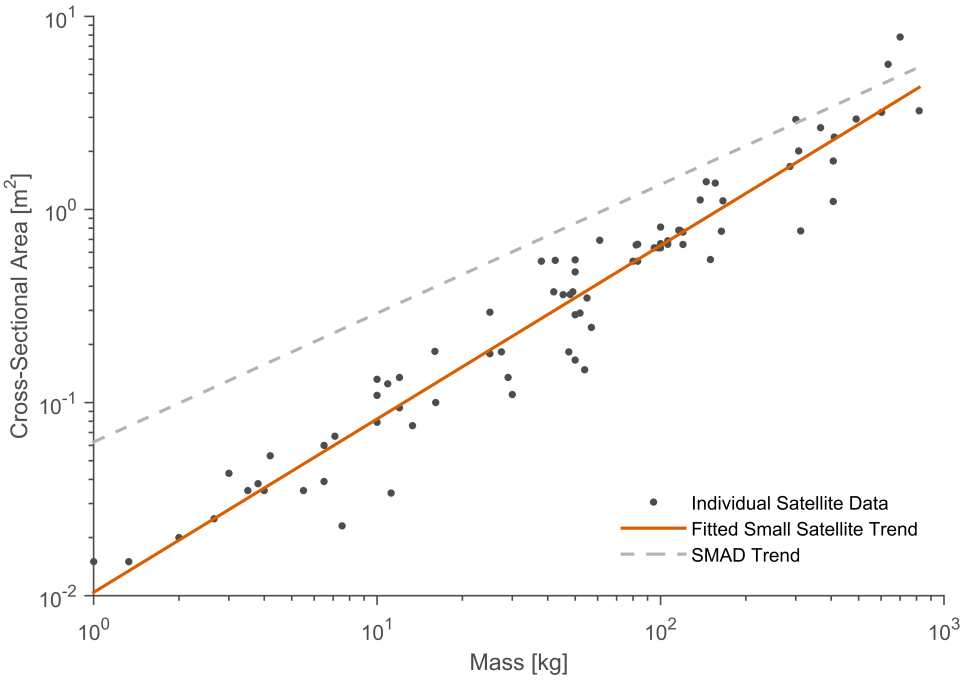

Figure 5.14: Relationship between mass and cross-sectional area of small satellites.

In order to develop a new sizing relationship for small satellites, primarily to provide a method for estimating the cross-sectional area, a survey of small satellites for which both mass and external dimensions was available was performed. The cross-sectional area for each satellite was subsequently calculated using modified forms of Eqn. (5.13) based on the particular shape of each satellite. The relationship between mass and calculated cross-sectional area of these satellites is presented in Figure 5.14. The resulting trend can be characterised by the power function shown in Eqn. (5.25) and as the trend-line in Figure 5.14.

$$A = 0.0104m^{0.8980} \tag{5.25}$$

5.2.2 Sizing of Carrier Vehicle Spacecraft

The exercise of sizing carrier-type vehicles for constellation deployment can be treated as analogous to the specification of other orbital transfer vehicles or "space-tugs". A number of existing studies have been performed which include mass-budgets or information about the design of such vehicles. The relevant aspects of these studies is discussed herein.

In the study of constellation deployment using EML-1, Chase et al. [68] specify a spacecraft bus to payload mass fraction of 0.80 and a bipropellant propulsion system sized to 18 % of the required propellant mass given a specific impulse of 315 s. The mass of the ballute aerocapture device was not included in the mass of the spacecraft bus, but was included as a discrete component during the calculation of the total vehicle mass.

The sizing of pallet-vehicles by King and Beidleman [65] specifies a dry-mass of 56.66 kg to support the deployment of four microsatellites of 11.3 kg, resulting in a payload fraction of 0.80. However, in this study it was assumed that the pallet-vehicle was comprised of primarily the solid-rocket motor casing, also providing the primary structure of the vehicle, and the separation mechanisms for the individual satellites, resulting in a high payload fraction.

The Surrey Small-Satellite Transfer Vehicle (S3TV), presented by Ward et al. [63] is designed to deploy up to 36 3U CubeSats or 4 microsatellite payloads with a nominal mass of 15 kg. A Nitrous Oxide and HDPE hybrid propulsion system with a specific impulse of 250 s is proposed to provide a nominal of ΔV of 500 m s^{-1}. With an approximate launch mass of 170 kg, the payload to spacecraft dry-mass fraction can be calculated to be 0.43.

The design of a microsatellite space-tug vehicle is explored by Baker et al. [64]. The vehicle was designed to perform large orbit-transfer manoeuvres using a bipropellant system with a

specific impulse of 250 s. With a payload mass of 100 kg at maximum specification, the wet mass of the vehicle is stated to be 180 kg providing a ΔV of 130 m s^{-1}, corresponding to a payload to dry-mass fraction of 0.59.

A dispenser-spacecraft was designed to carry the 92 10 kg nanosatellites for the DRACO constellation mission to investigate the dynamics of the magnetotail [198]. The mass-budget of the dispenser-ship indicates a dry-mass of 216.9 kg, including a 50 kg allocation for the bipropellant propulsion system but excluding the mass of the payload. A further 202 kg of propellant mass is specified in order to provide the necessary ΔV for the orbital transfers. The resulting payload fraction can be calculated to be 0.81.

Carrier Vehicle Sizing Procedure

The sizing process for a generic host-vehicle carrying multiple sub-satellites to be deployed can be performed using the same process described previously and shown in Figure 5.13. However, the initial mass of the carrier vehicle is dependent on the mass of the satellites contained, and cannot therefore be determined prior to the sizing of the individual satellites.

In order to provide a dry-mass estimate of the carrier vehicle the manifested satellites are considered to be the payload of the spacecraft. A suitable ratio of payload mass to dry-mass of the spacecraft can then be used to define the dry mass. Typical payload mass to spacecraft dry-mass ratios are stated by Wertz and Larson [28] to lie in the range of 1:2 to 1:7, or as fractions approximately 0.14 to 0.50. However, as evidenced by the other studies which have investigated the design of transfer or carrier-type vehicles, the payload fraction can exceed this typical range due to the simple requirements of the spacecraft.

Following specification of the payload and propulsion system mass, the remaining mass of the spacecraft is allocated to the remaining subsystems, often referred to as the bus, for example: structure, thermal, power, communications, attitude determination and control, command and data handling. By imposing a minimum fraction of the spacecraft dry-mass which is reserved for these subsystems, the propulsion system and vehicle can be sized accordingly given only the payload mass which is to be carried.

An iterative procedure is proposed which steadily decreases the specified payload fraction of the spacecraft until the required fraction of the spacecraft allocated to the bus-systems is obtained. The operation of this procedure is described graphically in Figure 5.15.

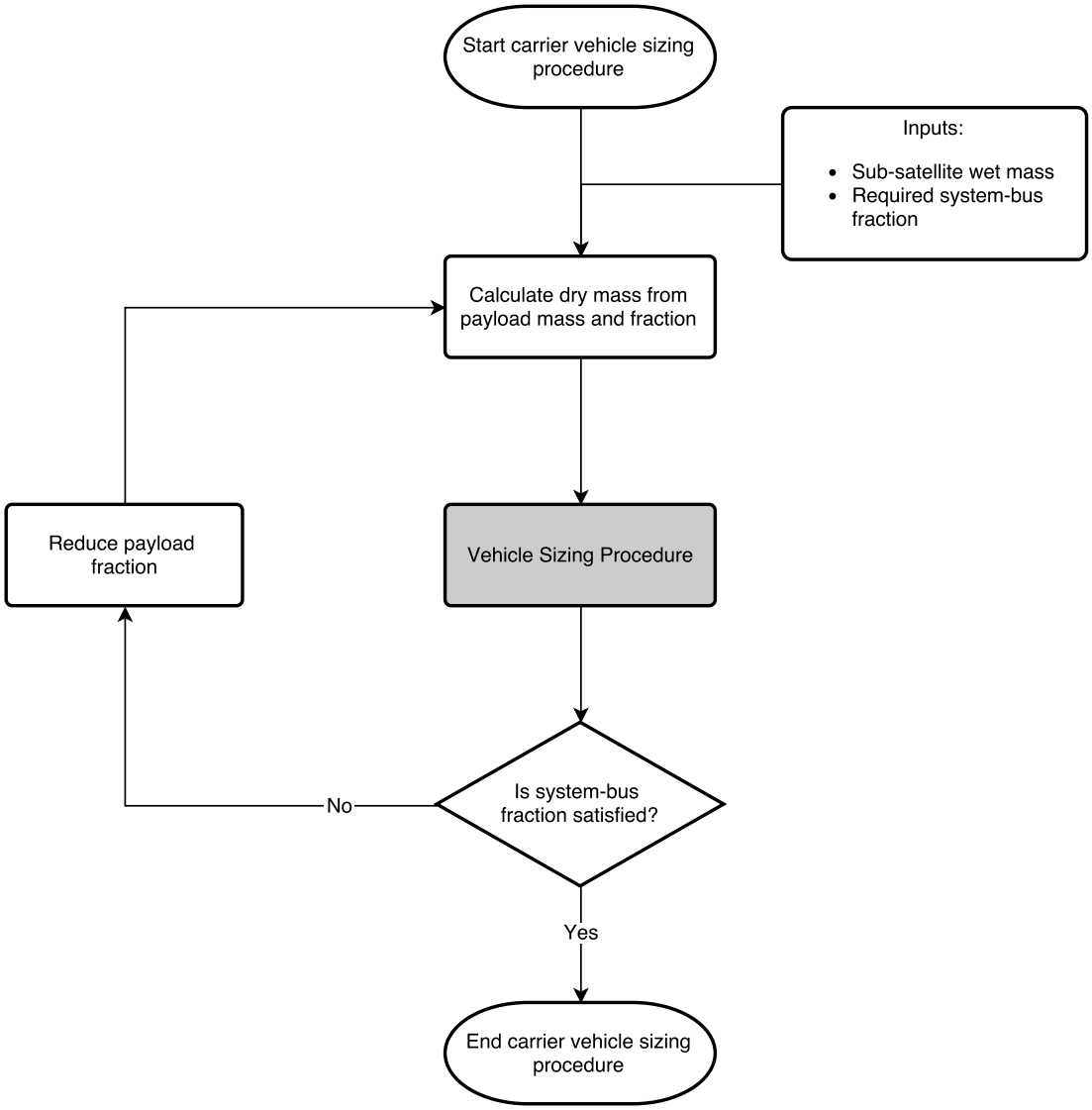

Figure 5.15: Modification of spacecraft sizing procedure for carrier-type vehicles.

5.2.3 Propulsion System Characterisation

A method of defining the major characteristics of different propulsion systems is required to provide information needed to perform the preliminary sizing of a spacecraft. In the absence of detailed information about the vehicle design and the actual propulsion systems to be used a surrogate modelling method can be used to provide representative information. Most importantly the specific impulse of the propulsion system is required in order to calculate the mass of propellant needed to perform the orbital manoeuvres. However, additional parameters such as the mass of propulsion system hardware and power requirement of the system can be used

to determine the feasibility and cost of integrating the chosen propulsion system with the rest of the spacecraft.

A method of modelling these primary propulsion system characteristics was developed by Chiasson and Lozano [195], focusing on low-thrust propulsion systems of less than 10 N. The developed method operates by identifying trends or relationships that exist between the system characteristics of different propulsion system models contained in a master database. Once determined, these relationships can then be used to predict the major characteristics of thruster models not contained within the database.

The methodology of Chiasson and Lozano [195] has been used in this study with an extended database of propulsion system models and newly fitted relationships. These relationships determined by regression methods are presented in Appendix C, categorised by propulsion system type.

Using this method, a minimum of three inputs are required in order to generate a characteristic propulsion system: propulsion system type, propellant type, and required thrust. In order to ensure that the available thrust range is feasible for the propulsion system type and propellant chosen, a thrust scalar (value from 0 to 1) can be used instead, enabling a thrust value between the minimum and maximum thrust values in the database to be chosen.

Given the inputs and system relationships, the propulsion system model provides the following outputs: specific impulse, pressure, power, and thruster mass. Depending on state, the propellant and pressurant molar mass, density, specific volume of vapour at saturation, and vapour pressure are also provided to enable the sizing of the required tanks.

This method of propulsion system modelling enables flexibility in the system types and propellant combinations which can be considered by the design-space exploration method. With improving propulsion system technology and the development of novel systems, the database can be expanded and new trends and relationships identified. The existing propulsion system types can then be updated using the new relationships, or new propulsion system types defined.

5.2.4 Validation of Spacecraft Sizing Method

Validation of the spacecraft and propulsion system sizing methodology can be performed by comparing the design of actual spacecraft and satellites to the parameters which can be obtained using the developed method. The required input variables to perform the sizing of a spacecraft are total mission ΔV, dry mass, thrust, and propulsion system and propellant type. The total

mass of the spacecraft, masses of the propulsion subsystem and components, power requirement, specific impulse and cross-sectional area can then be compared to actual missions.

Whilst the use of the sizing method ensures that all of these parameters are enumerated, the available and published information about actual missions is often incomplete. The system parameters obtained from the sizing methodology may therefore have to be compared against incomplete sets of data. In the following sections, the developed sizing method is validated using four actual spacecraft of a range of different sizes, missions, and propulsion system types.

RapidEye

RapidEye is a commercial Earth observation constellation consisting of five identical microsatellites based on the SSTL-150 platform. The RapidEye satellites are of cuboid shape with three body-mounted solar panels, a three-axis attitude control system, and an approximate mass of 155 kg each. A Xenon "warm gas" resistojet propulsion system providing a ΔV of 35.4 $\mathrm{m\,s^{-1}}$ is used by the satellites to perform insertion orbit corrections and constellation set-up and management manoeuvres [199]. The propulsion system features a single resistojet thruster of nominal 0.018 N, requiring 30 W of power during operation, and a spherical propellant tank manufactured from Titanium alloy Ti-6Al-4V.

The comparison between the actual system parameters and parameters predicted by the developed sizing procedure are presented in Table 5.6. The input variables used to direct the sizing procedure are also presented at the top, derived from the actual mission and spacecraft parameters.

Table 5.6: Comparison of actual and modelled propulsion system and physical parameters of RapidEye satellite. Input variables required by the sizing method are shown in the top section.

	Actual [200, 199]	**Calculated**
ΔV [$\mathrm{m\,s^{-1}}$]	35.4	
Dry Mass [kg]	143	
Thrust [N]	0.018	
Wet Mass [kg]	155	154.9
Propulsion System Mass (dry) [kg]	-	18.6
Propellant Mass [kg]	12	11.94
Thruster Mass [kg]	0.065	0.676
Tank Mass [kg]	4.5	3.83
Propulsion System Power [W]	30	29
Specific Impulse [s]	48.3	45
Cross-sectional Area [$\mathrm{m^2}$]	1.37	0.95

A number of differences exist between the actual and predicted system parameters. Most significantly, the predicted thruster mass is much greater than the actual thruster mass utilised on the satellite. This difference can be attributed to the lack of relationship used to predict the thruster mass from the required thrust magnitude. Due to the sparsity of available data on resistojet thruster systems, no reliable trend could be identified between thrust magnitude and thruster mass. An average value of the thruster mass is therefore used.

Secondly, the sizing method predicts a smaller tank mass than specified for the actual spacecraft. Whilst the sizing method and actual design utilise the optimal spherical tank for minimum mass, the design of the actual tank will encompass issues relating to the manufacture of the pressure vessel. In order to produce a spherical tank welded or riveted seams are required which will contribute additional mass to the structure. Further mass may also be required in order to ensure that the pressure vessel satisfies the safety requirements when potential material and manufacturing defects are considered.

Finally, a smaller average cross-sectional area of the satellite is predicted by the sizing method than is true of the actual satellite. This difference in cross-sectional may be due to the payload carried by the satellite, a multi-spectral imaging system consisting of three mirrors to achieve the required optical resolution. The internal volume required by optical systems is typically greater than other payload types, thus resulting in above average external dimensions and therefore cross-sectional area.

THEMIS

The THEMIS (Time History of Events and Macroscale Interactions during Substorms) mission is a constellation of five identical microsatellites designed to investigate substorms in the magnetosphere of the Earth [201]. The THEMIS satellites, frequently referred to as probes, require significant propulsive capabilities in order to achieve the required spatial separation in the magnetotail to perform the mission. The probes each use a hydrazine monopropellant propulsion system to achieve and maintain the highly elliptical orbits with required inclinations between 4.5° to 9° and apogee radii ranging from ∼10 R_E to ∼30 R_E. A total ΔV of 940 $m\,s^{-1}$ was required by the probe with the largest apogee radius to achieve the desired mission orbit. Each satellite was equipped with the same volume of propellant and identical propulsion systems consisting of two spherical propellant tanks, a single helium pressurant tank, and four 4.4 N thrusters.

Table 5.7: Comparison of actual and modelled propulsion system and physical parameters of THEMIS satellite. Input variables required by the sizing method are shown in the top section.

	Actual [201]	**Calculated**
ΔV [m s^{-1}]	940	
Dry Mass [kg]	77	
Thrust [N]	4 x 4.4	
Wet Mass [kg]	126	119.0
Propulsion System Mass (dry) [kg]	<12	11.2
Propellant Mass [kg]	49	42.0
Thruster Mass [kg]	-	1.13
Tank Mass [kg]	-	9.80
Propulsion System Power [W]	-	7.86
Specific Impulse [s]	200	220
Cross-sectional Area [m^2]	0.78	0.75

Comparison of the actual and predicted system values for the THEMIS satellites, shown in Table 5.7, indicates that the sizing method has been able to generate a system which is generally characteristic of the actual spacecraft.

However, this validation case illustrates one of the shortcomings of the propulsion system modelling method. Whilst four thrusters are specified by the actual system, the sizing method only predicts the use of a two thrusters due to the range of the underlying database. The relationship between thruster mass and thrust magnitude, shown in Appendix C, is used to predict thruster mass. For comparison, the selection of four 4.4 N thrusters would result in a combined mass of 1.67 kg, whilst the the two 8.8 N thrusters result in a mass of 1.13 kg.

Whilst the issue of thruster selection contributes to the overall under-prediction of the satellite wet mass, the difference in propellant mass of 7 kg is more significant. This difference may result from the lower reported specific impulse of the actual system in comparison to that predicted by the propulsion system characteristics model. A greater mass is therefore required to produce the same ΔV.

CNES DEMETER

The DEMETER (Detection of Electromagnetic Emissions Transmitted from Earthquake Regions) spacecraft is a 130 kg satellite developed by the French government agency CNES. The DEMETER satellite is based on the cuboid-shaped Myriade, EADS Astrosat-100, small satellite platform with a two panel external solar array for power generation. The satellite operates in a nominally 715 km Sun Synchronous Orbit (SSO), studying the ionosphere for the effects of geophysical activity, primarily earthquakes. A blowdown hydrazine monopropellant propulsion

Table 5.8: Comparison of actual and modelled propulsion system and physical parameters of DEMETER satellite. Input variables required by the sizing method are shown in the top section.

	Actual [202, 203]	**Calculated**
ΔV [m s^{-1}]	100	
Dry Mass [kg]	95.5	
Thrust [N]	4 x 1	
Wet Mass [kg]	100	100.03
Propulsion System Mass (dry) [kg]	4.83	2.14
Propellant Mass [kg]	4.5	4.53
Thruster Mass [kg]	1.55	0.36
Tank Mass [kg]	1.2	1.06
Propulsion System Power [W]	-	7.9
Specific Impulse [s]	(BoL) 220	220
Cross-sectional Area [m^2]	0.690	0.643

system is specified for the spacecraft, principally to perform orbit raising manoeuvres using four thrusters each with a thrust of 1 N. A ΔV of 100 m s^{-1} was used as the reference propulsive requirement for the system development [202].

Similarly to the case study performed for the THEMIS satellite previously, the sizing method does not automatically consider the use of four individual thrusters when a single thruster satisfying the thrust requirement can be specified. For the DEMETER satellite, this results in the generation of a single thruster of 0.36 kg rather than four thrusters with a combined mass of 0.64 kg. In either case, the thruster mass is significantly less than the thruster mass reported by Salome [202] for the actual spacecraft. This difference in thruster mass, and a small difference in tank mass also contribute to the overall difference in propulsion system dry mass between the predicted and actual system.

Whilst the predicted cross-sectional area of the spacecraft appears to agree well with the actual value (<7 % error), this does not include the area contribution of the solar array which has an additional area of 9 m^2. Depending on the attitude of the spacecraft, the cross-sectional area with respect to the velocity vector may actually vary significantly from the predicted value. However, due to the altitude of the mission orbit of 715 km, the error in cross-sectional area has little effect on the drag experienced by the satellite compared to missions operating in orbits with lower altitudes.

TacSat-2 and MicroSat Systems Roadrunner

TacSat-2 is a technology demonstration satellite developed by the US Air Force Research Laboratory (AFRL). The objective of the development of the satellite is to demonstrate new rapid

Table 5.9: Comparison of actual and modelled propulsion system and physical parameters of TacSat-2 satellite. Input variables required by the sizing method are shown in the top section.

	Actual [204]	**Calculated**
ΔV [m s^{-1}]	154	
Dry Mass [kg]	362.5	
Thrust [N]	0.0128	
Wet Mass [kg]	367	365.7
Propulsion System Mass (dry) [kg]	-	28.7
Propellant Mass [kg]	4.5	3.2
Thruster Mass [kg]	<1	2.16
Tank Mass [kg]	-	1.05
Propulsion System Power [W]	200	1508
Specific Impulse [s]	1390	1784
Cross-sectional Area [m^2]	(Stowed) 2.65	2.06

design, build, and test processes, responsive launch and on-orbit operations, and test a number of different sensors and technologies. The TacSat-2 spacecraft, based on the MicroSat Systems Roadrunner platform, has a launch mass of 367 kg, is 3-axis stabilised, and features two external solar arrays deployed after launch and separation.

The demonstration and test of a low-power Hall-effect thruster is a key goal of the TacSat-2 mission. The specified Busek BHT-200-X3 Hall-effect thruster utilises Xenon propellant and is capable of up to 1600 s specific impulse whilst requiring less than 300 W (200 W nominal) of input power. The system properties for TacSat-2 are presented in Table 5.9.

The nominal specification and capability of the MicroSat Systems Roadrunner platform is different from the TacSat-2 spacecraft, and is presented in Table 5.10. Compared to TacSat-2, the dry mass of the spacecraft is significantly smaller, enabling a greater ΔV capability from the same nominal propellant mass.

Given the slightly differing specifications of the TacSat-2 satellite and the reference Roadrunner platform, the spacecraft sizing method was applied to both configurations. The result for TacSat-2 input variables is presented in Table 5.9, and for the Roadrunner platform in Table 5.10.

Comparison of these results illustrates a problem with predicting the performance of a low-power Hall-effect thruster system using the database of propulsion systems available. Due to the number of higher-powered systems in the database, the identified relationship between thrust and power favours high-power systems. Consequently, for a system requiring approximately 12.5 mN of thrust, a power of 1.5 kW and a specific impulse of 1783 s is specified. Furthermore,

Table 5.10: Comparison of actual and modelled propulsion system and physical parameters of MicroSat Systems Roadrunner platform. Input variables required by the sizing method are shown in the top section.

	Actual [205]	**Calculated**
ΔV [m s^{-1}]	260	
Dry Mass [kg]	305.42	
Thrust [N]	0.0125	
Wet Mass [kg]	309.9	310.0
Propulsion System Mass (dry) [kg]	12.9	29.3
Propellant Mass [kg]	4.5	4.58
Thruster Mass [kg]	1.12	2.16
Tank Mass [kg]	3.1	1.50
Propulsion System Power [W]	330	1504
Specific Impulse [s]	1300	1783
Cross-sectional Area [m^2]	(Stowed) 2.42	1.77

due to this overestimation of input power requirement, the propulsion system mass budget is also affected due to the accounting of power system mass required to operate the propulsion system. In response to this problem, an improvement to the propulsion system characterisation method was implemented. The database of Hall-effect thrusters was separated into high and low-power systems and two distinct sets of relationships generated. These relationships are presented in Appendix C.

Using the newly developed relationships for low-power Hall-effect thrusters, for the thrust requirement of 12.5 mN, a power of 272 W, a specific impulse of 1330 s, and thruster mass of 0.73 kg are predicted, matching the actual system properties of the Busek BHT-200 thruster much more closely.

Interestingly, for the case of the Roadrunner platform the predicted propellant mass required is greater than specified by the available documentation, in spite of the overestimation of specific impulse. However, on consideration of the ΔV requirement and the nominal and maximum specific impulse of the Busek BHT-200 system [206], the minimum propellant requirement can be calculated using the rocket equation, Eqn. (5.15), to be 5.85 kg and 5.09 kg respectively. In both cases, this is greater than the 4.5 kg that is specified for the actual Roadrunner platform.

Summary of Validation Cases

Whilst the comparison of actual satellite systems to those produced using the developed method of spacecraft and propulsion system sizing has indicated a number of problems with replicating

specific system parameters, the process of validation has demonstrated that the method is capable of generating characteristic propulsion systems and physical spacecraft parameters given the required inputs. The development of the vehicle sizing method can therefore be considered successful in the objective of supporting the analysis of different constellation deployment implementations.

A key factor in the development of the vehicle sizing method is the generation of the empirical relationships supported by databases of historical subsystem performance and satellite data. However, for certain system parameters or data-ranges, the sparsity or inconstancy of the available historical data can affect the developed relationships. Furthermore, the choice of system boundaries can have an equally significant effect, demonstrated by the example of the thrust-power relationship for Hall-effect systems previously. In this case, the benefits of low-power Hall-effect thrusters were overlooked due to the bias of the fitted relationship over the complete set of Hall-effect thrusters to high-powered systems.

Chiasson and Lozano [195] identify a number of further limitations of the propulsion system modelling method. Primarily, only spherical tank geometries are considered for simplicity of calculation. However, whilst a spherical tank is the most efficient design for minimum mass, cylindrical tanks with hemispherical or elliptical ends are often used when internal spacecraft volume and packing of components is an issue [194]. In addition to this, only a limited number of singular materials are considered for the tank construction, whereas many different materials and combinations may actually be used. Secondly, if able to, the propulsion system characterisation method will only specify the use of a single thruster with the necessary capability when on many missions multiple smaller thrusters are used for attitude control, additional manoeuvrability, or redundancy. Finally, only a single value of power density is considered for the calculation of required power subsystem mass. Additional values or scaling relationships relating to different power generation or storage technologies could be integrated to the method to enable the consideration of different power system architectures.

5.3 Cost Modelling

To determine the effect of different constellation deployment architectures on the cost of the spacecraft a method of estimating the cost is required. However, during the conceptual and preliminary design phases information about the design of the spacecraft is severely limited. A

method of bottom-up cost estimation by the addition of the different subsystem and integration costs is therefore unsuitable.

For system trade studies, in which the response of cost with variation in system parameters is of interest, parametric cost models are typically used [28]. A parametric cost model utilises a database of historical information to develop relationships between cost or other cost-related variables (eg labour, hours) and independent system design variables (eg weight, power, data-rate), typically using simple regression methods. These CERs can then be combined, aggregated, and averaged to generate a single cost estimate for the system.

In the context of the design-space exploration to be performed, the estimation of relative cost between different design architectures enables the system design team to understand the tradeoff in cost between designs. Relative cost is therefore of greater importance than the accuracy of the absolute cost estimate of the system which is output by the CERs. Furthermore, due to the high level of design uncertainty during the conceptual design phase, the accuracy of the absolute cost estimate is likely to be low.

A number of different parametric cost models for space systems are publicly available. However, many of these models are based on traditional large satellites and are therefore not appropriate for small satellite cost estimation which require different sets of CERs [207]. Ongoing technological development within the domain of small satellites may even necessitate the use of different cost models for different classes of satellite, illustrated by the emergence of the Aerospace Picosatellite Cost Model (A-PICOMO) for satellites with mass of 0.1 kg to 50 kg [208].

As the development of a new parametric cost model or set of CERs is beyond the scope of this research, the SSCM of the Aerospace Corporation and the USCM of the US Air Force is utilised.

Small Satellite Cost Model

The Small Satellite Cost Model (SSCM) is a set of CERs derived specifically for small satellites by the Aerospace Corporation [209]. The CERs are derived using a proprietary database of modern small satellites for which cost and technical system and subsystem data was collected. The CERs were identified by first examining linear and non-linear regression of individual variables against cost. Multi-variable relationships were then investigated and the appropriate CERs selected following comparison and analysis of the errors [210].

Due to the lack of available design information during the conceptual design phase many of the parameters required to enumerate the CERs of the Small Satellite Cost Model (SSCM) are not yet known. However, as evaluation of the relative cost between different design architectures for constellation deployment is the objective of the cost modelling module, only the CERs with parameters affected by the constellation deployment strategy need to be utilised.

In the absence of additional design data, only one appropriate CER is identified, shown in Eqn. (5.26). This relationship equates the cost of the spacecraft (Y_1 in FY97 \$M), to the downlink data rate (X_1 in kbps), average power (X_2 in W) and the propulsion subsystem dry mass (X_3 in kg) of the spacecraft.

$$Y_1 = 1.53 \left(X_1^{0.0107} \times X_2^{0.509} \times 1.0096^{X_3} \right) \tag{5.26}$$

To eliminate the additional dependent variables, the CER can be modified to become a simple proportional relationship, shown in Eqn. (5.27), valid for spacecraft with a dry bus mass of less than 400 kg and propulsion subsystems of dry mass of less than 35 kg. However, when made proportional, the cost is no longer an absolute measure and is only useful in comparing the relative cost between different designs. Alternatively, the additional dependent variables X_1 and X_2 can be replaced with suitable constant values set using assumptions based on the mission type.

$$Y_1 \propto 1.0096^{X_3} \tag{5.27}$$

Due to the limit on maximum spacecraft dry bus mass and propulsion subsystem dry mass that can be used to estimate satellite cost using the SSCM, an additional CER is required to enable the cost estimation of larger satellites or carrier vehicle spacecraft. For this purpose, the US Air Force (USAF) USCM will be used.

USAF Unmanned Space Vehicle Cost Model

The Unmanned Space Vehicle Cost Model (USCM) is a publicly available parametric cost model developed by the US Air Force to estimate the cost of satellite development and production. The model consists of a database of commercial, non-commercial (eg NASA, NOAA), and military satellite missions from which linear and non-linear CERs are derived.

The CERs, listed by Wertz and Larson [28], are taken from the theoretical first unit estimates from the 7th edition of the Unmanned Space Vehicle Cost Model (USCM). The relevant CER

is shown in Eqn. (5.28), relating the spacecraft dry bus mass (X_4 in kg) to the spacecraft cost (Y_2 in \$M).

$$Y_2 = \frac{43}{1000} X_4 \tag{5.28}$$

To enable compatibility of the two disparate CERs, a correction factor is applied which forces the two relations to be comparable at the crossover point of 400 kg spacecraft dry bus mass and 35 kg dry propulsion system mass.

Shortcomings of Cost Modelling Method

Whilst the method detailed herein enables a basic assessment of the comparative cost of different systems based on the drivers of propulsion system mass or dry bus mass, the method falls short of generating a true and representative cost of the total system. This is primarily due to the lack of vehicle design information which is necessary to utilise the full set of CERs of the SSCM or USCM to produce a complete cost estimate for the spacecraft. Information relating to the specific mission or operations of the constellation may be required to determine parameters such the pointing accuracy or downlink data rate, featured in the CERs of the SSCM. Additionally, in the absence of other design information, a tool for conceptual spacecraft design is necessary to perform the sizing of the different subsystems to estimate the mass and power budget needed by the cost models.

Furthermore, whilst the CERs used in this work enable comparison of systems with different propulsion architectures through the use of propulsion system dry mass or dry bus mass, additional characteristics of the different propulsion systems are not captured by the cost model and thus not reflected in the output cost metric. These overlooked characteristics may include factors such as complexity of design and manufacture; propellant safety, storability and material compatibility; and technology maturity which may significantly affect the cost of design and manufacture of the spacecraft.

5.4 Feasibility Screening

To reduce the computational burden of performing the full deployment analysis process for designs which result in infeasible solutions a coarse screening procedure can be implemented. The primary source of solution infeasibility for the different deployment strategies is due to

decay of the payloads before the required deployment is completed. This may be a result of low-altitude insertion orbit or mission orbits, long drift periods, or low ballistic coefficient.

The deployment strategy can also be checked to ensure that the required deployment of the constellation can be completed before an implemented deadline. To an approximation, using J2 perturbations only, the time required for two orbital planes to separate by a fixed angle can be calculated using Eqn. (2.4). Thus, using the maximum plane separation and the initial and mission orbit properties, an approximate deployment time for the constellation can be calculated.

In addition, using reduced-order analytical models for the required orbit transfer manoeuvres, an approximate ΔV for each vehicle can be calculated. Using the vehicle sizing method and propulsion system models described previously, the feasibility of vehicle design can assessed, primarily to check that a propulsion system mass fraction of 1 is not exceeded.

Whilst the estimated lifetime of the satellites in orbit could be determined using the semi-analytical orbit propagation method, the process for doing this for a population of designs would require a significant period of time. To reduce the time required to perform the feasibility check a surrogate model for orbital decay was developed, described below.

5.4.1 Predicting Orbital Decay

Response Surface Methodology (RSM) is an established metamodelling technique which utilises linear regression methods to generate a multidimensional surface or hypersurface to approximate a response given a set of selected input factors [211]. A Response Surface Equation (RSE), often of polynomial form, represents this surface as a function of the input factors. The RSE can therefore be used to estimate the value of the response given values for the different input factors.

To generate a RSE, a series of experiments are first carried out to measure the response variable for different specific combinations of the input factors. These combinations of the input factors are typically selected using Design of Experiments (DoE) methods which are driven by the expected form of the RSE [212].

A set of RSEs for time to decay were produced for different levels of solar flux and geomagnetic index, indicated in Table 5.11. Input factors of semi-major axis, eccentricity, inclination, and ballistic coefficient were selected to model the response of time to decay from orbit. Using these generated RSEs the time to decay of a satellite can be estimated for the different regimes

Table 5.11: Solar flux and geomagnetic index magnitude used to generate orbital decay RSEs.

Regime	**Solar Flux [SFU]**	**Geomagnetic Index [nT]**
Low	75	3
Average	150	15
High	200	28

of solar flux and geomagnetic index. These predictions for time to decay for different space weather regimes can then be used to screen the initial population for feasibility and filter the designs which feature satellites which decay from orbit before the planned deployment can be performed.

The low magnitude space weather regime corresponds to the minimum solar flux and geomagnetic index conditions expected, for example at solar minima, resulting in a maximum orbital lifetime prediction. If the time to decay constraint is violated under these conditions the strategy can therefore be considered infeasible. The RSEs for average and maximum space weather magnitude can be used similarly to determine whether the deployment strategy features marginal feasibility or no risk of orbital decay before the deployment is complete.

Initially, an *I-optimal* design using the JMP statistical software of the SAS Institute was used to to generate points to fit a third-order polynomial response surface. The RSE was then generated for each set of data and analysed for fit and residual violations. For this structured DoE formulation of 29 runs, the default size for 4 inputs, the matrix of input factors is shown in Figure 5.16. A set of 200 randomly generated points used for the validation of the RSEs are also shown in Figure 5.16 for reference. The structure of the DoE formulation is illustrated by the pattern of the points in the input factor matrix plot.

The fit of the model and residual analysis are shown in Figure 5.17. The plot of actual against predicted time to decay shows a linear relationship, indicating that the generated response surface is capable of estimating the time to decay. In the plot of residuals the error in time to decay is shown against the predicted time to decay. A negative error indicates a longer time to decay predicted by the RSE than the time to decay calculated by propagation. Consideration of the residuals reveals that significant errors are present in the time to decay predicted by the model. Whilst the error in time to decay of the points used to generate the RSE appear low, the error for the randomly generated points are significant and also appear to grow with the time to decay. Furthermore, the errors appear to show a negative bias, indicating that the RSE

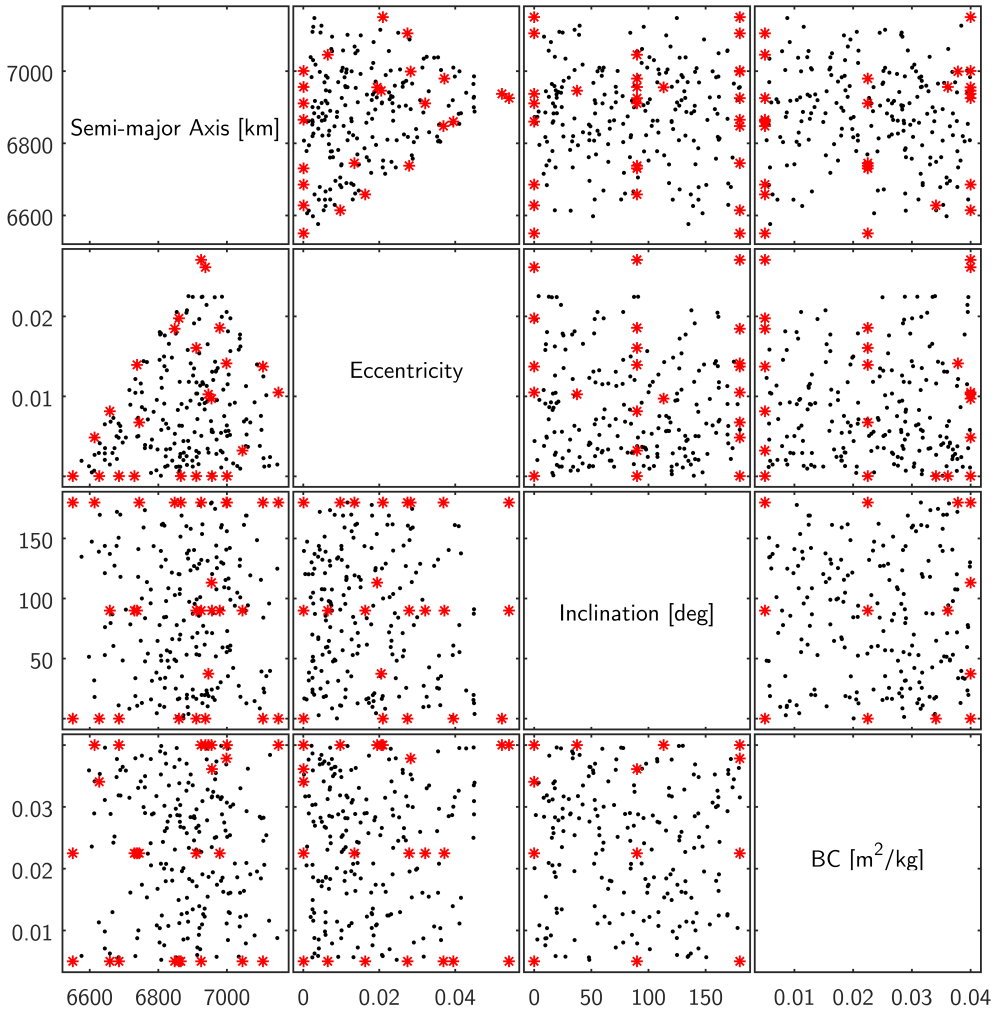

Figure 5.16: Matrix plot showing combinations of input factors for 29-point DoE formulation to generate RSE. Randomly generated combinations of input factors (200 points) for validation of the RSE are also shown for reference.

may have some tendency over-predict the time to decay from orbit and under-predict the effect of atmospheric drag on the satellite.

Following this result, DoE formulations with increasing numbers of run-points were performed to investigate the effect on the fit, error, and bias of the generated RSE. The error analysis for each formulation is conducted using the same 200 random points used previously to validate the 29-point formulation, shown in Figure 5.16. The average, average absolute, and maximum error of different DoE formulations are shown in Figure 5.18. Significantly, for these formulations with increasing numbers of run-points the average error is consistently negative, indicating a similar bias in each RSE. Furthermore, no reliable trend appears to exist in the

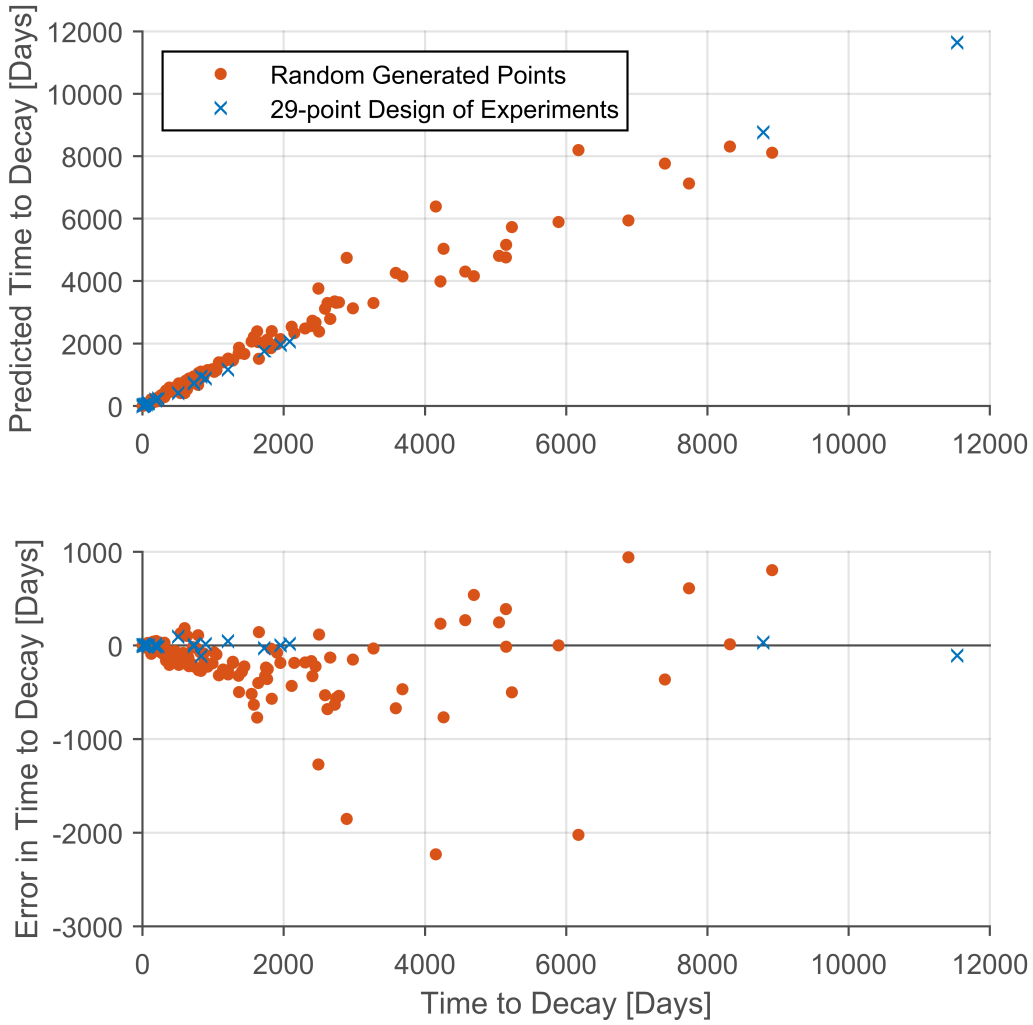

Figure 5.17: Fit and residual analysis of average solar flux and geomagnetic index RSE using 29-point design of experiments formulation.

average absolute and maximum error with increasing number of run-points. This negative bias in the RSEs indicates systematic over-prediction of the time to decay from orbit and under-prediction of the effects of atmospheric drag. For the purpose of assessing the initial population for infeasible designs the presence of this bias in the model will result in fewer designs being removed by the screening process.

The presence of bias in the RSEs may be due to the patterned sampling of the input factors by the structured DoE formulations to produce the expected third-order polynomial response surface. Thus, a set of 200 points, comprised of the the default 29-point structured DoE and a further 171 randomly defined points, was used to generate a new RSE. The input matrix of this

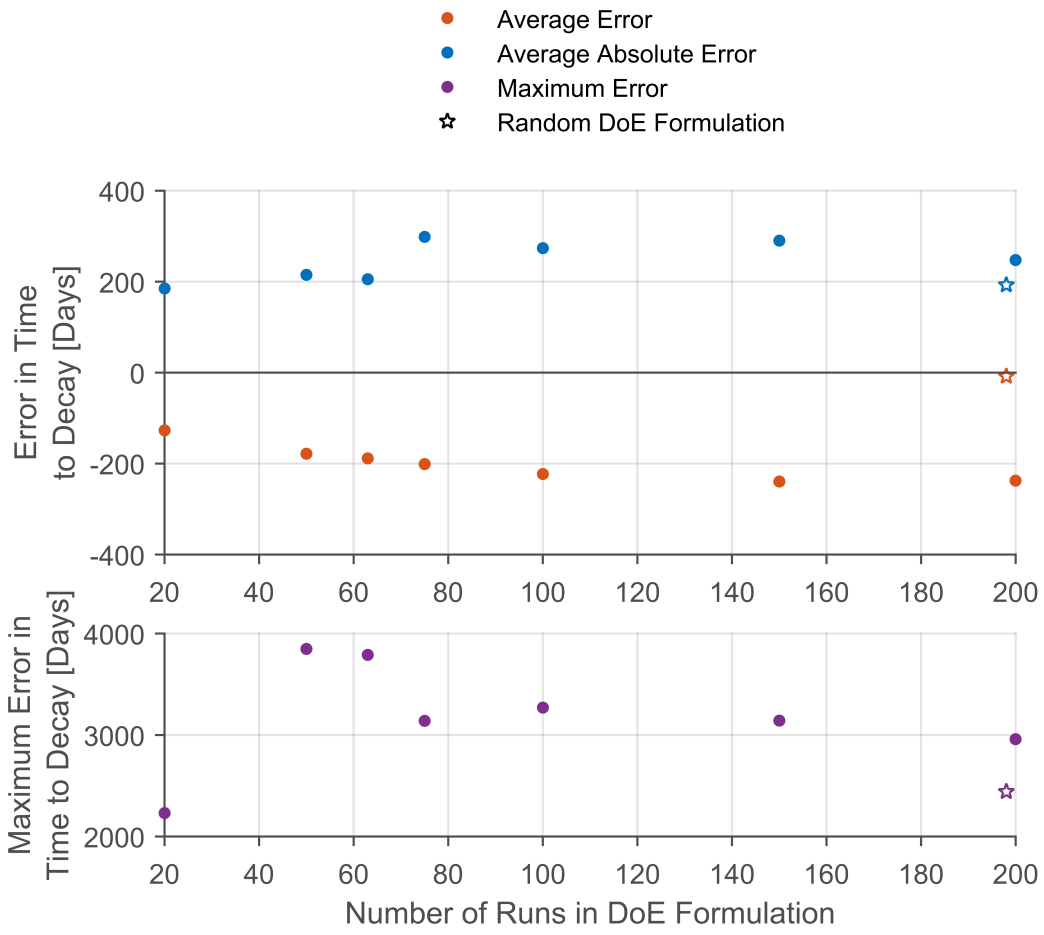

Figure 5.18: Average error, average absolute error, and maximum error of RSEs generated using DoE formulations with varying number of runs. Corresponding errors for the random 189-point DoE formulation are also shown.

formulation is shown in Figure 5.19, indicating both the base DoE structure and the additional randomly generated points. Of the total 200 random points, 189 resulted in a calculated decay time. A maximum period of propagation of 100 years was chosen to limit the computational time expended. The remaining 11 points were found to exceed this maximum propagation period and were thus disregarded.

The fit and residual analysis of the generated RSE corresponding to this random DoE formulation is shown in Figure 5.20. The errors are also shown in Figure 5.18 for comparison against the standard DoE formulations with varying number of run-points. The average absolute error and maximum error of the random formulation are similar to the 29-point DoE formulation. However, most significantly the errors appear to be reasonably evenly distributed about the x-axis, indicating that there is no significant bias in the RSE. This result is confirmed by the very

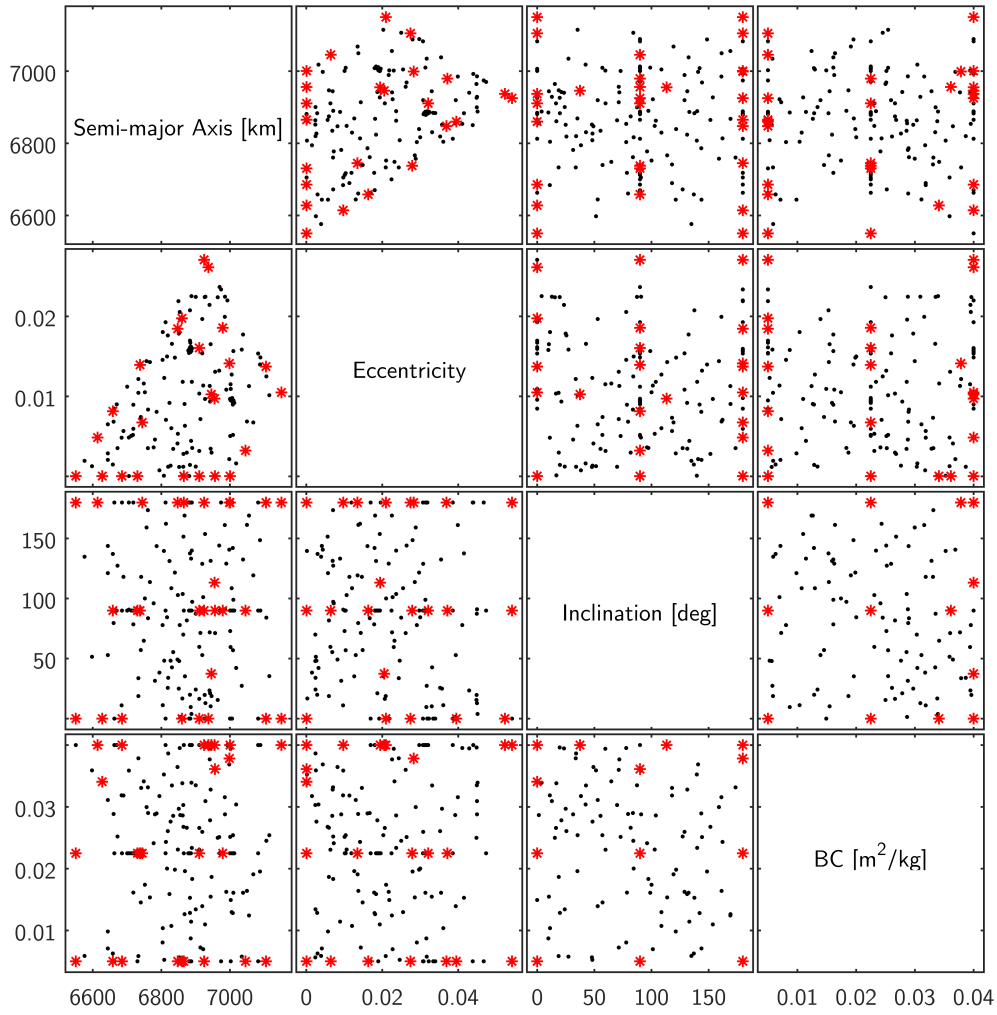

Figure 5.19: Matrix plot showing combinations of input factors for 189-point DoE formulation to generate RSE. Structured base DoE formulation of 29-points and additional randomly generated points are both shown.

low value of average error in time to decay for this formulation in comparison to the structured DoE formulations. The reduction in bias of the RSE is attributed to the sampling of a greater proportion of the input factor space by the randomly generated points. However, the error or variance in the values predicted by the model still exists, and is likely due to a factor or effect which is not captured by the third-order polynomial form of the response surface. The surface model corresponding to this RSE is shown in Figure 5.21 as a series of three-dimensional plots each composed of two input variables against the response of time to decay.

Errors present in the output time to decay by the developed RSE will result in a incorrect screening of some designs which may not actually result in decay prior to the deployment of

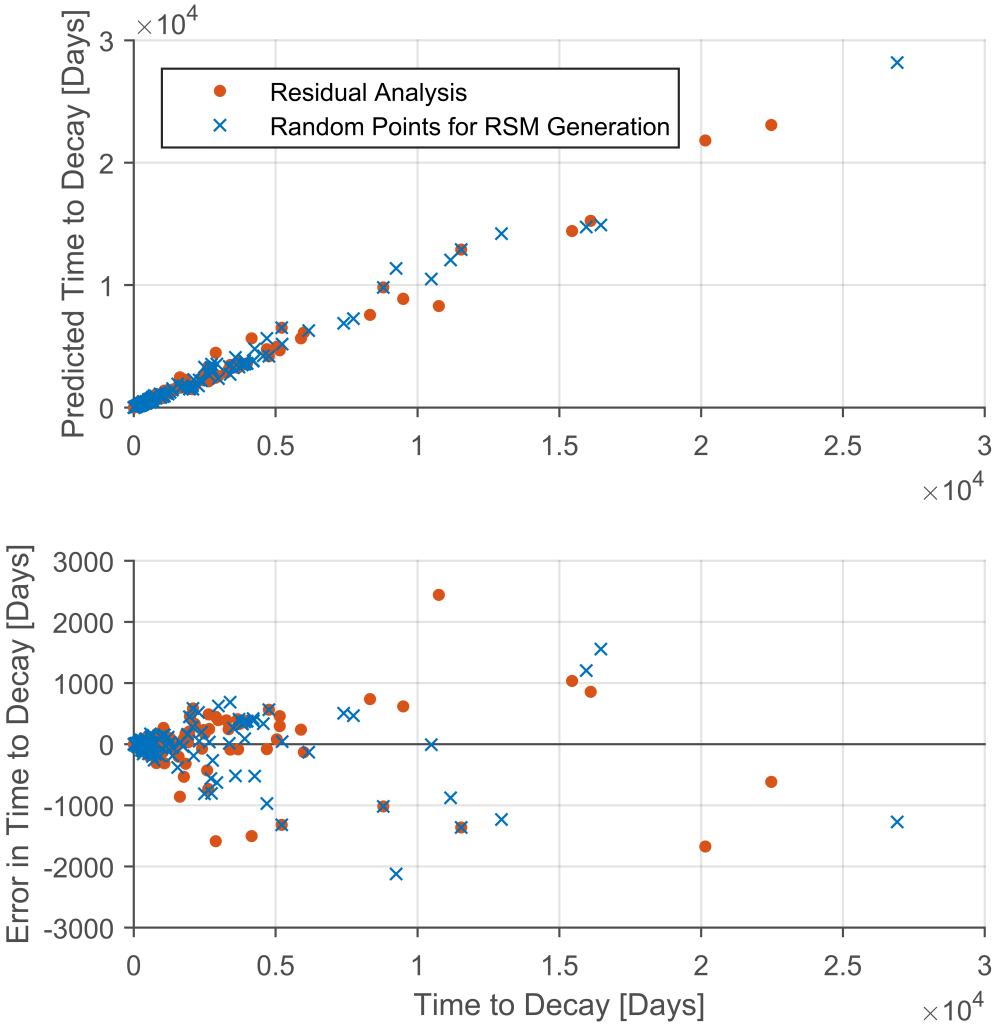

Figure 5.20: Fit and residual analysis of average solar flux and geomagnetic index RSE using a randomly generated set of 189-points.

the constellation. Similarly, some designs may also be passed which will prove to be infeasible when propagation is performed. However, reduction of the number of infeasible designs prior to the full analysis results in less wasted computational time and increases the number of active population members in the design-space exploration.

Improvements to the RSEs for time to decay from orbit could be investigated by considering different effects including higher-order polynomials and trigonometric relationships. Different DoE formulations including space-filling designs can also be considered. Alternatively, different meta-modelling techniques such as neural networks or Gaussian process regression could be investigated. Finally, with respect to the implementation of the RSE in the screening process,

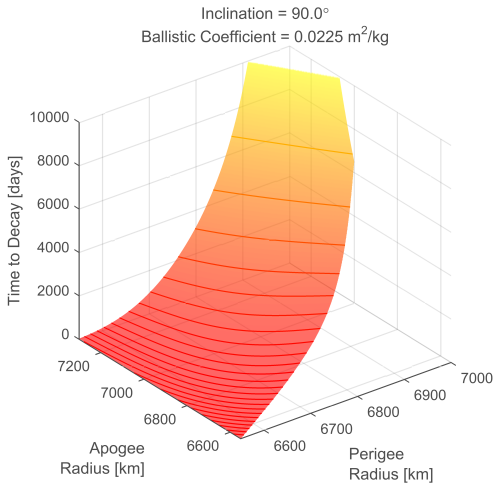

(a) Response of time to decay with apogee and perigee radius.

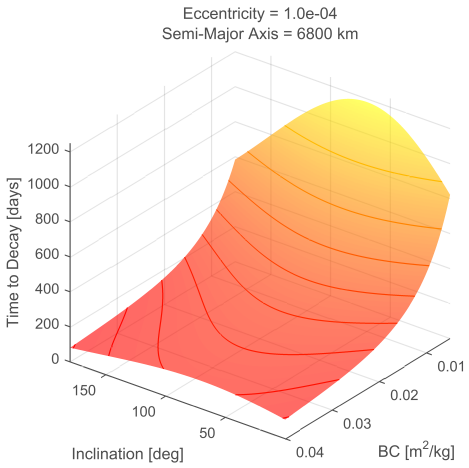

(b) Response of time to decay with inclination and ballistic coefficient.

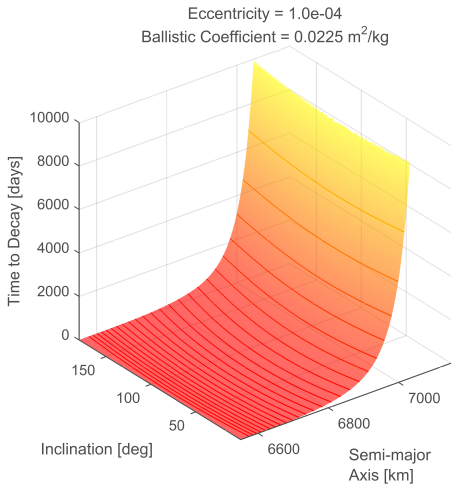

(c) Response of time to decay with semi-major axis and inclination.

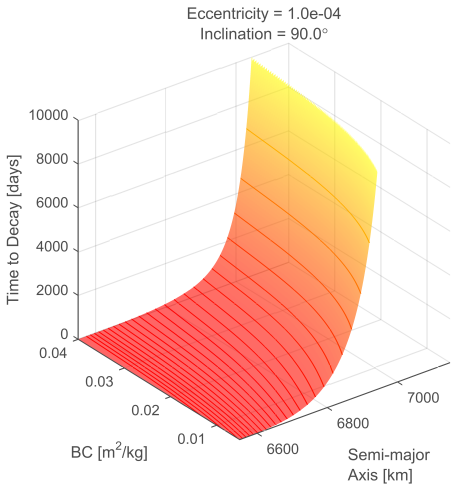

(d) Response of time to decay with semi-major axis and ballistic coefficient.

Figure 5.21: Graphical representation of response surface of time to decay for average solar flux of SI150SFU) and geomagnetic index of 15 nT, generated using the final 189-point DoE formulation. Factors not shown in each subplot are held at static values.

marginal infeasibility of designs could be considered to allow some solutions which are labelled infeasible but within the range of error of the RSE to be passed through to the full analysis. Thus, it can be ensured that potentially good solutions are not removed from the design-space exploration process.

Chapter 6

Implementation and Mission Case Studies

In this chapter, the results of implementing the developed methodology with the reduced-order analysis framework, presented in Figure 3.3, to a set of small satellite constellations are presented. The results of the test cases presented herein first demonstrate the capability and effectiveness of performing the exploration of the design-space using the multiobjective genetic algorithm method. Following this, the overall aim of improving the design process for small satellite constellations is explored by considering the different deployment architectures and system designs which are identified by the design-space exploration process.

The test cases presented in this chapter were chosen to demonstrate the different capabilities of the design-space exploration method and encompass different constellation configurations, payload sizes, and mission types. Initially, the test cases are modelled on existing constellation systems, enabling comparison with actual design-points. Proposed missions and configurations are then considered.

To explore the effectiveness of the design-space exploration method the effect of varying the parameters of the genetic algorithm on the diversity and performance of the developed solutions is investigated. First, changing of the population size and number of generations over which the analysis is performed is investigated. Subsequently, the effects of different population initiation methods are examined.

Finally, the results of the design exploration for each case study are examined to determine the effectiveness in the developed methodology in identifying suitable architectures for constellation deployment. These mission specific results focus on the Pareto set of solutions obtained using the genetic algorithm and are compared to existing design-points where available. To be successful in improving the design of small satellite constellation missions, the developed method should illustrate the tradeoffs which exist in the design-space and identify a range of both effective and diverse solutions for consideration by the system design team in the ongoing design process.

6.1 Evaluation of the Design Space Exploration Method

Before the developed methodology is used to generate final results for the chosen constellation missions the performance of the design-space exploration method can be investigated and appropriate operating parameters for the GA chosen.

First the balance between number of individuals in the working population and the number of generations over which the GA is executed is explored. These two parameters contribute to the overall number of analysis function calls which are used to perform the design-space exploration and therefore the length of time of the total process. If the working population is small, the GA may become stuck at local optima. However, large populations can require a greater number of generations to converge towards the Pareto set.

Secondly, different methods of generating the initial population are tested. These different methods can be used to ensure that the initial population is composed of individuals which are distributed across the whole design-space. By generating populations with initially high diversity in the design-space, convergence to global optima rather than locally optimal solutions can be promoted.

For these initial analyses two representative missions will be used and the results of different implementations of the design-space exploration compared to offer insight into the GA optimisation process. Furthermore, by comparing these different case studies to each other it can be determined whether the selection of GA parameters is mission specific. The two case studies used for these investigations are based on the FORMOSAT-3/COSMIC and ORBCOMM missions, labelled as Mission 1 and Mission 2 respectively, for which the orbital parameters and Walker Delta constellation configuration are summarised in Table 6.1.

Table 6.1: Constellation configuration and orbital parameters of example missions used for investigation of the design-space exploration method. Mission 1 is based on the FORMOSAT-3/COSMIC mission, whilst Mission 2 is based on the ORBCOMM constellation.

	Mission 1	**Mission 2**
Number of Satellites	6	32
Number of Planes	6	4
Spread in RAAN [°]	180	360
Semi-major Axis [km]	7178	7203
Inclination [°]	72	45
Eccentricity	0.01	0.001

Due to the presence of only a single satellite in each orbital plane, the number of design variables for Mission 1 is relaxed to 6, whilst for Mission 2 the number of design variables is 11, shown previously in Eqn. (4.2). The number of design variables involved in the problem of interest determines the dimensionality of the design-space and can therefore have an impact on the effectiveness of the exploration and the results generated using the GA method. For both missions, the objectives of total system mass, time to deploy, and cost, discussed at the beginning of Chapter 5, are used to direct the GA optimisation method.

6.1.1 Population Size and Number of Generations

In the implementation of a GA the number of individuals contained within the working population and the number of generations for which the GA is run for are important parameters. If the population size is too small the optimisation method can easily converge towards the presently known dominant individuals which may be suboptimal in the global objective space. However, if the population is very large, convergence of the algorithm towards the Pareto set may be slow and a large number of generations may be required.

In order to experiment with the effects of changing population size and number of generations the following two rules used in a similar experiment by Vrajitoru [213] are implemented:

1. The total number of analysis function calls during each run of the genetic algorithm should be held constant. The total number of function calls is equal to the number of individuals in the population multiplied by the number of generations. For each case study a total of 2500 function calls is implemented, chosen primarily due to the computational time required to execute each study. The combinations of population size and number of generations used in this study are shown in Table 6.2. A single run of 2500 individuals

is also included to enabled comparison to the process of simple random sampling in the design-space.

2. The population for each run is created using the same pool of randomly selected individuals. For each GA run of a different working population size, the initial population selection is performed using a PRNG but with the same random seeding value. Thus, each initial population of increasing size contains the same individuals used to initiate the previous smaller populations and new randomly generated individuals required to complete the population. In this manner it can be ensured that the smaller populations do not contain genetic information which is not available to the larger populations.

Table 6.2: Combinations of working population size and number of generations used to evaluate the design-space exploration method. The total of 2500 function calls is held constant for each run.

Run ID	Working Population Size	Number of Generations
2500/1	2500	1
500/5	500	5
250/10	250	10
100/25	100	25
50/50	50	50
25/100	25	100

To investigate the effect of runs with different population size and number of generations the average values of different weighted-sum objective formulations can be compared to investigate the quality of the identified solutions. The effect of different combinations of population size and number of generations on diversity can also be examined by considering the number of non-dominated solutions generated by the design-space exploration method, the distance between the nondominated points in the design and objective spaces and the spacing or spread of the solutions in the nondominated set.

Comparison of Diversity, Spacing, and Spread Metrics

Diversity in the design and objective spaces, referred to as genotypic and phenotypic diversity respectively, can be measured by calculating the crowding-distance between points in the non-dominated set. The crowding-distance for each point is computed using the algorithm of Deb et al. [102] which calculates the perimeter of the hyper-parallelepiped which has vertices at the nearest neighbouring points on each side of the design-point in each dimension. A greater value of the average crowding-distance measure of solutions in either the design or objective space

indicates a greater level of diversity in either the designs or solutions obtained which is typically desired for purposes of design-space exploration.

The distribution of the nondominated solutions in the objective space can also be considered. In the absence of knowledge of the true Pareto front by which spread metrics can be calculated (eg Spread metric Δ of Deb et al. [102]), the spacing metric of Schott [214] can be evaluated. The spacing metric S can be calculated using Eqn. (6.1) by considering the number of nondominated solutions N, the nearest-neighbour distance of each nondominated solution in the objective space d_i and the average distance $\bar{d}$. The distance d_i of each point is calculated as in Eqn. (6.2), where $f_m^{i,j}$ is the objective value of the i^{th} or j^{th} individual in the m^{th} dimension. Normalised fitness values are used for the calculation of distance to ensure that objectives of different magnitudes are of equal importance and do not dominate each other. A spacing metric value of 0 indicates that the set of known nondominated solutions is equally spaced.

$$S = \sqrt{\frac{1}{N-1}\sum_{i=1}^{N}\left(\bar{d} - d_i\right)^2} \tag{6.1}$$

$$d_i = \min_{j}^{N}\left(\sum_{m=1}^{M}|f_m^i - f_m^j|\right) \tag{6.2}$$

However, the spacing metric can be somewhat misleading as the true Pareto-front may be composed of points which are not equally spread, therefore yielding a non-zero value. Furthermore, the spacing metric can in some cases wrongly indicate a more uniform spread than is truly represented due to the use of the nearest-neighbour distance measure, identified by Bandyopadhyay et al. [215]. This effect arises when pairs of points are each-others nearest neighbour but located at a distance from other clusters of points.

The total spread of the the identified Pareto front can also be measured by the maximum spread metric D of Zitzler et al. [216] shown in Eqn. (6.3), where f_m^i is the objective value of the i^{th} individual in the m^{th} dimension. If absolute values for the maximum and minimum of each objective are known, an upper bound on the value of the maximum spread metric can be determined.

$$D = \sqrt{\sum_{m=1}^{M}\left(\max_{i=1}^{N} f_m^i - \min_{i=1}^{N} f_m^i\right)^2} \tag{6.3}$$

The crowding-distance, spacing and maximum spread measures for the GA runs of Missions 1 and 2 for varying population size and number of generations are presented in Table 6.3.

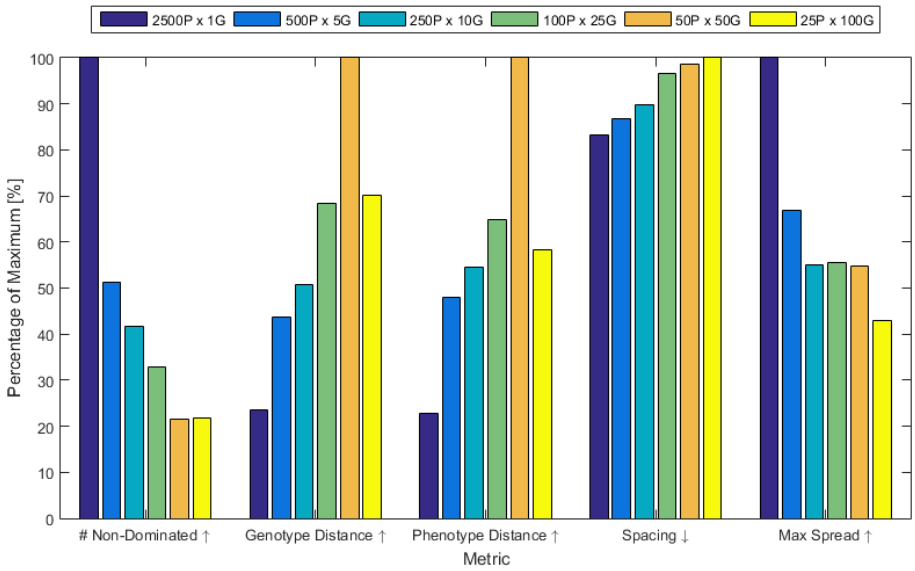

(a) Mission 1.

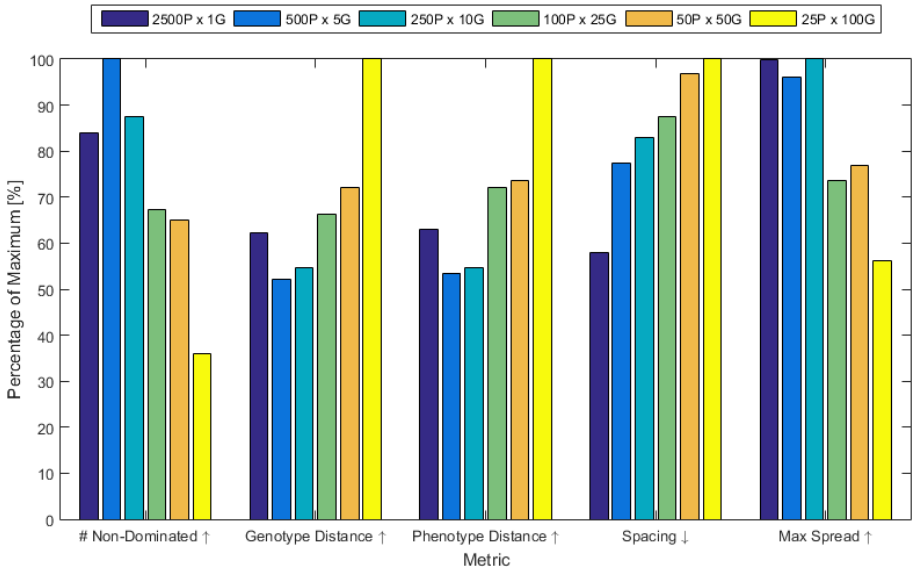

(b) Mission 2.

Figure 6.1: Comparison of diversity, spacing and spread metrics of all identified nondominated solutions generated by GA runs with varying population size and number of generations. The arrow by each label indicates direction of preference of the metric.

Table 6.3: Diversity, spacing, and spread metrics of all identified nondominated solutions generated by GA runs with varying population size and number of generations.

(a) Mission 1.

Run ID	No of ND Solutions	Average Distance		Spacing	Max Spread
		Genotype	Phenotype		
2500/1	**604**	0.0035	0.0034	**0.0169**	**0.8339**
500/5	310	0.0065	0.0070	0.0177	0.5572
250/10	252	0.0076	0.0080	0.0183	0.4594
100/25	189	0.0102	0.0095	0.0197	0.4633
50/50	130	**0.0149**	**0.0147**	0.0201	0.4567
25/100	131	0.0105	0.0086	0.0204	0.3591

(b) Mission 2.

Run ID	No of ND Solutions	Average Distance		Spacing	Max Spread
		Genotype	Phenotype		
2500/1	363	0.0168	0.0077	**0.0030**	0.8402
500/5	**432**	0.0141	0.0065	0.0041	0.8087
250/10	378	0.0148	0.0066	0.0044	**0.8422**
100/25	291	0.0179	0.0088	0.0046	0.6190
50/50	281	0.0195	0.0090	0.0051	0.6472
25/100	155	**0.0270**	**0.0122**	0.0053	0.4722

The results for Mission 1 (shown in Table 6.3a and Figure 6.1a) indicate that a larger number of nondominated solutions are generated by the GA runs with increasing population size. This demonstrates the exploratory capability of a large working population which can sample a larger portion of the design-space in a single generation than a run which has a smaller population size. Furthermore, with a larger working population, a greater number of nondominated solutions can be taken forward to the next generation. However, there is no guarantee that these identified nondominated solutions are either globally nondominated or true-Pareto solutions. This effect is similarly reflected in the results for Mission 2 (shown in Table 6.3b and Figure 6.1b). However, the 2500P x 1G run which is clearly dominant in the diversity result for Mission 1, does not perform as well for Mission 2. As this run approximates a random search of the design-space by 2500 individuals, this result may be affected by the initialisation of the population using random design vector selection.

The spacing metrics for Missions 1 and 2 show that runs with a larger working population size in general return a better result than the runs of a larger number of generations. This indicates that the distance between the identified nondominated solutions are more uniformly spread. Similarly, the runs with larger population size attain a generally greater maximum

spread in nondominated solutions than the runs of smaller population size. This again indicates the ability of larger population sizes to search the whole design-space.

The result of phenotypic distance corresponds to the results obtained for number of non-dominated solutions and maximum spread. For a fewer number of nondominated solutions or a larger maximum spread, the distance between solutions in the objective space is likely to be larger. Interestingly, for both Missions 1 and 2, the result of phenotypic distance closely resembles the genotypic distance measure, indicating that the individuals in the design-space are similarly distributed to those in the objective space.

Comparison of Weighted-Sum Objective Functions

The quality of the solutions generated by each run of the GA can be compared using the fitness of the nondominated population which is generated. A single measure of fitness can be generated by combining the three objectives using different weighted-sum formulations following the form of Eqn. (6.4). The three objectives are first normalized using the global maximum values such that each is of approximately the same magnitude. These normalised objectives are then multiplied by the weightings and then summed. The three extreme forms of the weighted-sum equation simply consider each objective in isolation. A forth simple case is presented when each objective is given an equal weighting. These formulations are presented in Table 6.4. A number of further weighted-sum formulations can then be considered by randomly selecting weightings which sum to one.

$$f(x) = \lambda_1 f(x)_1 + \lambda_2 f(x)_2 + \lambda_3 f(x)_3 \tag{6.4}$$

$$\lambda_1 + \lambda_2 + \lambda_3 = 1$$

The minimum value of each objective and the equal-weighting formulation for the GA runs of varying population size and number of generations are shown in Table 6.5. For a set of 100 000 randomly generated weighted-sum formulations the number of times each combination of population size and number of generations run was dominated, ie produced the worst result, or was the dominating result is shown in Table 6.6.

The results of objective fitness for Mission 1, illustrated in Figure 6.2a, generally indicate that the best overall performance is obtained by the GA implementations which have large population sizes. This is demonstrated by the performance of the 250P x 10G run which

Table 6.4: Weighted sum formulations used for the comparison of GA runs with varying population size and number of generations.

Label	Weighted-Sum Formulation		
	Mass	**Time**	**Cost**
w_1	1	0	0
w_2	0	1	0
w_3	0	0	1
w_4	0.33	0.33	0.33

Table 6.5: Normalised fitness of best individual, minimum fitness, in total population using different weighted-sum formulations for GA runs with varying population size and number of generations.

(a) Mission 1.

Run ID	Weighted-Sum			
	w_1	w_2	w_3	w_4
2500/1	0.3992	**0.2497**	0.5501	0.3996
500/5	0.3996	0.2512	0.5501	0.4003
250/10	**0.3991**	0.2497	**0.5498**	**0.3995**
100/25	0.3992	0.2538	0.5501	0.4010
50/50	0.3993	0.2572	0.5502	0.4022
25/100	0.4154	0.2574	0.5504	0.4077

(b) Mission 2.

Run ID	Weighted-Sum			
	w_1	w_2	w_3	w_4
2500/1	0.0723	0.1579	0.0671	0.0991
500/5	**0.0722**	0.1574	**0.0671**	**0.0989**
250/10	0.0733	0.1576	0.0671	0.0993
100/25	0.0735	**0.1565**	0.0672	0.0991
50/50	0.0734	0.1566	0.0672	0.0991
25/100	0.0738	0.1609	0.0673	0.1006

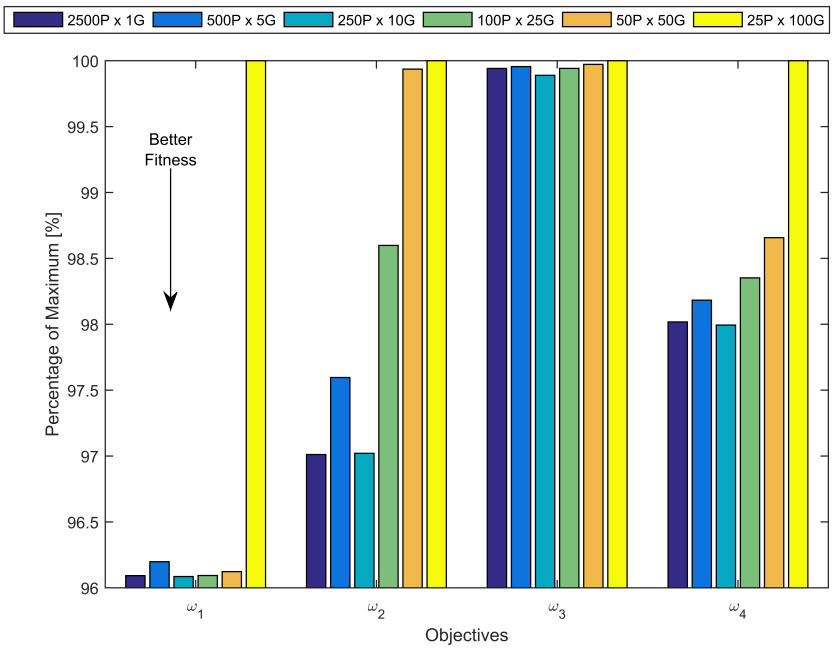

(a) Mission 1.

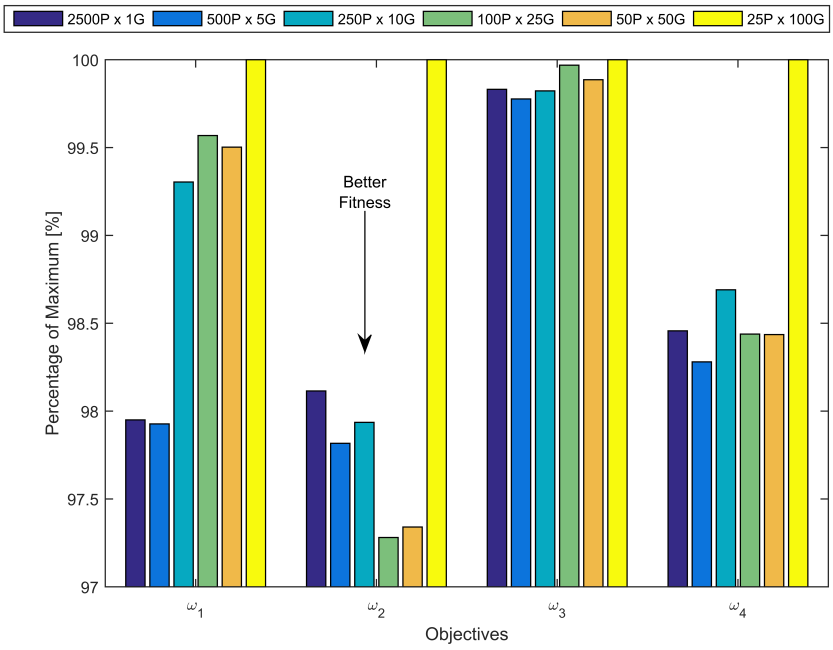

(b) Mission 2.

Figure 6.2: Comparison of best individual, minimum fitness, for different weighted-sum formulations for GA runs with varying population size and number of generations. The relative performance to the maximum value is shown. A lower value of percentage from maximum indicates better obtained fitness weighted-sum fitness metric.

Table 6.6: Performance comparison of GA runs with varying population size and number of generations. A random set of 100 000 weighted-sum formulations was generated and the minimum fitness for each run evaluated for domination.

(a) Mission 1.

	Run ID					
	2500/1	500/5	250/10	100/25	50/50	25/100
% Dominated	0.32	0.39	0.99	2.25	3.08	**92.98**
% Dominating	4.83	7.81	**83.87**	1.17	2.89	0.10

(b) Mission 2.

	Run ID					
	2500/1	500/5	250/10	100/25	50/50	25/100
% Dominated	34.23	0.31	**60.18**	1.24	0.93	3.64
% Dominating	8.68	1.01	0.38	3.99	**85.96**	0.05

generates the best fitness values for each objective and weighting except the ω_2 formulation where it is marginally outperformed by the 2500P x 1G run. The 2500P x 1G and 500P x 5G runs also show good overall performance, whilst the smallest population size runs, 50P x 50G and 25P x 100G, show generally poor performance comparatively. The application of 100 000 random weighted-sum formulations to Mission 1 generally reflects the results obtained for the individual objectives. These results, presented in Table 6.6a, show that the 250P x 10G run generates the best fitness value in 83.9 % of the cases, whilst the 25P x 100G run generates the worst result 93.0 % of the time.

In Figure 6.2b, the results for Mission 2 show that the best fitness in the different objectives is generated by different combinations of population size and number of generations. This is demonstrated by the performance of the 100P x 25G run which generates the best result in the ω_2 formulation, but performs relatively poorly in the ω_1 and ω_3 formulations in which the 500P x 5G run generates the best results. When the random weighted-sum formulations are applied to the results of Mission 2 (Table 6.6b), the 50P x 50G run is identified as dominant, generating the minimum result in 86.0 % of the cases. This result can be attributed to the overall good performance of the 50P x 50G across all of the objectives.

Overall, the results for Mission 1 indicate that a larger population size is beneficial in generating good solutions which address all of the objectives simultaneously. However, a random search with a large population (ie the 2500P x 1G run) only produces the best result in 4.8 % of

cases, indicating that execution of the GA over multiple generations is necessary. In comparison, the results for Mission 2 suggest that individuals with better fitness can be obtained by runs which have a smaller population size but are executed for a greater number of generations.

This difference in the two sets of results is reflective of the change in complexity between the design-space of the two missions. Due to the presence of multiple satellites per orbital plane in the constellation configuration of Mission 2 the number of design variables increases from 6 to 11 in comparison to Mission 1. With increased design complexity, a greater number of generations may be able to generate better results through the increased use of selection, crossover, and mutation operators. In comparison, for a substantially smaller design-space, the initial population has a greater chance of containing good individuals and therefore fewer generations may be required to produce good results.

In both missions the 25P x 100G run can be seen to perform extremely poorly against one of the objectives in comparison to the other GA runs. For ω_1 for Mission 1 and ω_2 for Mission 2, the low performance indicates that the GA has become stuck at a local minima and genetic information which can improve the performance in these objectives is not present in the small population. Whilst increased rate of mutation may enable these runs to escape local minima, the use of probabilistic operators cannot be used to guarantee an increase in performance.

Summary of Study on Population Size and Number of Generations

For the two missions studies presented, it is indicated that a larger working population size is advantageous for generating the maximum diversity in the overall nondominated population. This result is expected as a larger population size enables greater exploration of the design-space and the retention of a larger range of genetic information than a smaller population size.

For performance in the objective space, a balance between working population size and number of executed generations is found to be preferable. For a more complex design-space with a greater number of design variables, a smaller population size executed for a larger number of generations is found to generate a better set of overall solutions. For the simpler design-space, a larger population executed for fewer generations is shown to produce better results. Alternatively, a dynamic population size could be investigated which balances exploration and exploitation of the design-space. This method would initially utilise a large population size to enable exploration of the design-space. Over subsequent generations, the population size can

be decreased increasing selection pressure and exploitation of the best identified individuals in the population.

The results of this studies, whilst somewhat trivial, provide some valuable information about the topology of the design-space. The comparison of distance measures shows correlation between the diversity between the input and output spaces, indicating that the distribution of input designs and output solutions is similar. In addition, differences in behaviour of the two missions also demonstrates the effect of changing the complexity of the design-space by adding design variables. This suggests that the selection of different tuning parameters for each mission studies can be performed to improve the performance of the optimisation method.

6.1.2 Comparison of Initial Population Generation Methods

In this study of population initialisation, two alternative methods, Latin Hypercube Sampling (LHS) and Quasi-Random Number Generator (QRNG) are compared to the basic method of random population generation using PRNG sampling. In each run, the working population size and number of generations is held constant, resulting in an equal number of function calls. To reduce the probabilistic effects of the different population initialisation methods, each implementation is performed a number of times using a scrambled seeding value for the random number generator and the average values of the resulting diversity metrics and minimum fitness used for comparison.

The different methods of initial population generation can first be compared by examining the coverage of the design-space and the corresponding diversity metrics of the generated designs. The effect of the different initialisation methods on the generated output can then be investigated by considering the quality and fitness of the nondominated solutions.

For Mission 1 a population size of 250 individuals was chosen to provide the best compromise between diversity metrics and output solution performance following the result of the previous study detailed in Section 6.1.1. Similarly, for Mission 2 a population size of 50 individuals was selected.

Comparison of Initial Populations

For the simplified case of Mission 1, where there are 6 effective design variables, example input variable matrices for the three different initial population generation methods are shown in

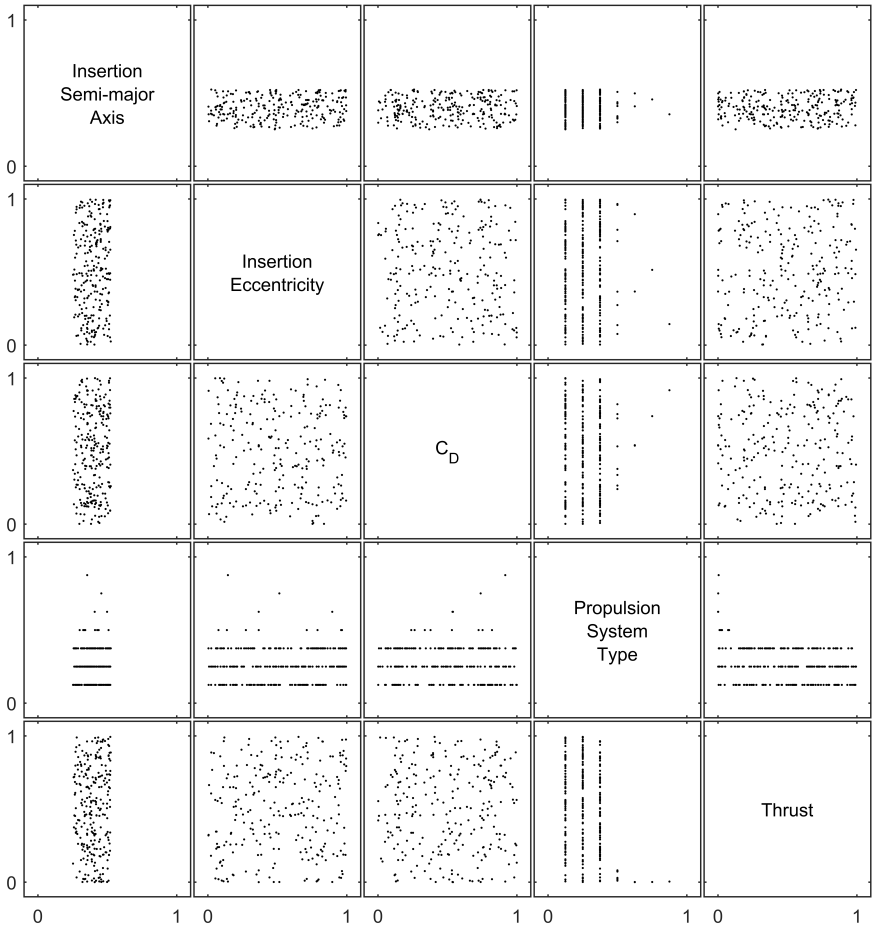

(a) Pseudo-random number population generation.

Figure 6.3: Example Scatter-plot matrix of input variables of the initial population of 250 individuals for different initialisation methods for Mission 1. Each variable is shown normalised between the bounds specified during the population initialisation phase.

Figure 6.3. The Inclination variable has been eliminated as the range of this parameter was highly constrained in the mission definition.

These plots clearly indicate the range of feasibility and infeasibility in the initial population, indicated by the areas of the design-space which filled with points and areas which are devoid of points. The Semi-major Axis variable demonstrates this effect, showing only a band of feasible solutions in the normalised range of 0.3 to 0.5, corresponding to approximately 6770 km to 6950 km. Outside of this range, solutions are either infeasible or few feasible solutions exist and are therefore not identified by the probabilistic operation of the population initialisation methods.

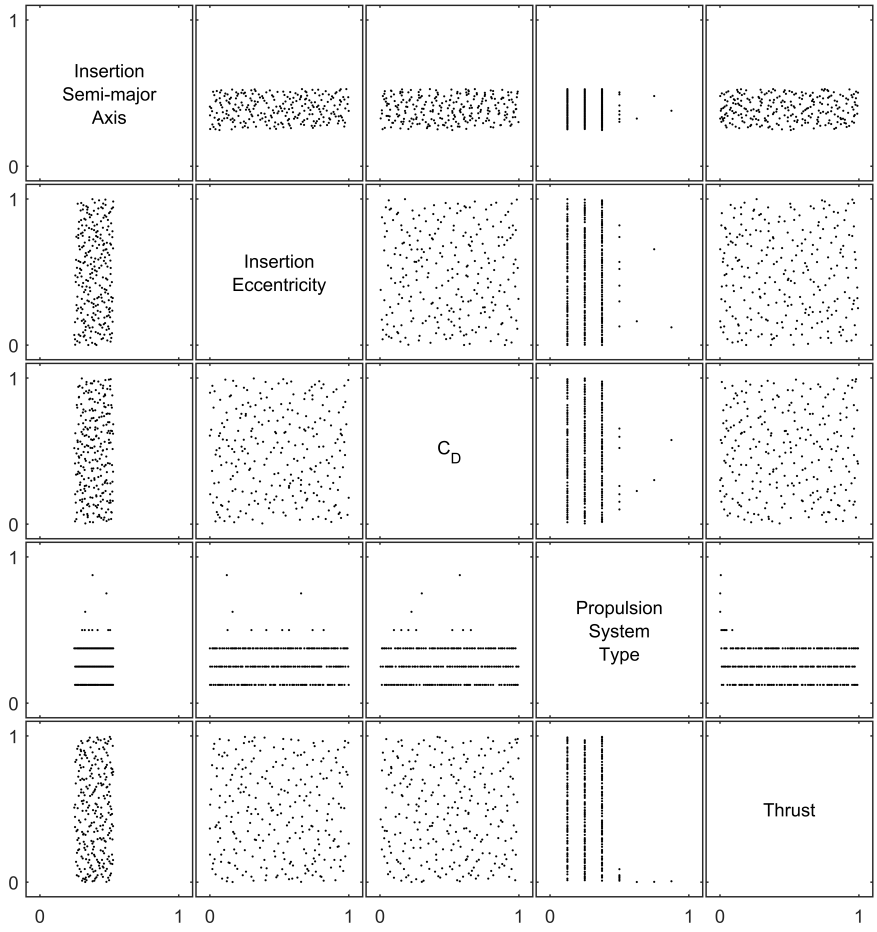

(b) Quasi-random number population generation.

Figure 6.3: Example Scatter-plot matrix of input variables of the initial population of 250 individuals for different initialisation methods for Mission 1. Each variable is shown normalised between the bounds specified during the population initialisation phase.

Comparison of the three different initialisation methods for Mission 1, shown in Figure 6.3, indicates that each method is capable of a similar total coverage of the design-space. However, the QRNG method can be observed to generate a more even or uniform coverage of the identified feasible space, than the PRNG or LHS methods, indicated by the lack of clumping or grouping of points. This observation is expected and is attributable to the aim of the QRNG method to produce a sequence of numbers which have enhanced uniformity and low discrepancy.

Example input variable matrices for Mission 2 are shown in Figure 6.4. Due to the orbital configuration of the Mission 2 constellation with multiple-satellites in each orbital plane, all 11 design variables are relevant and considered in the analysis. In Figure 6.4, 9 design variables are shown, the Inclination variable disregraded as in Mission 1, whilst the Carrier Vehicle Use

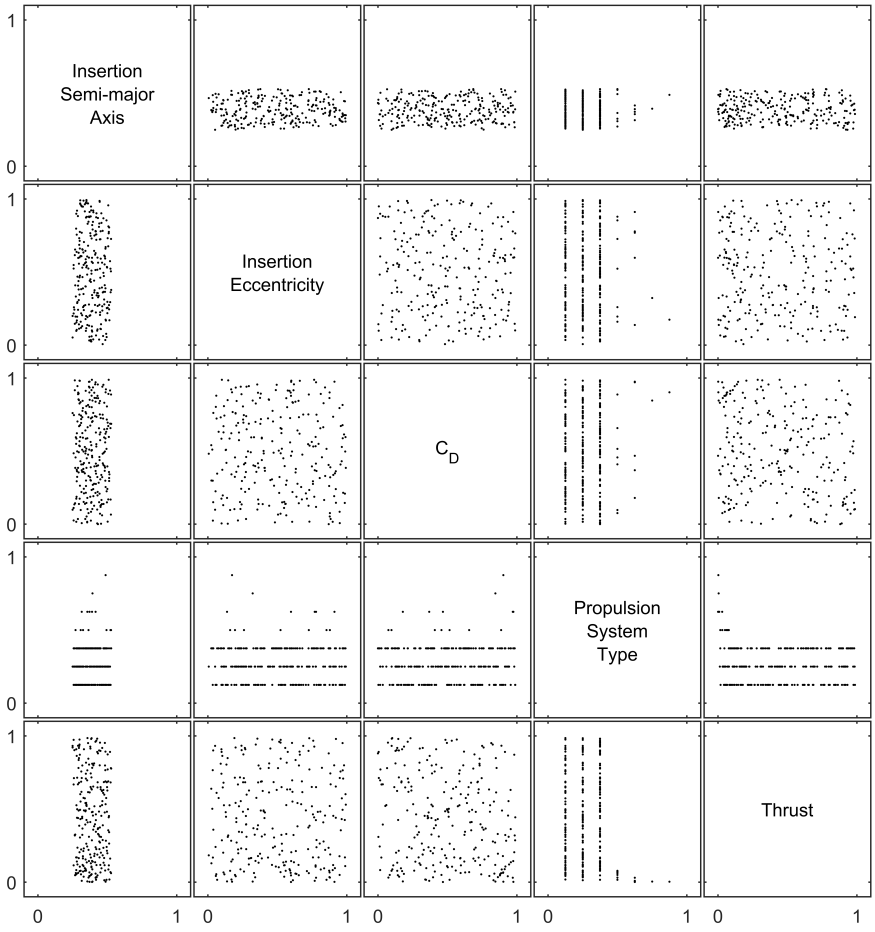

(c) Latin-hypercube population generation.

Figure 6.3: Example Scatter-plot matrix of input variables of the initial population of 250 individuals for different initialisation methods for Mission 1. Each variable is shown normalised between the bounds specified during the population initialisation phase.

variable is effectively a binary operator and is therefore also excluded. Furthermore, in the plots for the final four variables, points are only shown for the designs which utilise carrier vehicles. These plots are therefore more sparsely populated than the plots for the first five variables.

Similarly to Mission 1, ranges of feasibility and infeasibility can be identified in the input variable matrices for Mission 2, shown in Figure 6.4. However, due to the sparsity of the plots due to the reduced number of individuals in the initial population, identification of areas of infeasibility rather than areas which are simply missed by the initialisation methods is more difficult. Comparison of the three different input variable matrices for Mission 2 similarly demonstrates an increased uniformity in coverage achieved by the QRNG method. This effect

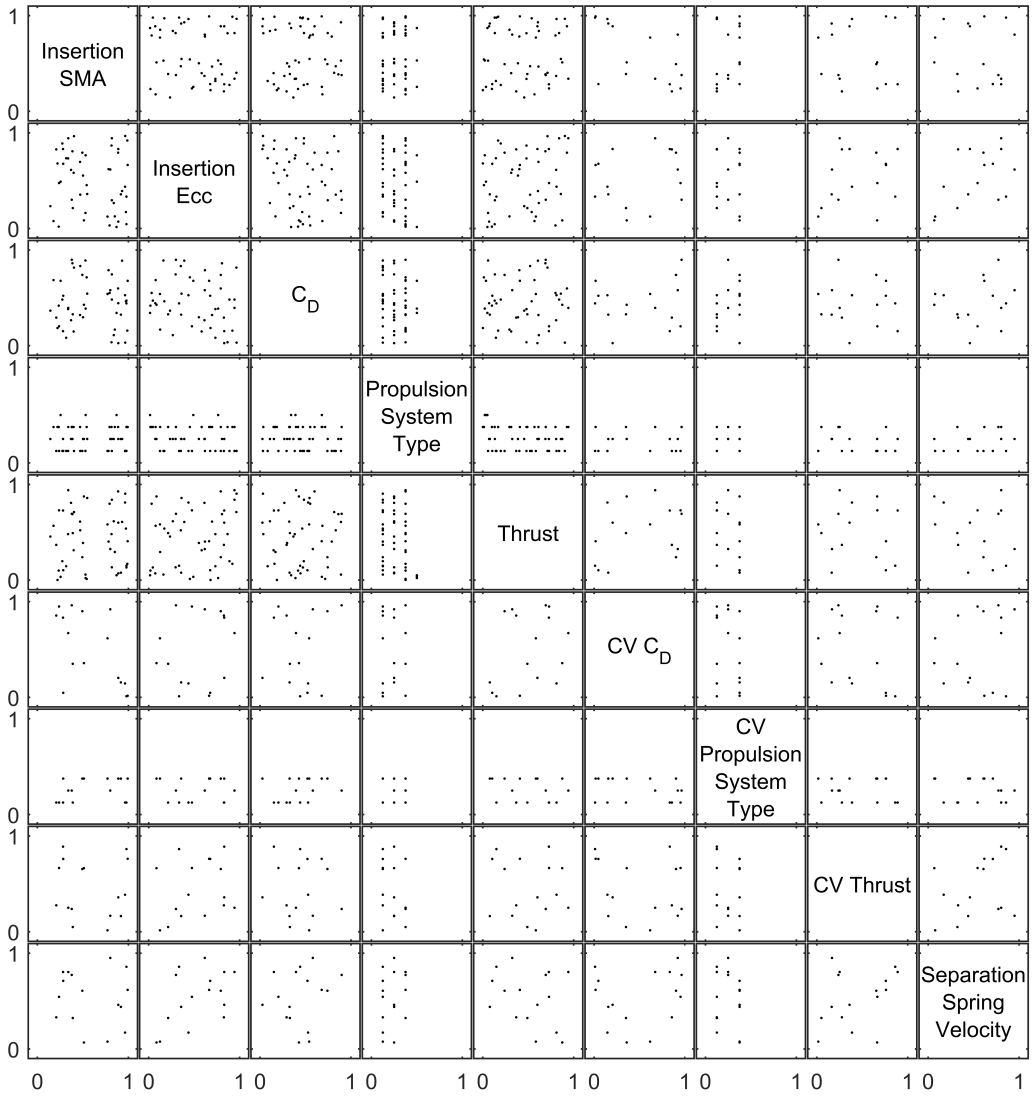

(a) Pseudo-random number population generation.

Figure 6.4: Example scatter plot matrices of input variable matrices of the initial population of 50 individuals for different initialisation methods for Mission 2. Each variable is shown normalised between the bounds specified during the population initialisation phase.

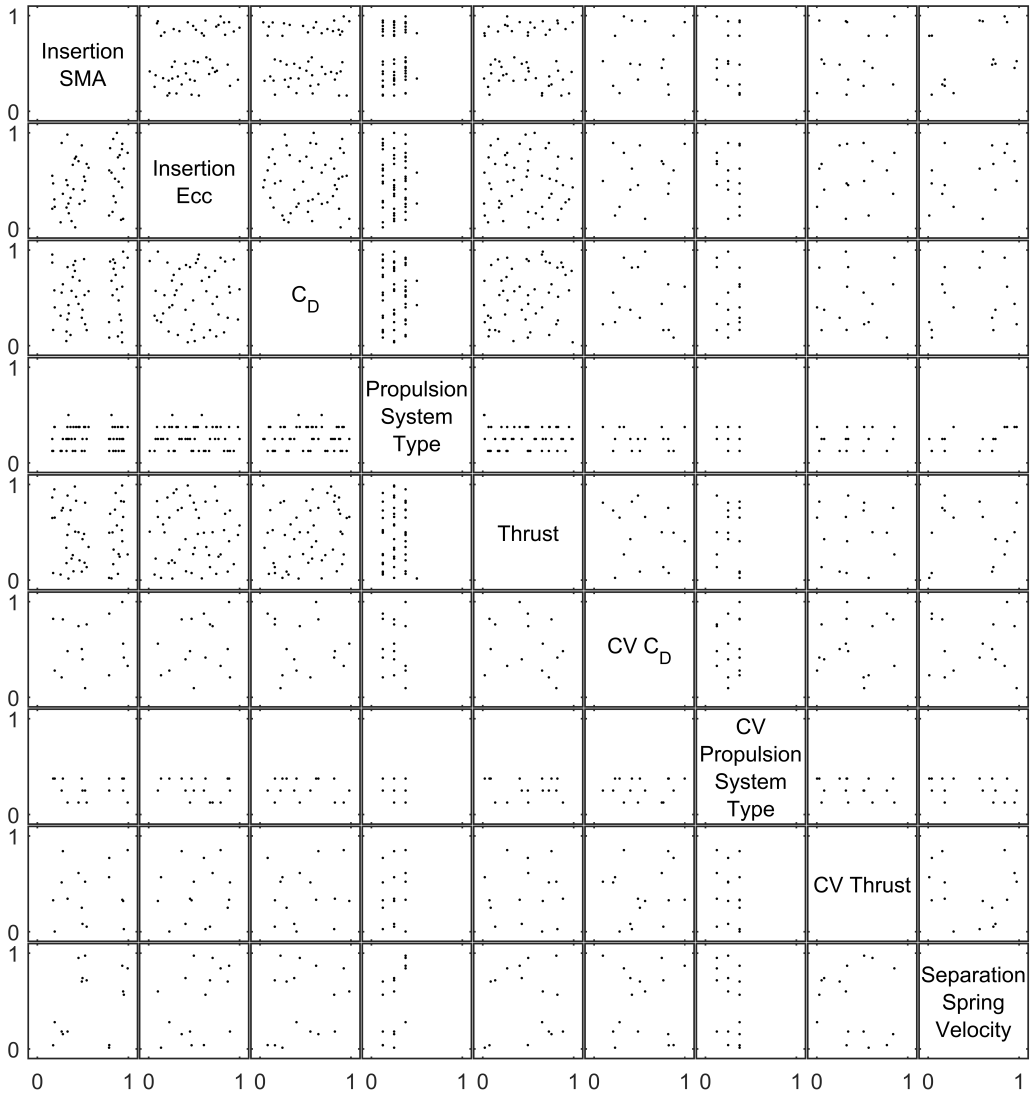

(b) Quasi-random number population generation.

Figure 6.4: Example scatter plot matrices of input variable matrices of the initial population of 50 individuals for different initialisation methods for Mission 2. Each variable is shown normalised between the bounds specified during the population initialisation phase.

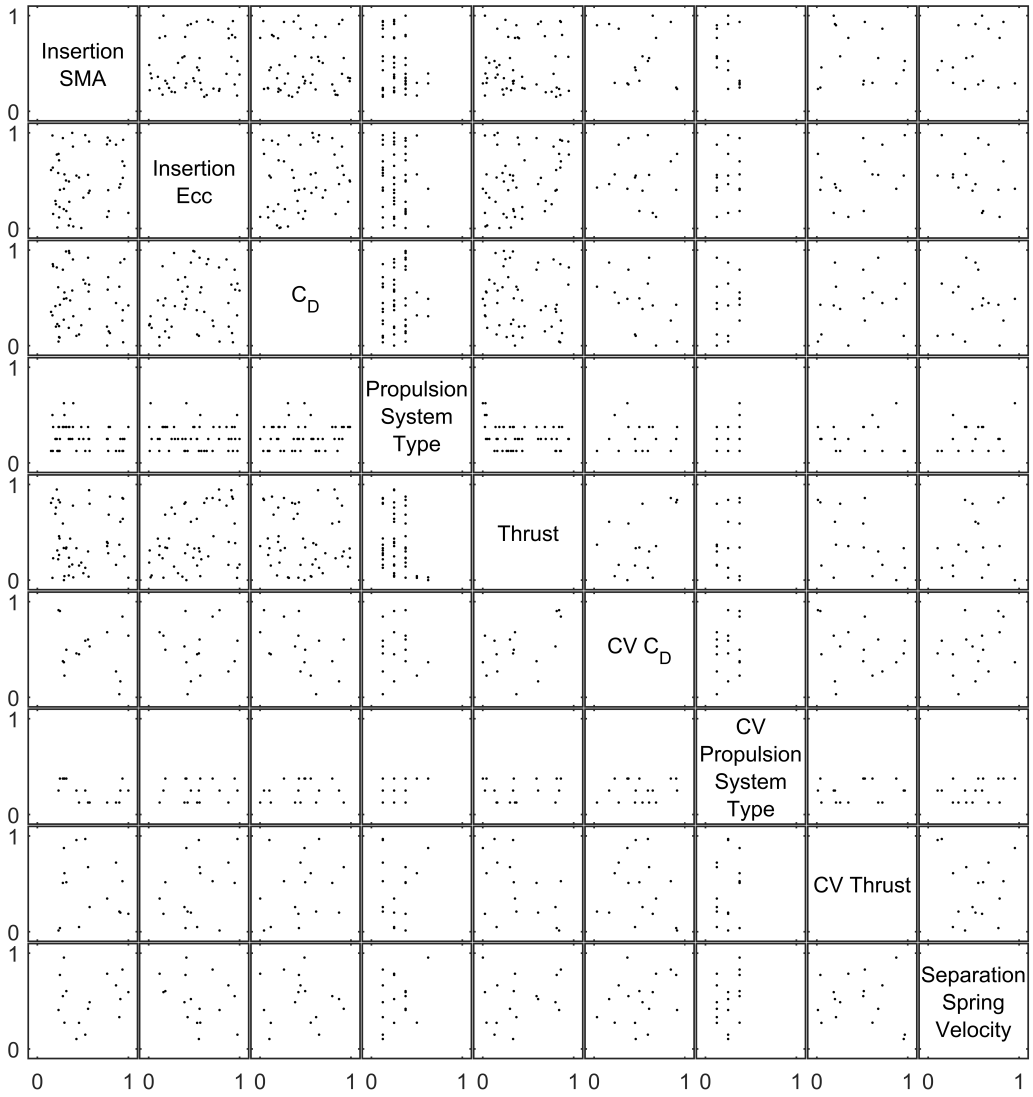

(c) Latin-hypercube population generation.

Figure 6.4: Example scatter plot matrices of input variable matrices of the initial population of 50 individuals for different initialisation methods for Mission 2. Each variable is shown normalised between the bounds specified during the population initialisation phase.

Table 6.7: Diversity, spacing, and spread metrics of initial population generated different population initialisation methods.

(a) Mission 1: averaged data of 10 random initialisations with a population of 250 individuals.

	Run ID	**Avg Distance**	**Spacing**	**Max Spread**
Genotype	Pseudo-Random	0.0077	0.0828	**1.885**
	Quasi-Random	**0.0078**	**0.0690**	1.882
	Latin Hypercube	0.0074	0.0806	1.867
Phenotype	Pseudo-Random	**0.0126**	**0.0282**	0.8151
	Quasi-Random	0.0125	0.0295	**0.8334**
	Latin Hypercube	0.0124	0.0287	0.8029

(b) Mission 2: averaged data of 10 random initialisations with a population of 50 individuals.

	Run ID	**Avg Distance**	**Spacing**	**Max Spread**
Genotype	Pseudo-Random	0.2699	0.2422	2.626
	Quasi-Random	0.2871	**0.2131**	2.630
	Latin Hypercube	**0.2979**	0.2327	**2.654**
Phenotype	Pseudo-Random	0.0650	**0.0666**	0.9021
	Quasi-Random	0.0679	0.0698	0.9394
	Latin Hypercube	**0.0703**	0.870	**0.9905**

is especially noticeable when considering the carrier-vehicle specific variables in which design points are most sparse.

Analysis of Initial Population Diversity

A qualitative comparison of the diversity of the initial populations generated by the three different procedures is presented in Table 6.7. For both Mission 1 and Mission 2 the diversity metrics presented are an average of 10 populations generated using each initialisation method.

The results of diversity in the design-space show that the QRNG method generates the lowest average value of the spacing metric for both missions. This supports the observations of the input variable matrices made previously, primarily that the QRNG method produces an initial population that has high uniformity in coverage of the identified feasible design-space. The LHS method also demonstrates a lower value of the genotypic spacing metric than the PRNG method for both missions, indicating that greater uniformity of points in the design-space is achieved using this method. For Mission 1, this result is also supported by the average distance in the design-space which indicates less grouping of the points is present in the QRNG populations. However, the difference in magnitude of the average distance metric between the different initialisation methods is small, suggesting that the average distance between the points

generated by each population initialisation method are very similar. For Mission 2, the greatest average distance measure is generated by the LHS method. In each case, for average distance and spacing in the design-space, the PRNG method is found to be bettered by either the QRNG or LHS methods.

The results of the maximum spread measure in the design-space are less clear. For Mission 1 the greatest spread is produced by the PRNG method, whilst for Mission 2 the LHS method produces the greatest maximum spread metric. However, in comparison to the upper bound on the maximum spread metric calculated using Eqn. (6.3) and the maximum, range of each active variable, the difference in spread generated by each initialisation method is less than 1 %. This indicates that each method of population initialisation is similarly capable of generating designs which cover the maximum range of the design-space.

The corresponding metrics for diversity in the objective space are also shown in Table 6.7. The result of the phenotype spacing metric appears to be opposite to that of the genotypic spacing metric, indicating that uniformity of points in the design-space does not map directly to uniformity of solutions in the objective space. The results of average distance in the objective space are also not consistent with the trends in spacing metric. However, the difference in magnitude between the average phenotype spacing results are relatively small, indicating that each method generates a solution set with a very similar average distance between the solutions. Finally, for Mission 1 the maximum spread in the objective space is achieved by the QRNG method, whilst for Mission 2, the maximum spread is attained by the LHS method. However, there is no apparent trend in the maximum spread achieved in the objective space by the different methods of population initialisation.

Comparison of Weighted-Sum Objective Functions

The solutions generated by each population initialisation method can be compared by considering the fitness of the individuals in each initial population. Similarly to the previous study on population size and number of generations, both the individual objective values and weighted-sum formulations can be used to compare the overall performance of the populations generated using the different initialisation procedures. The performance of each population initialisation method against the three objectives and the equal-weighting formulation is shown in Table 6.8. For each initialisation method, the value reported is an average of the minimum fitness obtained

Table 6.8: Average normalised fitness of best individual, minimum fitness, in initial population using different weighted-sum formulations for different population initialisation methods. For each of 10 runs of the three populations initialisation methods the average minimum fitness against each weighted-sum formulation is presented.

(a) Mission 1.

Run ID	**Weighted-Sum**			
	w_1	w_2	w_3	w_4
Pseudo-Random	**0.3987**	0.2517	0.5510	**0.4005**
Quasi-Random	0.4001	0.2519	**0.5508**	0.4009
Latin Hypercube	0.4003	**0.2502**	0.5511	0.4005

(b) Mission 2.

Run ID	**Weighted-Sum**			
	w_1	w_2	w_3	w_4
Pseudo-Random	0.1748	0.1738	0.1051	0.1568
Quasi-Random	**0.1743**	**0.1664**	**0.1050**	**0.1553**
Latin Hypercube	0.1743	0.1670	0.1051	0.1553

in each of the 10 runs performed and normalised using the overall maximum value in each objective. Using the same 100 000 weighted-sum formulations as the previous study, the overall performance of each population initialisation method can be investigated by a full-factorial comparison of each of the 10 runs for domination. The average dominance of each initialisation method is reported in Table 6.9.

In the analysis of Mission 1, the PRNG method is shown to perform well when considering the individual objectives and the equal-weighting formulation, generating the lowest average fitness for ω_1 and ω_4 in Table 6.8a. However, when the 100 000 weighted-sum formulations are considered in Table 6.9a, the PRNG method is found to be dominated in 49.3 % of cases. In comparison, the LHS method generates the best overall results and is dominant 46.3 % of the time.

For Mission 2, the QRNG generates the lowest average minimum fitness value in each objective, indicated in Table 6.8b. When each initialisation method is assessed for dominance in Table 6.9b, the QRNG method is shown to be most dominant, whilst the PRNG method is found to be dominated most often. However, the difference in dominance between the initialisation methods in Mission 2 is less clear than the result for Mission 1. This may be attributable to the presence of the additional variables used in the analysis of Mission 2 for carrier vehicle based solutions. For non-carrier vehicle solutions, these variables are allocated by the population

Table 6.9: Average performance comparison of different population initialisation methods. For each initialisation process, 10 initial populations were generated and enumerated. A full factorial pairing of the runs is performed and used to determine the average domination when tested against a random set of 100 000 weighted-sum formulations

(a) Mission 1.

	Pseudo-Random	**Quasi-Random**	**Latin Hypercube**
% Dominated	**49.29**	26.78	23.93
% Dominating	17.35	36.32	**46.33**

(b) Mission 2.

	Pseudo-Random	**Quasi-Random**	**Latin Hypercube**
% Dominated	**42.26**	27.81	29.93
% Dominating	29.64	**38.54**	31.82

generation method, but not utilised. Due to the binary Carrier Vehicle Use variable, the effectiveness of the structured QRNG and LHS methods may be reduced for the conditional variables.

Evidence of this effect can be observed in Figure 6.4, in which the distribution and uniformity of points in the carrier vehicle specific variables for the QRNG and LHS initialisation methods is much less apparent than the first five design variables.

Summary of Study on Initial Population Generation

Study of three different methods of initial population generation confirms that space-filling design methods can be used to promote genotypic diversity of an initial population. Furthermore, the space-filling designs have also been shown on average to produce initial populations with generally better performing individuals. In comparison to the typical method of population generation using PRNG, these methods are therefore preferable for design-space exploration, exploitation, and the ultimate identification of nondominated or Pareto solutions.

Further improvements to the initial population generation may be possible by iteratively measuring the distribution of identified feasible individuals and subsequently searching for feasible individuals within poorly covered areas. Additionally, sphere-packing or other space-filling design methods could also be investigated.

6.2 Case Study I: FORMOSAT-3/COSMIC

The FORMOSA Satellite Series No.3/Constellation Observing System for Meteorology, Ionosphere and Climate (FORMOSAT-3/COSMIC) mission, described by Fong et al. [43] and previously in Section 5.1.9, is a GPS-RO constellation consisting of six microsatellites. The configuration of the constellation is a modified Walker Delta with six orbital planes equally distributed about 180° in RAAN, shown in Figure 6.5. The satellites are also phased with respect to each other their orbits to maximise the volume of data that can be downlinked.

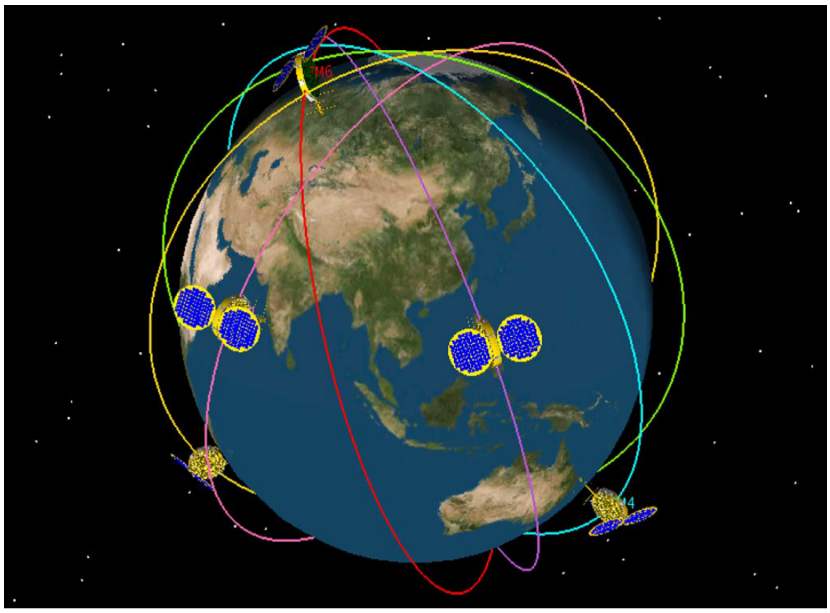

Figure 6.5: Planned configuration of FORMOSAT-3/COSMIC constellation [43].

The design-point of the true FORMOSAT-3/COSMIC deployment strategy can be compared to the solutions developed by the design exploration method. In this analysis, two different solutions to the true FORMOSAT-3/COSMIC mission can be defined, the *actual* deployment and the *simulated* deployment. For the actual deployment solution the system mass and deployment time are taken from Fong et al. [43], whilst calculation of the comparative cost of the system was enabled by evaluation of the actual propulsion system using the known spacecraft parameters and propellant mass. The derived propulsion system mass fraction was then used to determine the cost. The simulated deployment solution was determined using a set of input variables defined using the known mission and spacecraft parameters, indicated in Figure 6.6, and used to enumerate the output solution using the developed analysis method. The output

vectors for the actual and simulated design-points are shown in Eqns. (6.5a) and (6.5b).

$$f_{actual} = \begin{bmatrix} \text{mass} \\ \text{time} \\ \text{cost} \end{bmatrix} = \begin{bmatrix} 366.3 \\ 549.0 \\ 6.137 \end{bmatrix} \begin{matrix} [\text{kg}] \\ [\text{days}] \\ [-] \end{matrix} \tag{6.5a}$$

$$f_{sim} = \begin{bmatrix} \text{mass} \\ \text{time} \\ \text{cost} \end{bmatrix} = \begin{bmatrix} 347.7 \\ 503.1 \\ 6.097 \end{bmatrix} \begin{matrix} [\text{kg}] \\ [\text{days}] \\ [-] \end{matrix} \tag{6.5b}$$

The differences between the actual and simulated FORMOSAT-3/COSMIC deployment solutions are attributable to the method by which the propulsion system of the satellite is modelled in the developed analysis and due to anomalies present in the execution of the actual mission which are not reflected in the simulated deployment. Specifically, the propulsion system modelling process does not account for systems in which the thrust and specific impulse vary with tank pressure. Nominal values for each of these parameters were therefore used to analyse the simulated deployment solution, and ultimately result in differences in the calculated propulsion system mass and propellant mass compared to the actual FORMOSAT-3/COSMIC mission. In addition, the FORMOSAT-3/COSMIC satellites were loaded with significantly more propellant than required to perform the necessary orbital manoeuvres to perform the deployment. The approximately 2 kg additional propellant per satellite, corresponding to a margin of about 45 %, contributes to the significant difference in total mass between the systems. The reason for this considerable margin on fuel mass is not explicitly stated in the literature. Finally, the during the actual FORMOSAT-3/COSMIC mission deployment a number of issues were encountered, documented by Fong et al. [43], which resulted in significant delays to the deployment of the constellation. Most significantly, thrust-burn failures due to incorrect manoeuvre and moment of inertia modelling and calculation of the Sun-vector during daylight periods caused delays in the deployment of the constellation and increased the ΔV required by each satellite and therefore the mass of propellant consumed.

6.2.1 Problem Definition

The required input parameters used in the application of the design-space exploration method to the FORMOSAT-3/COSMIC mission are listed in Table 6.10. These parameters were chosen

to most closely resemble the parameters used in the deployment of the actual system, described by Fong et al. [43]. The Deployment Deadline parameter is chosen as a limiting factor to the length of the deployment strategy and is not derived from the actual start date for the mission. This extended period of deployment of 42 months, compared to the actual deployment time of 20 months, enables the consideration of deployment strategies which may utilise significantly different propulsion systems or initial insertion orbits and allows for exploration of the larger design-space for this mission.

Table 6.10: FORMOSAT-3/COSMIC design-space exploration input parameters [43].

Property	**Value**
Number of Satellites	6
Number of Orbital Planes	6
Satellite Dry Mass [kg]	54
Insertion Date	15 April 2006
Deployment Deadline	01 January 2010
Mission Semi-major Axis, a_i [km]	7178
Mission Eccentricity, e_i	0.01
Mission Inclination, i_i [°]	71.992
Mission RAAN, Ω_i [°]	Ω_1, $(\Omega_1 - 30)$, $(\Omega_1 - 60)$, $(\Omega_1 - 90)$, $(\Omega_1 - 120)$, $(\Omega_1 - 150)$ ± 5
Mission Mean Anomaly, M_i [°]	M_1, $(M_1 - 52.5)$, $(M_1 - 105)$, $(M_1 - 157.5)$, $(M_1 - 210)$, $(M_1 - 262.5)$ ± 8

Further constraint of the design-space is provided by the upper and lower bounds on the design variables required by the genetic algorithm optimisation method. These bounds are listed in Table 6.11 and were selected to direct the design-space exploration to the known areas of feasibility and viability. For example, bounding of the launch inclination to the mission inclination of the constellation was performed to enable comparison to the true FORMOSAT-3/COSMIC mission which was launched directly into the correct orbital plane by a Minotaur I launch vehicle.

Table 6.11: Bound constraints on design variables for GA design-space exploration of FORMOSAT-3/COSMIC mission.

	Lower Bound	**Upper Bound**
Insertion Semi-major Axis [km]	6600	7300
Insertion Eccentricity	1×10^{-6}	1×10^{-2}
Insertion Inclination [°]	71.992	71.992
Coefficient of Drag	2.0	2.5

Given the bounds provided in Table 6.11 and the mission parameters in Table 6.10, the initial population shown in Figure 6.6 was generated using LHS initiation and a population size of 250 individuals. The corresponding parameters for the true FORMOSAT-3/COSMIC design point are also shown for comparison. This initial population indicates a definite region of feasibility, approximately 0.25 to 0.5 in the normalised Semi-major Axis variable, corresponding to 6775 km to 6950 km. The upper limit of feasibility is established by the requirement to perform the deployment within a prescribed time period, imposing a minimum bound on the rate at which plane separation must occur. The presence of atmospheric drag imposes the lower limit on feasibility, as low initial orbital altitudes cause the satellites to decay before the deployment can be performed. In comparison to the Semi-major Axis, for the given bounds, the Eccentricity and Coefficient of Drag variables do not exhibit clear regions of infeasibility. The spread of initial solutions across the Propulsion System Type variable indicates that fewer feasible solutions exist for the more energetic resistojet, arcjet, ion, and Hall effect propulsion systems. Furthermore, for these higher-power systems, the Thrust variable indicates that only low-thrust systems are feasible in comparison to Cold Gas Thruster (CGT), monopropellant, and bipropellant systems.

6.2.2 Tradespace Analysis

After performing exploration of the design-space by execution of 10 generations of the GA method, a total of 2500 analysis function calls, the set of output solutions can be analysed. These results, categorised by Propulsion System Type, are shown in Figure 6.7 plotted in the 3-dimensional tradespace of System Mass, Deployment Time, and Cost. A 2-dimensional projection of System Mass against Time to Deploy is also shown. For the FORMOSAT-3/COSMIC mission, the output space shown in Figure 6.7 indicates that the fastest deployment can be achieved by either CGT, monopropellant, or bipropellant propulsion systems. These systems are similarly capable of generating the lowest cost solutions in the output space. However, for minimum total system mass, arcjet and low-power Hall effect thruster systems demonstrate the most promising output characteristics.

The subset of nondominated solutions, or Pareto efficient solutions, are shown in Figure 6.8. These results demonstrate that a range of propulsion system types are capable of generating feasible and Pareto efficient results. Without considering viability or preferability in the design or output tradespace, these solutions are equal in overall performance and a single best solution

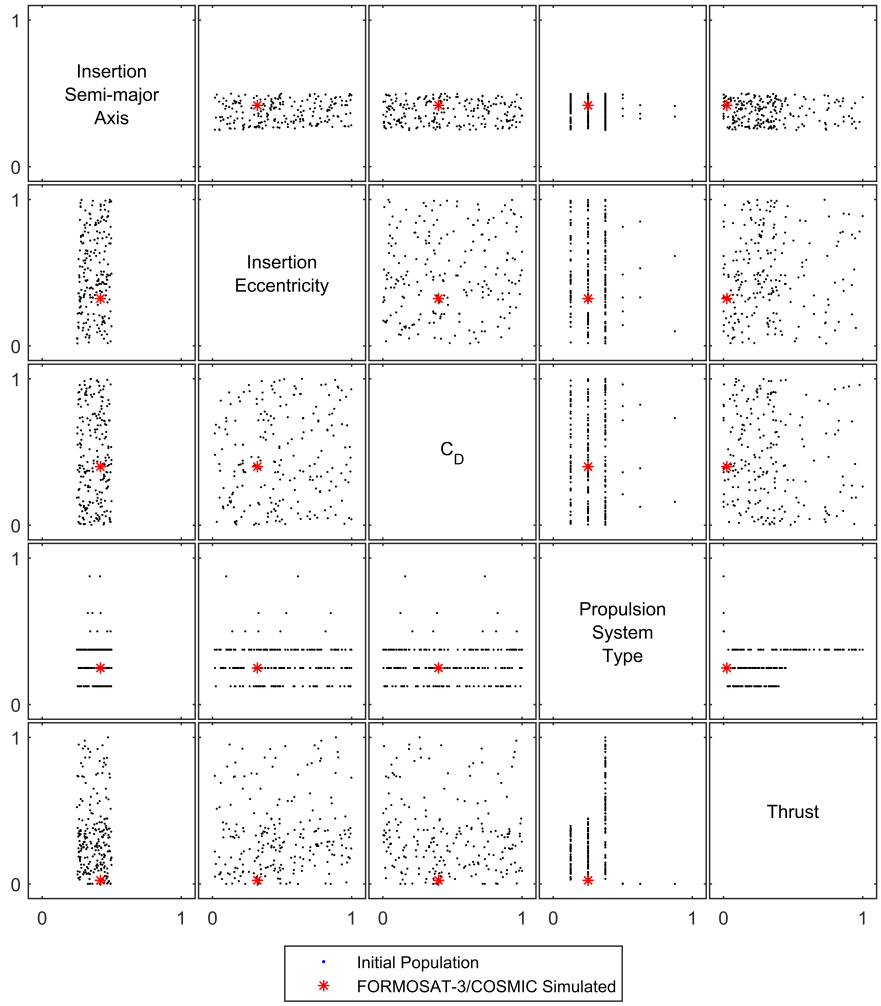

Figure 6.6: Scatter-plot matrix of input variables of initial population members for FORMOSAT-3/COSMIC mission analysis. Initialisation was performed using Latin Hypercube sampling to generate a population of 250 individuals.

cannot be selected. For the propulsion system types which are well represented, a clear trade-off between time to execute the deployment and total mass of the system is exhibited which corresponds to to the known trade-off between planar drift-rate and the ΔV magnitude required to perform the necessary in-plane manoeuvres. This trade is primarily a function of the insertion orbit semi-major axis and the propellant mass required to perform the in-plane manoeuvres. The order in which the propulsion systems appear with respect to the system mass axis is also indicative of the dominance of specific impulse in the rocket equation. For propulsion systems with low specific impulse the propellant mass required to perform deployment in a given time is greater. Furthermore, by this mechanism the increase in propellant mass required

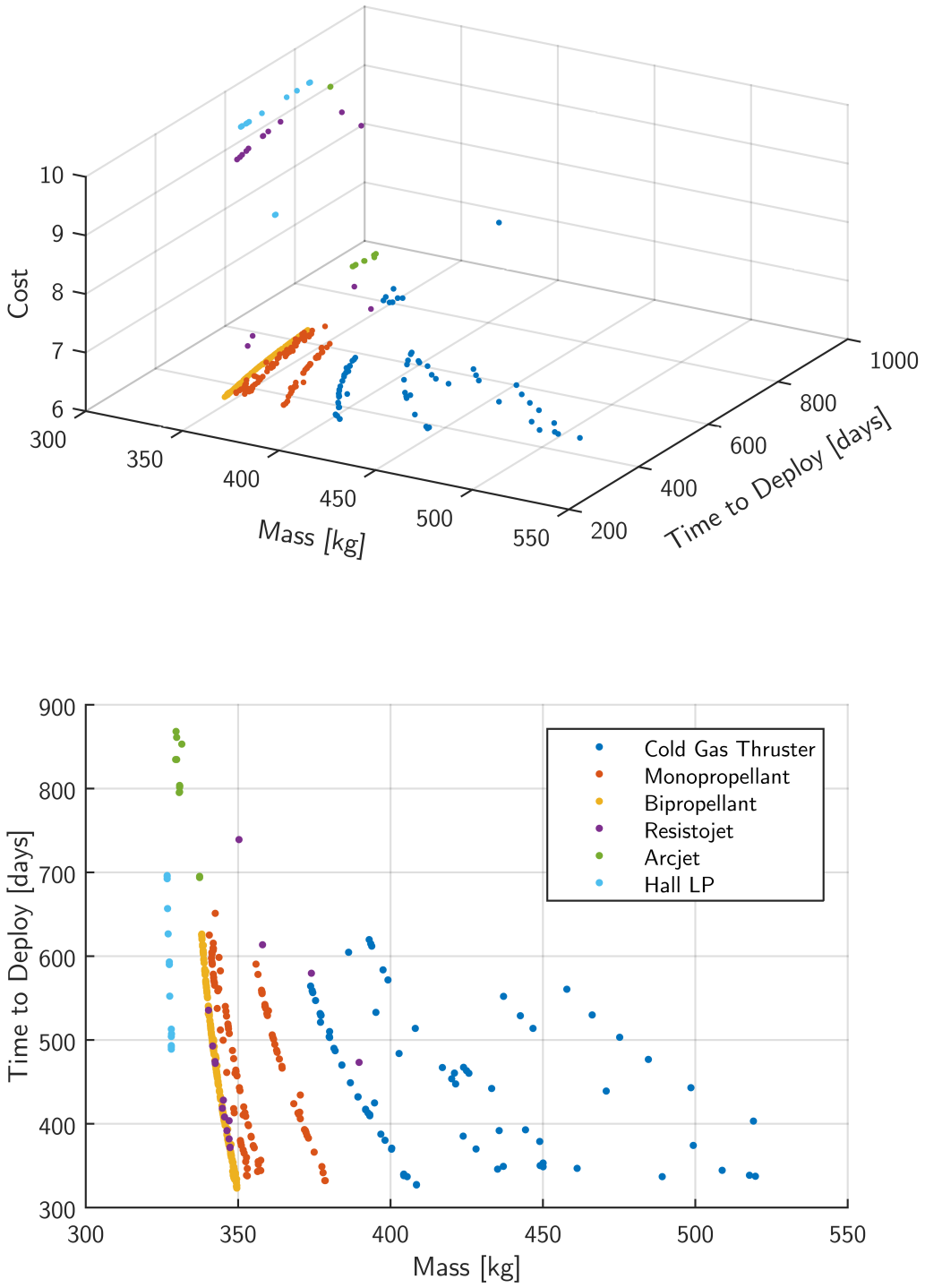

Figure 6.7: Output space of total solution set obtained using 10 generation GA design-space exploration method with a population size of 250 individuals.

to perform a larger ΔV manoeuvre is greater for smaller specific impulse. This therefore results in the difference in gradient of the trade between system mass and deployment time for each propulsion system type.

Relationships between the developed solutions and the input variables can also be examined by use of parallel coordinate plots, demonstrated in Figure 6.9. In the left-hand parallel coordinate plot the vertical axis represents the different variables or outputs of interest, whilst the horizontal axis indicates the normalised value of each of these variables. Each design is then shown as a series of connected points, one for each variable of interest, creating a single poly-line. In the right-hand plot a histogram corresponding to each variable shows the distribution of the designs over the normalised value range. The height of the histogram bins indicates the frequency of designs within that range.

In parallel coordinate plotting, the order in which the variables or outputs are shown can be changed to reveal different patterns or relationships between adjacent parameters. However, identification of the different interesting features in the dataset may require experimenting with many orderings. Interactive methods for exploring parallel coordinate plots can be used to aid the identification of trends or patterns by enabling quick reordering or inversion of the parameter axes and dynamic colouring, filtering, or selection of the poly-lines based on the range of data for a given variable.

The parallel coordinate plot in Figure 6.9 shows the set of nondominated solutions with monopropellant propulsion systems. In this plot, the values shown for each of the six relevant input variables are normalised with respect to the upper and lower bounds in the design-space. The values shown for the three output objectives are normalised with respect to the highest and lowest obtained by the design-space exploration method. Thus, using the parallel coordinate plot, the range of the input and output space over which designs exist can be identified. For example, in Semi-major Axis the total set of monopropellant solutions are shown to cover the normalised range 0.26 to 0.50. However, the corresponding nondominated solutions are all clustered between 0.45 to 0.48, approximately 6914 km to 6937 km. Similarly, the Thrust of the nondominated solutions is restricted to the normalised range 0.02 to 0.18, whilst the dominated solution set is shown to span the complete design-space. These observations are supported by the distribution histograms which also indicate the spread of the total solution set and clustering of the nondominated solutions. These trends can aid the identification of ranges in the design-space which can result in increased output solution performance.

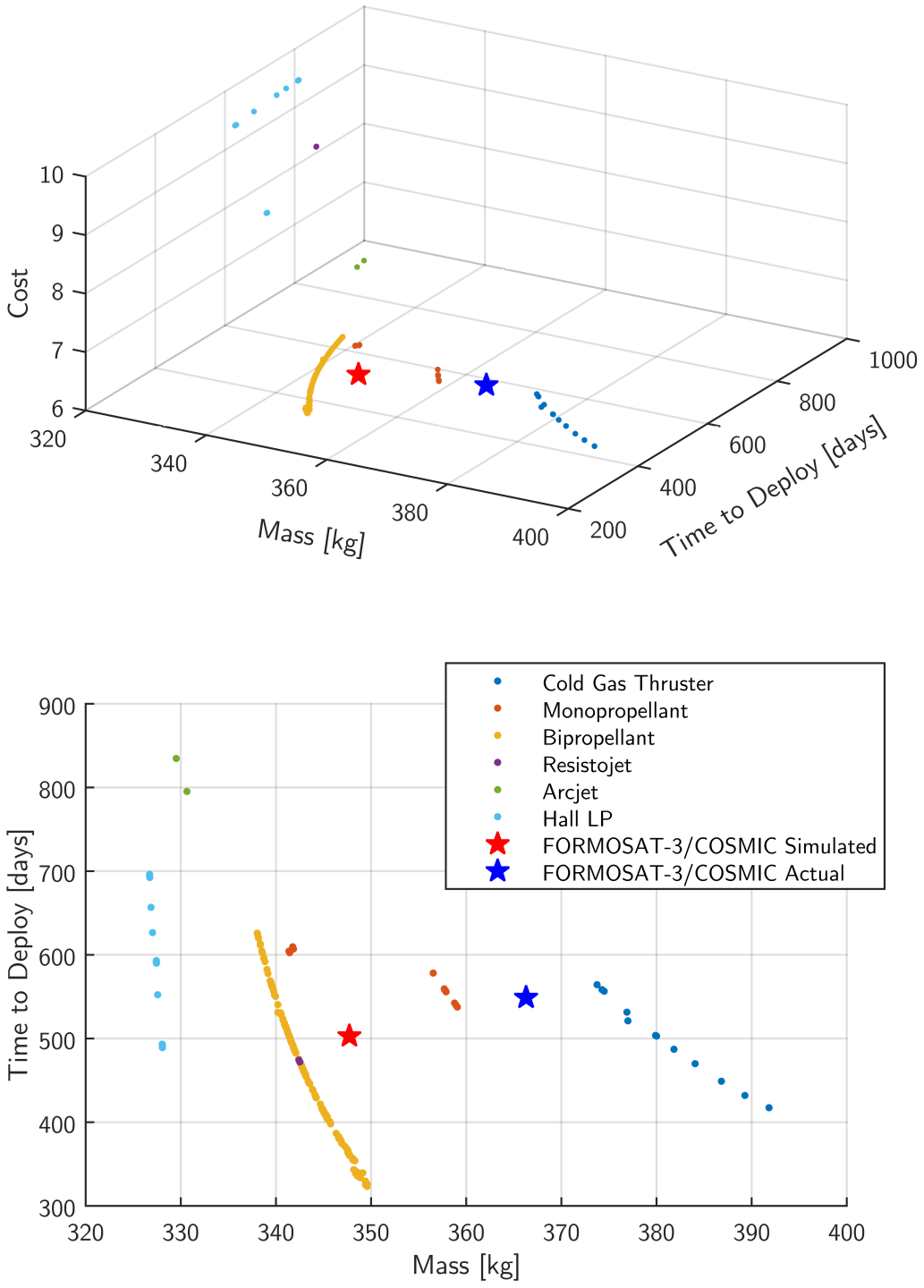

Figure 6.8: Output space of nondominated solutions obtained using 10 generation GA design-space exploration method with a population size of 250 individuals.

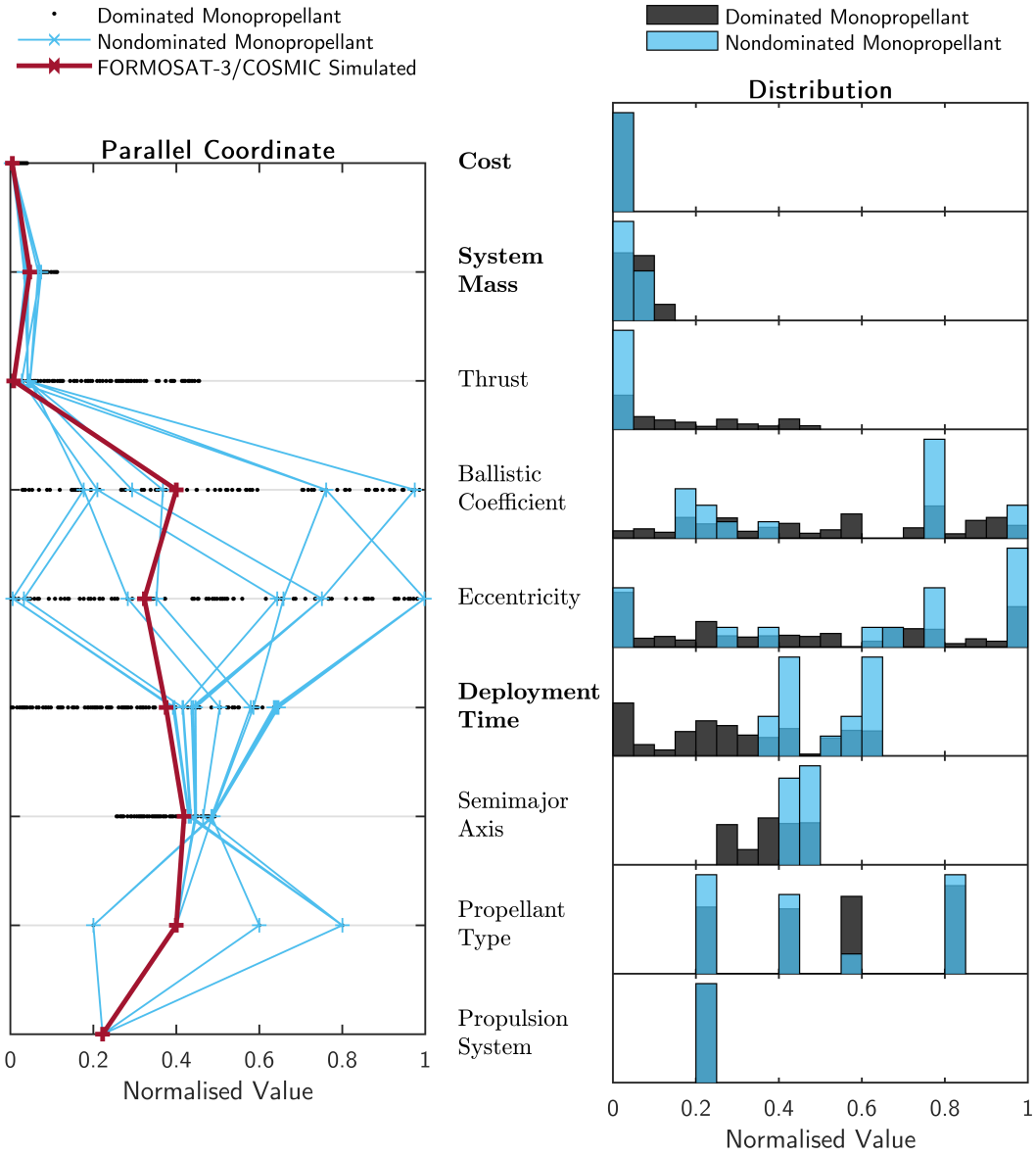

Figure 6.9: Parallel coordinate plot and distribution plot of nondominated monopropellant propulsion systems in the global design-space. Dominated solutions are also shown for reference. Normalised values of six input variables and three output objectives (**bold**) are shown for the range of designs of interest.

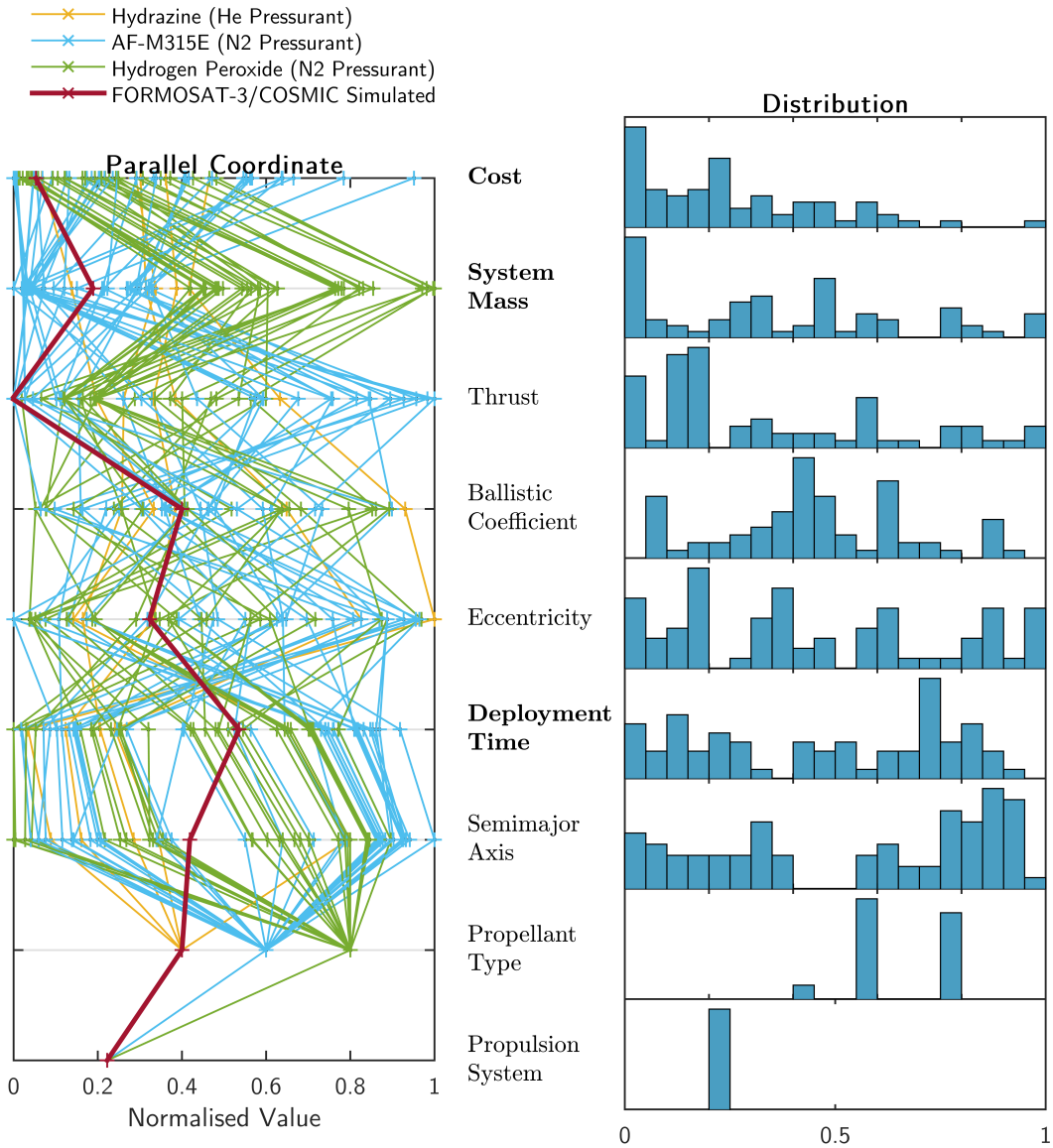

Figure 6.10: Parallel coordinate plot and distribution plot of the set of nondominated solutions for monopropellant propulsion systems only. Normalised values with respect to only monopropellant designs of six input variables and three output objectives (**bold**) are shown for the range of designs of interest.

However, examination of the output space for the nondominated monopropellant designs is difficult due to the clustering of points in small ranges of each of the objectives. Thus, in Figure 6.10, the set of nondominated solutions for only monopropellant propulsion systems is shown for the same six design variables and three output objectives. In this case, normalisation of the variables on the horizontal scale of the parallel coordinate plot is performed using the maximum and minimum values for designs with monopropellant propulsion systems. In Figure 6.10, the most identifiable pattern is between the Semi-major Axis variable and Deployment Time output. These two variables show a predominately linear mapping with few points of crossover, indicating that the Deployment Time is highly dependent on Semi-major Axis. Of the four different propellant and pressurant combinations available in the propulsion system database, three are featured in the nondominated set, indicated by the three different colours shown. Examination of the designs indicates a pattern between the System Mass and Cost objectives for the different propellant/pressurant types. Propulsion systems with Hydrogen Peroxide with Nitrogen pressurant appear to generate relatively high System Mass, but lower Cost. Contrastingly, AF-M315E with Nitrogen pressurant propulsion systems result in lower System Mass but cover the normalised range in the Cost objective. Due to the limited number of systems with Hydrazine propellant and Helium pressurant a similar trend between System Mass and Cost is not apparent.

An alternative method of presentation or visualisation of the results of the design-space exploration method is presented in Figure 6.11, in which the active input variables of the identified nondominated solutions are paired against the output objectives. However, these plots do not provide any significant new information or understanding of the design and output space compared to the parallel coordinate plot presented previously.

6.2.3 Comparison to the True FORMOSAT-3/COSMIC Mission

The location of the two FORMOSAT-3/COSMIC design-points, actual and simulated, in the output space are shown in Figure 6.8. However, due to the dominance of bipropellant propulsion systems comparison of these design-points to similar designs with monopropellant propulsion systems is difficult. Whilst the results of the design-space exploration indicate that bipropellant systems clearly dominate most monopropellant systems, these systems have a significant complexity penalty. In particular, these systems require multiple propellant and pressurant tanks and additional flow control apparatus. Furthermore, there may be significant safety concerns

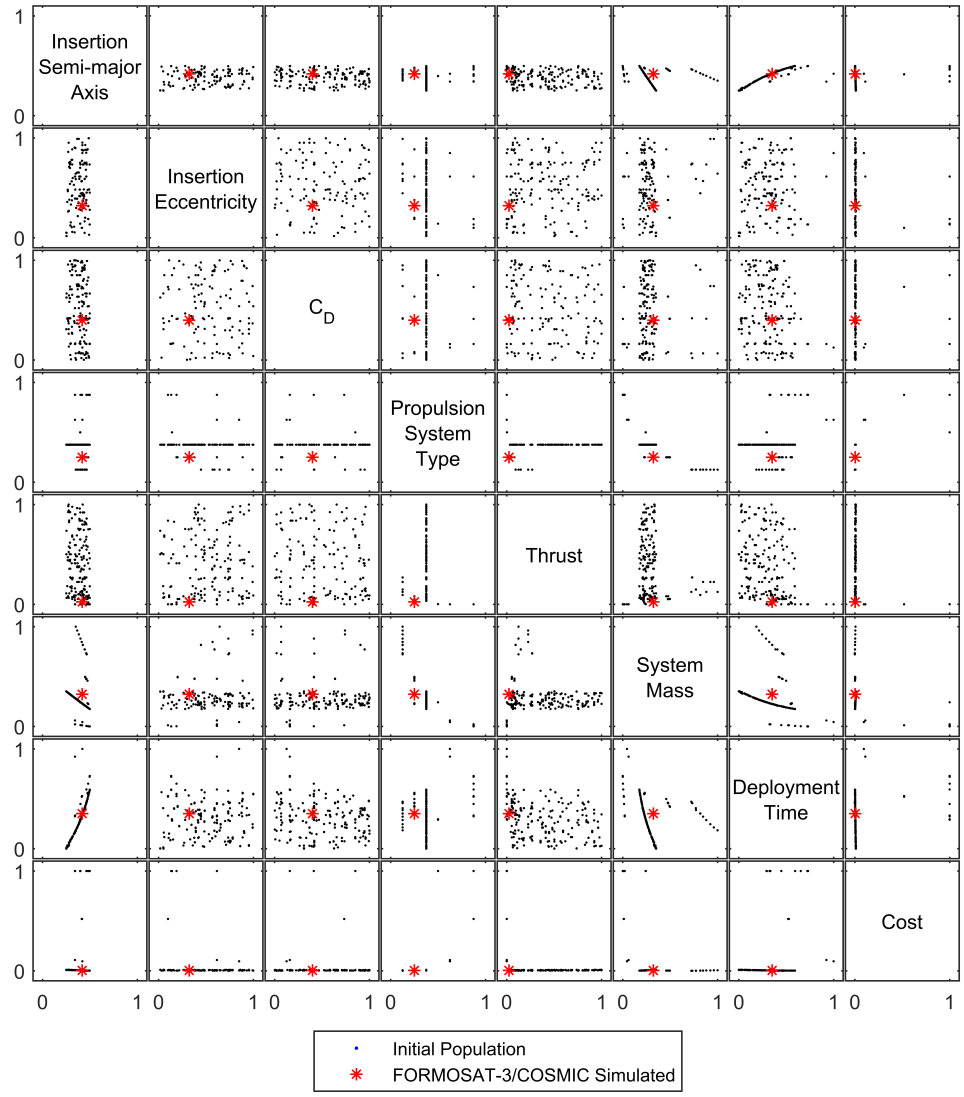

Figure 6.11: Scatter-plot matrix of selected input and output variables of the nondominated set of solutions identified during design-space exploration of the deployment of the FORMOSAT-3/COSMIC mission.

regarding the handling, storage and material compatibility of hypergolic propellant combinations or powerful oxidising agents. For these reasons, bipropellant propulsion systems may be overlooked in favour of systems which may be of simpler design and manufacture or have cheaper operational overheads. Thus, the selection of a monopropellant propulsion system for the FORMOSAT-3/COSMIC system against the better performing bipropellant systems may reflect a factor that is not captured by the presented analysis and design-space exploration methods. However, if this preference for simplicity is known or applied a posteriori, the examination of the results output by the design-space exploration method can be directed accordingly.

In Figure 6.12, the two design-points are plotted against the set of nondominated solutions if only monopropellant systems are considered from the total solution set. In this reduced set of solutions, the simulated result expectedly appears on the line of solutions featuring the same propulsion system, monopropellant Hydrazine with gaseous Helium pressurant. Systems using this combination of propellant and pressurant are generally of higher mass than systems utilising the green propellant AF-M315E for the same deployment time, but have a slightly lower comparative cost. Monopropellant systems using Hydrogen Peroxide propellant result in systems with much greater mass for the same deployment time, but are also the cheapest identified.

Compared to the identified solutions, the actual result is clearly dominated. This is attributable to issues with the mission operations discussed previously and the additional propellant mass carried by the FORMOSAT-3/COSMIC spacecraft.

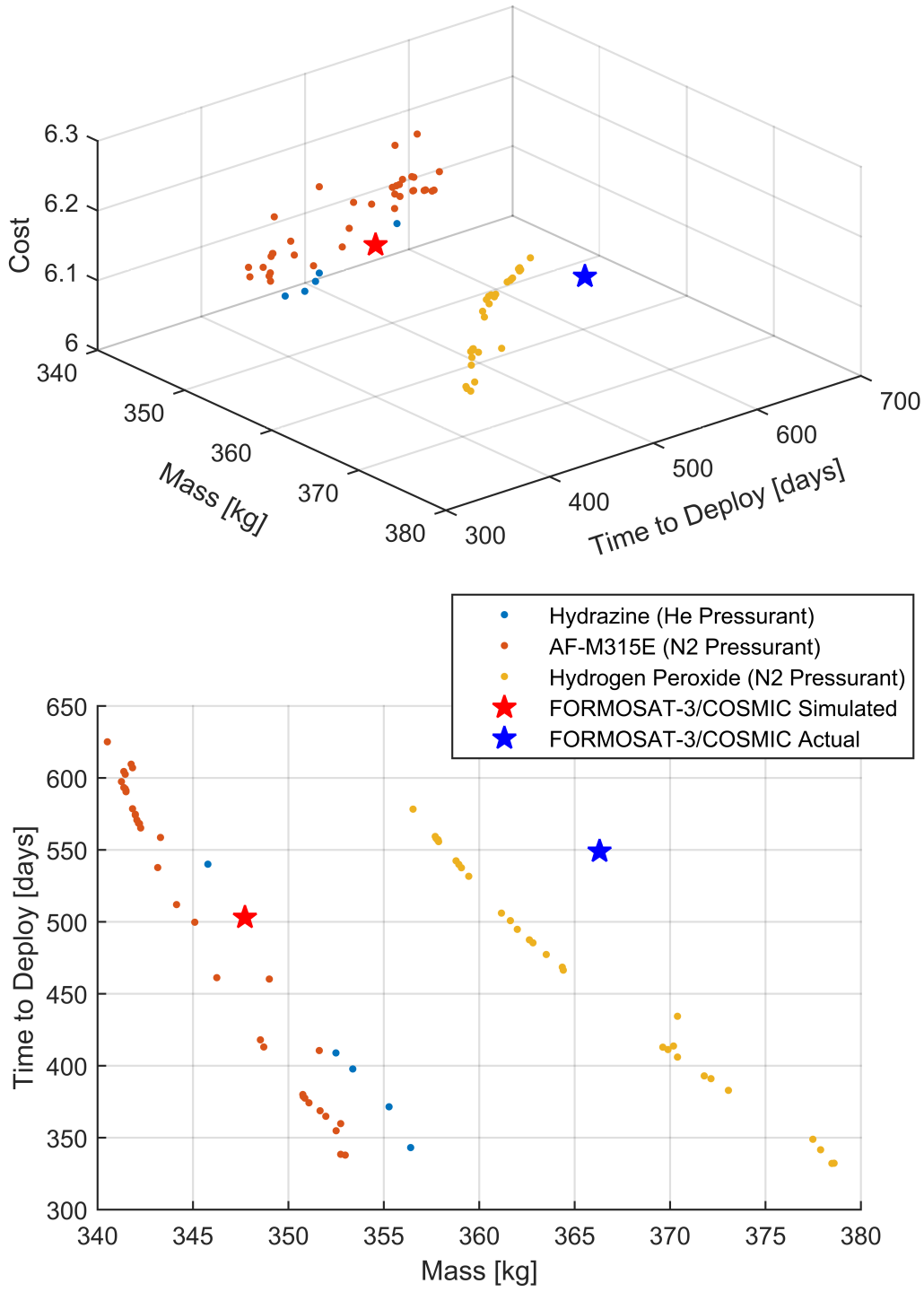

Figure 6.12: Output space of nondominated subset of solutions for monopropellant propulsion systems. The solutions are categorised by propellant and pressurant combination.

6.3 Case Study II: The ORBCOMM Constellation

The ORBCOMM system is a LEO satellite communications constellation launched between 1995 and 1999 to provide global wireless data transfer and messaging services. The plan for the first generation constellation, shown in Figure 6.13, consisted of a total of 47 satellites, of which 32 are arranged in a Walker Delta configuration with 4 equispaced orbital planes at 45° inclination. The remaining satellites were allocated to a pair of high-inclination orbits of 4 satellites each at 70° and 108°, and an equatorial orbit of 7 satellites [38, 39]. However, the final equatorial orbit of the constellation was never populated and only two satellites were placed into each of the high-inclination orbits due to economic and financial issues culminating in the filing of Chapter 11 bankruptcy protection [29].

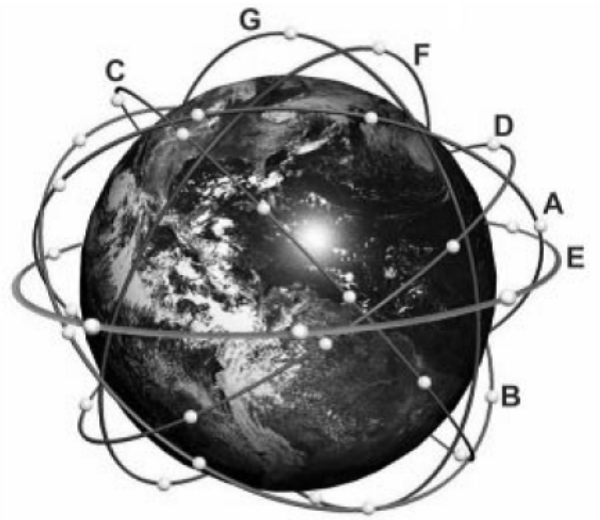

Figure 6.13: Planned ORBCOMM satellite constellation configuration [38]. Planes A–D are arranged in a Walker Delta pattern of 4 planes each containing 8 satellites at 45° inclination. Plane E is an equatorial orbit containing 7 satellites. Planes F and G each contain 4 satellites and are inclined at 70° and 108° respectively.

The deployment of the ORBCOMM constellation was performed by a series of 6 commissioned launches, detailed in Table 6.12. For each launch, the payload consisted of the total compliment of satellites required to population a single orbital plane. Thus, to complete the deployment of the constellation, only small insertion corrections and phasing of the satellites within each orbital plane was required. These manoeuvres were performed using an individual Nitrogen CGT propulsion system on each satellite.

Table 6.12: List of launches of first ORBCOMM constellation satellites [217].

Payload	Date	Launch Vehicle
ORBCOMM F1–F2	Pegasus-H	03-04-1995
ORBCOMM A1–A8	Pegasus-XL HAPS	23-12-1997
ORBCOMM G1–G2	Taurus-2210	10-02-1998
ORBCOMM B1–B8	Pegasus-XL HAPS	02-08-1998
ORBCOMM C1–C8	Pegasus-XL HAPS	23-09-1998
ORBCOMM D2–D8	Pegasus-XL HAPS	04-12-1999

Delivery to orbit of the core Walker Delta configuration of the constellation, planes A–D, was performed by 4 launches over 721 days. The mass of each of these satellites launched was 45 kg [40], resulting in a total mass of 1440 kg. A complete output vector for comparison of the true ORBCOMM constellation launch cannot be determined as cost of these satellites is not reported in the literature. However, the system deployment and total mass can be compared to the results of the design-space exploration nonetheless.

6.3.1 Problem Definition

The input parameters for the planned Walker Delta constellation of 32 satellites forming the core of the ORBCOMM system are presented in Table 6.13. Due to the requirement of multiple satellites in each orbital plane of the constellation, deployment strategies which utilise carrier vehicles can be considered for this mission. The Insertion Date for the analysis was chosen to coincide with the launch of the first set of satellites in the Walker Delta configuration of the actual ORBCOMM constellation such that representative space weather data is used for the calculation of atmospheric density and the evaluation of drag effects. In this analysis, observed solar flux and geomagnetic index data is used as a full archive of predicted space weather index data for the analysis period is not available [218].

Table 6.13: ORBCOMM design-space exploration input parameters.

Property	Value
Number of Satellites	32
Number of Orbital Planes	4
Satellite Dry Mass [kg]	45
Insertion Date	23 December 1997
Deployment Deadline	01 January 2002
Mission Semi-major Axis, a_i [km]	7203
Mission Eccentricity, e_i	0.001
Mission Inclination, i_i [°]	45

The upper and lower bounds for each variable provided to the GA method are presented in Table 6.14. For this mission study, the Inclination was bounded to that of the required mission inclination and the bounds on Semi-major Axis relaxed such that a larger range of orbital altitudes, including those above the mission orbit could be considered by the design-space exploration method.

Table 6.14: Bound constraints on design variables for GA design-space exploration of ORBCOMM mission.

	Lower Bound	**Upper Bound**
Insertion Semi-major Axis [km]	6600	7500
Insertion Eccentricity	1×10^{-6}	1×10^{-2}
Insertion Inclination [°]	45	45
Coefficient of Drag	2.0	2.5
Separation Spring Velocity [$\mathrm{m\,s^{-1}}$]	0.1	2.0

Using a population size of 50 individuals and the QRNG method of initialisation, the initial population shown in Figure 6.14 was generated. In this initial population of total 50 individuals, 8 are solutions which utilise carrier vehicles in order to perform the in-plane orbital manoeuvres required to achieve the spacing in RAAN. The initial population generated covers a range in insertion Semi-major Axis between the normalised values of 0.15 to 1, corresponding to approximately 6750 km to 7500 km. Solutions with a Semi-major Axis below approximately 6750 km were found to be infeasible due to the decay of one or more of the payloads before the deployment could be completed. In addition, an exclusion area between approximately 0.6 to 0.8 or 7140 km to 7320 km is present, due to the Deployment Deadline parameter which mandates a minimum rate at which the insertion orbit and mission orbit planes must separate. However, due to the sparsity of the points, a factor of the working population size, these ranges are only indicative of true feasibility limits in the design-space.

In the initial population, shown in Figure 6.14, the spread of Propulsion System Type for both individual spacecraft and subsatellite/carrier-vehicle combinations appears to be restricted to CGT, monopropellant, bipropellant, and resistojet systems. Additionally, in the Separation Spring Velocity parameter, each of the identified solutions in the initial population are below the normalised value of 0.4, or $0.86\,\mathrm{m\,s^{-1}}$. Due to the use of space-filling QRNG population generation, this indicates that designs which specify the use of Separation Spring Velocities

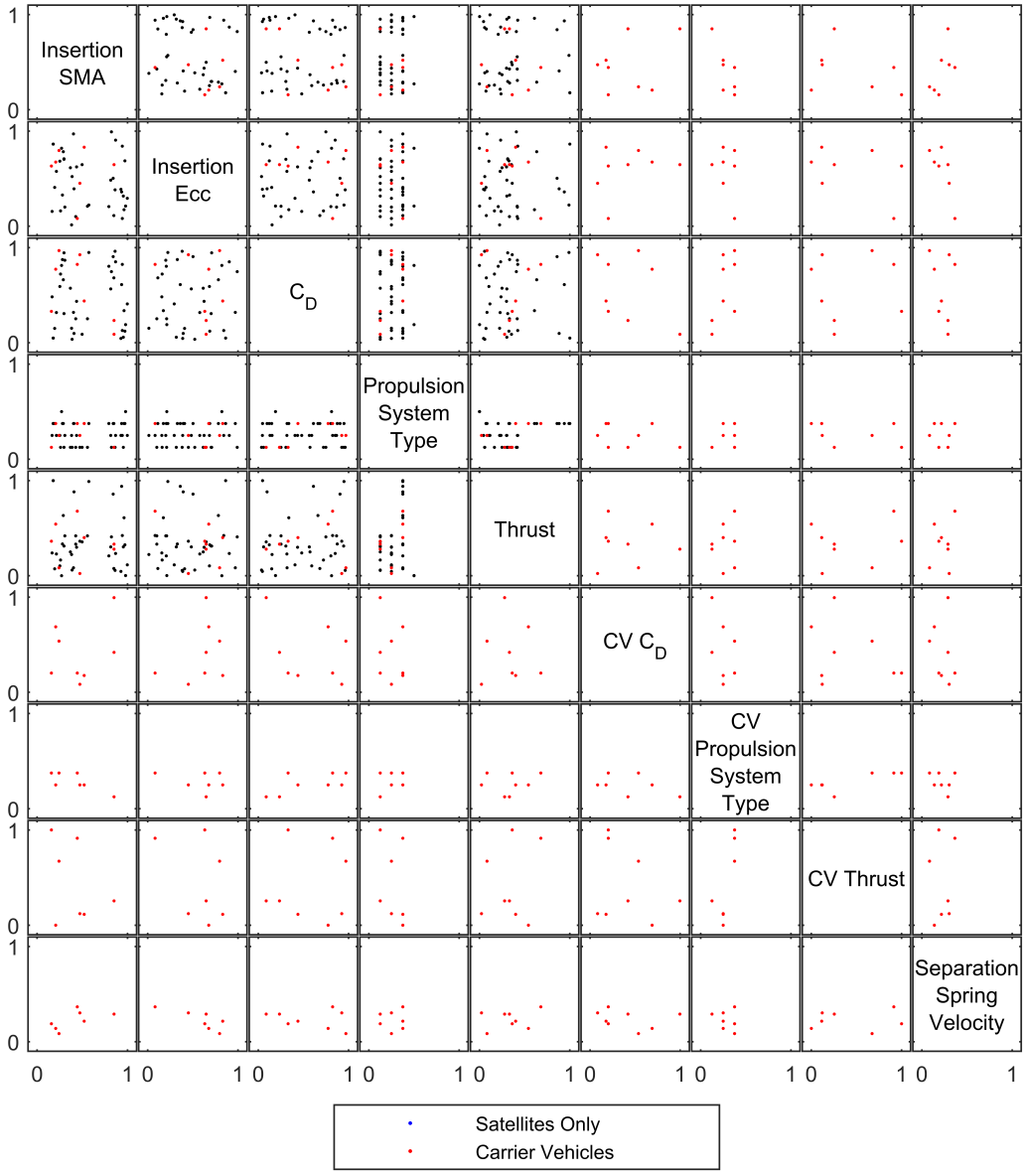

Figure 6.14: Scatter-plot matrix of input variables of initial population members for ORBCOMM mission analysis. Initialisation was performed using Quasi-Random Number Generation sampling to generate a population of 50 individuals.

greater than this, solutions are generally infeasible. This is likely due to the propulsive requirements required by the subsatellites to return to the required mission orbit from the phasing orbit achieved using the spring velocity.

6.3.2 Tradespace Analysis

The total set of solutions obtained by the GA implementation of 50 generations with a working population size of 50 individuals is shown in Figure 6.15. Designs which do not use carrier vehicles are shown as points with colour indicating the Propulsion System Type of the individual satellites. Designs which utilise carrier vehicles are shown as open shapes of which the colour indicates the Propulsion System Type of the carrier vehicle. The Propulsion System Type of the subsatellites deployed by these carrier vehicles is not shown to maintain clarity of the figure.

In the tradespace shown, designs which utilise carrier vehicles are demonstrated to have a greater comparative cost than designs of individual satellites. Furthermore, the total mass of these systems is shown to be greater than individual satellites, with the exception of individual satellites with CGT propulsion systems. However, designs utilising carrier vehicles are also shown to be capable of achieving the shortest Time to Deploy of all solutions identified during the performed design-space exploration. In addition, an example of the explorative capability of the GA optimisation method is demonstrated by the appearance of a carrier vehicle vehicle design which utilises an arcjet propulsion system. As no arcjet systems were identified during the analysis of the initial population shown in Figure 6.14, the introduction of this Propulsion System Type is purely attributable to the mutation operator of the GA optimisation method.

In Figure 6.16 the set of nondominated solutions corresponding to designs which do not utilise carrier vehicles are shown. These solutions demonstrate that designs which utilise individual satellites with bipropellant propulsion systems are capable of generating both the shortest deployment time and lowest mass systems in the set of identified designs. However, designs with monopropellant propulsion systems are also well represented in the nondominated set due to their lower relative cost. A single CGT system is also present in the nondominated set due to a lower cost than bipropellant systems with comparative deployment times. However, the mass of this system is significantly greater than the other nondominated solutions, a result of the relatively low specific impulse of CGT propulsion systems. In comparison to the complete set of results shown in Figure 6.15, no resistojet systems are represented in the nondominated set, primarily due to their increased cost in comparison to the other propulsion

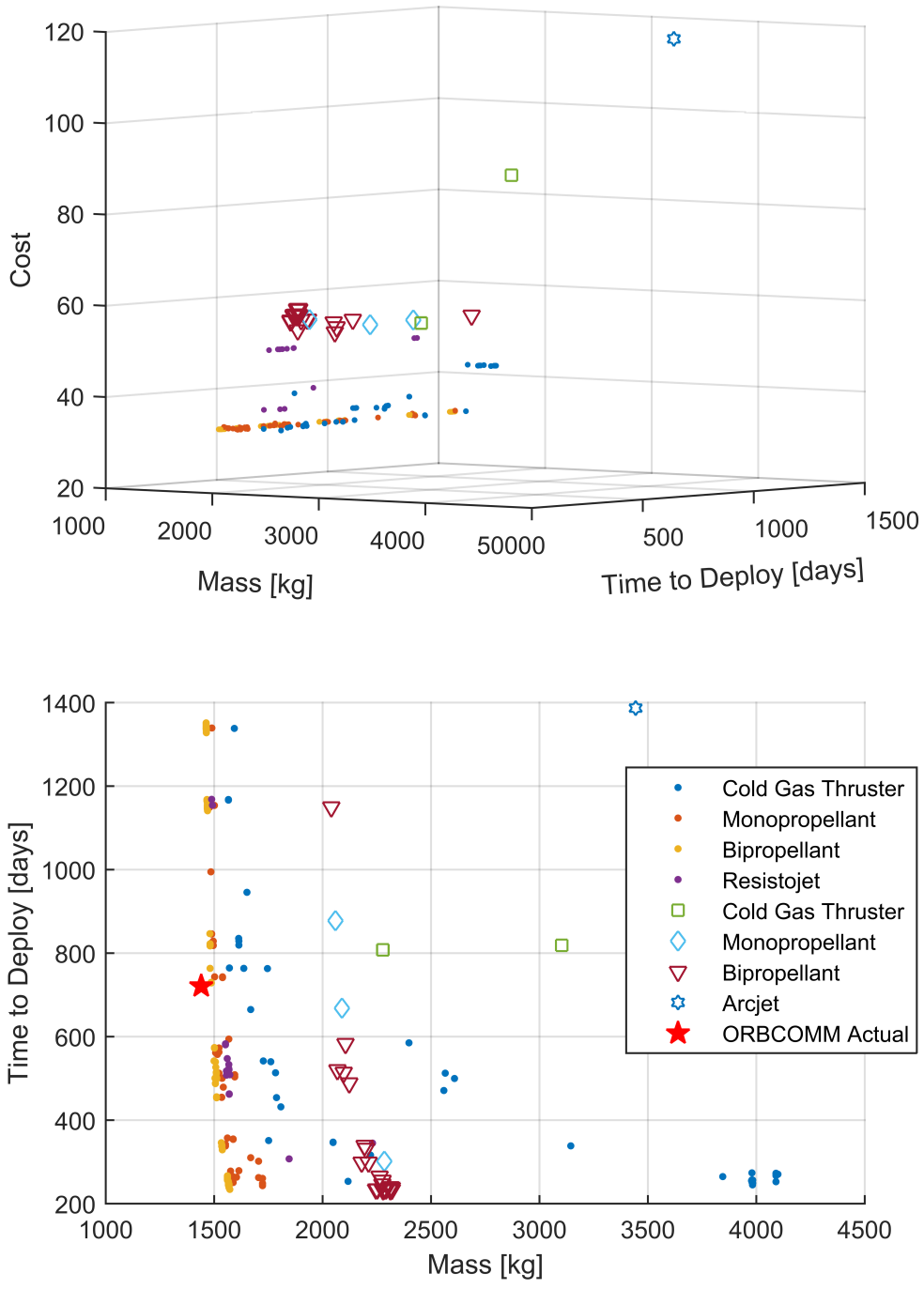

Figure 6.15: Output space of total solution set obtained using 50 generation GA design-space exploration method with a population size of 50 individuals. Designs which do not use carrier vehicles are shown as points with colour indicating the Propulsion System Type of the individual satellites. Designs which utilise carrier vehicles are shown as open shapes of which the colour indicates the Propulsion System Type of the carrier vehicle.

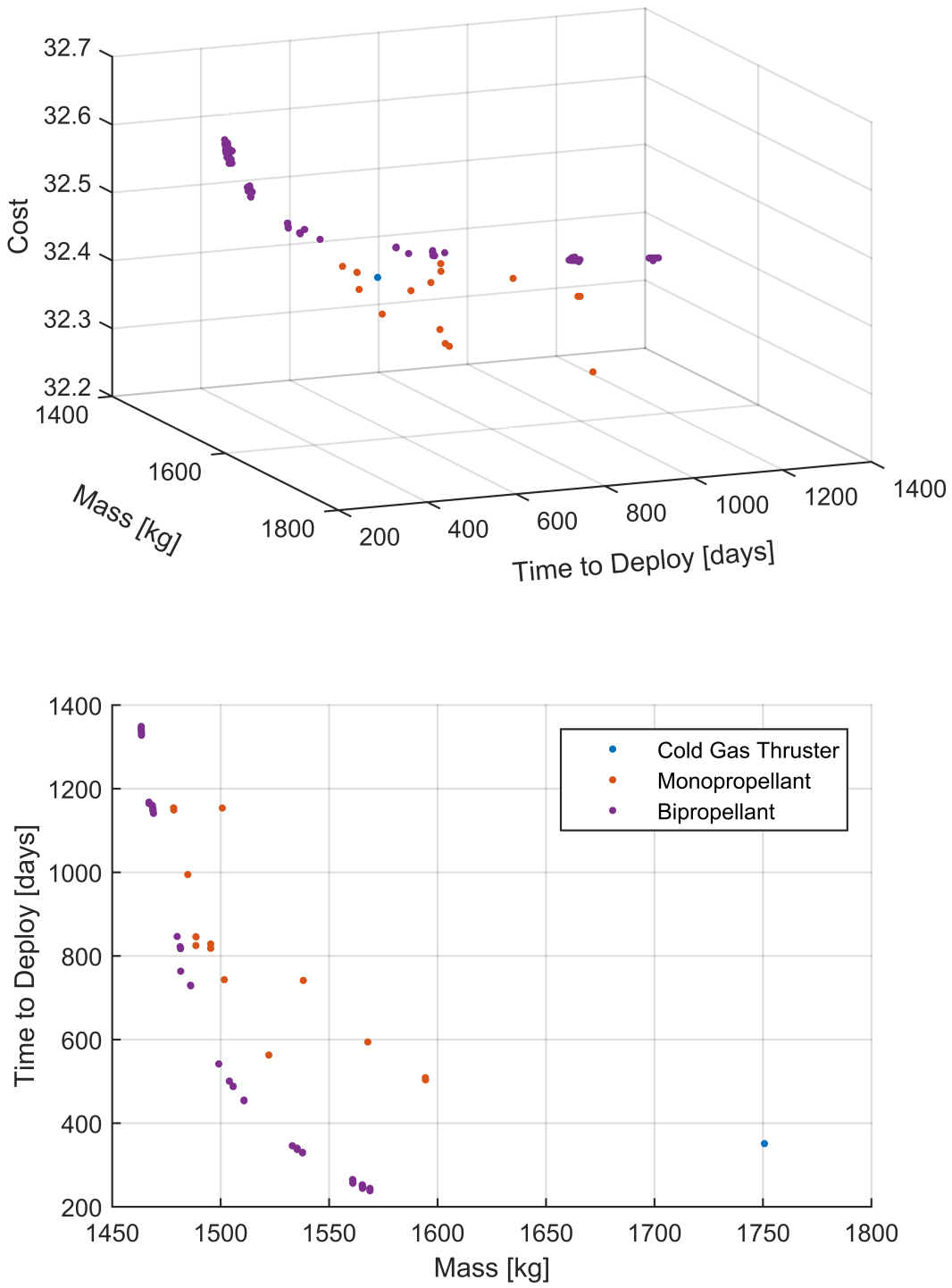

Figure 6.16: Output space of nondominated set of solutions which utilise individual satellite deployment strategies. The solutions are categorised by propulsion system type.

system types. Similarly to the analysis of the first case study presented in Section 6.2.2, an identifiable tradeoff between deployment time and system mass can be observed in the well represented monopropellant and bipropellant propulsion system types.

The nondominated set of solutions which utilise carrier vehicles is shown in Figure 6.17. Of the solutions identified by the design-space exploration, all but one of the nondominated solutions utilise a bipropellant propulsion system for the carrier vehicle, whilst the remaining solution uses a monopropellant propulsion system. Due to the relationship between propulsive requirement and rate of planar separation, a tradeoff between deployment time and total mass also exists for these designs which utilise carrier vehicles.

Comparison of designs which utilise carrier vehicles to designs which do not, using Figure 6.15, indicates a mass penalty which is associated with the use of carrier vehicles to perform the deployment of a constellation within a similar time period. Furthermore, the cost of these systems which utilise carrier vehicles is observed to be greater than the use of individual satellite deployment architectures. However, as discussed in Section 5.3, the method of cost estimation implemented only considers the mass of the propulsion system calculated by the vehicle sizing method. The benefits of use of carrier vehicles may therefore not be captured by the comparative cost measure. For example, use of a smaller propulsion system on the subsatellites may reduce design constraints and result in simplification of the design and manufacturing process. Similarly, the propulsion system of the carrier vehicle may be less constrained or complex due to size and therefore less costly to design, produce, and integrate.

The method of system cost estimation implemented, considering only propulsion system dry-mass, may disadvantage strategies which utilise carrier vehicles in the design-space exploration process, as these solutions which may be preferable when other aspects of the system design are considered are indicated to be inferior. Thus, during the selection phase of the genetic algorithm, these designs will be less likely to be passed through to subsequent generations, and will not contribute to the on-going optimisation process.

6.3.3 Comparison to Launch of the Actual ORBCOMM Constellation

In the 2D projection of deployment time against total system mass in Figure 6.15, the corresponding result of the true ORBCOMM system is shown for comparison to the results of the design-space exploration. As the actual constellation was launched as a series of satellite

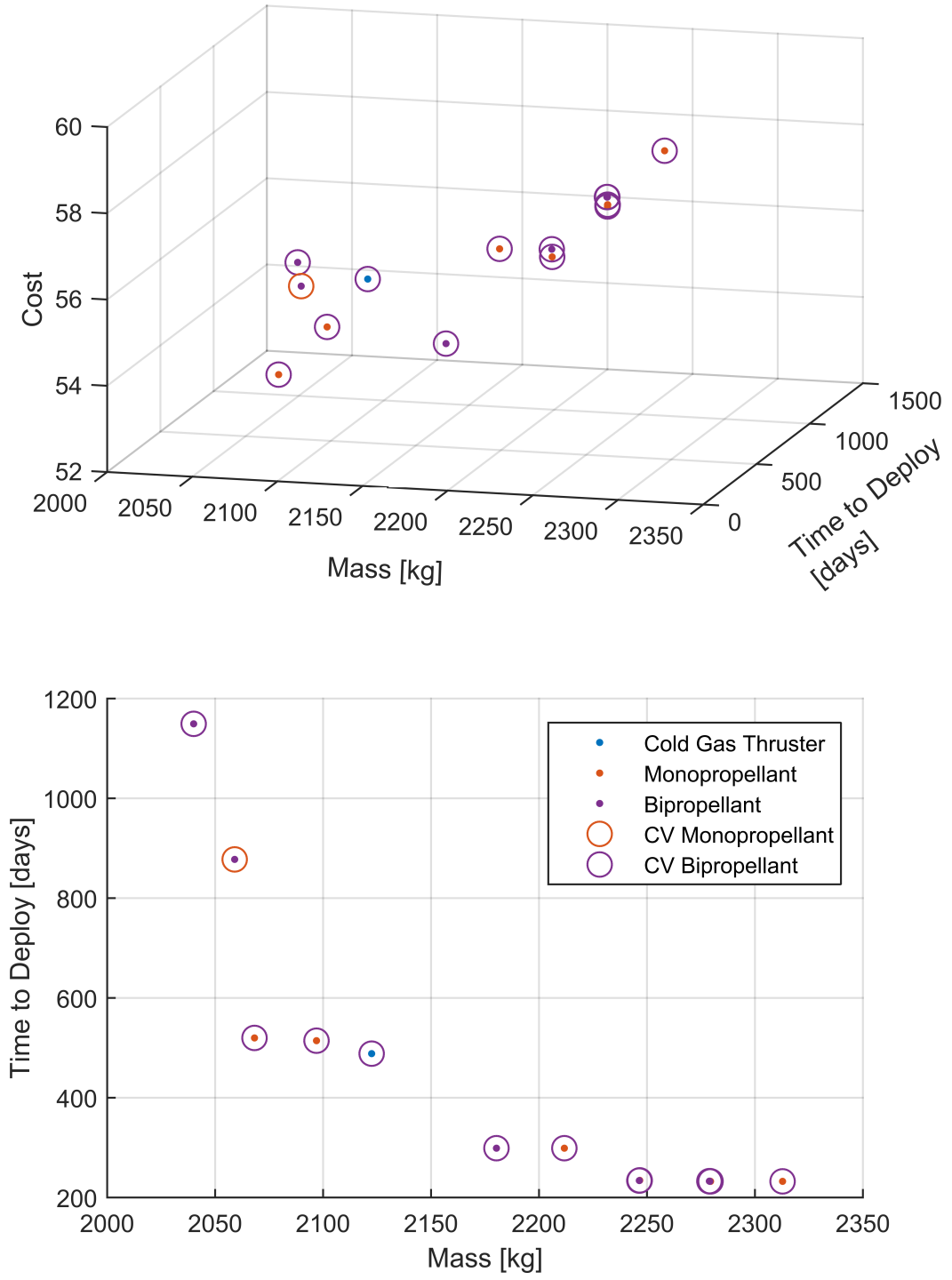

Figure 6.17: Output space of nondominated set of solutions which utilise carrier vehicles. The propulsion system of the carrier vehicle is indicated by the colour of the retaining circle, whilst the propulsion system of the corresponding subsatellites is indicated by the contained point.

clusters, each to the correct orbital plane, each satellite was only required to perform phasing manoeuvred to complete the deployment. None of the solutions identified by the design-space exploration were therefore able to achieve a smaller total system mass. However, a significant number of solutions demonstrate a shorter time to deploy than the actual ORBCOMM mission, indicating that deployment using a single launch vehicle and indirect plane separation could have enabled completion of the core Walker Delta configuration of the constellation in a much shorter time period. In addition, the difference in cost between a single launch and 4 discrete and dedicated launches may be significant. Using the nominal cost for the Pegasus-XL HAPS launch vehicle reported by Isakowitz et al. [219], the total cost of launch of the actual ORBCOMM constellation would have been $100M. However, launch of the complete system on a single vehicle, assuming a total system mass of less than 2000 kg, could be achieved for about $45M using a Delta-II launch vehicle [219]. This represents a saving of 55 % on launch costs alone, corresponding to approximately 17 % of the reported total system cost of $330M [49, 220].

This comparison, however, does not take into account the constraint on launch schedule which was somewhat affected by the manufacture of the large number of satellites comprising the constellation [40]. Furthermore, launch of the complete set of satellites comprising a constellation on a single launch vehicle may represent a significantly greater risk than multiple launches of fewer payloads and using different vehicles. Whilst able to potentially provide a shorter time to full system capability, launch in this manner may therefore be less desirable from an operations, investment, or insurance perspective [221].

6.4 Case Study III: Earth Imaging Nanosatellite System

This third case study is inspired by the notional Earth imaging constellation proposed by Andrews [222] for low revisit time, of the order of 20 minutes. This constellation, depicted in Figure 6.18, is comprised of 80 nanosatellites in a "low-ball" configuration, a Walker Delta pattern with 8 planes at 500 km altitude and 55° inclination, and a further two "high-ball" planes in SSO of 10 satellites each. The proposed satellites are of 6U CubeSat form factor, approximately 8 kg mass, and capable of 3.5 m GSD.

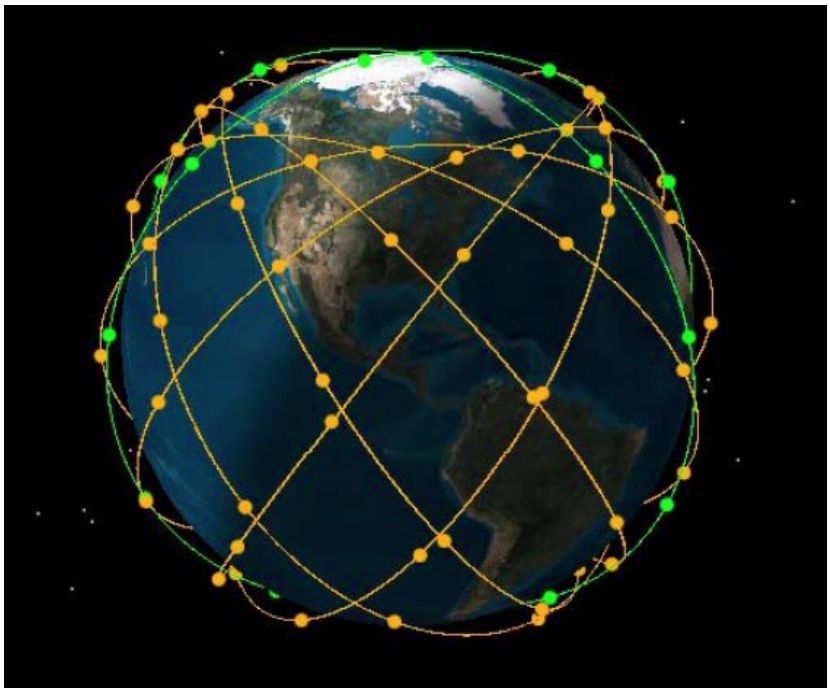

Figure 6.18: Proposed Earth imaging nanosatellite constellation, comprised of 8 planes in Walker Delta configuration at 55° inclination (yellow) and 2 planes in SSO (green) [222].

6.4.1 Problem Definition

The input parameters for this proposed Earth imaging nanosatellite constellation are presented in Table 6.15. For this case study, in contrast to the previous two analyses, the selected insertion date of the payloads is in the future, requiring the use of predicted solar flux and geomagnetic index data rather than observed values. Thus, the results of this design-space exploration will be associated with additional uncertainty as the accuracy of the predicted space weather index data is not known.

Table 6.15: Earth imaging nanosatellite constellation design-space exploration input parameters.

Property	**Value**
Number of Satellites	80
Number of Orbital Planes	10
Satellite Dry Mass [kg]	8
Insertion Date	06 June 2016
Deployment Deadline	06 June 2018
Mission Semi-major Axis, a_i [km]	6871
Mission Eccentricity, e_i	0.001
Mission Inclination, i_i [°]	55

Due to the relatively low on-orbit lifetime of the proposed spacecraft, specified as 36 months by Andrews [222], the allowable deployment phase for such a system must be kept short to ensure that the period of full mission capability is not impacted. A period of 2 years was therefore selected such that any identified designs would result in at least a complete year of full mission capability following the completion of deployment before the design lifetime of the satellites is exceeded.

The bounds on the design variables for the GA are shown in Table 6.16. In this initial analysis of this mission, it is assumed that a dedicated launch of the "low-ball" constellation is performed. Thus, the inclination of the initial orbit is constrained to that of the mission orbit.

Table 6.16: Bound constraints on design variables for GA design-space exploration of Earth imaging nanosatellite constellation.

	Lower Bound	**Upper Bound**
Insertion Semi-major Axis [km]	6600	7500
Insertion Eccentricity	1×10^{-6}	1×10^{-2}
Insertion Inclination [°]	55	55
Coefficient of Drag	2.0	2.5
Separation Spring Velocity [$\mathrm{m\,s^{-1}}$]	0.1	2.0

Using a population size of 100 individuals, the initial population shown in Figure 6.19 was generated using the QRNG method. In the input variable matrix of the initial population shown, 18 solutions which utilise carrier vehicles are indicated. In this initial population a clear range of feasibility is indicated in the Semi-major Axis variable as no solutions below approximately 0.5, corresponding to 7050 km are shown. The infeasibility of solutions with a smaller Semi-major Axis is attributable to two limitations, either that one or more satellites will

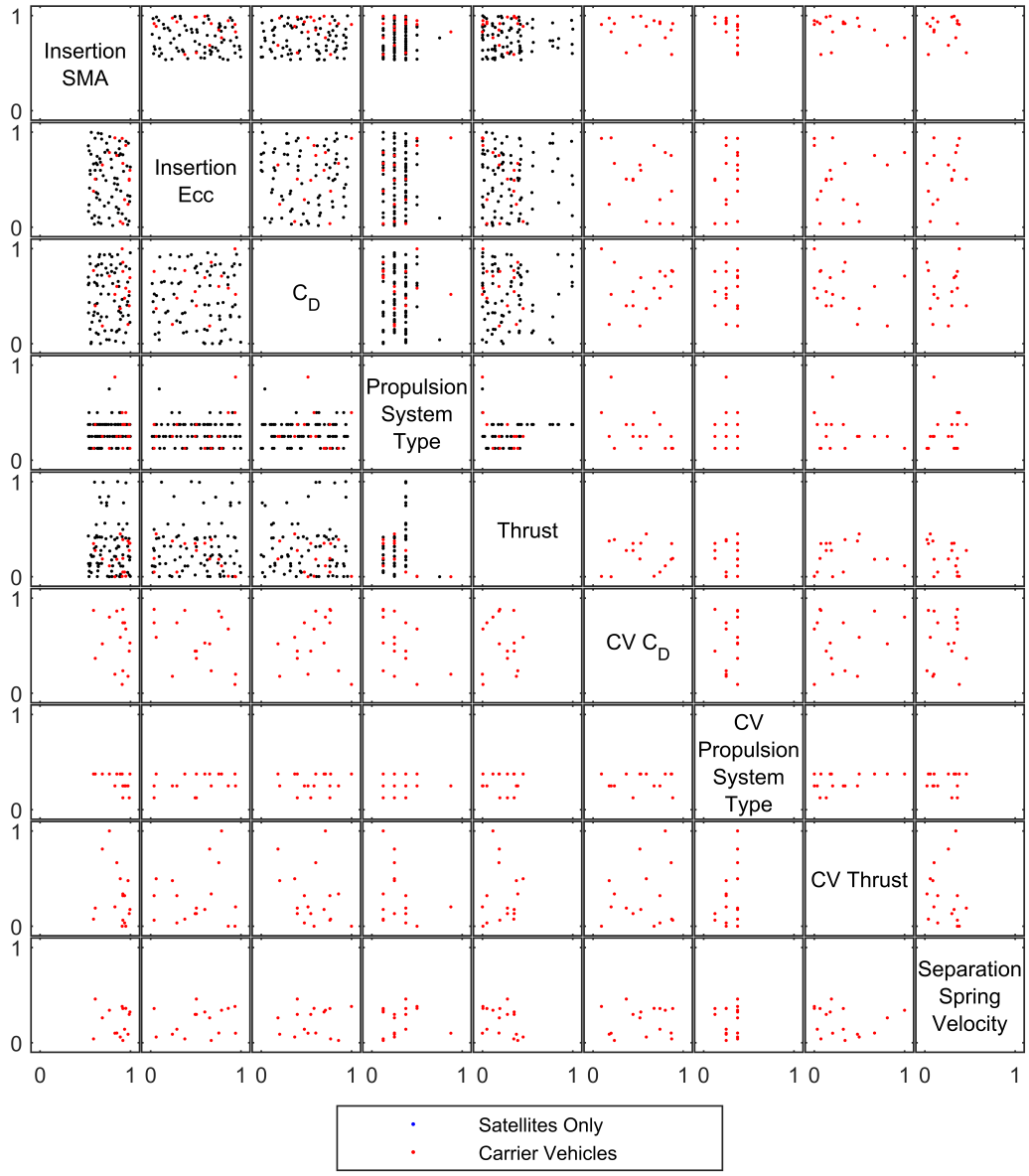

Figure 6.19: Scatter-plot matrix of input variables of initial population members for Earth imagining nanosatellite constellation analysis. Initialisation was performed using Quasi-Random Number Generation sampling to generate a population of 100 individuals.

decay before the deployment is completed, or that the drift-rate between the initial and mission orbital planes is not fast enough to satisfy the Deployment Deadline parameter imposed.

A range of different propulsion systems are identified in the initial population shown in Figure 6.19. CGT, monopropellant, bipropellant, resistojet, low-power Hall-effect and ion systems are identified for individual satellites or subsatellites, whilst CGT, monopropellant, and bipropellant systems are indicated for carrier vehicles. However, this is only an indication of

feasibility as the QRNG initialisation method may not have sampled from all feasible regions of the design-space. Of the identified solutions, the maximum thrust of the subsatellites for carrier vehicle solutions is shown to be less than the maximum thrust for individual satellite solutions. This is due to the propulsion system sizing relationships between thrust and thruster mass, which result in a restricted thrust to limit the mass of the individual subsatellites. Finally, similarly to the previous case study, the Separation Spring Velocity appears to be limited to a normalised value of about 0.45, or $0.97\,\mathrm{m\,s^{-1}}$.

6.4.2 Tradespace Analysis

The total set of results of the GA design-space exploration process is shown in Figure 6.20. In the output tradespace shown, the carrier vehicle designs are shown to have generally greater comparative cost than individual satellites. However, with respect to the system mass, the penalty for carrier-vehicle use appears to be less than that demonstrated in the previous case study of the ORBCOMM constellation. For this mission, in which the satellites are of much smaller dry-mass, the effects of propulsion system scaling become more pronounced. Furthermore, as 10 satellites are required in each orbital plane, the duplication of this propulsive requirement magnifies this effect.

The output tradespace for the set of nondominated designs for deployment strategies using individual satellites is shown in Figure 6.21. In this tradespace satellites with low-power Hall-effect and ion propulsion systems are shown to achieve the lowest total system mass, due to the higher specific impulse of these systems. However, due to their higher thruster mass, these systems have a greater propulsion system mass fraction. Furthermore, these systems are limited to deployment times in excess of 600 days. The shortest deployment times are achieved by satellites with either monopropellant or bipropellant propulsion systems with thrust magnitude enough to perform the larger in-plane manoeuvres required. The satellites with CGT propulsion systems are capable of similarly short deployment times, but have much greater mass due to the lower specific impulse of the system. With respect to the cost metric, the Hall-effect and ion systems are shown to have a higher comparative cost than the CGT, monopropellant, and bipropellant systems, attributable to their higher propulsion system dry-mass used in the SSCM CERs.

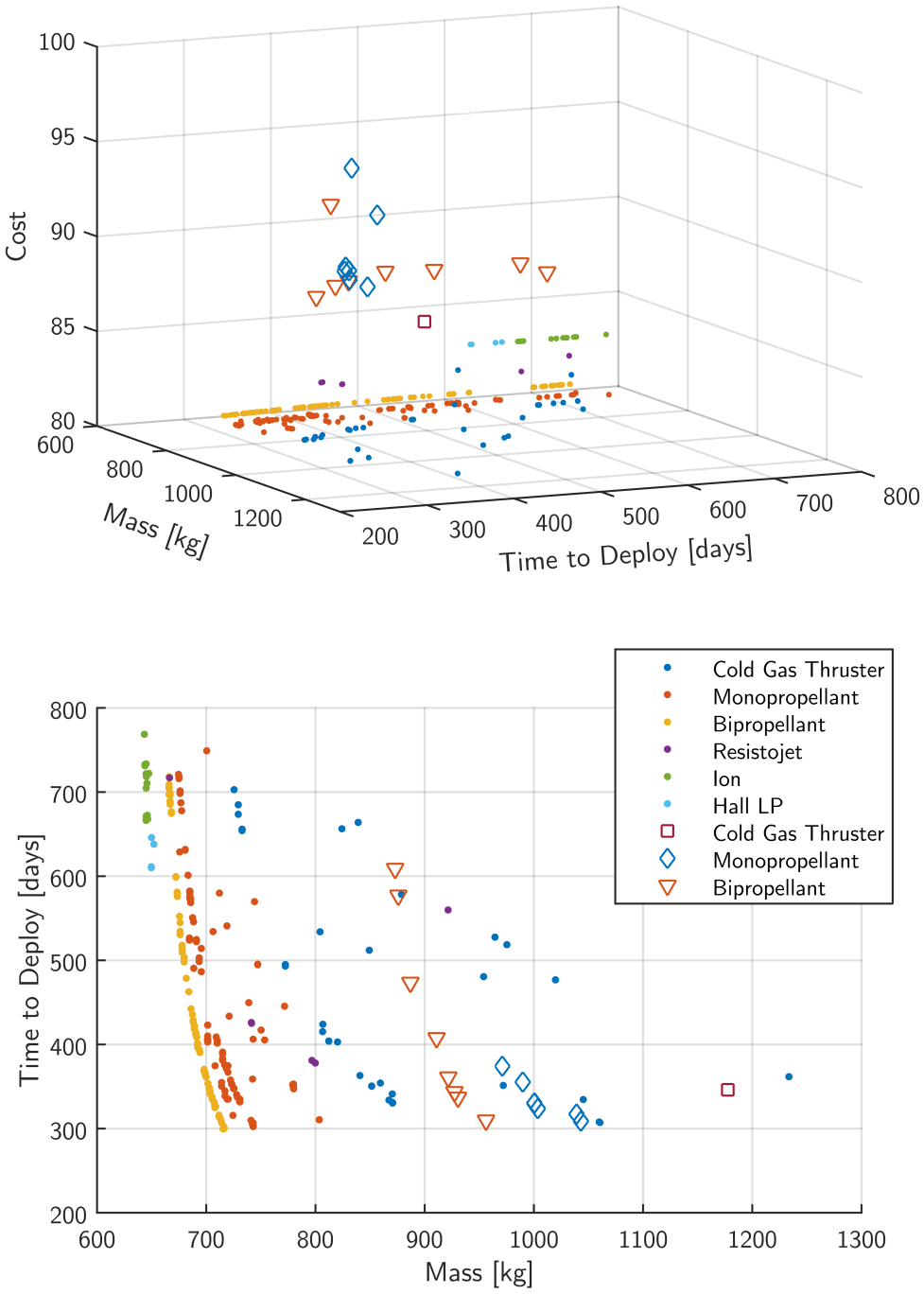

Figure 6.20: Output space of total solution set obtained using 10 generation GA design-space exploration method with a population size of 100 individuals. Designs which do not use carrier vehicles are shown as points with colour indicating the Propulsion System Type of the individual satellites. Designs which utilise carrier vehicles are shown as open shapes of which the colour indicates the Propulsion System Type of the carrier vehicle.

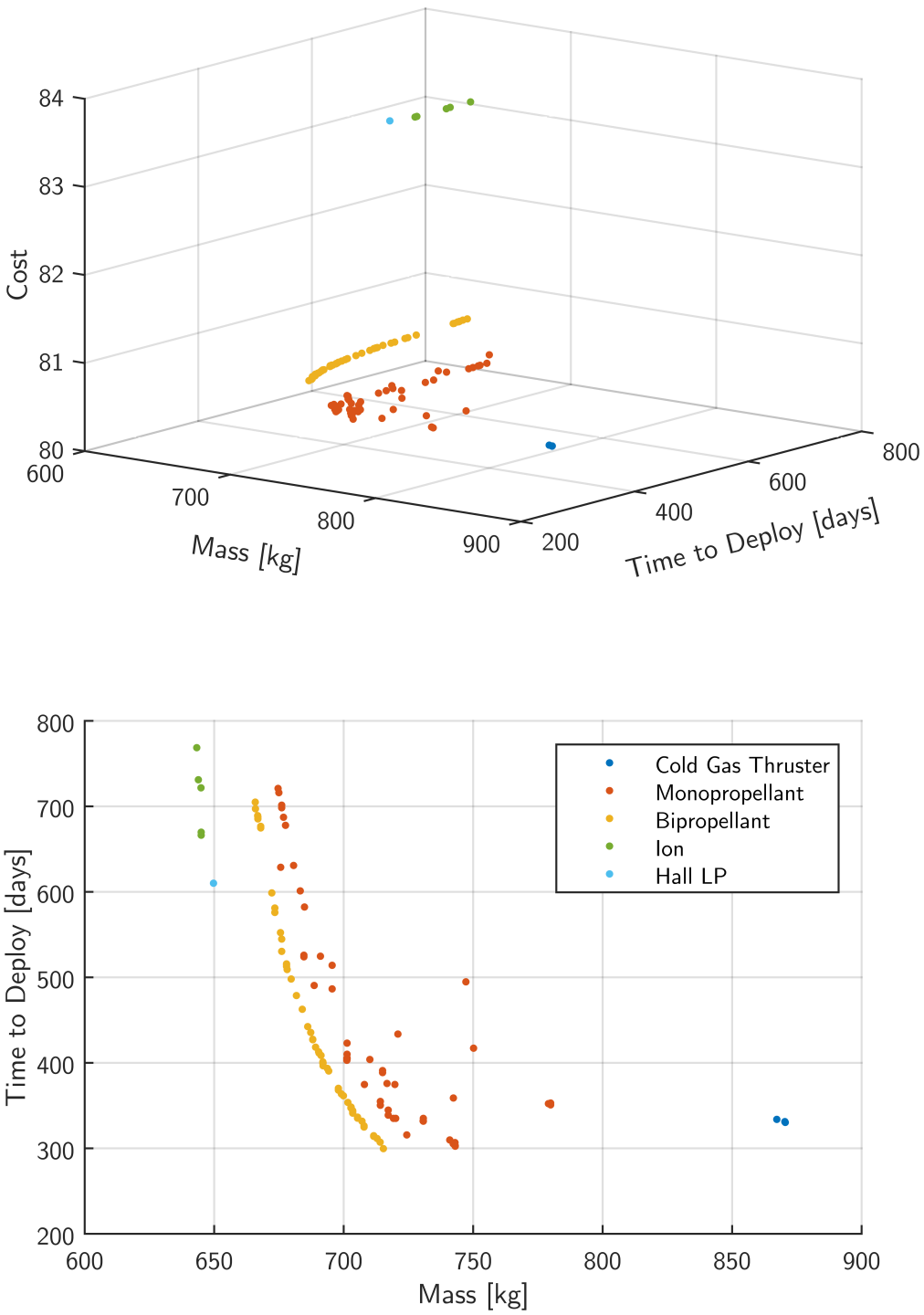

Figure 6.21: Output space of nondominated solutions which utilise individual satellite deployment strategies. The solutions are categorised by propulsion system type.

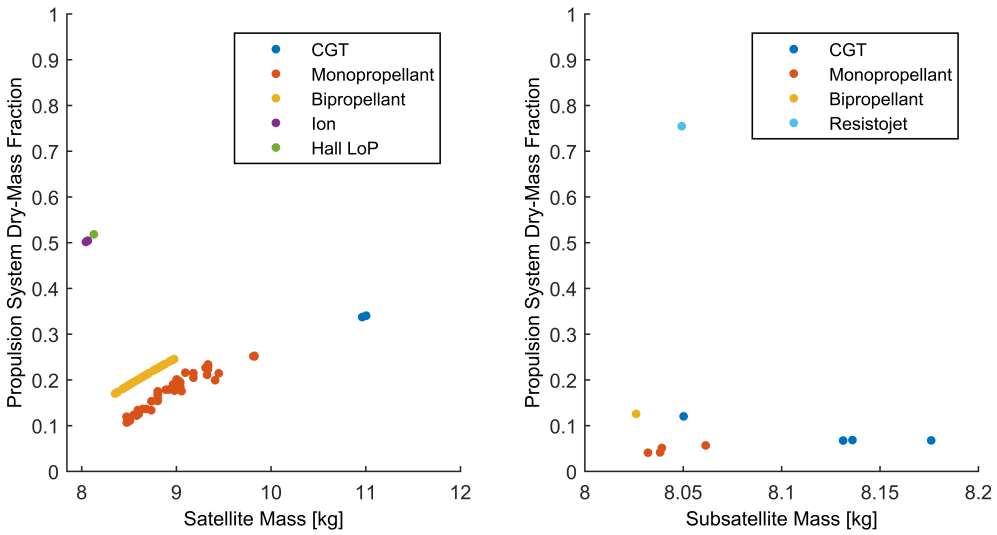

Figure 6.22: Comparison of propulsion system mass fraction for different propulsion system types. Left: Individual satellite designs, Right: Subsatellites of carrier vehicle designs

The set of nondominated carrier vehicle designs is shown in Figure 6.23. Similarly to the previous design-space exploration of the ORBCOMM constellation, the number of carrier vehicle strategies analysed may have been limited by the method of system cost-estimation and dependence of cost on propulsion system dry-mass. The tradeoff between system mass and deployment time for these carrier-vehicle solutions is clearly demonstrated in the tradespace. A single CGT solution is present in the nondominated set due to its low comparative cost, a result of the low propulsion system dry-mass. However, the system mass for this design is high due to the low specific impulse of CGT propulsion systems.

No identifiable tradeoff is apparent between the different propulsion systems of the subsatellites shown in the tradespace in Figure 6.23. However, due to smaller mass of the subsatellite propulsion system in comparison to the carrier vehicle propulsion system and and its use in only performing the necessary orbital phasing manoeuvres, the result of different subsatellite propulsion systems may not be easily identifiable in the tradespace. Furthermore, sparsity of solutions in the tradespace makes any trends difficult to identify.

The mass budget of the subsatellite propulsion systems can also be investigated in more detail. In Figure 6.22, the propulsion system mass fraction of satellite-only deployment strategies is compared to that of the subsatellites in carrier-vehicle deployment strategies. The propulsion system mass fraction for the subsatellite resistojet system solution is shown to be approximately

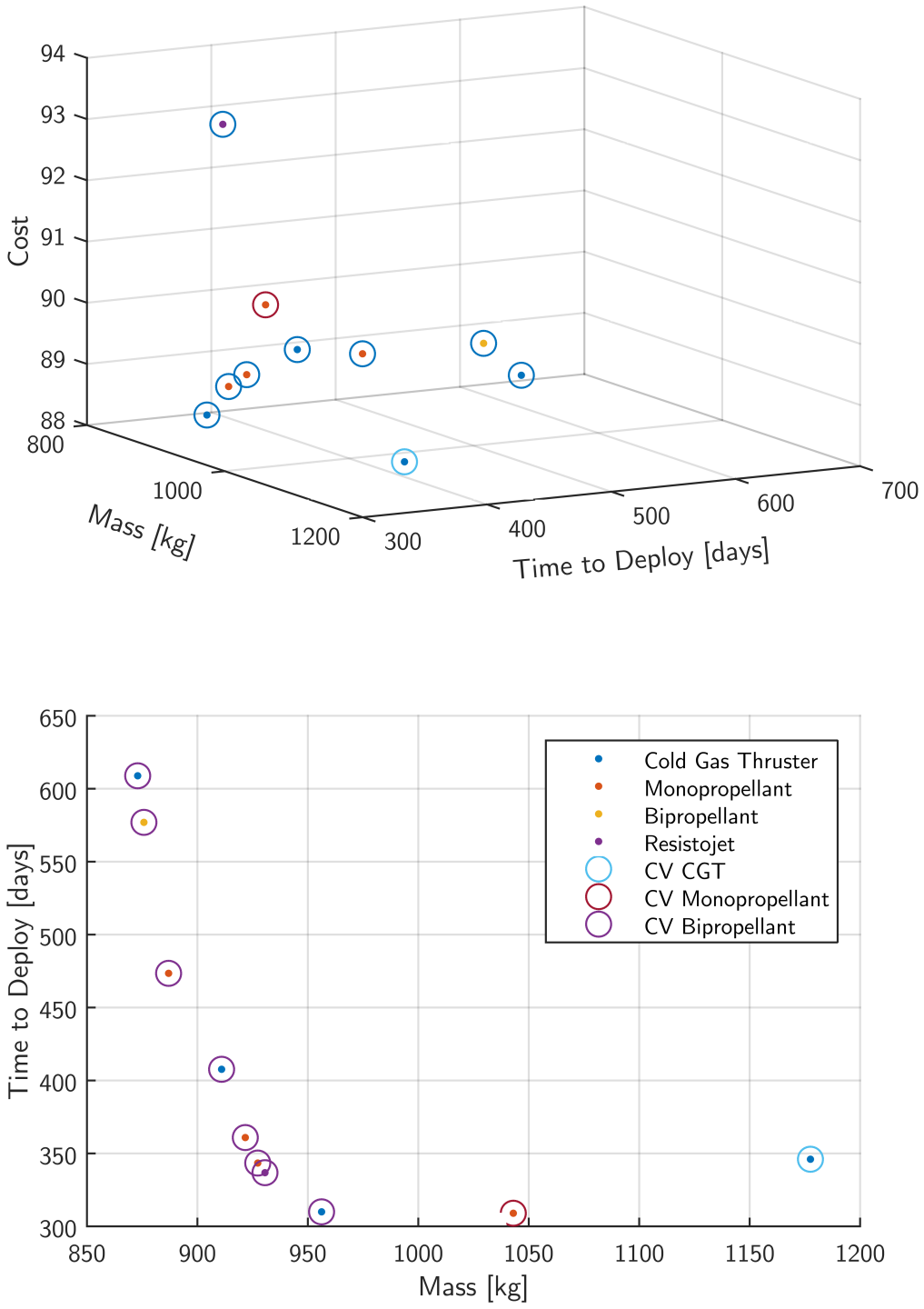

Figure 6.23: Output space of nondominated set of solutions which do not utilise carrier vehicles. The propulsion system of the carrier vehicle is indicated by the colour of the retaining circle, whilst the propulsion system of the corresponding subsatellite is indicated by the contained point.

0.75, indicating that only 25 % of the subsatellite mass is left for the payload and remaining subsystems. In comparison, the CGT, monopropellant, and bipropellant systems have much lower propulsion system dry-mass fractions and may therefore result in more viable vehicle designs. The propulsion system mass fraction for individual satellite designs is shown to trend positively with satellite mass. This is due to the propellant mass required to perform the in-plane orbital transfers of varying magnitude depending on the selected insertion orbit.

6.4.3 Launch using a Secondary Payload Opportunity

For constellations of small satellites the most viable or affordable method of launch may be using available piggyback launch opportunities. However, for these launches, the insertion orbit is typically chosen by the primary payload operator and therefore may not be optimal for the mission of the secondary payloads. For a launch of this type, the design-space is significantly reduced as the insertion orbit properties, Semi-major Axis, Eccentricity, and Inclination, are known and are not variable. However, as the insertion orbit Inclination may be different to that of the mission orbit of the constellation, out-of-plane transfer manoeuvres may be required in order to achieve the specified deployment.

Table 6.17: Bound constraints on design variables for GA design-space exploration of Earth imaging nanosatellite constellation launched using a secondary payload opportunity.

	Lower Bound	**Upper Bound**
Insertion Semi-major Axis [km]	6798.1	6798.1
Insertion Eccentricity	1×10^{-4}	1×10^{-4}
Insertion Inclination [°]	51.6	51.6
Coefficient of Drag	2.0	2.5
Separation Spring Velocity [$\mathrm{m\,s^{-1}}$]	0.1	2.0

The chosen secondary payload launch opportunity is based on a scheduled launch of a resupply mission to the ISS in May 2016, to be fulfilled by a SpaceX Falcon 9 vehicle [91]. These ISS resupply missions are a frequent source of secondary-payload launch opportunities. The planned insertion orbit of this launch is to an altitude of 420 km and inclination of 51.6°, corresponding to the approximate orbit of the ISS. However, the selected insertion orbit altitude for this analysis has been increased to 720 km to ensure that the planned plane separation can be performed before the selected Deployment Deadline and decay of the payloads occurs. This increase in orbital altitude could be achieved using an upper-stage or secondary payload transfer vehicle such as that offered by Andrews [223]. Given this chosen launch opportunity and insertion orbit, the Semi-major Axis, Eccentricity, and Inclination variables for the design-space analysis are constrained, reflected in the design variables bounds in Table 6.17.

The initial population for this analysis, generated using the QRNG method, is shown in Figure 6.24. Due to the previously provided constraints on the insertion orbit properties, the Semi-major Axis, Eccentricity, and Inclination variables have been neglected in this input variable matrix. The initial population generated for this analysis features 40 designs which utilise

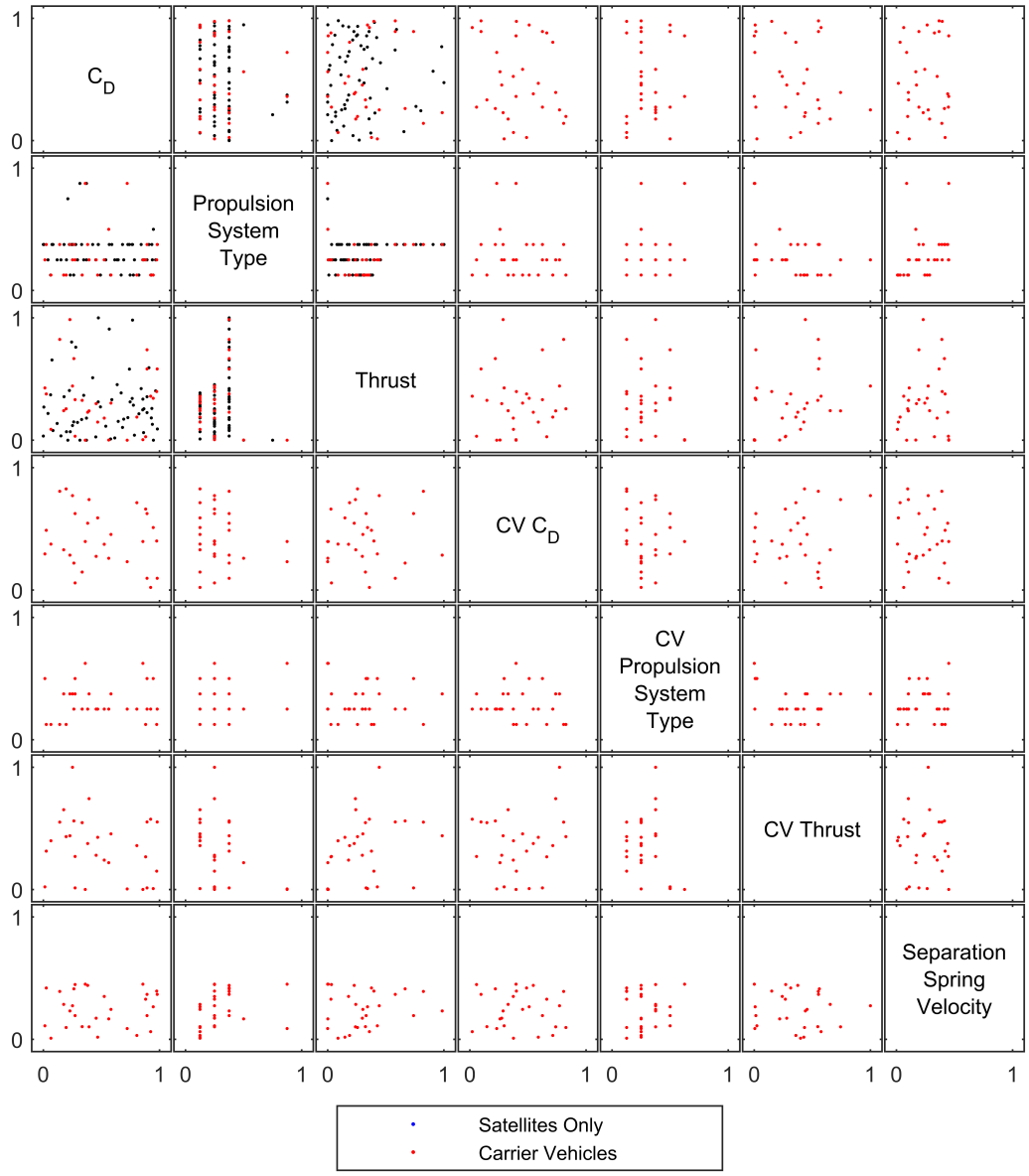

Figure 6.24: Scatter-plot matrix of input variables of initial population members for Earth imagining nanosatellite constellation analysis using secondary payload launch opportunity. Initialisation was performed using Quasi-Random Number Generation sampling to generate a population of 100 individuals.

carrier vehicles. The significant fraction of these designs identified in this initial population compared to the previous less constrained case indicates the additional propulsive requirement of the change in orbital inclination.

The nondominated sets of individual satellite and carrier vehicle designs are shown in Figure 6.26. In this output space, the designs of lowest system mass are achieved by satellite-only

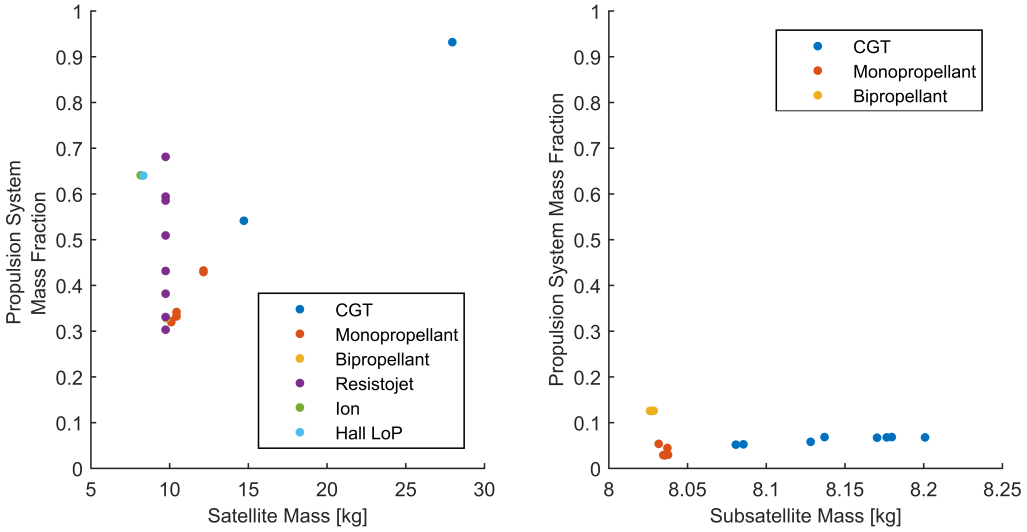

Figure 6.25: Comparison of propulsion system mass fraction, including propellant mass, for different propulsion system types. Left: Individual satellite designs, Right: Subsatellites of carrier vehicle designs

deployment strategies utilising low-power Hall and ion propulsion systems, a virtue of the high specific impulse of these systems. Comparatively the shortest system deployment times are achieved using either individual satellite or carrier vehicle deployment strategies with CGT systems. Due to the highly constrained design-space the total spread in deployment time between the different strategies is small in comparison to the results of the previous analysis when the insertion orbit was less constrained.

The propulsion system mass fraction, including propellant mass, of the nondominated designs of individual satellites and subsatellites is shown in Figure 6.25. Comparison of these vehicles demonstrates the additional propulsion system mass which is required by the individual satellites to perform the inclination change and orbit raising manoeuvres. The results for individual satellite deployment strategies show each of the vehicles has a propulsion system mass fraction of more than 0.3. Many of these strategies are therefore unlikely to result in viable vehicle designs when the mass of other subsystems and payload is considered. Comparatively, subsatellites of the nondominated carrier vehicle designs have much lower propulsion system mass fractions, less than 0.15, presenting less of an issue to the vehicle design process.

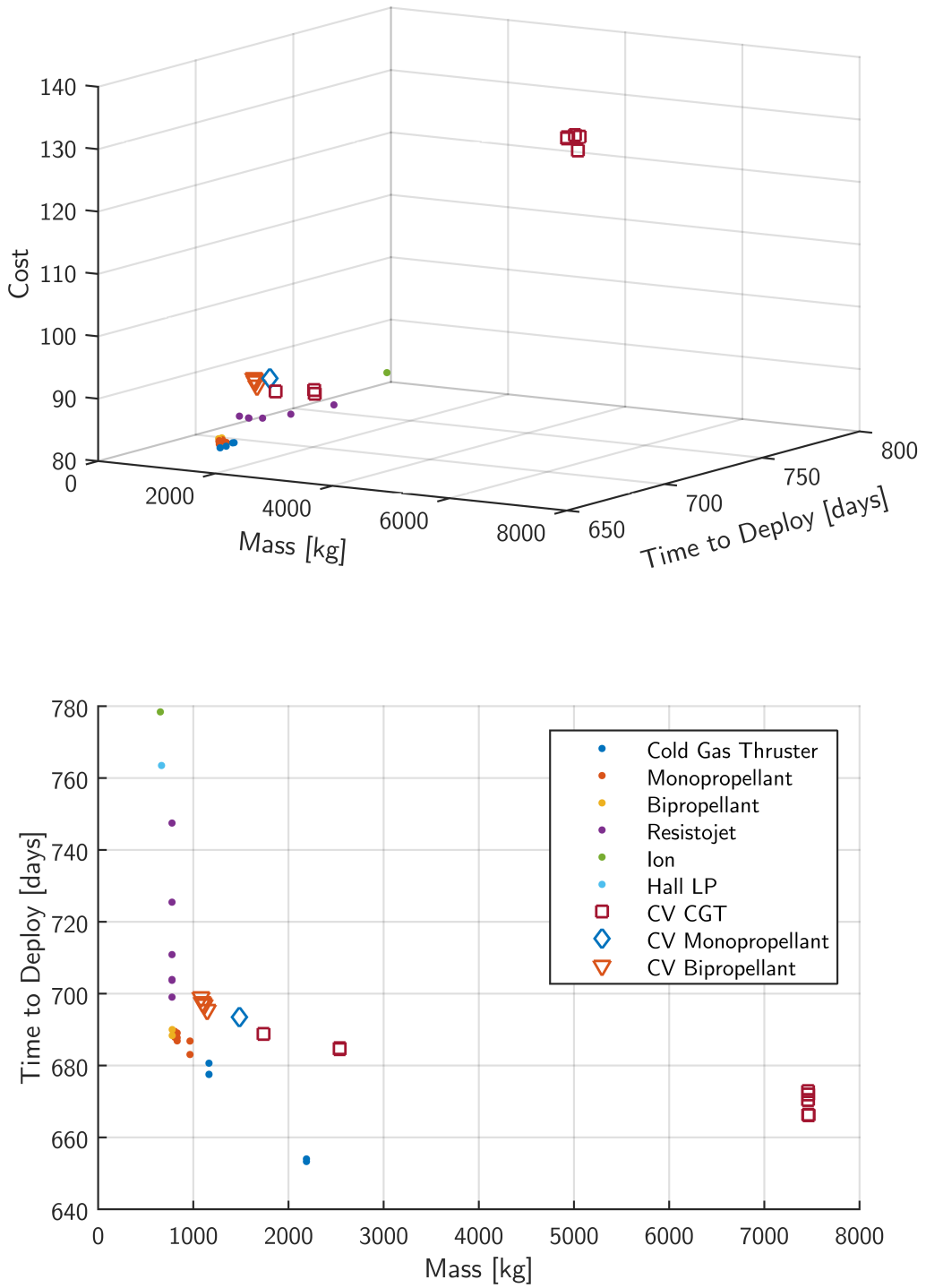

Figure 6.26: Output space of nondominated set of solutions obtained using 10 generation GA design-space exploration method with a population size of 100 individuals. Designs which do not use carrier vehicles are shown as points with colour indicating the Propulsion System Type of the individual satellites. Designs which utilise carrier vehicles are shown as open shapes of which the colour indicates the Propulsion System Type of the carrier vehicle.

6.5 Chapter Summary

The example design-space explorations performed in this study have produced informative results in the conceptual design of small satellite constellations. Three case-studies were used to demonstrate the use of the developed methodology for satellite constellations with different orbital properties, configurations, and payload size. The first two of these case-studies were based on previous constellations deployed in Earth orbit, enabling a comparison of the generated results to real-world systems. In both cases, the design-space exploration indicated that improvements to the deployment strategy of each system could have been made, resulting in reduced overall system mass, system launch and deployment cost, or shorter deployment time following launch.

Of particular note, the study of the FORMOSAT-3/COSMIC mission indicated that reduced system mass could have been achieved using bipropellant propulsion systems or monopropellant systems with the alternative green propellant AF-M315E. Alternatively, these propulsion system choices could also have been used to realise the deployment of the constellation in a shorter period of time, enabling commencement of the scientific mission sooner after launch and extending the useful lifetime of the satellites. Similarly, for the ORBCOMM constellation, the results of the performed study demonstrated that a system of similar mass could be deployed from a single launch vehicle in a significantly shorter period of time than the actual mission. In addition to this insight, the design-space exploration process also indicated that a number of different propulsion system type and propellant combinations could be used to support this alternative launch strategy whilst maintaining the cost-savings associated with using a single launch vehicle.

The final case study investigated the deployment options for a proposed nanosatellite constellation for Earth observation. The results of this study indicated that a range of strategies and different propulsion system and propellant combinations could be used to deploy a constellation of this type using only a single launch. Furthermore, identification of suitable deployment strategies following launch using a secondary payload or piggyback launch opportunity was demonstrated using the design-space exploration method. In this case-study, identified designs using carrier-vehicle deployment strategies were also found to be more competitive with individual satellite designs, particularly when an inclination change manoeuvre was required as part of the deployment process. The contrasting ranges of propulsion system mass fraction

for the carrier vehicle and individual satellite solutions demonstrate a key benefit of the use of carrier-vehicle strategies by increasing the viability of the vehicle design.

A number of additional trends were identified during the examination of the results of the design-space explorations. First, a clear tradeoff between total system mass and deployment time of the constellation is present in each of the studies performed. Whilst this tradeoff was expected due to the underlying relationship between the orbital mechanics and rocket-propulsion physics which define the deployment, the ability to evaluate and enumerate the specific tradeoff for a given mission or system profile is useful and enables the system designer to identify deployment strategies which better match the priorities of the mission. Secondly, the selection of propulsion system type on system mass was demonstrated to have a similar effect in each mission case study, a result of the dependence of propellant mass on the specific impulse of the chosen propulsion system. Whilst this relationship is somewhat trivial and known a priori, the quantification of this tradeoff is beneficial in identifying which propulsion system types may be most appropriate for constellations of different size, configuration, or mass classification. Lastly, the design-space exploration method, in particular the developed screening process, has been shown to enable identification of the feasible insertion orbit properties which can be used to perform the constellation deployment before an imposed deadline or without resulting in the decay of any assets before the correct configuration is achieved. This information is particularly useful during the conceptual design phase and can be used in combination with knowledge of the corresponding system mass to evaluate the range of different available launch opportunities.

A final note should be made on the identified issue of the model used to generate comparative system cost, one of the objectives for minimisation by GA optimisation. Whilst the minimisation of the system cost is a logical choice given that the budget of small satellite systems is often highly constrained, the implemented cost model only considers the propulsion system dry-mass of the spacecraft. A truly representative system cost cannot be generated without a more detailed analysis of the vehicle design. As a result, it was found that deployment strategies which utilise carrier vehicles were disadvantaged in the optimisation process, and may therefore not have featured as prominently in the design-space exploration. The development of a more capable conceptual vehicle design method to support a more comprehensive cost model would enable evaluation of a less biased and more useful cost metric to be used in the optimisation method.

Chapter 7

Conclusion

Advancement in the capability of small satellites and associated technologies has resulted in the growth in interest and development of constellations or distributed systems of these spacecraft. However, given the current paradigm of launch and access to orbit of these systems, the establishment of these systems in orbit is restricted. Whilst secondary-payload launch opportunities have somewhat alleviated the difficulty and cost of small payloads achieving Earth orbit, delivery to a non-optimal orbit or restrictions on propulsive capability can significantly reduce the impact and mission success of these spacecraft. For constellations or other formations of multiple small satellites, these issues are intensified by the necessity to achieve a specified orbital configuration or distribution of the payloads in orbit in order to successfully perform the mission. It is with this realisation that the necessity to focus on the deployment of these systems was identified. In particular it was established that constellations with multiple orbital planes required the greatest attention due to the increased complexity and greater propulsive requirement of their deployment.

The deployment of multi-plane constellations of satellites from a single insertion point can be performed using a number of strategies, some of which are able to significantly reduce the propulsive requirement, albeit at the cost of increased deployment time. However, these strategies are yet to be used routinely for the establishment of such systems in orbit.

A review of design methods and tools for the conceptual design of satellite constellations indicated an absence of appreciation of constellation deployment appropriate for small satellites. Design processes for deployment of traditional constellations of satellites were found to focus

on only the selection of a set of launch vehicles for a given orbital configuration. Furthermore, it was found that current design methods for small satellite constellations are not capable of investigating the different deployment strategies available, despite the benefits to the mission that can be achieved. Rather, the selection of a deployment strategy is typically chosen a priori or without a complete analysis.

In order to address these deficiencies identified in current design practices, this thesis presented a novel methodology to integrate the analysis of deployment into the design process for satellite constellation missions. Using an analysis framework approach, this methodology enables the examination of small satellite constellation deployment design using strategies or methods which were previously poorly supported in the design process. Integration of the deployment analysis with other aspects of the mission and vehicle design process is facilitated by the framework through exchange of necessary information and variables, forwards and backwards as required, between the different contributing analysis modules.

In the developed methodology, exploration of the design-space formed by the analysis framework is used to increase the knowledge available to the system design team. To perform this exploration, a multiobjective optimisation process is applied to investigate the relationships and tradeoffs between the input variables and output objectives of interest. Furthermore, by examining the output tradespace resulting from this optimisation process, the best performing system architectures or individual solutions can be identified and selected for further development. Use of this methodology to increase knowledge of discrete elements of the overall design-space can also support the ability to concurrently influence other aspects of the design process which may not be explicitly included in the analysis framework, such as the constellation configuration, vehicle design, or launch selection. This enables more informed decision making and further supports the development of improved overall system and mission designs.

Implementation of the developed methodology was performed using a reduced-order analysis framework, focusing on the design of small satellite constellations deployed using the method of indirect plane separation. A GA optimisation method was selected and applied to explore the design space and uncover the tradeoffs between the design variables and output objectives of time required for deployment, satellite mass, and system cost.

To support this implementation, an original analysis method for the deployment of satellite constellations by indirect plane separation was developed during the course of this research. Complementary vehicle-sizing and propulsion system models were also applied to evaluate the

effect of the deployment strategies on the system-level design of the satellites. A screening process based on a novel approach for estimating orbital decay using RSM was also implemented to eliminate infeasible designs and improve the computational efficiency of the design-space exploration process.

7.1 Conclusions of the Developed Methodology

The chosen optimisation method, reduced-order analysis framework, and contributing analysis were used to examine the three mission case-studies presented in Chapter 6, demonstrating the methodology proposed in this research. Two initial studies were also performed to investigate the effect of varying population size, number of generations, and method of population initialisation on the effectiveness of the GA optimisation method. The results of these initial studies illustrated the relationship between optimum population size, number of generations, and the dimensionality of the design-space and indicated that performance improvements could be achieved through the use of space-filling design methods for population initialisation.

Analysis of the input space enumerated by the design-space exploration process for each mission case-study illustrated the capability to identify ranges of infeasibility in the selected input variables. Such information can be used to inform the design team and reduce the design-space for future studies, limiting wasted time and resources. The resulting tradespace for each of the mission case-studies showed the presence of multiple nondominated solutions in the output tradespace, affirming that a single optimal solution for these objectives does not exist without knowing the preferences of the decision maker. Examination of these tradespaces enabled the identification of relationships between the system mass, vehicle cost, and time required to deploy each constellation. Trends based on the propulsion system and propellant type were also observed. Through the quantification of the tradespace and enumeration of the chosen objectives, the effect of different system choices on the selected objectives can be assessed, different designs compared, and the most promising system architectures identified.

The results of the three mission case-studies demonstrated the benefits of exploring the design-space for the deployment of the constellation. In particular, for the FORMOSAT-3/COSMIC and ORBCOMM missions which could be compared to the actual system parameters, improvements in time to complete the deployment or total system mass were identified,

increasing launch opportunities or mission lifetime. Furthermore, for the ORBCOMM system, significant cost savings were identified through launch using a single launch vehicle rather than a separate launch per orbital plane. Simultaneously, the time to complete the deployment of the constellation and therefore the time to achieve full system capability was also able to be reduced considerably. In the third mission study, for an Earth observation nanosatellite constellation, deployment following secondary payload and piggyback launch opportunities was examined. Amongst the variety of feasible system designs which were identified, solutions which use carrier-vehicles were shown to be of interest due to their short time to deploy and the increased viability and flexibility afforded to the individual satellite design. These mission-specific results demonstrate that significant and valuable information can be generated using the developed methodology. This information can be used by the system design team to aid selection of the most appropriate or effective system architectures for further and more detailed investigation.

The reduced-order analysis framework, used to evaluate design vectors for the mission case-studies, provides support for the hypothesis that the analysis of deployment can be integrated as a contributing analysis to the framework for small satellite constellation mission design. In the reduced-order analysis framework, the exchange of information into and from the deployment strategy design module is demonstrated with the vehicle-design and cost analysis modules, including an iterative mechanism involving ΔV and system mass. Verification of the framework is provided by the verification of the individual contributing analyses, and subsequently by comparison of the FORMOSAT-3/COSMIC mission to a solution generated using known input parameters. The successful implementation of the reduced-order analysis framework also supports the development of more complex analysis frameworks which embody more aspects of the full life-cycle design and analysis of small satellite constellation missions. Realisation of these higher-order design studies would enable exploration of the wider design-space for these missions and support the identification and selection of the best overall system solutions.

In order to demonstrate the developed methodology, a novel analysis method for small satellite constellation deployment using indirect plane separation was successfully developed and verified. The method utilises semi-analytical orbit propagation to simulate the necessary manoeuvres and orbital position of the vehicles comprising the constellation throughout the process of deployment. A time-varying atmospheric density model is also used to evaluate the

effects of atmospheric drag and predict the decay of the satellite orbits. Verification of the atmospheric model and orbit propagation method was performed by comparison of the simulated orbit parameters and lifetime to true satellite orbit data obtained from US AFSPC TLE sets. The constellation deployment analysis method was subsequently verified using the known deployment profile of the FORMOSAT-3/COSMIC mission. The successful development of this method confirms the hypothesis that the analysis of small satellite constellation deployment can be performed by simulation using a method of orbit propagation. During the development and subsequent implementation of this analysis, a number of improvements or modifications to the method were identified. These alternative approaches and enhancements are discussed in detail in the following section.

7.2 Recommended Improvements and Future Work

Whilst the methodology generated in this study has successfully demonstrated the ability to explore the design-space for small satellite constellation deployment a number of improvements to its implementation and further developments have been identified over the course of this research. Furthermore, the application of this methodology to the wider design process for small satellite constellations should be pursued. These recommended improvements and opportunities for further study or development are discussed below.

Constellation Deployment Strategies

A number of improvements and additions can be made to the analysis for deployment by the method of indirect plane separation presented in Section 5.1. To provide a more complete analysis the method should consider the use of opposite in-plane manoeuvres, enabling the satellites to separate at a greater rate and therefore reducing the time required to perform the deployment. Furthermore, to increase the efficiency of any inclination changes required, the capability to perform the plane-change manoeuvre after the necessary in-plane manoeuvres should be considered. Combined plane-change manoeuvres could also be examined.

During the review of satellite constellation deployment, other methods were also identified which could be considered using additional analyses to more completely represent the design-space for constellation deployment. These alternative methods, discussed in Section 2.2.2, are direct orbit transfer and deployment using EML-1. Investigation of deployment using an

optimally selected set of individual launch vehicles or secondary payload opportunities could be also performed, similar to the launch of traditional constellations or the establishment of ad hoc constellations by Marinan et al. [90], Gangestad et al. [91].

In addition, for the methods of direct plane transfer and indirect plane separation the use of multiple secondary payload or piggyback launch opportunities with varying dates rather than a single insertion orbit could be considered. Assessment of differential drag manoeuvres or carrier vehicles which are capable of inserting each payload into its required orbital slot and thus able to completely eliminate the requirement of a propulsion system on each satellite could also be investigated.

Whilst each of these additions would increase the dimensionality and complexity of the design-space for constellation deployment, the exploration of the increased design-space would support the identification and selection of the most appropriate deployment method and implementation for different missions, constellation configurations, and system design preferences.

Orbit Propagation

The deployment analysis method developed during this research utilises a semi-analytical propagation method to evaluate the orbits of the vehicles during each simulated deployment whilst accounting for orbital perturbations due to non-spherical geopotential and atmospheric drag. However, whilst this method of propagation supported the integration of a complex atmospheric density model, the computational cost of the implemented method was high.

To support the use of design-space exploration methods during the early mission and system design phases computationally efficient contributing analyses are required. An improved implementation or alternative methods of orbital propagation should therefore be investigated, enabling an increase in computational efficiency per function call. An adaptive propagation method could also be considered in which a reduced fidelity method of propagation could be used for some orbit regimes, those at higher-altitude with less significant drag effects for example. A more efficient method would allow an increased number of different designs to be considered by the optimisation method in a given time, enabling either more rapid or more comprehensive design-space exploration.

Furthermore, the use of up-to-date forecast solar flux and geomagnetic index data may be unnecessary during the early design phases when uncertainty in the launch date may be present. However, consideration of the time-varying space-weather environment may still be important

due to the significant drift-periods required for constellation deployment. Representative data for the projected space-weather environment, for example using the aggregating method of Oltrogge and Chao [176] could therefore be used. Simplification or substitution of the atmospheric density model may therefore also be considered, further reducing the computational complexity of the propagation method.

System Cost Modelling

As identified above and previously in Section 5.3, the method of cost modelling implemented during this research is only capable of generating a comparative system cost based on the dry-mass of the spacecraft and the utilised propulsion system. Support for a more comprehensive cost model which accounts for additional effects of utilising different deployment strategies or propulsion systems should therefore be sought.

A requirement to the implementation of such a cost model is the development or integration of a more detailed conceptual spacecraft design method or tool. Given a payload or instrument mass, mission type, propulsion system options, and orbit properties, a mass and power budget for the system could be developed which can be utilised to more comprehensively assess the cost of the spacecraft using the CERs of the SSCM, USCM, or recent A-PICOMO.

An improved cost model and associated vehicle design methods are components which contribute to a more extensive integrated design environment, discussed in greater detail below.

Wider Design Process Integration

In this thesis an integrated method for the design-space exploration of small satellite constellation deployment was demonstrated using a reduced-order analysis framework and without consideration of many other important aspects of the constellation design process. However, to realise the perceived benefits of increasing the available knowledge during the conceptual design phase, the design-space exploration process should include and benefit from these other contributing analyses which may affect the overall system design.

Thus, the implementation of this developed methodology with a more detailed system design process for small satellite constellations should be investigated. In addition to the consideration of deployment, such an design framework for distributed small satellite missions might include consideration of the constellation configuration and orbit design, preliminary vehicle design, launch vehicle or opportunity selection, ground-segment and mission operations, end-of-life compliance, and a life-cycle system cost model.

Additionally, different objectives of the design-space exploration process could be used to identify deployment strategies which consider priorities other than deployment time, system mass, or cost. For example, for a communications or data-transfer constellation the level of system capability during the system deployment phase may be of particular interest. Similarly, for an Earth imaging constellation, deployment strategies which minimise the revisit time or maximise the coverage during the deployment may be preferred.

In the context of a more complete analysis framework, the chosen objective functions can be used to identify improved or optimal system-level designs from a design-space which more closely represents the true breadth of design candidates. Alternatively, utility functions or value models can be used to identify and select system-level designs based on stakeholder preferences or economic analysis.

7.3 Concluding Remarks

The utilisation of small satellites in distributed systems will continue to grow, fuelled by the increasing demand for remote sensing capability, Earth observation data, and global communication and data transfer. Moreover, advances in technology development and miniaturisation will increase the capability of these systems, enabling new applications and missions.

The research presented in this thesis has laid the foundations of a methodology by which the deployment of small satellite constellations can be investigated during the early design process, enabling a greater understanding of the design-space. A method of analysis for deployment using indirect plane separation strategies was developed and subsequently verified, enabling the investigation of deployment of different constellation configurations and mission types. A multiobjective GA optimisation method was subsequently applied in this research as a means to effectively perform the exploration of the large design-space for deployment of small satellite constellations and enable an understanding of the system-level tradeoffs between different deployment strategies. It is hoped that the methodology presented in this thesis will continue to be developed to support the design of future distributed systems and constellations of small satellites.

References

[1] Rainer Sandau, Klaus Brieß, and Marco DErrico. Small satellites for global coverage: Potential and limits. *ISPRS Journal of Photogrammetry and Remote Sensing*, 65(6): 492–504, 2010. ISSN 09242716. doi:10.1016/j.isprsjprs.2010.09.003.

[2] William W. Saylor, Kyle Smaagard, Nathan Nordby, and David J. Barnhart. New Scientific Capabilities Enabled by Autonomous Constellations of Smallsats. In *21st Annual AIAA/USU Conference on Small Satellites*, number 719, Logan, UT, 2007. American Institute of Aeronautics and Astronautics (AIAA).

[3] Nicholas H. Crisp, Katharine L. Smith, and Peter M. Hollingsworth. Small Satellite Launch to LEO: A Review of Current and Future Launch Systems. *Transactions of the Japan Society for Aeronautical and Space Sciences, Aerospace Technology Japan*, 12 (ists29), 2014. ISSN 1884-0485. doi:10.2322/tastj.12.Tf_39.

[4] Nicholas H. Crisp, Katharine L. Smith, and Peter M. Hollingsworth. Launch and deployment of distributed small satellite systems. *Acta Astronautica*, 114:65–78, 2015. ISSN 00945765. doi:10.1016/j.actaastro.2015.04.015.

[5] Irene A. Budianto and John R. Olds. Design and Deployment of a Satellite Constellation Using Collaborative Optimization. *Journal of Spacecraft and Rockets*, 41(6):956–963, 2004. ISSN 0022-4650. doi:10.2514/1.14254.

[6] Cyrus D. Jilla and David W. Miller. Multi-Objective, Multidisciplinary Design Optimization Methodology for Distributed Satellite Systems. *Journal of Spacecraft and Rockets*, 41(1):39–50, 2004. ISSN 0022-4650. doi:10.2514/1.9206.

[7] Adam M. Ross, Daniel E. Hastings, Joyce M. Warmkessel, and Nathan P. Diller. Multi-Attribute Tradespace Exploration as Front End for Effective Space System Design. *Journal of Spacecraft and Rockets*, 41(1):20–28, 2004. ISSN 0022-4650. doi:10.2514/1.9204.

[8] Nicholas H. Crisp, Katharine L. Smith, and Peter M. Hollingsworth. Small Satellite Launch to LEO: a Review of Current and Future Launch Systems. In *29th International Symposium on Space Technology and Science*, Nagoya-Aichi, Japan, 2013. Japan Society for Aeronautical and Space Sciences (JSASS).

[9] Nicholas H. Crisp, Katharine L. Smith, and Peter M. Hollingsworth. Launch and Deployment of Distributed Small Satellite Systems. In *65th International Astronautical Congress*, pages 1–15, Toronto, Canada, 2014. International Astronautical Federation (IAF).

[10] Michael Swartwout. University-Class Satellites: From Marginal Utility to 'Disruptive' Research Platforms. In *18th Annual AIAA/USU Conference on Small Satellites*, pages 9–13, Logan, UT, 2004. American Institute of Aeronautics and Astronautics (AIAA).

[11] Siegfried W. Janson. 25 Years of Small Satellites. In *25th Annual AIAA/USU Conference on Small Satellites*, Logan, UT, 2011. American Institute of Aeronautics and Astronautics (AIAA).

[12] Herbert J. Kramer and Arthur P. Cracknell. An Overview of Small Satellites in Remote Sensing. *International Journal of Remote Sensing*, 29(15):4285–4337, 2008. ISSN 0143-1161. doi:10.1080/01431160801914952.

[13] Daniel Selva and David Krejci. A survey and assessment of the capabilities of Cubesats for Earth observation. *Acta Astronautica*, 74:50–68, 2012. ISSN 00945765. doi:10.1016/j.actaastro.2011.12.014.

[14] Freddy M. Pranajaya and Robert E. Zee. Nanosatellite Tracking Ships: From Concept to Launch in 7 Months. In *23rd Annual AIAA/USU Conference on Small Satellites*, pages 1–6, Logan, UT, 2009. American Institute of Aeronautics and Astronautics (AIAA).

[15] Wayne L. Nicholson, Antonio J. Ricco, Elwood Agasid, Christopher Beasley, Millan Diaz-Aguado, Pascale Ehrenfreund, Charles Friedericks, Shakib Ghassemieh, Michael Henschke, John W. Hines, Christopher Kitts, Ed Luzzi, Diana Ly, Nghia Mai, Rocco Mancinelli, Michael McIntyre, Giovanni Minelli, Michael Neumann, Macarena Parra,

Matthew Piccini, R Mike Rasay, Robert Ricks, Orlando Santos, Aaron Schooley, David Squires, Linda Timucin, Bruce Yost, and Anthony Young. The O/OREOS Mission: First Science Data from the Space Environment Survivability of Living Organisms (SESLO) Payload. *Astrobiology*, 11(10):951–8, 2011. ISSN 1557-8070. doi:10.1089/ast.2011.0714.

[16] Christopher Kitts, John W. Hines, Elwood Agasid, Antonio J. Ricco, Bruce Yost, Karolyn Ronzano, and Jordi Puig-Suari. The GeneSat-1 Microsatellite Mission : A Challenge in Small Satellite Design. In *20th Annual AIAA/USU Conference on Small Satellites*, pages 1–6, Logan, UT, 2006. American Institute of Aeronautics and Astronautics (AIAA).

[17] Michael Swartwout. Attack of the CubeSats: A Statistical Look. In *25th Annual AIAA/USU Conference on Small Satellites*, Logan, UT, 2011. American Institute of Aeronautics and Astronautics (AIAA).

[18] Hank Heidt, Jordi Puig-Suari, Augustus S. Moore, Shinichi Nakasuka, and Robert J. Twiggs. CubeSat: A New Generation of Picosatellite for Education and Industry Low-Cost Space Experimentation. In *14th Annual AIAA/USU Conference on Small Satellites*, Logan, UT, 2000. American Institute of Aeronautics and Astronautics (AIAA). ISBN 6507238651.

[19] Kirk Woellert, Pascale Ehrenfreund, Antonio J. Ricco, and Henry R. Hertzfeld. Cubesats: Cost-effective science and technology platforms for emerging and developing nations. *Advances in Space Research*, 47(4):663–684, 2011. ISSN 02731177. doi:10.1016/j.asr.2010.10.009.

[20] Freddy M. Pranajaya and Robert E. Zee. Generic Nanosatellite Bus for Responsive Mission. In *5th Responsive Space Conference*, Los Angeles, CA, 2007. American Institute of Aeronautics and Astronautics (AIAA). ISBN 4166677799.

[21] Freddy M. Pranajaya and Robert E. Zee. The NEMO Bus: A Third Generation High-Performance Nanosatellite for Earth Monitoring and Observation. In *24th Annual AIAA/USU Conference on Small Satellites*, Logan, UT, 2010. American Institute of Aeronautics and Astronautics (AIAA).

[22] NASA. CubeSat Backgrounder. Technical report, Wallops Flight Facility, Goddard Space Flight Center, Wallops Island, VA, 2009. URL `http://www.nasa.gov/centers/wallops/pdf/326337main_Cubesatbackgrounder.pdf`.

[23] Martin N. Sweeting. Space at Surrey: Micro-Mini-Satellites for Affordable Access to Space. *Air & Space Europe*, 2(1):38–52, 2000. ISSN 12900958. doi:10.1016/S1290-0958(00)80009-X.

[24] Jeff Foust. Emerging Opportunities for Low-Cost Small Satellites in Civil and Commercial Space. In *24th Annual AIAA/USU Conference on Small Satellites*, Logan, UT, 2010. American Institute of Aeronautics and Astronautics (AIAA).

[25] Gerry Webb and Alex da Silva Curiel. Is It Really That Hard to Get Your Hardware Into Space? In *23rd Annual AIAA/USU Conference on Small Satellites*, Logan, UT, 2009. American Institute of Aeronautics and Astronautics (AIAA).

[26] Kirk Woellert. Space Access: Still the Major Issue for the Small Satellite Community. *Journal of Small Satellites*, 1(2):45–47, 2012.

[27] Loren Lemmerman, Carol Raymond, Robert Shotwell, James Chase, Kul Bhasin, and Robert Connerton. Advanced platform technologies for Earth science. *Acta Astronautica*, 56(1-2):199–208, 2005. ISSN 00945765. doi:10.1016/j.actaastro.2004.09.031.

[28] James R. Wertz and Wiley J. Larson, editors. *Space Mission Analysis and Design*. Microcosm Press/Kluwer Academic Publishers, El Segundo, CA, 3 edition, 1999. ISBN 978-1-881883-10-4.

[29] Peter Fortescue, Graham Swinerd, and John Stark, editors. *Spacecraft Systems Engineering*. John Wiley & Sons, Ltd., Chichester, UK, 4 edition, 2011. ISBN 9780470750124.

[30] R. David Luders. Satellite Networks for Continuous Zonal Coverage. *ARS Journal*, 31 (2):179–184, 1961. doi:10.2514/8.5422.

[31] L. Rider. Optimized Polar Orbit Constellations for Redundant Earth Coverage. *Journal of the Astronautical Sciences*, 33:147–161, 1985.

[32] L. Rider. Analytic Design of Satellite Constellations for Zonal Earth Coverage using Inclined Circular Orbits. *Journal of the Astronautical Sciences*, 34:31–64, 1986.

[33] J.G. Walker. Some Circular Orbit Pattern Providing Continuous Whole Earth Coverage. *Journal of the British Interplanetary Society*, 24:369–384, 1971.

[34] A.H. Ballard. Rosette Constellations of Earth Satellites. *IEEE Transactions on Aerospace and Electronic Systems*, AES-16(5):656–673, 1980. ISSN 0018-9251. doi:10.1109/TAES.1980.308932.

[35] Joseph C. Pizzicaroli. Launching and Building the Iridium Constellation. In Jozef C. van der Ha, editor, *Mission Design & Implementation of Satellite Constellations*, chapter 2.2. Springer-Science+Business Media, B.V., Dordrecht, 1998. doi:10.1007/978-94-011-5088-0_10.

[36] Leonard Schiff and Ananthanarayanan Chockalingam. Signal design and system operation of Globalstar versus IS-95 CDMA similarities and differences. *Wireless Networks*, 6(1): 47–57, 2000. ISSN 10220038. doi:10.1023/A:1019164909332.

[37] ASD-Eurospace. Space Trends: Global Space Activity Overview 1986-2011. Technical Report May, ASD-Eurospace, Paris, 2012.

[38] Sarah Reid. ORBCOMM System Overview. Technical Report G, ORBCOMM LLC, Dulles, VA, 2001.

[39] Maria J. Evans and Timothy D. Maclay. Mission Design of the ORBCOMM Constellation. In Jozef C. van der Ha, editor, *Mission Design & Implementation of Satellite Constellations*, chapter 2.1. Springer-Science+Business Media, B.V., Dordrecht, the Netherlands, 1998. doi:10.1007/978-94-011-5088-0_9.

[40] Bhavesh T. Patel, Susanne Schroll, and Andrew Lewin. On-orbit Performance of the ORBCOMM Spacecraft Constellation. In *13th Annual AIAA/USU Conference on Small Satellites*, Logan, UT, 1999. American Institute of Aeronautics and Astronautics (AIAA).

[41] George Tyc, John Tulip, Daniel Schulten, Manfred Krischke, and Michael Oxfort. The RapidEye Mission Design. In *Acta Astronautica*, volume 56, pages 213–219, 2005. ISBN 0094-5765. doi:10.1016/j.actaastro.2004.09.029.

[42] Paul Stephens, John Cooksley, Alex da Silva Curiel, Lee Boland, Susan Jason, James Northham, Andrew Brewer, Javad Anzalchi, Hugh Newell, Craig Underwood, Stephen Machin, Wei Sun, and Martin N. Sweeting. Launch of the International Disaster Monitoring Constellation; the Development of a Novel International Partnership in Space. In

International Conference on Recent Advances in Space Technologies, Istanbul, Turkey, 2003. IEEE. ISBN 0-7803-8142-4. doi:10.1109/RAST.2003.1303972.

[43] Chen-Joe Fong, Wen-Tzong Shiau, Chen-Tsung Lin, Tien-Chuan Kuo, Chung-Huei Chu, Shan-Kuo Yang, Nick L. Yen, Shao-Shing Chen, Ying-Hwa Kuo, Yuei-An Liou, and Sien Chi. Constellation Deployment for the FORMOSAT-3/COSMIC Mission. *IEEE Transactions on Geoscience and Remote Sensing*, 46(11):3367–3379, 2008. doi:10.1109/TGRS.2008.2005202.

[44] David J. Barnhart, Tanya Vladimirova, Adam M. Baker, and Martin N. Sweeting. A low-cost femtosatellite to enable distributed space missions. *Acta Astronautica*, 64(11-12): 1123–1143, 2009. ISSN 00945765. doi:10.1016/j.actaastro.2009.01.025.

[45] Rainer Sandau. Status and trends of small satellite missions for Earth observation. *Acta Astronautica*, 66(1-2), 2010. ISSN 00945765. doi:10.1016/j.actaastro.2009.06.008.

[46] Christopher R. Boshuizen, James Mason, Pete Klupar, and Shannon Spanhake. Results from the Planet Labs Flock Constellation. In *28th Annual AIAA/USU Conference on Small Satellites*, Logan, UT, 2014. American Institute of Aeronautics and Astronautics (AIAA).

[47] Kiran Murthy, Michael Shearn, Byron D. Smiley, Alexandra H. Chau, Josh Levine, and Dirk Robinson. SkySat-1: Very High-Resolution Imagery from a Small Satellite. In *Sensors, Systems, and Next-Generation Satellites XVIII*, volume 92411E, Amsterdam, Netherlands, 2014. SPIE. doi:10.1117/12.2074163.

[48] Jaime Esper, Peter V. Panetta, Michael Ryschkewitsch, Warren Wiscombe, and Steven Neeck. NASA-GSFC Nano-Satellite Technology for Earth Science Missions. *Acta Astronautica*, 46(2-6):287–296, 2000. ISSN 00945765. doi:10.1016/S0094-5765(99)00214-3.

[49] David J. Barnhart, Tanya Vladimirova, and Martin N. Sweeting. Very-Small-Satellite Design for Distributed Space Missions. *Journal of Spacecraft and Rockets*, 44(6):1294–1306, 2007. ISSN 0022-4650. doi:10.2514/1.28678.

[50] Lars Dyrud, Stefan Slagowski, Jonathan Fentzke, Warren Wiscombe, Brian Gunter, Kerri Cahoy, Gary Bust, Aaron Rogers, Bob Erlandson, Larry Paxton, and Steven Arnold. Small-Sat Science Constellations: Why and How. In *27th Annual AIAA/USU Conference*

on Small Satellites, Logan, UT, 2013. American Institute of Aeronautics and Astronautics (AIAA).

[51] Alex da Silva Curiel, Meryl Lambert, Doug Liddle, Martin N. Sweeting, Chung-Huei Chu, Chen-Joe Fong, and Guey-Shin Chang. Introduction to FORMOSAT-7/COSMIC-2 Mission. In *27th Annual AIAA/USU Conference on Small Satellites*, Logan, UT, 2013. American Institute of Aeronautics and Astronautics (AIAA).

[52] S.R. Tsitas and J. Kingston. 6U CubeSat commercial applications. *Aeronautical Journal*, 116(1176):189–198, 2012.

[53] John R. London III, Mark E. Ray, David J. Weeks, and A. Brent Marley. The First US Army Satellite in Fifty Years: SMDC-ONE First Flight Results. In *25th Annual AIAA/USU Conference on Small Satellites*, Logan, UT, 2011. American Institute of Aeronautics and Astronautics (AIAA).

[54] USASMDC/ARSTRAT. SMDC-ONE Nanosatellite Technology Demonstration. Technical report, Huntsville, AL, 2012.

[55] USASMDC/ARSTRAT. Kestrel Eye Visible Imagery Nanosatellite Technology Demonstration. Technical report, Huntsville, AL, 2012.

[56] Michael Scardera, Matt Baker, Reid Reynolds, Shalini Reddy, Kevin Kellogg, Michael Mahoney, Paul Silversmith, Natalie Rodriguez, and Peter Dohm. ALTAIR: Millennium's DARPA SeeMe Satellite Solution Technical (R)evolution. In *28th Annual AIAA/USU Conference on Small Satellites*, Logan, UT, 2014. American Institute of Aeronautics and Astronautics (AIAA).

[57] Matt Bille, Paul Kolodziejski, and Tom Hunsaker. Distant Horizons : Smallsat Evolution In The Mid-to-Far Term. In *25th Annual AIAA/USU Conference on Small Satellites*, Logan, UT, 2011. American Institute of Aeronautics and Astronautics (AIAA).

[58] Charles D. Norton, Sergio Pellegrino, and Michael Johnson. Findings of the KECK Institute for Space Studies Program on Small Satellites : A Revolution in Space Science. In *27th Annual AIAA/USU Conference on Small Satellites*, Logan, UT, 2013. American Institute of Aeronautics and Astronautics (AIAA).

[59] Tanya Vladimirova, Xiaofeng Wu, Kawsu Sidibeh, David J. Barnhart, and Abdul-Halim Jallad. Enabling Technologies for Distributed Picosatellite Missions in LEO. In *First NASA/ESA Conference on Adaptive Hardware and Systems*, Istanbul, Turkey, 2006. IEEE Computer Society. ISBN 0769526144. doi:10.1109/AHS.2006.33.

[60] Office of Commercial Space Transportation (AST) and the Commercial Space Transportation Advisory Committee (COMSTAC). 2009 Commercial Space Transportation Forecasts. Technical report, Federal Aviation Administration, Washington, DC, 2009.

[61] Christopher P. Bridges, Luke Sauter, and Phil Palmer. Formation Deployment & Separation Simulation of Multi- Satellite Scenarios using SatLauncher. In *IEEE Aerospace Conference*, Big Sky, MT, 2011. IEEE. doi:10.1109/AERO.2011.5747258.

[62] Howard D. Curtis, editor. *Orbital Mechanics for Engineering Students*. Butterworth-Heinemann, Boston, MA, 2 edition, 2010. ISBN 978-0-12-374778-5.

[63] Catherine Ward, Alex da Silva Curiel, Martin N. Sweeting, Gulielmo S. Aglietti, and Jake Schaffner. Surrey Small Satellite Transfer Vehicle. In *56th International Astronautical Congress of the International Astronautical Federation, the International Academy of Astronautics, and the International Institute of Space Law*, Fukuoka, Japan, 2005. International Astronautical Federation (IAF). doi:10.2514/6.IAC-05-B5.3.B5.5.06.

[64] Adam M. Baker, Alex da Silva Curiel, Jake Schaffner, and Martin N. Sweeting. You can get there from here: Advanced low cost propulsion concepts for small satellites beyond LEO. *Acta Astronautica*, 57(2-8):288–301, 2005. ISSN 00945765. doi:10.1016/j.actaastro.2005.03.046.

[65] J.A. King and N.J. Beidleman. Method and Apparatus for Deploying a Satellite Network, 1993. URL `www.google.co.uk/patents/US5199672`.

[66] Chen-Joe Fong, Cheng-Yung Huang, Vicky Chu, Nick Yen, Ying-Hwa Kuo, Yuei-An Liou, and Sien Chi. Mission Results from FORMOSAT-3/COSMIC Constellation System. *Journal of Spacecraft and Rockets*, 45(6):1293–1302, 2008. ISSN 0022-4650. doi:10.2514/1.34427.

[67] Frank Silvio Marzano, Domenico Cimini, Adelaide Memmo, Mario Montopoli, Tommaso Rossi, Mauro De Sanctis, Marco Lucente, Daniele Mortari, and Sabatino Di Michele.

Flower Constellation of Millimeter-Wave Radiometers for Tropospheric Monitoring at Pseudogeostationary Scale. *IEEE Transactions on Geoscience and Remote Sensing*, 47 (9):3107–3122, 2009. ISSN 0196-2892. doi:10.1109/TGRS.2008.2012349.

[68] James Chase, Naomi Chow, Erica Gralla, and N. Jeremy Kasdin. LEO Constellation Design Using the Lunar L1 Point. In *14th AAS/AIAA Space Flight Mechanics Meeting*, Maui, HI, 2004. American Astronautical Society (AAS).

[69] Mahdi Jafari Nadoushan and Alireza Basohbat Novinzadeh. Satellite Constellation Build-up via Three-Body Dynamics. *Journal of Aerospace Engineering*, 228(1):155–160, 2014. ISSN 0954-4100. doi:10.1177/0954410013476615.

[70] David C. Folta and Frank Vaughn. A Survey Of Earth-Moon Libration Orbits: Stationkeeping Strategies And Intra-Orbit Transfers. In *AIAA/AAS Astrodynamics Conference*, Providence, RI, 2004. American Institute of Aeronautics and Astronautics (AIAA). doi:10.2514/6.2004-4741.

[71] David C. Folta, T.A. Pavlak, K.C. Howell, M.A. Woodard, and D.W. Woodfork. Stationkeeping of Lissajous trajectories in the Earth-Moon system with applications to ARTEMIS. In *20th AAS/AIAA Space Flight Mechanics Meeting*, San Diego, CA, 2010. American Astronautical Society (AAS).

[72] Trevor C. Sorensen, Eric J. Pilger, Mark S. Wood, Miguel A. Nunes, and Lance K. Yoneshige. Mission Design and Operations of a Constellation of Small Satellites for Remote Sensing. In Khanh D. Pham, Joseph L. Cox, Richard T. Howard, and Genshe Chen, editors, *Sensors and Systems for Space Applications VI*, volume 8739, Baltimore, MD, 2013. SPIE. doi:10.1117/12.2016745.

[73] Jordi Puig-Suari, Guy Zohar, and Kyle Leveque. Deployment of CubeSat Constellations Utilizing Current Launch Opportunities. In *27th Annual AIAA/USU Conference on Small Satellites*, number 805, Logan, UT, 2013. American Institute of Aeronautics and Astronautics (AIAA).

[74] R.V. Ramanan. Strategy for Deployment of Multiple Satellites for Collision-Free Relative Orbital Motion. *Journal of Guidance, Control, and Dynamics*, 23(3):556–558, 2000. ISSN 0731-5090. doi:10.2514/2.4565.

[75] NovaNano. Separation Mechanisms for Satellites in 1-50kg Range. In *UNISEC Workshop*, Tokyo, Japan, 2013. University Space Engineering Consortium (UNISEC).

[76] Joseph W. Gangestad, Brian S. Hardy, and David A. Hinkley. Operations, Orbit Determination, and Formation Control of the AeroCube-4 CubeSats. In *27th Annual AIAA/USU Conference on Small Satellites*, Logan, UT, 2013. American Institute of Aeronautics and Astronautics (AIAA).

[77] Randy Rose, Will Wells, Jillian Redfern, Debi Rose, John Dickinson, Chris Ruf, Aaron Ridley, and Kyle Nave. NASA's Cyclone Global Navigation Satellite System (CYGNSS) Mission - Temporal Resolution of a Constellation Enabled by Micro-Satellite Technology. In *27th Annual AIAA/USU Conference on Small Satellites*, Logan, UT, 2013. American Institute of Aeronautics and Astronautics (AIAA). ISBN 7347646561.

[78] Alan S. Li and James Mason. Optimal Utility of Satellite Constellation Separation with Differential Drag. In *AIAA/AAS Astrodynamics Specialist Conference*, San Diego, CA, 2014. American Institute of Aeronautics and Astronautics (AIAA). ISBN 978-1-62410-308-7. doi:10.2514/6.2014-4112.

[79] Jeffrey L. Smith. Concurrent Engineering in the Jet Propulsion Laboratory Project Design Center. In *Aerospace Manufacturing Technology Conference & Exposition*, Long Beach, CA, 1998. Society of Automotive Engineers, Inc. doi:10.4271/981869.

[80] Joseph A. Aguilar, Andrew Dawdy, and Glenn W. Law. The Aerospace Corporation's Concept Design Center. In *8th Annual International Symposium of the International Council on Systems Engineering*, Vancouver, Canada, 1998. International Council on Systems Engineering (INCOSE).

[81] Irene A. Budianto. *A Collaborative Optimization Approach to Improve the Design and Deployment of Satellite Constellations*. Phd thesis, Georgia Institute of Technology, 2000.

[82] Graeme B. Shaw, D.W. Miller, and D.E. Hastings. Development of the Quantitative Generalized Information Network Analysis Methodology for Satellite Systems. *Journal of Spacecraft and Rockets*, 38(2):257–269, 2001. ISSN 0022-4650. doi:10.2514/2.3679.

[83] Cyrus D. Jilla. *A Multiobjective, Multidisciplinary Design Optimization Methodology for the Conceptual Design of Distributed Satellite Systems*. Phd thesis, Massachusetts Institute of Technology, 2002.

[84] Nathan P. Diller. *Utilizing Multiple Attribute Tradespace Exploration with Concurrent Design for Creating Aerospace Systems Requirements*. Msc thesis, Massachusetts Institute of Technology, 2002.

[85] Adam M. Ross. *Multi-Attribute Tradespace Exploration with Concurrent Design as a Value-Centric Framework for Space System Architecture and Design*. Dual-msc thesis, Massachusetts Institute of Technology, 2003.

[86] Nathan P. Diller and Joyce M. Warmkessel. Applying Multi-Attribute Utility Analysis to Architecture Research for the Terrestrial Observer Swarm. In *20th Digital Avionics Systems Conference*, volume 1, pages 1–9, Daytona Beach, FL, 2001. IEEE. ISBN 0-7803-7034-1. doi:10.1109/DASC.2001.963373.

[87] Stefania Cornara, Theresa W. Beech, Miguel Belló-Mora, and Guy Janin. Satellite Constellation Mission Analysis and Design. *Acta Astronautica*, 48(5-12):681–691, 2001. ISSN 00945765. doi:10.1016/S0094-5765(01)00016-9.

[88] Stefania Cornara, Theresa W. Beech, Miguel Belló-mora, and Antonio Martinez de Aragon. Satellite Constellation Launch, Deployment, Replacement and End-of-Life Strategies. In *13th Annual AIAA/USU Conference on Small Satellites*, Logan, UT, 1999. American Institute of Aeronautics and Astronautics (AIAA).

[89] Olivier L. de Weck, Richard de Neufville, and Mathieu Chaize. Staged Deployment of Communications Satellite Constellations in Low Earth Orbit. *Journal of Aerospace Computing, Information, and Communication*, 1(3):119–136, 2004. doi:10.2514/1.6346.

[90] Anne Marinan, Austin Nicholas, and Kerri Cahoy. Ad hoc CubeSat constellations: Secondary launch coverage and distribution. In *IEEE Aerospace Conference*, Big Sky, MT, 2013. IEEE. ISBN 9781467318112. doi:10.1109/AERO.2013.6497174.

[91] Joseph W. Gangestad, James R. Wilson, Kristin L Gates, and John V Langer. Rideshare-Initiated Constellations: Future CubeSat Architectures with the Current Launch Manifest. In *31st Space Symposiym*, number April, Colorado Springs, CO, 2015. The Space Foundation.

[92] Eunsuk Kang, Ethan Jackson, and Wolfram Schulte. *An Approach for Effective Design Space Exploration*, volume 6662 of *Lecture Notes in Computer Science*. Springer Berlin Heidelberg, Berlin, Heidelberg, 2011. ISBN 978-3-642-21291-8. doi:10.1007/978-3-642-21292-5_3.

[93] Dimitri N. Mavris and Olivia J. Pinon. An Overview of Design Challenges and Methods in Aerospace Engineering. In Omar Hammami, Daniel Krob, and Jean-Luc Voirin, editors, *Complex Systems Design & Management*, chapter 1. Springer-Verlag, Berlin, Heidelberg, 2012. ISBN 978-3-642-25202-0. doi:10.1007/978-3-642-25203-7.

[94] Kalyanmoy Deb. *Multi-Objective Optimization using Evolutionary Algorithms*. John Wiley & Sons, Ltd., Chichester, UK, 2001. ISBN 978-0-471-87339-6.

[95] Kalyanmoy Deb. Multi-objective Optimisation Using Evolutionary Algorithms: An Introduction. In *Multi-objective Evolutionary Optimisation for Product Design and Manufacturing*, pages 3–34. Springer, London, 2011. ISBN 978-0-85729-617-7. doi:10.1007/978-0-85729-652-8_1.

[96] Carlos A. Coello Coello, Gary B. Lamont, and David A. Van Veldhuizen. *Evolutionary Algorithms for Solving Multi-Objective Problems*. Springer-Science+Business Media, LLC, New York, NY, 2nd edition, 2007. ISBN 9780387310299. doi:10.1007/978-0-387-36797-2.

[97] R. Timothy Marler and Jasbir S. Arora. Function-transformation methods for multi-objective optimization. *Engineering Optimization*, 37(6):551–570, 2005. ISSN 0305-215X. doi:10.1080/03052150500114289.

[98] Todd Mosher. Conceptual Spacecraft Design Using a Genetic Algorithm Trade Selection Process. *Journal of Aircraft*, 36(1):200–208, 1999. doi:10.2514/2.2426.

[99] David A. Coley. *An Introduction to Genetic Algorithms for Scientists and Engineers*. World Scientific Publishing Co. Pte. Ltd., Singapore, 1999. ISBN 978-981-02-3602-1. doi:10.1142/3904.

[100] Darrell Whitley, Soraya Rana, and Robert B. Heckendorn. Island model genetic algorithms and linearly separable problems. In *Evolutionary Computing*, pages 109–125. Springer Berlin Heidelberg, New York, NY, 1997. ISBN 3-540-63476-2. doi:10.1007/BFb0027170.

[101] M. Srinivas and L.M. Patnaik. Adaptive probabilities of crossover and mutation in genetic algorithms. *IEEE Transactions on Systems, Man, and Cybernetics*, 24(4):656–667, 1994. ISSN 00189472. doi:10.1109/21.286385.

[102] Kalyanmoy Deb, Amrit Pratap, Sameer Agarwal, and T. Meyarivan. A Fast and Elitist Multiobjective Genetic Algorithm: NSGA-II. *IEEE Transactions on Evolutionary Computation*, 6(2):182–197, 2002. doi:10.1109/4235.996017.

[103] Eckart Zitzler, Marco Laumanns, and Lothar Thiele. SPEA2: Improving the Strength Pareto Evolutionary Algorithm. Technical report, Computer Engineering and Networks Laboratory (TIK), ETH Zurich, 2001.

[104] J.D. Knowles and D.W. Corne. Approximating the nondominated front using the Pareto Archived Evolution Strategy. *Evolutionary Computation*, 8(2):149–172, 2000. ISSN 1063-6560. doi:10.1162/106365600568167.

[105] Joshua Knowles. ParEGO: A hybrid algorithm with on-line landscape approximation for expensive multiobjective optimization problems. *IEEE Transactions on Evolutionary Computation*, 10(1):50–66, 2006. ISSN 1089778X. doi:10.1109/TEVC.2005.851274.

[106] James Kennedy and Russell Eberhart. Particle swarm optimization. In *IEEE International Conference on Neural Networks*, Perth, 1995. IEEE. doi:10.1109/ICNN.1995.488968.

[107] Riccardo Poli, James Kennedy, and Tim Blackwell. Particle swarm optimization. *Swarm Intelligence*, 1(1):33–57, 2007. ISSN 1935-3812. doi:10.1007/s11721-007-0002-0.

[108] P. N. Suganthan. Particle swarm optimiser with neighbourhood operator. In *IEEE Congress on Evolutionary Computation*, volume 3, pages 1958–1962, Washington, DC, 1999. IEEE. ISBN 0-7803-5536-9. doi:10.1109/CEC.1999.785514.

[109] Andrew Stacey, Mirjana Jancic, and Ian Grundy. Particle swarm optimization with mutation. In *IEEE Congress on Evolutionary Computation*, Canberra, 2003. IEEE. ISBN 0-7803-7804-0. doi:10.1109/CEC.2003.1299838.

[110] Carlos A. Coello Coello, Gregorio Toscano Pulido, and Maximino Salazar Lechuga. Handling multiple objectives with particle swarm optimization. *IEEE Transactions on Evolutionary Computation*, 8(3):256–279, 2004. ISSN 1089-778X. doi:10.1109/TEVC.2004.826067.

[111] S. Kitayama, M. Arakawa, and K. Yamazaki. Penalty function approach for the mixed discrete nonlinear problems by particle swarm optimization. *Structural and Multidisciplinary Optimization*, 32(3):191–202, 2006. ISSN 1615-147X. doi:10.1007/s00158-006-0021-2.

[112] Ahmad Rezaee Jordehi and Jasronita Jasni. Particle swarm optimisation for discrete optimisation problems: a review. *Artificial Intelligence Review*, 43(2):243–258, 2015. ISSN 0269-2821. doi:10.1007/s10462-012-9373-8.

[113] S. Kirkpatrick, C.D. Gelatt, and M.P. Vecchi. Optimization by Simulated Annealing. *Science*, 220(4598):671–680, 1983. ISSN 0036-8075. doi:10.1126/science.220.4598.671.

[114] B. Suman and P. Kumar. A survey of simulated annealing as a tool for single and multiobjective optimization. *Journal of the Operational Research Society*, 57(10):1143–1160, 2006. ISSN 0160-5682. doi:10.1057/palgrave.jors.2602068.

[115] Piotr Czyzak and Adrezej Jaszkiewicz. Pareto simulated annealing - a metaheuristic technique for multiple objective combinatorial optimization. *Journal of Multi-Criteria Decision Analysis*, 7(1):34–47, 1998. ISSN 10579214. doi:10.1002/(SICI)1099-1360(199801)7:1<34::AID-MCDA161>3.0.CO;2-6.

[116] A. Suppapitnarm, K.A. Seffen, G.T. Parks, and P.J. Clarkson. A Simulated Annealing Algorithm for Multiobjective Optimization. *Engineering Optimization*, 33(1):59–85, November 2000. ISSN 0305-215X. doi:10.1080/03052150008940911.

[117] Sanghamitra Bandyopadhyay, Sriparna Saha, Ujjwal Maulik, and Kalyanmoy Deb. A Simulated Annealing-Based Multiobjective Optimization Algorithm: AMOSA. *IEEE Transactions on Evolutionary Computation*, 12(3):269–283, 2008. ISSN 1941-0026. doi:10.1109/TEVC.2007.900837.

[118] E. George. Optimization of Satellite Constellations for Discontinuous Global Coverage via Genetic Algorithms. *Advances in the Astronautical Sciences*, 97(Aug), 1997.

[119] William A. Crossley and Edwin A. Williams. Simulated Annealing and Genetic Algorithm Approaches for Discontinuous Coverage Satellite Constellation Design. *Engineering Optimization*, 32(3):353–371, 2000. doi:10.1080/03052150008941304.

[120] T.A. Ely, William A. Crossley, and E.A. Williams. Satellite Constellation Design for Zonal Coverage Using Genetic Algorithms. *Journal of the Astronautical Sciences*, 47(3-4), 1999.

[121] W.J. Mason, V. Coverstone-Carroll, and J.W. Hartmann. Optimal Earth Orbiting Satellite Constellations Via a Pareto Genetic Algorithm. In *AIAA/AAS Astrodynamics Specialist Conference and Exhibit*, Boston, MA, 1998. American Institute of Aeronautics and Astronautics (AIAA). doi:10.2514/6.1998-4381.

[122] Matthew P. Ferringer and David B. Spencer. Satellite Constellation Design Tradeoffs Using Multiple-Objective Evolutionary Computation. *Journal of Spacecraft and Rockets*, 43(6):1404–1411, 2006. ISSN 0022-4650. doi:10.2514/1.18788.

[123] Matthew P. Ferringer, Ronald S. Clifton, and Timothy G. Thompson. Efficient and Accurate Evolutionary Multi-Objective Optimization Paradigms for Satellite Constellation Design. *Journal of Spacecraft and Rockets*, 44(3):682–691, 2007. ISSN 0022-4650. doi:10.2514/1.26747.

[124] Olivier L. de Weck and Darren Chang. Architecture Trade Methodology for LEO Personal Communication Systems. In *20th International Communicatuions Satellite Systems Conference*, Montreal, Canada, 2002. American Institute of Aeronautics and Astronautics (AIAA). ISBN 978-1-62410-111-3. doi:10.2514/6.2002-1866.

[125] Douglas O. Stanley, Theodore A. Talay, Roger A. Lepsch, W.D. Morris, and Kathryn E. Wurster. Conceptual Design of a Fully Reusable Manned Launch System. *Journal of Spacecraft and Rockets*, 29(4):529–537, 1992. ISSN 0022-4650. doi:10.2514/3.25496.

[126] John R. Olds. *Multidisciplinary Design Techniques Applied to Conceptual Aerospace Vehicle Design.* Phd thesis, North Carolina State University, 1993.

[127] John R. Olds. System Sensitivity Analysis Applied to the Conceptual Design of a Dual-Fuel Rocket SSTO. In *5th Symposium on Multidisciplinary Analysis and Optimization*,

Panama City Beach, FL, 1994. American Institute of Aeronautics and Astronautics (AIAA).

[128] Robert D. Braun, Richard W. Powell, Roger A. Lepsch, Douglas O. Stanley, and Ilan M. Kroo. Comparison of Two Multidisciplinary Optimization Strategies for Launch-Vehicle Design. *Journal of Spacecraft and Rockets*, 32(3):404–410, 1995. ISSN 0022-4650. doi:10.2514/3.26629.

[129] Lawrence F. Rowell, Robert D. Braun, John R. Olds, and Resit Unal. Multidisciplinary Conceptual Design Optimization of Space Transportation Systems. *Journal of Aircraft*, 36(1), 1999. doi:10.2514/2.2428.

[130] P. Cage, I. Kroo, and R. Braun. Interplanetary trajectory optimization using a genetic algorithm. In *AAS/AIAA Astrodynamics Specialists Conference*, volume 43, Reston, Virigina, August 1994. American Institute of Aeronautics and Astronautics. doi:10.2514/6.1994-3773.

[131] Douglas J. Bayley, Roy J. Hartfield, John E. Burkhalter, and Rhonald M. Jenkins. Design Optimization of a Space Launch Vehicle Using a Genetic Algorithm. *Journal of Spacecraft and Rockets*, 45(4):733–740, 2008. ISSN 0022-4650. doi:10.2514/1.35318.

[132] John T. Hwang, Dae Young Lee, James W. Cutler, and Joaquim R.R.A. Martins. Large-Scale Multidisciplinary Optimization of a Small Satellites Design and Operation. *Journal of Spacecraft and Rockets*, 51(5):1648–1663, 2014. ISSN 0022-4650. doi:10.2514/1.A32751.

[133] C.J. Lowe and Malcolm Macdonald. Rapid model-based inter-disciplinary design of a CubeSat mission. *Acta Astronautica*, 105(1):321–332, 2014. ISSN 00945765. doi:10.1016/j.actaastro.2014.10.002.

[134] Nichols F. Brown and John R. Olds. Evaluation of Multidisciplinary Optimization Techniques Applied to a Reusable Launch Vehicle. *Journal of Spacecraft and Rockets*, 43(6): 1289–1300, 2006. ISSN 0022-4650. doi:10.2514/1.16577.

[135] Joaquim R.R.A. Martins and Andrew B. Lambe. Multidisciplinary Design Optimization: Survey of Architectures. *AIAA Journal*, 2013. doi:10.2514/1.J051895.

[136] Adam M. Ross and Daniel E. Hastings. The Tradespace Exploration Padadigm. In *INCOSE International Symposium*, Rochester, NY, 2005. INCOSE.

[137] Nicolas E. Antoine and Ilan M. Kroo. Framework for Aircraft Conceptual Design and Environmental Performance Studies. *AIAA Journal*, 43(10):2100–2109, 2005. ISSN 0001-1452. doi:10.2514/1.13017.

[138] Andrew March, Ian Waitz, and Karen Willcox. A Methodology for Integrated Conceptual Design of Aircraft Configuration and Operation to Reduce Environmental Impact. In *9th AIAA Aviation Technology, Integration, and Operations Conference (ATIO) and Aircraft Noise and Emissions Reduction Symposium (ANERS)*, Hilton Head, SC, 2009. American Institute of Aeronautics and Astronautics (AIAA). ISBN 978-1-60086-977-8. doi:10.2514/6.2009-7026.

[139] Lorenz Drack and Hossein S. Zadeh. Applications of Stochastic Optimisation in Non-Linear and Discontinuous Design Spaces. In *12th International Conference on Analytical and Stochastic Modelling Techniques and Applications*, Riga, Latvia, 2005. ISBN 1842331124.

[140] Serpil Sayn. Measuring the quality of discrete representations of efficient sets in multiple objective mathematical programming. *Mathematical Programming*, 87(3):543, 2000. ISSN 00255610. doi:10.1007/s101070050128.

[141] Stacey L. Faulkenberg and Margaret M. Wiecek. On the quality of discrete representations in multiple objective programming. *Optimization and Engineering*, 11(3):423–440, 2010. ISSN 13894420. doi:10.1007/s11081-009-9099-x.

[142] Kenneth Moe and Mildred M. Moe. GasSurface Interactions and Satellite Drag Coefficients. *Planetary and Space Science*, 53(8):793–801, 2005. ISSN 00320633. doi:10.1016/j.pss.2005.03.005.

[143] Borhan Kazimipour, Li Xiaodong, and A.K. Qin. A Review of Population Initialization Techniques for Evolutionary Algorithms. In *IEEE Congress on Evolutionary Computation*, pages 2585–2592, Beijing, China, 2014. IEEE. ISBN 978-1-4799-1488-3. doi:10.1109/CEC.2014.6900618.

[144] H. Maaranen, K. Miettinen, and M.M. Mäkelä. Quasi-Random Initial Population for Genetic Algorithms. *Computers and Mathematics with Applications*, 47(12):1885–1895, 2004. ISSN 08981221. doi:10.1016/j.cainwa.2003.07.011.

[145] Mohammad Hamdan and Osamah Qudah. The Initialization of Evolutionary Multi-objective Optimization Algorithms. In *Advances in Swarm and Computational Intelligence*, volume 2, pages 495–504. Springer International Publishing, Switzerland, 2015. ISBN 9783319204659. doi:10.1007/978-3-319-20466-6_52.

[146] Silvia Poles, Yan Fu, and Enrico Rigoni. The Effect of Initial Population Sampling on the Convergence of Multi-Objective Genetic Algorithms. In Vincent Barichard, Matthias Ehrgott, Xavier Gandibleux, and Vincent T'Kindt, editors, *Multiobjective Programming and Goal Programming*, volume 618, pages 123–133. Springer Berlin Heidelberg, Berlin, Heidelberg, 2009. ISBN 978-3-540-85646-7. doi:10.1007/978-3-540-85646-7_12.

[147] Pedro A. Diaz-Gomez and Dean F. Hougen. Initial Population for Genetic Algorithms: A Metric Approach. In *International Conference on Genetic and Evolutionary Methods*, pages 43–49, Las Vegas, NV, 2007.

[148] E. Osaba, R. Carballedo, F. Diaz, E. Onieva, P. Lopez, and A. Perallos. On the influence of using initialization functions on genetic algorithms solving combinatorial optimization problems: A first study on the TSP. In *IEEE Conference on Evolving and Adaptive Intelligent Systems (EAIS)*, pages 1–6, Linz, Austria, 2014. IEEE. ISBN 978-1-4799-3347-1. doi:10.1109/EAIS.2014.6867465.

[149] Joaquim R.R.A. Martins. A Short Course on Multidisciplinary Design Optimization. Technical report, University of Michigan, Ann Arbor, MI, 2012.

[150] Larry J. Eshelman, Richard A. Caruana, and J. David Schaffer. Biases in the crossover landscape. In *Third International Conference on Genetic Algorithms*, pages 10–19, Fairfax, VA, 1989. George Mason University. ISBN 1-55860-006-3.

[151] William M. Spears. Crossover or Mutation? In *Foundations of Genetic Algorithms*, volume 2, pages 221–237. Morgan Kaufmann Publishers Inc., San Francisco, CA, 1993. doi:10.1016/B978-0-08-094832-4.50020-9.

[152] A.E. Eiben and C.A. Schippers. On evolutionary exploration and exploitation. *Fundamenta Informaticae*, 35, 1998. ISSN 0169-2968. doi:10.3233/FI-1998-35123403.

[153] David A. Vallado. *Fundamentals of Astrodynamics and Applications*. Microcosm Press/Springer, Hawthorne, CA, 4 edition, 2013.

[154] J.J.F. Liu and R.L. Alford. Semianalytic Theory for a Close-Earth Artificial Satellite. *Journal of Guidance, Control, and Dynamics*, 3(4):304–311, 1980. doi:10.2514/3.55994.

[155] P.J. Cefola. Equinoctial orbit elements - Application to artificial satellite orbits. In *AAS/AIAA Astrodynamics Specialists Conference*, Reston, VA, 1972. American Institute of Aeronautics and Astronautics (AIAA). doi:10.2514/6.1972-937.

[156] Felix R. Hoots and Richard G. France. An analytic satellite theory using gravity and a dynamic atmosphere. *Celestial Mechanics*, 40(1):1–18, 1987. ISSN 0008-8714. doi:10.1007/BF01232321.

[157] J.J.F. Liu and R.L. Alford. A Semi-Analytic Theory for the Motion of a Close- Earth Artificial Satellite with Drag. In *17th Aerospace Sciences Meeting*, New Orleans, LA, 1979. American Institute of Aeronautics and Astronautics (AIAA).

[158] Vladimir A. Chobotov, editor. *Orbital Mechanics*. American Institute of Aeronautics and Astronautics (AIAA), Reston, VA, 3 edition, 1993. ISBN 1563475375. doi:10.2514/4.862250.

[159] G.E. Cook and R.N.A. Plimmer. The Effect of Atmospheric Rotation on the Orbital Plane of a Near-Earth Satellite. *Proceedings of the Royal Society A: Mathematical, Physical and Engineering Sciences*, 258(1295):516–528, nov 1960. ISSN 1364-5021. doi:10.1098/rspa.1960.0204.

[160] D.G. King-Hele. *Satellite Orbits in an Atmosphere: Theory and Applications*. Blackie and Son Ltd., Glasgow, UK, 1987.

[161] D.G. King-Hele and R.R. Allan. The Rotational Speed of the Upper Atmosphere. *Space Science Reviews*, 6(2):81–87, November 1966. doi:10.1007/BF00222595.

[162] David A. Vallado and David Finkleman. A Critical Assessment of Satellite Drag and Atmospheric Density Modeling. In *AIAA/AAS Astrodynamics Specialist Conference and Exhibit*, Honolulu, HI, 2008. The American Institute of Aeronautics and Astronautics (AIAA). doi:10.2514/6.2008-6442.

[163] R.C. Nigam. Secular Decrease in the Inclination of Artificial Satellites. *AIAA Journal*, 1 (6):1454–1455, 1963. ISSN 0001-1452. doi:10.2514/3.1836.

[164] L.G. Jacchia. Revised Static Models of the Thermosphere and Exosphere with Empirical Temperature Profiles. Technical report, Smithsonian Astrophysical Observatory, Cambridge, MA, 1971.

[165] J.M. Picone, A.E. Hedin, D.P. Drob, and A.C. Aikin. NRLMSISE-00 Empirical Model of the Atmosphere: Statistical Comparisons and Scientific Issues. *Journal of Geophysical Research*, 107(A12), 2002. ISSN 0148-0227. doi:10.1029/2002JA009430.

[166] C. Pardini and L. Anselmo. Comparison and Accuracy Assessment of Semi-Empirical Atmopshere Models through the Orbital Decay of Spherical Satellites. *Journal of Astronautical Sciences*, 49(2), 2001.

[167] Keith A. Akins, Liam Healy, Shannon Coffey, and J.M. Picone. Comparison of MSIS and Jacchia Atomposheric Density Models for Orbit Determination and Propagation. In *13th AAS/AIAA Space Flight Mechanics Meeting*, Ponce, Puerto Rico, 2003. American Astronautical Society (AAS).

[168] J. Park, Y.-J. Moon, K.-H. Kim, K.-S. Cho, H.-D. Kim, Y.-S. Kwak, Y.-H. Kim, Y.-D. Park, and Y Yi. Comparison between the KOMPSAT-1 drag derived density and the MSISE model density during strong solar and/or geomagnetic activities. *Earth, Planets and Space*, 60(6):601–606, jun 2008. ISSN 1880-5981. doi:10.1186/BF03353123.

[169] Jianpeng Guo, Weixing Wan, Jeffrey M. Forbes, Eric Sutton, R. Steven Nerem, T. N. Woods, Sean Bruinsma, and Libo Liu. Effects of solar variability on thermosphere density from CHAMP accelerometer data. *Journal of Geophysical Research: Space Physics*, 112 (A10), oct 2007. doi:10.1029/2007JA012409.

[170] L.G. Jacchia, J.W. Slowey, and I.G. Campbell. An analysis of the solar-activity effects in the upper atmosphere. *Planetary and Space Science*, 21(11):1835–1842, nov 1973. ISSN 00320633. doi:10.1016/0032-0633(73)90114-1.

[171] L.G. Jacchia. New Static Models of the Thermosphere and Exosphere with Empirical Temperature Profiles. *SAO Special Report*, 313(May), 1970.

[172] Jeffrey M. Forbes, Gang Lu, Sean Bruinsma, Steven Nerem, and Xiaoli Zhang. Thermosphere density variations due to the 1524 April 2002 solar events from CHAMP/STAR

accelerometer measurements. *Journal of Geophysical Research*, 110(A12), 2005. doi:10.1029/2004JA010856.

[173] E.K. Sutton, J.M. Forbes, and D.J. Knipp. Rapid response of the thermosphere to variations in Joule heating. *Journal of Geophysical Research: Space Physics*, 114(A4), apr 2009. doi:10.1029/2008JA013667.

[174] David A. Vallado and T.S. Kelso. Using EOP and Space Weather Data for Satellite Operations. In *15th AAS/AIAA Astrodynamics Specialist Conference*, Lake Tahoe, CA, 2005. American Institute of Aeronautics and Astronautics (AIAA).

[175] David A. Vallado and T.S. Kelso. Earth Orientation Parameter and Space Weather Data for Flight Operations. In *23rd AAS/AIAA Space Flight Mechanics Meeting*, Kauai, HI, 2013. American Institute of Aeronautics and Astronautics (AIAA).

[176] Daniel L. Oltrogge and Chia-Chun Chao. Standardized Approaches for Estimating Orbital Lifetime after End-of-Life. In *AIAA/AAS Astrodynamics Specialist Conference*, volume 129, Mackinac Island, MI, 2007. American Astronautical Society (AAS).

[177] G.E. Cook. Satellite Drag Coefficients. *Planetary and Space Science*, 13(10):929–946, 1965. ISSN 00320633. doi:10.1016/0032-0633(65)90150-9.

[178] ISO TC 20/SC 14. Space systems Estimation of orbit lifetime. Technical report, International Organization for Standardization, Geneva, Switzerland, 2011.

[179] Daniel L. Oltrogge and Kyle Leveque. An Evaluation of CubeSat Orbital Decay. In *25th Annual AIAA/USU Conference on Small Satellites*, Logan, UT, 2011. American Institute of Aeronautics and Astronautics (AIAA). ISBN 6508594621.

[180] K. M. Borkowski. Accurate algorithms to transform geocentric to geodetic coordinates. *Bulletin Géodésique*, 63(1):50–56, 1989. ISSN 00074632. doi:10.1007/BF02520228.

[181] Yoshihide Kozai. The motion of a close earth satellite. *The Astronomical Journal*, 64: 367–377, 1959.

[182] J.J.F. Liu. Satellite Motion about an Oblate Earth. *AIAA Journal*, 12(11):1511–1516, 1974. doi:10.2514/3.49537.

[183] J. Lean, J.M. Picone, S. Knowles, A. Hedin, and G. Moore. Validating NRLMSIS Using Atmospheric Densities Derived from Spacecraft Drag: Starshine Example. In *AIAA/AAS Astrodynamics Specialist Conference and Exhibit*, number August, Monterey, CA, 2002. American Institute of Aeronautics and Astronautics (AIAA). doi:10.2514/6.2002-4736.

[184] A. Bezděk and D. Vokrouhlický. Semianalytic Theory of Motion for Close-Earth Spherical Satellites Including Drag and Gravitational Perturbations. *Planetary and Space Science*, 52(14):1233–1249, 2004. ISSN 00320633. doi:10.1016/j.pss.2004.08.004.

[185] Bruce R. Bowman and Kenneth Moe. Drag Coefficient Variability at 175-500km from the Orbit Decay Analyses of Spheres. In *AAS/AIAA Astrodynamics Specialists Conference*, number 1, page 21, Lake Tahoe, CA, 2005. American Astronautical Society (AAS).

[186] J. Kabeláč and L. Sehnal. Atmospheric effects on the dynamics of the MIMOSA satellite. *Journal of Geodesy*, 76(9-10):536–542, 2003. ISSN 09497714. doi:10.1007/s00190-002-0275-4.

[187] Ken Fujiwara, Kuniyuki Omagari, Thomas Iljic, Shinji Masumoto, Yasumi Konda, Tomio Yamanaka, Yohei Tanaka, Masaki Maeno, Taihei Ueno, Hiroki Ashida, Junichi Nishida, Takuro Ikeda, and Saburo Matunaga. Tokyo Tech Nano-Satellite CUTE-1.7 + APD Flight Operation Results and the Succeeding Satelliite. In *17th IFAC Symposium on Automatic Control in Aerospace*, Toulouse, France, 2007. International Federation of Automatic Control.

[188] Cheinway Hwang, Ting Jung Lin, Tzu Pang Tseng, and Benjamin Fong Chao. Modeling Orbit Dynamics of FORMOSAT-3/COSMIC Satellites for Recovery of Temporal Gravity Variations. *IEEE Transactions on Geoscience and Remote Sensing*, 46(11):3412–3423, 2008. ISSN 01962892. doi:10.1109/TGRS.2008.2004789.

[189] Hiroki Ashida, Kota Fujihashi, Shinichi Inagawa, Yoshiyuki Miura, Kuniyuki Omagari, Naoki Miyashita, Saburo Matunaga, Takahiro Toizumi, Jun Kataoka, and Nobuyuki Kawai. Design of Tokyo Tech nano-satellite Cute-1.7+APD II and its operation. *Acta Astronautica*, 66(9-10):1412–1424, 2010. ISSN 00945765. doi:10.1016/j.actaastro.2009.10.035.

[190] Anna University Chennai. ANUSAT - Anna University Satellite, 2009. URL `https://www.annauniv.edu/anusat/`.

[191] Christopher Kitts, Karolyn Ronzano, Richard Rasay, Ignacio Mas, Jose Acain, Michael Neumann, Laura Bica, Paul Mahacek, Giovanni Minelli, Erin Beck, Steve Li, Brian Gamp, Seamus Agnew, John Shepard, John Hines, Elwood Agasid, Charlie Friedericks, Matthew Piccini, Macarena Parra, Linda Timucin, C. Beasley, Mike Henschke, Ed Luzzi, Nghia Mai, Mike McIntyre, Robert Ricks, Antonio Ricco, David Squires, Bruce Yost, Greg Defouw, Aaron Schooley, Diana Ly, Millan Diaz-Aguado, Eric Stackpole, Orlando Diaz, Tammy Doukas, David Niesel, and Michael McGinnis. Initial Flight Results from the PharmaSat Biological Microsatellite Mission. In *23rd Annual AIAA/USU Conference on Small Satellites*, Logan, UT, 2009. American Institute of Aeronautics and Astronautics (AIAA).

[192] D.C. Redding. Highly Efficient, Very Low-Thrust Transfer to Geosynchronous Orbit: Exact and Approximate Solutions. *Journal of Guidance, Control, and Dynamics*, 7(2): 141–147, 1984. ISSN 0731-5090. doi:10.2514/3.8559.

[193] Robert A. Bettinger and Jonathan T. Black. Mathematical Relation Between the Hohmann Transfer and Continuous-Low Thrust Maneuvers. *Acta Astronautica*, 96:42–44, 2014. ISSN 00945765. doi:10.1016/j.actaastro.2013.11.020.

[194] Ronald W. Humble, Gary N. Henry, and Wiley J. Larson, editors. *Space Propulsion Analysis and Design*. McGraw-Hill, New York, NY, 1 edition, 1995.

[195] Thomas M. Chiasson and Paulo C. Lozano. *Modeling the Characteristics of Propulsion Systems Providing Less Than 10 N Thrust*. Msc., Massachusetts Institute of Technology, 2012.

[196] Clyde Space Ltd. Small Satellite Solar Panels. Datasheet, Glasgow, UK, 2012.

[197] GomSpace. NanoPower P110 Series Solar Panels. Datasheet, Aalborg, Denmark, 2013.

[198] NASA Science and Technology Definition Team for the Megnetospheric Constellation Mission DRACO. The Magnetospheric Constellation Dynamic Response and Coupling Observatory (DRACO): Understanding the Global Dynamics of the Structured Magnetotail. Technical Memorandum May, Goddard Space Flight Center, Greenbelt, MD, 2001.

[199] Mark Pollard. The Design, Build, Test and In-Orbit Performance of Low Cost Xenon Warm Gas Propulsion Systems. In *Space Propulsion*, San Sebastian, Spain, 2010. European Space Agency (ESA).

[200] I. Coxhill, D. Gibbon, and M. Drube. The Evolution of Xenon Resistojet Propulsion Systems at SSTL. In *5th International Spacecraft Propulsion Conference*, Heraklion, Greece, 2008.

[201] J. L. Burch and V. Angelopoulos, editors. *The THEMIS Mission*. Springer-Science+Business Media, B.V., New York, NY, 2009. ISBN 978-0-387-89819-3. doi:10.1007/978-0-387-89820-9.

[202] Roland Salome. The Propulsion Subsystem of the CNES Microsatellite Product Line. In *3rd International Conference on Spacecraft Propulsion*, Cannes, France, 2000. European Space Agency (ESA).

[203] Philippe Landiech and Paul Rodrigues. Overview on CNES Micro Satellites Missions: In Flight, Under Development and Next. In *Small Satellite Missions for Earth Observation*, pages 3–18. Springer-Verlag Berlin Heidelberg, Berlin, Heidelberg, 2010. ISBN 9789292212247. doi:10.1007/978-3-642-03501-2_1.

[204] Herbert J. Kramer. TacSat-2, 2015. URL `https://directory.eoportal.org/web/eoportal/satellite-missions/t/tacsat-2`.

[205] Terrance Yee. Roadrunner, a High-Performance Responsive Space Mission. In *18th Annual AIAA/USU Conference on Small Satellites*, Logan, UT, 2004. American Institute of Aeronautics and Astronautics (AIAA).

[206] Busek Co. Inc. Busek Low Power Hall Thrusters. Datasheet, Natick, MA, 2013. URL `http://www.busek.com/technologies__hall.htm`.

[207] David A. Bearden. Small-Satellite Costs. *Crosslink*, 2(1):33–44, 2001.

[208] Mary Boghosian and Ricardo Valerdi. A Cost Estimating Methodology for Very Small Satellites. In *Summer CubeSat Developers' Workshop*, pages 1–14, Logan, UT, 2011. The Aerospace Corporation.

[209] N.Y. Lao, Todd J. Mosher, and J.M. Neff. Small Satellite Cost Model Version 98 INTRO. User's guide, The Aerospace Corporation, El Segundo, CA, 1998.

[210] Eric Mahr and Greg Richardson. Development of the Small Satellite Cost Model (SSCM) Edition 2002. In *IEEE Aerospace Conference*, Big Sky, MT, 2003. IEEE. ISBN 0-7803-7651-X. doi:10.1109/AERO.2003.1235567.

[211] Debora D. Daberkow and Dimitri N. Mavris. An Investigation of Metamodeling Techniques for Complex Systems Design. In *9th Symposium on Multidisciplinary Analysis and Optimization*, Atlanta, GA, 2002. American Institute of Aeronautics and Astronautics (AIAA). ISBN 978-1-62410-120-5. doi:10.2514/6.2002-5457.

[212] André I. Khuri and Siuli Mukhopadhyay. Response Surface Methodology. *Wiley Interdisciplinary Reviews: Computational Statistics*, 2(2):128–149, 2010. ISSN 19395108. doi:10.1002/wics.73.

[213] Dana Vrajitoru. Large Population or Many Generations for Genetic Algorithms? Implications in Information Retrieval. In *Soft Computing in Information Retrieval*, Studies in Fuzziness and Soft Computing, chapter Part III, pages 199–222. Physica-Verlag HD, Heidelberg, 2000. ISBN 978-3-7908-2473-5. doi:10.1007/978-3-7908-1849-9_9.

[214] Jason. R Schott. *Fault Tolerant Design Using Single and Multicriteria Genetic Algorithm Optimization.* Msc, Massachusetts Institute of Technology, 1995.

[215] Sanghamitra Bandyopadhyay, Sankar K. Pal, and B. Aruna. Multiobjective GAs, Quantitative Indices, and Pattern Classification. *IEEE Transactions on Systems, Man and Cybernetics, Part B: Cybernetics*, 34(5):2088–2099, 2004. ISSN 1083-4419. doi:10.1109/TSMCB.2004.834438.

[216] Eckart Zitzler, Kalyanmoy Deb, and Lothar Thiele. Comparison of Multiobjective Evolutionary Algorithms: Empirical Results. *Evolutionary Computation*, 8(2):173–195, 2000. ISSN 1063-6560. doi:10.1162/106365600568202.

[217] Office of Commercial Space Transportation (AST) and the Commercial Space Transportation Advisory Committee (COMSTAC). 2002 Commercial Space Transportation Forecasts. Technical report, Federal Aviation Administration, Washington, DC, 2002.

[218] T.S. Kelso. Space Weather Data Query. Personal Email Communication, April 2014.

[219] Steven J. Isakowitz, Joshua B. Hopkins, and Joseph P. Hopkins Jr. *International Reference Guide to Space Launch Systems*. The American Institute of Aeronautics and Astronautics (AIAA), Reston, VA, 4 edition, 2004. ISBN 978-1-56347-591-7. doi:10.2514/4.475917.

[220] Quentin Hardy. Orbcomm Aims to Corner Low-Orbit Satellite Market, February 1997. URL `http://www.wsj.com/articles/SB855707661315821500`.

[221] Joseph Howard, Dipak Oza, and Danford S. Smith. Best Practices for Operations of Satellite Constellations. In *SpaceOps 2006 Conference*, Rome, 2006. American Institute of Aeronautics and Astronautics (AIAA). doi:10.2514/6.2006-5866.

[222] Jason Andrews. Constellation of Distributed NanoSats for Real Time Earth Observation. In *8th IAA Symposium on Small Satellites for Earth Observation*, Berlin, Germany, 2011. DLR.

[223] Jason Andrews. Spaceflight Secondary Payload System (SSPS) and SHERPA Tug - A New Business Model for Secondary and Hosted Payloads. In *26th Annual AIAA/USU Conference on Small Satellites*, Logan, UT, 2012. American Institute of Aeronautics and Astronautics (AIAA).

[224] Gerry Webb and Alex da Silva Curiel. The Changing Launcher Solutions of the Small Satellite Sector. In *62nd International Astronautical Congress*, Cape Town, SA, 2011. International Astronautical Federation (IAF).

[225] Gregory J. Kehrl and Matt Steele. Technical and Programmatic Challenges for Dedicated Ride Share Missions. In *26th Annual AIAA/USU Conference on Small Satellites*, Logan, UT, 2012. American Institute of Aeronautics and Astronautics (AIAA).

[226] Dustin Doud, Brian Bjelde, Christian Melbostad, and Lauren Dreyer. Secondary Launch Services and Payload Hosting Aboard the Falcon and Dragon Product Lines. In *26th Annual AIAA/USU Conference on Small Satellites*, Logan, UT, 2012. American Institute of Aeronautics and Astronautics (AIAA).

[227] Spaceflight Services. Deployed Payloads: Pricing Plans, 2013. URL `http://spaceflightservices.com/pricing-plans/`.

[228] US. Airforce/Lou Hernandez. Spaceflight Now: Payload Cache Prepared for Launch. URL `http://spaceflightnow.com/minotaur/stps26/101112cleanroom`.

[229] Orbital Sciences Corporation. 8 ORBCOMM Satellites Integrated to Pegasus. URL `http://www.orbital.com/NewsInfo/ImagesMultimedia/Images/SpaceLaunch/index.shtml`.

[230] Henry R. Hertzfeld, Ray A. Williamson, and Nicolas Peter. The relevance of economic data in the decision-making process for orbital launch vehicle programs, a U.S. perspective. *Acta Astronautica*, 61(11-12):1076–1084, 2007. ISSN 00945765. doi:10.1016/j.actaastro.2006.12.015.

[231] Andrew D. Ketsdever, Marcus P. Young, Jason B. Mossman, and Anthony P. Pancotti. Overview of Advanced Concepts for Space Access. *Journal of Spacecraft and Rockets*, 47 (2):238–250, 2010. ISSN 0022-4650. doi:10.2514/1.46148.

[232] Takashi Arime, Masanori Sugimine, Seiji Matsuda, Jun Yokote, Takayoshi Fuji, Kenji Sasaki, Dominic Depasquale, Hideki Kanayama, and Mitsuteru Kaneoka. ALSET - Air Launch System Enabling Technology R&D Program. In *25th Annual AIAA/USU Conference on Small Satellites*, number 5, Logan, UT, 2011. American Institute of Aeronautics and Astronautics (AIAA).

[233] David J. Weeks, Steven H. Walker, and Robert L. Sackheim. Small satellites and the DARPA/Air Force FALCON program. *Acta Astronautica*, 57(2-8):469–477, 2005. ISSN 00945765. doi:10.1016/j.actaastro.2005.03.058.

[234] Tessaleno Devezas, Francisco Cristovão L. de Melo, Maria Luisa Gregori, Maria Cristina V. Salgado, Joana R. Ribeiro, and Christian B.C. Devezas. The Struggle for Space: Past and Future of the Space Race. *Technological Forecasting and Social Change*, 79(5):963–985, 2012. ISSN 00401625. doi:10.1016/j.techfore.2011.12.006.

[235] Mitchell Burnside Clapp. Airborne Launch Assist Space Access (ALASA). In *SeeMe Industry Day Briefing*, Arlington, VA, 2012. DARPA Tactical Technology Office.

[236] Makeyev State Rocket Centre. SHTIL LV, 2009. URL `http://www.makeyev.ru/rocspace/rkkshtil/`.

[237] IAI MLM Division. Shavit Brochure, 2005.

[238] Orbital Sciences Corporation. Pegasus Users Guide 7.0. Technical report, Dulles, VA, 2010.

[239] Office of Commercial Space Transportation (AST) and the Commercial Space Transportation Advisory Committee (COMSTAC). 2012 Commercial Space Transportation Forecasts. Technical report, Federal Aviation Administration, Washington, DC, 2012.

[240] Orbital Sciences Corporation. Minotaur I User's Guide 2.1. Technical report, Orbital Sciences Corporation, Dulles, VA, 2006.

[241] Lockheed Martin Space Systems Company. Athena Mission Planner's Guide (MPG). Technical Report August 2011, Lockheed Martin Space Systems Company, Denver, CO, 2012.

[242] Space Exploration Technologies. Falcon 1 Launch Vehicle Payload User's Guide. Technical report, Hawthorne, CA, 2008.

[243] Space Exploration Technologies. Falcon 1 Overview, 2007. URL `http://www.spacex.com/falcon1.php`.

[244] Orbital Sciences Corporation. Taurus Launch System Payload User's Guide 4.0. Technical report, Dulles, VA, 2006.

[245] Arianespace. Vega User's Manual Issue 3 Revision 0. Technical report, Arianespace, Évry-Courcouronnes, France, 2006.

[246] Gerry Webb. Launching Small Satellites in Russia. In *Small Satellites Systems and Services - The 4S Symposium*, pages 1–12, Portorož, Slovenia, 2012.

[247] EUROKOT Launch Services GmbH. Rockot User's Guide 5.0. Technical Report 5, Bremen, 2011.

[248] Office of Commercial Space Transportation (AST). The Annual Compendium of Commercial Space Transportation: 2012. Technical report, Federal Aviation Adminstration, Washington, DC, 2013.

[249] Japan Aerospace Exploration Agency (JAXA). Epsilon Launch Vehicle. Technical report, Japan Aerospace Exploration Agency (JAXA), Tokyo, Japan, 2012.

[250] Stephen Harner. Amid Stock Market Summer Doldrums, Japan's JAXA Launching New World-Beating Epsilon Rocket, 2013. URL `http://www.forbes.com/sites/`

stephenharner/2013/08/22/amid-stock-market-summer-doldrums-japans-jaxa-launching-new-world-beating-epsilon-rocket/.

[251] Office of Commercial Space Transportation (AST). 2011 U.S. Commercial Space Transportation Developments and Concepts: Vehicles, Technologies, and Spaceports. Technical report, Federal Aviation Administration, Washington, DC, 2011.

[252] A.C. Charania, Dominic DePasquale, Seiji Matsuda, Hideki Kanayama, and Takayoshi Fuji. NanoLauncher: Efficient Orbital Transport for Nanosatellites. In *2nd UN/Japan Nano-Satellite Symposium*, Graz, Austria, 2011.

[253] Jeremy S. Goodwin and Peter Wegner. Evolved Expendable Launch Vehicle Secondary Payload Adapter. In *AIAA SPACE 2001 Conference and Exposition*, Albuquerque, NM, 2001. American Institute of Aeronautics and Astronautics (AIAA). doi:10.2514/6.2001-4701.

[254] Joseph R. Maly, Michael E. Evert, John T. Shepard, and Christian A. Smith. Space Access for Small Satellites on Rideshare Missions with ESPA and ESPA-Derived Payload Adapters. In *IEEE Aerospace Conference*, Big Sky, MT, 2011. IEEE. ISBN 978-1-4244-7350-2. doi:10.1109/AERO.2011.5747234.

[255] USASMDC/ARSTRAT. SWORDS: Soldier-Warfighter Operationally Responsive Deployer for Space. Technical report, Huntsville, AL, 2012. URL `http://www.smdc.army.mil/FactSheets/SWORDS.pdf`.

[256] Eduardo Viegas Dalle Lucca. Aerospace Science and Technology Department: Contributions Towards the Brazilian Space Program. In *Fiftieth Session of the Scientific and Technical Subcommittee on the Peaceful Uses of Outer Space*, number February, Vienna, Austria, 2013. United Nations Office for Outer Space Affairs.

[257] Fernando Hisas. Plan Espacial Nacional. Technical report, Comisión Nacional de Actividades Espaciales (CONAE), Buenos Aires, Argentina, 2011.

[258] Vadim Zakirov, Martin N. Sweeting, Peter Erichsen, and Timothy Lawrence. Specifics of Small Satellite Propulsion: Part 1. In *15th Annual AIAA/USU Conference on Small Satellites*, Logan, UT, 2001. American Institute of Aeronautics and Astronautics (AIAA).

[259] Steven Arestie, E. Glenn Lightsey, and Brian Hudson. Development of A Modular, Cold Gas Propulsion System for Small Satellite Applications. *Journal of Small Satellites*, 1(2): 63–74, 2012. URL http://www.jossonline.com/articles/0102-03/.

[260] David B. Scharfe and Andrew D. Ketsdever. A Review of High Thrust, High Delta-V Options for Microsatellite Missions. In *45th AIAA Joint Propulsion Conference and Exhibit*, volume 15, Denver, CO, 2009. American Institute of Aeronautics and Astronautics (AIAA).

[261] MOOG - ISP. MOOG Bipropellant Thrusters. Datasheet, Niagra Falls, NY, 2014. URL http://www.moog.com/literature/Space_Defense/Spacecraft/Propulsion/bipropellant_thrusters_rev_0914.pdf.

[262] Busek Co. Inc. 1cm RF Ion Thruster BIT-1. Datasheet, Natick, MA, 2014. URL http://www.busek.com/index_htm_files/70011950%20RevA%20Data%20Sheet%20for%20BIT-1%20Ion%20Thruster.pdf.

[263] Busek Co. Inc. Busek RF Ion Thrusters. Datasheet, Natick, MA, 2013. URL http://www.busek.com/index_htm_files/70008514E.pdf.

[264] Aerojet. Electric Propulsion Data Sheets. Datasheet, Redmond, WA, 2006. URL http://rocket.com/files/aerojet/documents/Capabilities/PDFs/Electric%20Propulsion%20Data%20Sheets.pdf.

[265] Busek Co. Inc. Busek Low Power Hall Thrusters. Datasheet, Natick, MA, 2013. URL http://www.busek.com/index_htm_files/70008510B.pdf.

[266] Busek Co. Inc. Busek High Power Hall Thrusters. Datasheet, Natick, MA, 2013. URL http://www.busek.com/index_htm_files/70008511B.pdf.

[267] Alta-Space. HT100 Brochure. Datasheet, Pisa, 2013. URL http://www.alta-space.com/uploads/file/brochures/Brochure_2013_HT100_D.pdf.

Appendix A

Launch of Small Satellites

To compliment their typically lower development costs, the launch of small satellites has traditionally been addressed through manifestation as secondary payloads utilising excess volume or mass on commissioned launches of larger satellites. This is typically known known as 'piggyback' launching [224]. The cost of these launch opportunities are much less than the cost of commissioning an individual launch. However, given the lower development costs for small satellites utilising COTS components, even with these reduced launch prices, see, Table A.1, access to orbit still represents a significant portion of the total mission budget. Additionally, the orbit achieved is often not ideal for the mission being performed, and the launch date can be subject to delays in the development of the primary payloads(s) [19]. Payloads designed to be launched by piggyback must therefore be agnostic to the destination orbit or be flexible enough in design to operate in a variety of LEO environments. As the missions performed by small satellites become increasingly useful, and potentially profitable, the compromises made in order to utilise piggyback launch opportunities become more detrimental to the success of the mission.

Cluster launch opportunities can offer a partial solution to the problems raised by piggyback launching. In cluster launches, the price of individual payload launch is similarly reduced by sharing the launch capacity with a number of payloads of different masses and sizes, as demonstrated in Figure A.1. Rideshare launches are typically classed as a subset of cluster launches where the payload consists of multiple similar satellites such as those forming a constellation or

Table A.1: Cost of advertised piggyback and cluster launch opportunities.

Vehicle/Provider	Mass/Form	Price [USD]	Specific Price [USD/kg]
Lockheed Martin Athena IIc [225]	3U P-POD	\$300k	\$60,000
	110kg microsatellite	\$12.5M	\$113,600
SpaceX Falcon 9 [226]	3U P-POD	\$200k-\$325k	\$40,000-\$65,000
	ESPA Class (180kg)	\$4M-\$5M	\$22,200-\$27,800
Spacecraft Services [227]	1U CubeSat	\$125k	\$125,000
	3U P-POD	\$325k	\$65,000
	6U P-POD	\$595k	\$59,500
	12U P-POD	\$995k	\$49,750
	50kg microsatellite	\$1.75M	\$35,000
	180kg microsatellite	\$4.95M	\$27,500
	300kg microsatellite	\$6.95M	\$23,200

swarm [224]. In particular, the Orbital Sciences' MicroStar satellite platform, used for the Orbcomm and FORMOSAT-3/COSMIC, is designed to support rideshare launch on the Pegasus, Taurus and Minotaur I vehicles, shown in Figure A.2.

In cluster launches the destination orbit is generally chosen to be mutually agreeable to the group of payloads and launch delays can be avoided by omitting the payloads which are not ready to launch. These opportunities have typically been arranged through launch brokerage companies by groups of satellite owners or operators. Recently, Lockheed Martin have begun to offer a specific launch opportunity labelled 'RideShare' for microsatellites and nanosatellites on their Athena vehicle [225]. The Dnepr and Polar Satellite Launch Vehicle (PSLV) launch vehicles are also often used for rideshare or cluster launches [224].

The dedicated option of launch offers the best conditions for access to orbit and is the preferred option for launch. For a dedicated launch, the satellite is either the only payload on the vehicle, or is labelled the primary payload and is therefore given priority over any secondary-manifested payloads. The required orbit for the mission of the payload can be selected and the launch date can be chosen with respect to the satellite development schedule. However, the price for dedicated launch, even on the smallest and cheapest vehicles, is typically much more expensive than the development cost of most small satellites, especially low-budget picosatellite and nanosatellite missions designed and built by education institutions. Dedicated launch is therefore generally only used for government minisatellite or large microsatellite missions.

Figure A.1: STP-S26 mission: multiple payloads integrated for Minotaur IV launch [228].

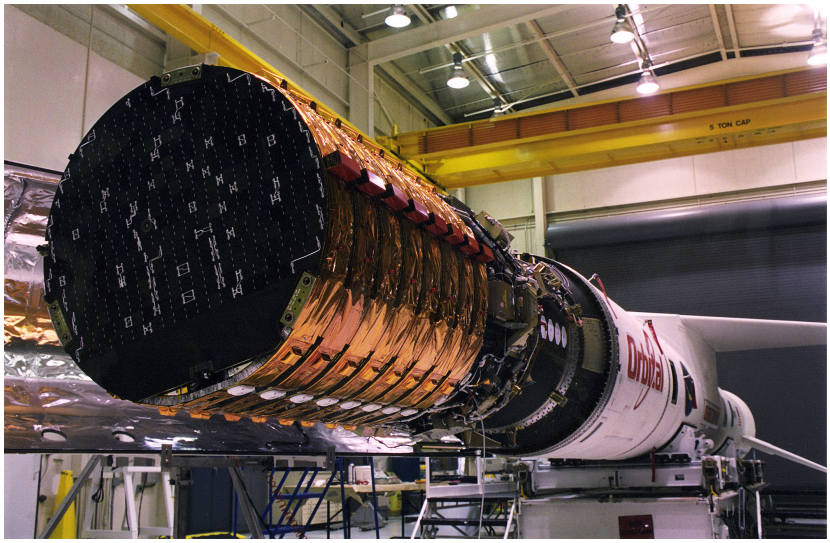

Figure A.2: ORBCOMM stack on Pegasus XL launch vehicle [229].

A.1 Small Launch Vehicles

The cost of payload delivery to orbit is often quoted as specific payload cost, the cost per unit mass of payload launched. This specific cost has been demonstrated, as in Figure A.3, to generally increase with decreasing payload capacity of the launch vehicles used for delivery to orbit [230, 231]. As a result, the specific launch cost for small payloads will typically be more expensive than those utilising cluster or piggyback launch opportunities. Furthermore, if the payload for a dedicated launch does not utilise the full capability of the launch vehicle the specific launch cost will actually be greater. Given the payload capacity of the available small launch vehicles, see Table A.2, most microsatellites and all nanosatellites and picosatellites will experience higher specific costs for dedicated launch.

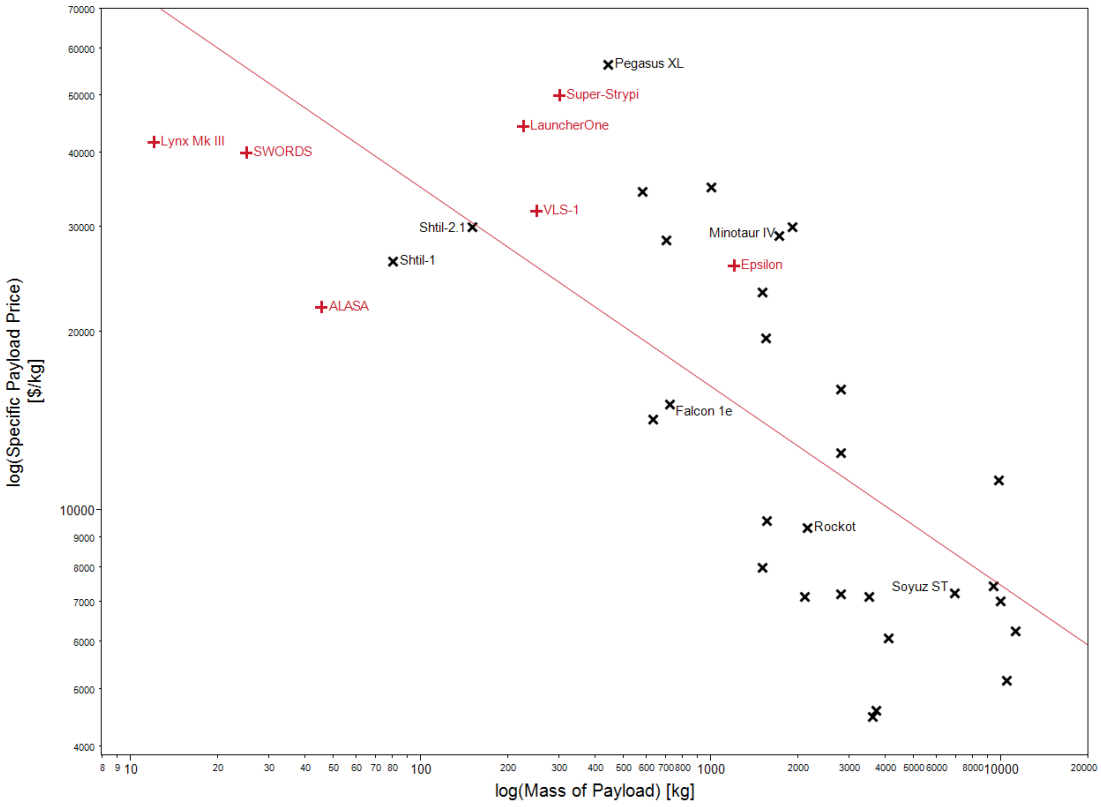

Figure A.3: Relationship between specific launch cost and launch vehicle payload capacity: existing launch vehicles (×), launch vehicles in development (+).

The proliferation of converted Intercontinental Ballistic Missile (ICBM) vehicles into the space launch market following the collapse of the former Soviet Union and the signing of Strategic Arms Reduction Treaty (START) resulted in the availability of a range of small and medium

launch vehicles. This range of vehicles benefited the developers of small satellites [11], and enabled the dedicated launch of minisatellites, some microsatellites and the clustered launch of smaller payloads. However, the ICBM heritage of these vehicles has since resulted in a number of issues relating to their ongoing availability for launch: storage, maintenance, re-lifing, and cost of conversion [224]. The availability of ICBM vehicles for commercial launch is also often uncertain or restricted.

The retirement and ongoing availability issues of ICBMs and other small launch vehicles, detailed in Table A.2, has resulted in a capability gap in the market for launch of small satellites, particularly for microsatellites and smaller classes [8].

A.1.1 Small Launch Vehicles in Development

Whilst piggyback and cluster launches have been successful in providing launch opportunities for small satellites at a more reasonable cost than individual launches, the compromises made with respect to schedule and orbit can be harmful to small satellites which are designed to be developed quickly or have inflexible mission requirements [25, 24]. As a result, a number of microsatellite and nanosatellite launch vehicles are in development to address the capability gap described previously. These new vehicles have been proposed by a variety of existing and emerging launch service providers and are shown in Table A.3 and have been included, where sufficient information was available, in Figure A.3.

Of these new small vehicles in development, three are to be air-launched vehicles and one launched from a suborbital spacecraft. The Pegasus and Pegasus-XL launchers are currently the only vehicle to have demonstrated operational air-launch capability. As a result, the method and associated technologies of air-launch to orbit are less mature than conventional vertical launch operations, and will involve additional development and testing prior to operation. The basic technologies and subsystems requiring development for a commercial air-launched system were outlined by the Air Launched System Enabling Technology (ALSET) project [232]. Specifically, the method and sequence of deployment and aerodynamic stabilization of the launch vehicle at ignition were identified as requiring substantial development and verification.

The immaturity of air-launched vehicles can also have an impact on the price of launch. For example, the price of the Pegasus launch vehicle has risen significantly since their introduction. Initially available for approximately $8M [233], in 1992 US Dollars, the price of launch has since risen to over $20M [234, 233, 27, 219]. This rise in cost has been attributed by different sources

Table A.2: Current small launch vehicles.

Vehicle	Payload [kg]	Altitude [km]	Approx. Cost [USD]	Specific Cost [USD/kg]	Notes/Known Issues	Source(s)
Shtil-1	80	500	$2.1M	$26,300	Submarine launched. Availability unknown.	[219, 236]
Shtil-2.1	150	500	$4.5M	$30,000	Submarine launched. Availability unknown.	[219, 236]
Shavit (LK-A)	350	420	Unknown	-	Commercial status unknown.	[219, 237]
Shavit-1 (LK-1)	350	700	Unknown	-	Commercial status unknown.	[219, 237]
Pegasus XL	443	200	$25M	$45,100	Air-launched	[219, 238]
Minotaur-1	580	185	$20M	$34,500	US Government sponsored payloads only. Planned retirement in 2017	[219, 239, 240]
Start-1	632	200	$9M	$14,200	Operation suspended: conversion of Svobodny to Vostochny cosmodrome.	[219]
Athena Ic	700	200	$20M	$28,600	No launches since 2001.	[224, 241]
Shavit-2 (LK-2)	800	700	Unknown	-	Commercial status unknown.	[219, 237]
Falcon 1e	1000	185	$10.9M	$10,900	Discontinued.	[242, 243]
Taurus (2110)	1000	500	$35M	$35,000	-	[224, 244]
Kosmos 3M	1500	250	$12M	$8,000	Discontinued.	[219]
Vega	1500	700	$35M	$23,300	Early operation phase.	[224, 245]
Athena IIc	1540	200	$30M	$19,500	No launches since 1999.	[241]
Minotaur IV	1720	184	$50M	$29,100	US Government sponsored payloads only. Planned retirement in 2017	[239]
PSLV-CA	2100	200	$15M	$7,100	-	[219, 239]
Rockot	2140	200	$20M	$9,300	-	[246, 247]

to a variety of reasons including life-cycle cost of the launch assist aircraft, range costs [235], and lack of competition [233].

In contrast, the VLM-1, VLS-1, Tronador II, and Long March 6 are vertically launched and utilise conventional launch vehicle technologies and systems. The development of these vehicles should therefore be less intensive as a result of the relative maturity of these technologies. Similarly, the Super-Strypi vehicle, based on the Strypi sounding rocket [248], should have reduced development requirements. The Epsilon launch vehicle will utilise new autonomous systems in order to reduce the time for ground operations in launch preparation [249] and allow control of the launch from any location in the world. These aim of these developments is to reduce the operational costs of launch and remove the requirement for launch control to be located at the launch site itself.

Of the vehicles identified in Table A.3, the Lynx Mk.III, GOLauncher2, and LauncherOne vehicles are being privately developed, and will be operated commercially. Commercial availability has also been announced for the Long March 6 [239] and Epsilon [239, 250] vehicles. However, there is some uncertainty regarding the commercial availability of the US Government-led vehicles in development: the Super-Strypi [248]; Soldier-Warfighter Operationally Responsive Deployer for Space (SWORDS) [251], previously known as the US Army Nanomissile; and THE Airborne Launch Assist Space Access (ALASA) program vehicles. The commercial availability of the VLM-1, Tronador II, and VLS-1 vehicles are similarly unknown at this time.

The projected specific launch prices of the vehicles in development have been included in Figure A.3. The specific launch prices of the new vehicles are similar to those offered by current launch vehicles and within the range of the secondary payload opportunities identified in Table A.1. The vehicles in development can also be seen to fit the trend of increasing specific launch price with decreasing payload capability.

The projected specific launch price of the ALASA program vehicle is significantly lower than the Pegasus-XL. However, the ALASA program predicts that the cost of launch per unit mass of payload can be reduced by up to 25% by avoiding range-related services through the use of an air-launched vehicle [235].

An additional benefit of air-launch systems is typically identified as increased operational flexibility [235, 252]. The use of a suitable carrier aircraft can enable launch from a variety of locations, potentially any runway of sufficient length. The existence of multiple launch sites can enable a greater number of launch opportunities and as a result more responsive launch. The

use of the carrier aircraft can also enable launch directly into any required orbital inclination whilst maximising the launchers payload performance to orbit and reducing the requirement for on-orbit manoeuvres. Disruptive weather systems and conditions can also be avoided, reducing the potential for delays in the launch. Finally, the call-up to launch of the system can be reduced through efficient payload integration operations and suitable transportation to the carrier aircraft take-off site.

A.2 Deployment of Small Satellites

The deployment of a satellite from the launch vehicle into its intended orbit is generally achieved through the use of a payload adapter and a separation system. The payload adapter serves to provide the appropriately sized interface to connect the payload to the structure of the launch vehicle. The separation system provides the physical connection between the payload and the payload adapter and contains a mechanism to release the payload and provide positive separation from the launch vehicle. The separation system provides a ΔV, typically using springs, on the order of 1–2 m/s in order to separate the launch vehicle and payload. In the case of multiple-manifested launches, multiple payload adapters and separation systems are required in order to mount and deploy all the payloads. The launcher itself may also perform some manoeuvring actions in order to avoid any accidental collisions and deploy all the payloads safely.

For the launch of small satellites, several standardised payload adapters and separation mechanisms have been developed and certified on multiple launch vehicles in order to increase the number of secondary payload opportunities. The most successful launch adapter is the EELV Secondary Payload Adapter (ESPA). The ESPA was initially designed for the United Launch Alliance (ULA) Evolved Expendable Launch Vehicle (EELV) vehicles, the Altas V and Delta IV, to support a primary payload of 6800 kg and 6 secondary payloads, with a 610x610x970mm volume envelope and mass up to 180kg [253], resulting in the recognition of the ESPA-class payload. The ESPA has since been made compatible with the Falcon 9 and Antares launch vehicles and new versions of the ESPA produced to either support launch of four 300kg payloads, the ESPA Grande, or six 100 kg payloads, the Small Launch ESPA, from the Minotaur IV, Falcon 1e, Taurus, and Delta II vehicles with varying volume constraints based on the payload faring of the different vehicles [254]. The ESPA has also been use as the primary

Table A.3: Review of small launch systems in development.

Vehicle	Payload [kg]	Altitude [km]	Approx. Cost [USD]	Specific Cost [USD/kg]	Development Status	Source(s)
Lynx Mk.III	12	LEO	$500,000	$41,667	Suborbital launch. First launch planned for 2016.	[248]
SWORDS	25	750	$1M	$40,000	Liquid CH4/LOX propellant. Vertical mobile launch. Responsive 24h call to launch. Test flight in 2014.	[255]
GOLauncher2	25	LEO	-	-	Hybrid propellant. Air-launch. First launch planned for 2018.	[248]
ALASA	45.4	LEO	<$1M	<$22,026	US Defense Advanced Research Projects Agency (DARPA) program. Three system concepts in development. Test launches in 2014/2015.	[235]
VLM-1	150	300	-	-	Solid Propellant. Vertical Launch. First launch planned for 2015.	[256]
LauncherOne	225	LEO	<$10M	<$44,444	Air-launch. First launch planned for 2015. Commercial operations beginning in 2016.	[248]
Tronador II	250	600	-	-	Hypergolic bi-propellant. Vertical Launch. First launch planned for 2015.	[257]
VLS-1	250	700	$8M	$32,000	Solid Propellant. Vertical launch. First launch planned for 2014.	[234, 256]
Super-Strypi	300	475	$15M	$50,000	Solid propellant. Vertical rail launch. Responsive 6 day call to launch. First launch planned for 2013.	[248]
Long March 6	1080	700	-	-	Kerosene/LOX propellant. Vertical launch. First launch planned for 2013.	[239]
Epsilon	1200	375	$31M	$25,833	Solid propellant. Vertical launch. First launch planned for 2013.	[239, 250, 249, 224]

structure for the Lunar Crater Observation and Sensing Satellite (LCROSS) mission, utilising the mounting points to attach the various subsystems and science payloads, and the internal volume to house a small monopropellant propulsion system. The Spaceflight Secondary Payload System (SSPS) and SHERPA in-space tug also utilise an ESPA Grande derived structure for the flexible deployment or on-orbit hosting of secondary launch payloads [223].

The P-POD and similar deployment systems, described in Section Section 2.1.1, contain both the separation system for the housed payloads and provide the physical interface between the launch vehicle and the payloads.

Once separated from the launch vehicle, the satellite requires a propulsion system in order to perform manoeuvres in order to adjust its orbit. For small satellites, particularly nanosatellites and picosatellites, the inclusion of a propulsion system can require a significant growth in mass and increase the total cost of development by a factor of two or three [258]. The constraints on mass and volume associated with secondary payload launching are further compounded by pressure and safety requirements allocated as a result of the use of a payload container or by the launch service provider in order to reduce the risk to the primary payload. As a result, most nanosatellites and picosatellites to date have been designed and launched without a propulsion system. However, as the usefulness of satellites in these classes increases, their ability to attain their mission orbit and perform station-keeping or in-plane manoeuvres has become increasingly necessary [259].

A.2.1 Small Satellite Propulsion

The variety of different propulsion systems which are suitable for use on small satellites are shown in Table A.4, adapted from the survey by Scharfe and Ketsdever [260]. For the data given in the table, the ranges of operation may not have been demonstrated or proven in flight. The Technology Readiness Level (TRL) of the various systems should therefore be investigated before being specified for use on the different sizes of small satellite.

A range of propulsion systems for satellites of mass 100 kg to 500 kg are known to be mature [259]. However, for nanosatellites and picosatellites with much smaller power capabilities and tighter mass and volume constraints, the traditionally used small satellite propulsion system technologies are not suitable [259].

Whilst development of new technologies is enabling the use of different propulsion systems for all classes of small satellite, not all propulsion systems are suitable for the missions and

on-orbit manoeuvres required. Low-thrust propulsion systems, for example, are not able to produce the impulsive ΔV required for coplanar or out-of-plane manoeuvres. If these types of propulsion system are to be used, low-thrust orbital manoeuvres and trajectories must be considered.

Table A.4: Summary of small satellite propulsion technologies. Adapted from Scharfe and Ketsdever [260]

Thruster Type	**Thrust [mN]**	I_{sp} **[s]**	**Power [W]**	**Thruster Mass [kg]**
Hall/Ion	0.4–20	300–3700	14–300	≤ 1
FEEP/Colloid	0.0001–1.5	450–9000	1-100	0.1–1
Electromagnetic	0.03–2	200–4000	≤ 10	0.06–0.5
Electrothermal	≤ 220	50–250	3–300	0.1–1
Cold Gas	0.5–3000	40–80	–	0.01–1
Monopropellant	0.001–1500	100–230	≤ 6	0.01–0.5
Bipropellant	0.001–45000	100–320	≤ 6	0.01–0.5
Decomoposing Solid	–	320	–	–
Laser Micro. (ablation)	0.001	100–300	2	–
Laser Micro. (ignition)	1–10	37–100	–	–
Laser Plasma	0.1–1	500–1000	2	≤ 1
Hollow Cathode	0.001–10	50-1200	5-1000	–
Solar Thermal	56–1000	200–1100	–	≤ 10

Appendix B

Supplementary Equations

Averaged Variational Equations due to Non-Spherical Geopotential

Explicit analytical expressions for the averaged variations of the mean Keplerian elements due to the zonal Earth harmonics, J_2, J_3, and J_4, used to solve the transformed equations of motion Eqn. (5.5), are given below, as per [154].

$$\langle \dot{a} \rangle_G = 0 \tag{B.1a}$$

$$\begin{aligned}\langle \dot{e} \rangle_G = &-\frac{3}{32} n J_2^2 \left(\frac{R_E}{p}\right)^4 \sin^2 i \left(14 - 15\sin^2 i\right) e \left(1 - e^2\right) \sin 2\omega \\ &- \frac{3}{8} n J_3 \left(\frac{R_E}{p}\right)^3 \sin i \left(4 - 5\sin^2 i\right) \left(1 - e^2\right) \cos\omega \\ &- \frac{15}{32} n J_4 \left(\frac{R_E}{p}\right)^4 \sin^2 i \left(6 - 7\sin^2 i\right) e \left(1 - e^2\right) \sin 2\omega\end{aligned} \tag{B.1b}$$

$$\begin{aligned}\langle \dot{i} \rangle_G = &- \frac{3}{64} n J_2^2 \left(\frac{R_E}{p}\right)^4 \sin 2i \left(14 - 15\sin^2 i\right) e^2 \sin 2\omega \\ &+ \frac{3}{8} n J_3 \left(\frac{R_E}{p}\right)^3 \cos i \left(4 - 5\sin^2 i\right) e \cos \omega \\ &- \frac{15}{64} n J_4 \left(\frac{R_E}{p}\right)^4 \sin 2i \left(6 - 7\sin^2 i\right) e^2 \sin 2\omega\end{aligned} \tag{B.1c}$$

$$\begin{aligned}\langle \dot{\omega} \rangle_G = &+ \frac{3}{4} n J_2 \left(\frac{R_E}{p}\right)^2 \left(4 - 5\sin^2 i\right) \\ &+ \frac{3}{16} n J_2^2 \left(\frac{R_E}{p}\right)^4 \left\{48 - 103\sin^2 i + \frac{215}{4}\sin^4 i + \left(7 - \frac{9}{2}\sin^2 i - \frac{45}{8}\sin^4 i\right) e^2 \right. \\ &\quad + 6\left(1 - \frac{3}{2}\sin^2 i\right)\left(4 - 5\sin^2 i\right)\sqrt{1 - e^2} - \frac{1}{4}\left[2\left(14 - 15\sin^2 i\right)\sin^2 i \right. \\ &\quad \left.\left. - \left(28 - 158\sin^2 i + 135\sin^4 i\right) e^2\right] \cos 2\omega \right\} \\ &+ \frac{3}{8} n J_3 \left(\frac{R_E}{p}\right)^3 \left[\left(4 - 5\sin^2 i\right) \frac{\sin^2 i - e^2 \cos^2 i}{e \sin i} + 2\sin i \left(13 - 15\sin^2 i\right) e\right] \sin \omega \\ &- \frac{15}{32} n J_4 \left(\frac{R_E}{p}\right)^4 \left\{16 - 62\sin^2 i + 49\sin^4 i + \frac{3}{4}\left(24 - 84\sin^2 i + 63\sin^4 i\right) e^2 \right. \\ &\quad \left. + \left[\sin^2 i \left(6 - 7\sin^2 i\right) - \frac{1}{2}\left(12 - 70\sin^2 i + 63\sin^4 i\right) e^2\right] \cos 2\omega \right\}\end{aligned} \tag{B.1d}$$

$$
\begin{aligned}
\langle \dot{\Omega} \rangle_G = & -\frac{3}{2} n J_2 \left(\frac{R_E}{p}\right)^2 \cos i \\
& -\frac{3}{2} n J_2^2 \left(\frac{R_E}{p}\right)^4 \cos i \left[\frac{9}{4} + \frac{3}{2}\sqrt{1-e^2} - \sin^2 i \left(\frac{5}{2} + \frac{9}{4}\sqrt{1-e^2}\right)\right. \\
& \left. + \frac{e^2}{4}\left(1 + \frac{5}{4}\sin^2 i\right) + \frac{e^2}{8}\left(7 - 15\sin^2 i\right)\cos 2\omega\right] \\
& -\frac{3}{8} n J_3 \left(\frac{R_E}{p}\right)^3 \left(15\sin^2 i - 4\right) e \cot i \sin\omega \\
& -\frac{15}{16} n J_4 \left(\frac{R_E}{p}\right)^4 \left[\left(4 - 7\sin^2 i\right)\left(1 + \frac{3}{2}e^2\right) - \left(3 - 7\sin^2 i\right) e^2 \cos 2\omega\right]
\end{aligned}
\tag{B.1e}
$$

$$
\begin{aligned}
\langle \dot{M} \rangle_G = & \, n + \frac{3}{4} n J_2 \left(\frac{R_E}{p}\right)^2 \left(1 - \frac{3}{2}\sin^2 i\right)\sqrt{1-e^2} \\
& + \frac{3}{2} n J_2^2 \left(\frac{R_E}{p}\right)^4 \left\{ \left(1 - \frac{3}{2}\sin^2 i\right)\left(1-e^2\right)\left[\frac{5}{4}\left(1 - \frac{5}{2}\sin^2 i + \frac{13}{8}\sin^4 i\right)\right.\right. \\
& \left.\left. + \frac{5}{8}\left(1 - \sin^2 i + \frac{5}{8}\sin^4 i\right)e^2 + \frac{1}{16}\sin^2 i\left(14 - 15\sin^2 i\right)\left(1 - \frac{5}{2}e^2\right)\cos 2\omega\right]\sqrt{1-e^2}\right\} \\
& + \frac{3}{8} n J_2^2 \left(\frac{R_E}{p}\right)^4 \frac{1}{\sqrt{1-e^2}}\left\{3\left[3 - \frac{15}{2}\sin^2 i + \frac{47}{8}\sin^4 i + \left(\frac{3}{2} - 5\sin^2 i + \frac{117}{16}\sin^4 i\right)e^2\right.\right. \\
& \left. - \frac{1}{8}\left(1 + 5\sin^2 i + \frac{101}{8}\sin^4 i\right)e^4\right]\frac{e^2}{8}\sin^2 i\left[70 - 123\sin^2 i + \left(56 - 66\sin^2 i\right)e^2\right]\cos 2\omega \\
& \left. + \frac{27}{128}e^4 \sin^4 i \cos 4\omega\right\} \\
& -\frac{3}{8} n J_3 \left(\frac{R_E}{p}\right)^3 \left(4 - 5\sin^2 i\right)\frac{1-4e^2}{e}\sqrt{1-e^2}\sin\omega \\
& -\frac{45}{128} n J_4 \left(\frac{R_E}{p}\right)^4 \left(8 - 40\sin^2 i + 35\sin^4 i\right)e^2\sqrt{1-e^2} \\
& + \frac{15}{64} n J_4 \left(\frac{R_E}{p}\right)^4 \sin^2 i \left(6 - 7\sin^2 i\right)\left(2 - 5e^2\right)\sqrt{1-e^2}\cos 2\omega
\end{aligned}
\tag{B.1f}
$$

First-Order Short-Period Variations

Explicit analytical expressions for first-order short periodic variations in the Keplerian elements due to the zonal Earth harmonics, J_2, J_3, and J_4, used to transform from mean to osculating orbital elements, Eqn. (5.2), are given below, as per [154].

$$a_{sp} = J_2 \left(\frac{R^2}{a}\right) \left\{ \left(\frac{a}{r}^3\right) \left[1 - \frac{3}{2}\sin^2 i + \frac{3}{2}\sin^2 i \cos 2\left(\omega + f\right)\right] - \left(1 - \frac{3}{2}\sin^2 i\right)\left(1 - e^2\right)^{-\frac{3}{2}} \right\} \tag{B.2a}$$

$$\begin{aligned} e_{sp} =& \frac{1}{2} J_2 \left(\frac{R}{p}\right)^2 \left(1 - \frac{3}{2}\sin^2 i\right) \left\{ \frac{1}{e}\left[1 + \frac{3}{2}e^2 - \left(1 - e^2\right)^{\frac{3}{2}}\right] \right. \\ & \left. + 3\left(1 + \frac{e^2}{4}\right)\cos f + \frac{3}{2}e\cos 2f + \frac{e^2}{4}\cos 3f \right\} \\ & \frac{3}{8} J_2 \left(\frac{R}{p}\right)^2 \sin^2 i \left[\left(1 + \frac{11}{4}e^2\right)\cos\left(2\omega + f\right) + \frac{3}{2}e\cos\left(2\omega - f\right) + 5e\cos\left(2\omega + 2f\right) \right. \\ & \left. + \frac{1}{3}\left(7 + \frac{17}{4}e^2\right)\cos\left(2\omega + 3f\right) + \frac{3}{2}e\cos\left(2\omega + 4f\right) + \frac{e^2}{4}\cos\left(2\omega + 5f\right) + \frac{3}{2}e\cos 2\omega \right] \end{aligned} \tag{B.2b}$$

$$i_{sp} = \frac{3}{8} J_2 \left(\frac{R}{p}\right)^2 \left[e\cos\left(2\omega + f\right) + \cos 2\left(\omega + f\right) + \frac{e}{3}\cos 2\left(2\omega + 3f\right) \right] \tag{B.2c}$$

$$\begin{aligned}\omega_{sp} = &+ \frac{3}{4}J_2\left(\frac{R}{p}\right)^2\left(4-5\sin^2 i\right)\left(f-M+e\sin f\right)\\
&+ \frac{3}{4}J_2\left(\frac{R}{p}\right)^2\left(1-\frac{3}{2}\sin^2 i\right)\left[\frac{1}{e}\left(1-\frac{1}{4}e^2\right)\sin nu+\frac{1}{2}\sin 2f+\frac{1}{12}e\sin 3f\right]\\
&- \frac{3}{2}J_2\left(\frac{R}{p}\right)^2\left\{\frac{1}{e}\left[\frac{1}{4}\sin^2 i+\frac{e^2}{2}\left(1-\frac{15}{8}\sin^2 i\right)\right]\sin\left(2\omega+f\right)+\frac{e}{16}\sin^2 i\sin\left(2\omega-f\right)\right.\\
&\quad + \frac{1}{2}\left(1-\frac{5}{2}\sin^2 i\right)\sin\left(2\omega+2f\right)-\frac{1}{e}\left[\frac{7}{12}\sin^2 i-\frac{e^2}{6}\left(1-\frac{19}{8}\sin^2 i\right)\right]\sin\left(2\omega+3f\right)\\
&\quad \left.- \frac{3}{8}\sin^2 i\sin\left(2\omega+4f\right)-\frac{1}{16}e\sin^2 i\sin\left(2\omega+5f\right)\right\}\\
&+ \frac{9}{16}J_2\left(\frac{R}{p}\right)^2\sin^2 i\sin 2\omega\end{aligned} \tag{B.2d}$$

$$\Omega_{sp} = -\frac{3}{2}J_2\left(\frac{R}{p}\right)^2\cos i\left[f-M+e\sin f-\frac{e}{2}\sin\left(2\omega+f\right)-\frac{1}{2}\sin\left(2\omega+2f\right)-\frac{e}{6}\sin\left(2\omega+3f\right)\right] \tag{B.2e}$$

$$\begin{aligned}M_{sp} = &- \frac{3}{2}J_2\left(\frac{R}{p}\right)^2\sqrt{\frac{1-e^2}{e}}\left\{\left(1-\frac{3}{2}\sin^2 i\right)\left[\left(1-\frac{1}{4}e^2\right)\sin nu+\frac{e}{2}\sin 2f+\frac{e^2}{12}\sin 3f\right]\right.\\
&\quad + \frac{1}{2}\sin^2 i\left[-\frac{1}{2}\left(1+\frac{5}{4}e^2\right)\sin\left(2\omega+f\right)-\frac{e^2}{8}\sin\left(2\omega-f\right)+\frac{7}{6}\left(1-\frac{e^2}{28}\right)\sin\left(2\omega+3f\right)\right.\\
&\quad \left.\left.+ \frac{3}{4}e\sin\left(2\omega+4f\right)+\frac{e^2}{8}\sin\left(2\omega+5f\right)\right]\right\}\\
&+ \frac{1}{4}J_2\left(\frac{R}{p}\right)^2\sqrt{1-e^2}\sin^2 i\sin 2\omega\end{aligned} \tag{B.2f}$$

Keplerian Orbital Elements to ECI State Vector

The following equations are used to transform the Keplerian orbital elements to position and velocity in the ECI frame. Eqns. (B.3a) and (B.3b) are used to calculate position and velocity in the perifocal coordinate system (PQW). Position and velocity vectors in the ECI frame are then obtained using the transformation matrix Eqn. (B.4) [153].

$$\vec{r}_{PQW} = \begin{bmatrix} \dfrac{p\cos f}{1+e\cos f} \\ \dfrac{p\sin f}{1+e\cos f} \\ 0 \end{bmatrix} \tag{B.3a}$$

$$\vec{v}_{PQW} = \begin{bmatrix} -\sqrt{\dfrac{\mu}{p}}\sin f \\ \sqrt{\dfrac{\mu}{p}}\,(e+\cos f) \\ 0 \end{bmatrix} \tag{B.3b}$$

$$\left[\frac{IJK}{PQW}\right] = \begin{bmatrix} \cos\Omega\cos\omega - \sin\Omega\sin\omega\cos i & -\cos\Omega\sin\omega - \sin\Omega\cos\omega\cos i & \sin\Omega\sin i \\ \cos\Omega\cos\omega - \sin\Omega\sin\omega\cos i & -\sin\Omega\sin\omega + \cos\Omega\cos\omega\cos i & -\cos\Omega\sin i \\ \sin\omega\sin i & \cos\omega\sin i & \cos i \end{bmatrix} \tag{B.4}$$

ECI to ECEF

Position and velocity in the ECEF coordinate system are obtained from position and velocity vectors in the rotating ECI frame using Eqns. (B.5a) and (B.5b) [153]. The GAST hour angle, θ, is required to define the rotation matrix $[T]$ and its derivative $[\dot{T}]$.

$$\vec{r}_{ECEF} = [T]\vec{r}_{ECI} \tag{B.5a}$$

$$\vec{v}_{ECEF} = [T]\vec{v}_{ECI} + [\dot{T}]\vec{r}_{ECI} \tag{B.5b}$$

$$[T] = \begin{bmatrix} \cos\theta & \sin\theta & 0 \\ -\sin\theta & \cos\theta & 0 \\ 0 & 0 & 1 \end{bmatrix} \tag{B.5c}$$

$$[\dot{T}] = \begin{bmatrix} -\omega_e \sin\theta & \omega_e \cos\theta & 0 \\ -\omega_e \cos\theta & -\omega_e \sin\theta & 0 \\ 0 & 0 & 0 \end{bmatrix} \tag{B.5d}$$

Appendix C

Propulsion System Models

The following tables contain thruster unit data, additional to that referred to by Chiasson and Lozano [195], which are used to determine the fitted relationships between the propulsion system characteristics shown in the corressponding figures.

Cold Gas Thrusters

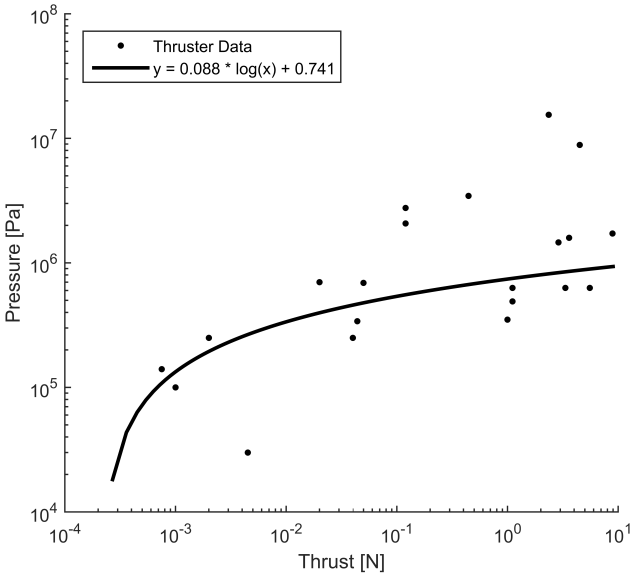

Figure C.1: Data and identified trend between thrust and pressure for CGT propulsion systems. Trend $R^2 = 0.145$

Monopropellant Thrusters

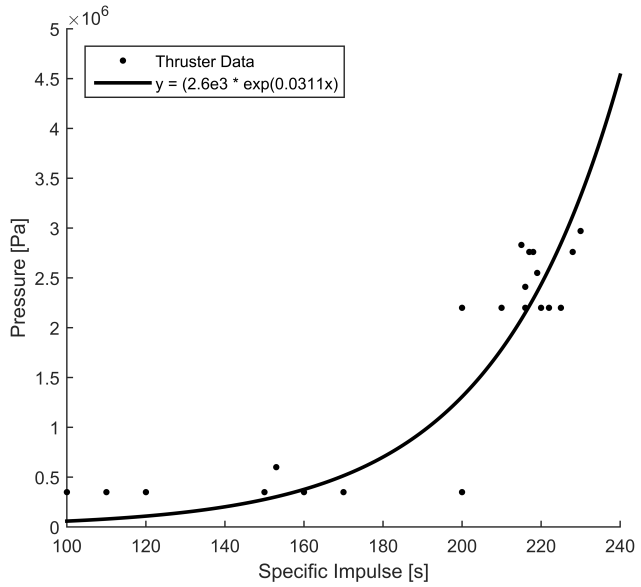

Figure C.2: Data and identified trend between specific impulse and pressure for monopropellant propulsion systems. Trend $R^2 = 0.777$

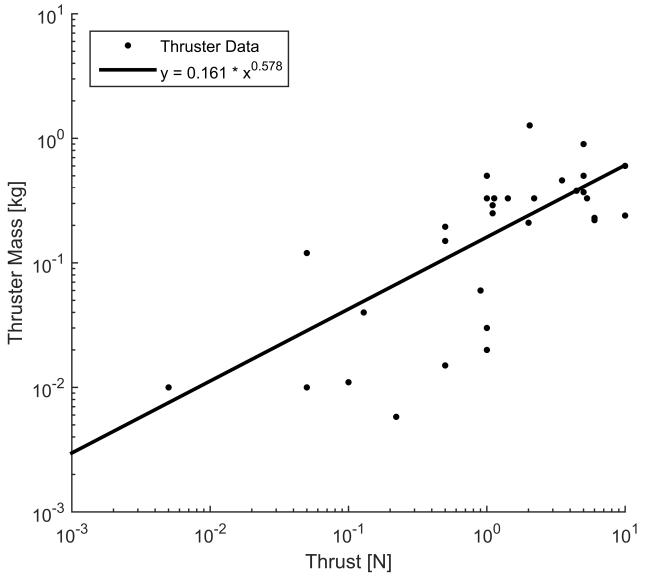

Figure C.3: Data and identified trend between thrust and thruster mass for monopropellant propulsion systems. Trend $R^2 = 0.612$

Bipropellant Thrusters

Table C.1: Additional bipropellant thruster data.

Thruster	Propellant	T_{max} [N]	p_{max} [W]	P_{in} [MPa]	m [kg]	I_{sp} [s]	Mix Ratio	Ref.
MOOG LLT	MON/MMH	9	27.0	1.97	0.78	274	1.65	[261]
MOOG 5lbf	MON/MMH	22	15.6	2.21	0.91	292	1.65	[261]
MOOG DST-11H	MON/MMH	22	41.0	2.76	0.77	310	0.85	[261]
MOOG DST-12	MON/MMH	22	9.0	2.76	0.64	302	1.61	[261]
MOOG DST-13	MON/MMH	22	41.0	2.76	0.68	298	1.65	[261]

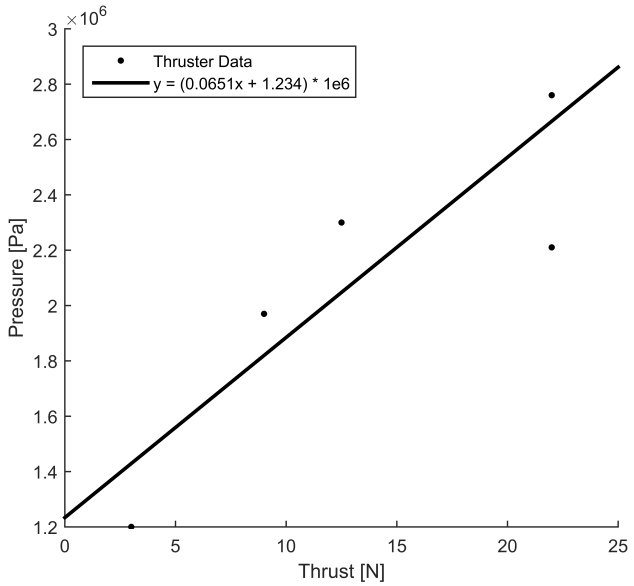

Figure C.4: Data and identified trend between thrust and pressure for bipropellant propulsion systems. Trend $R^2 = 0.810$

Resistojets

Table C.2: Additional resistojet thruster data.

Thruster	**Propellant**	$\mathbf{T_{max}}$ **[N]**	$\mathbf{p_{max}}$ **[W]**	$\mathbf{P_{in}}$ **[MPa]**	**m [kg]**	$\mathbf{I_{sp}}$ **[s]**	**Ref.**
UoSat-12	N_2O	0.125	100	1	1.240	127	[200]
Beijing 1	Xenon	0.018	15	0.1	0.065	42	[200]
RapidEye	Xenon	0.018	30	0.1	0.065	48	[200]

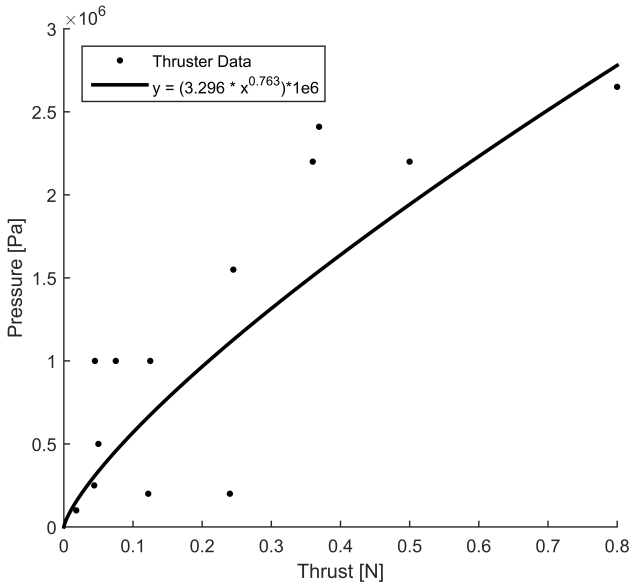

Figure C.5: Data and identified trend between thrust and pressure for resistojet propulsion systems. Trend $R^2 = 0.598$

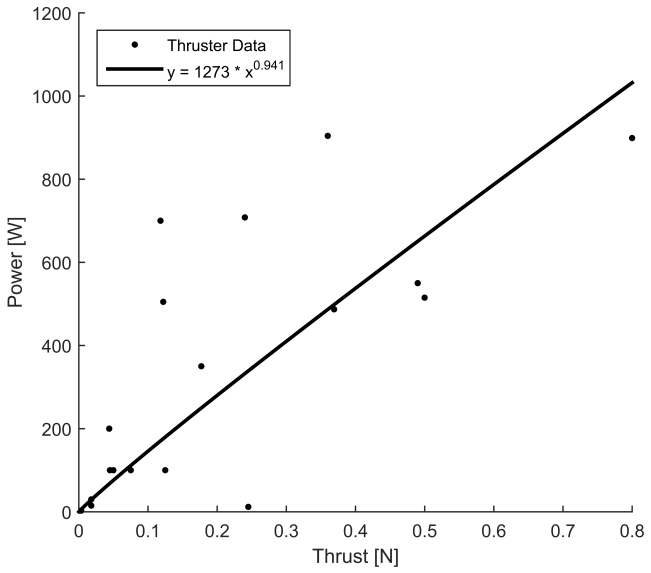

Figure C.6: Data and identified trend between thrust and power for resistojet propulsion systems. Trend $R^2 = 0.625$

Arcjets

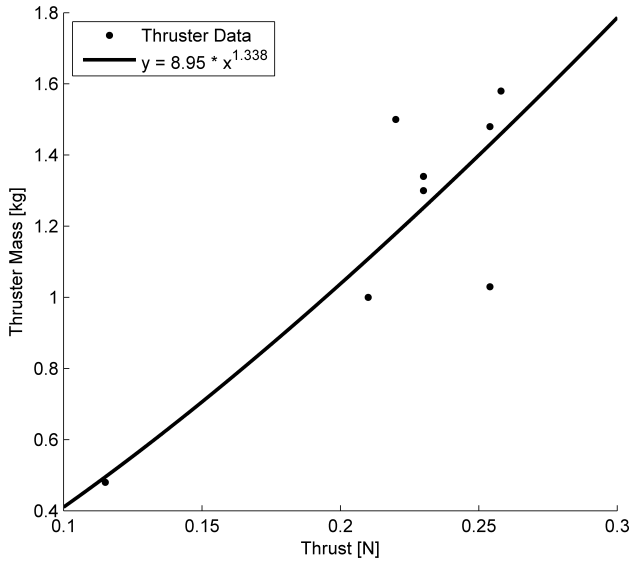

Figure C.7: Data and identified trend between thrust and thruster mass for arcjet propulsion systems. Trend $R^2 = 0.822$

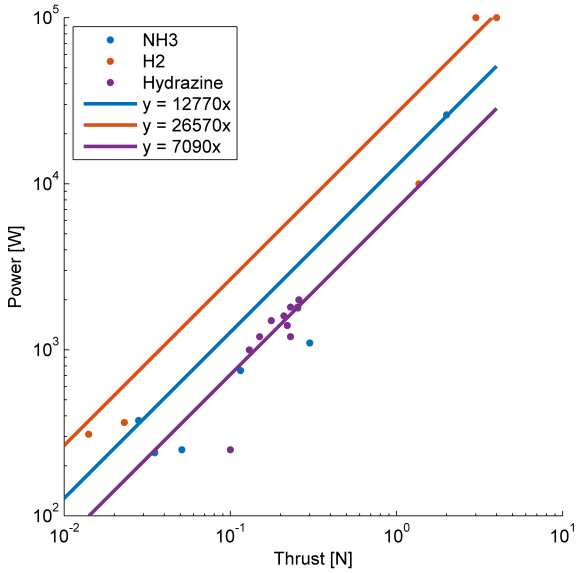

Figure C.8: Data and identified trend between thrust and power for arcjet propulsion systems of different propellants. NH3 trend $R^2 = 0.985$. H2 trend $R^2 = 0.898$. Hydrazine trend $R^2 = 0.762$.

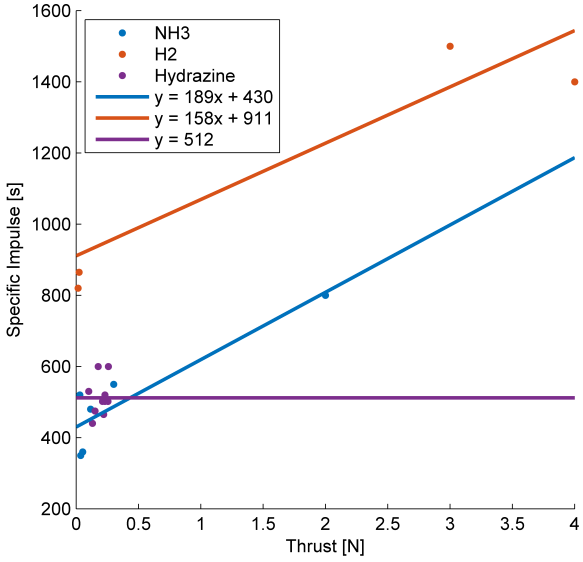

Figure C.9: Data and identified trend between thrust and specific impulse for arcjet propulsion systems of different propellants. NH3 trend $R^2 = 0.810$. H2 trend $R^2 = 0.808$.

Ion Thrusters

Table C.3: Additional ion thruster data.

Thruster	Propellant	T_{max} [mN]	p_{max} [W]	P_{in} [MPa]	m [kg]	I_{sp} [s]	η [%]	Ref.
Busek BIT-1 LP	Xenon	0.10	10	-	0.053	2150	28	[262]
Busek BIT-1 HP	Xenon	0.18	13	-	0.053	2300	36	[262]
Busek BIT-3	Xenon	1.4	60	-	0.2	3500	68	[263]
Busek BIT-7	Xenon	11	360	-	-	3850	73	[263]
Aerojet NEXT	Xenon	235	6900	-	13.3	4100	70	[264]

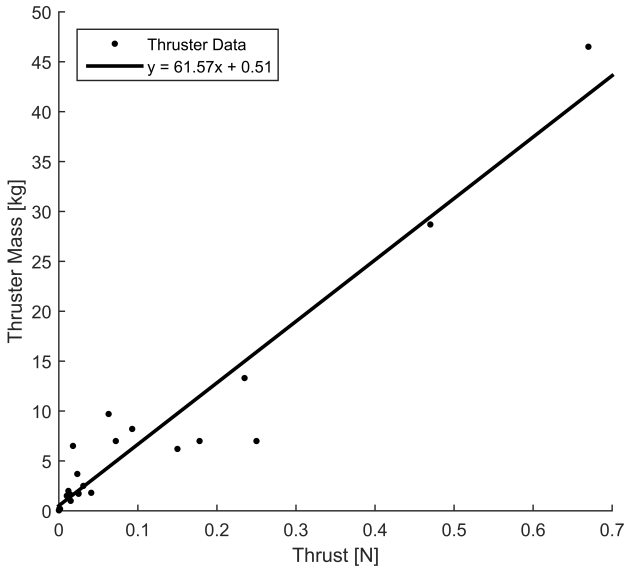

Figure C.10: Data and identified trend between thrust and thruster mass for ion propulsion systems. Trend $R^2 = 0.920$

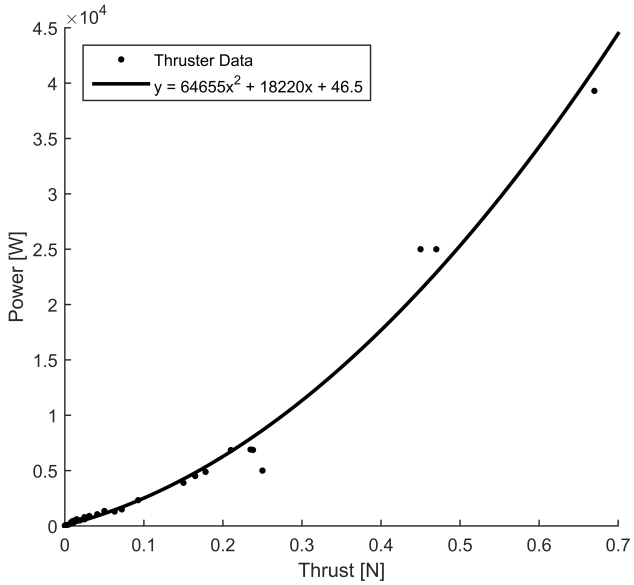

Figure C.11: Data and identified trend between thrust and power for ion propulsion systems. Trend $R^2 = 0.985$

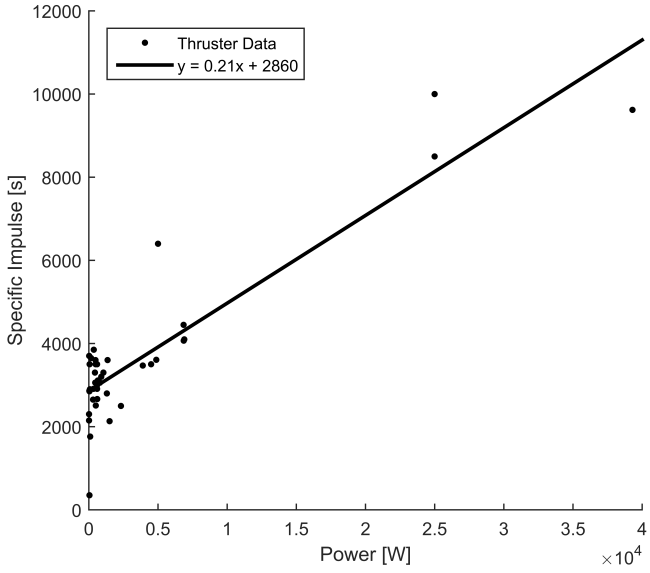

Figure C.12: Data and identified trend between power and specific impulse for ion propulsion systems. Trend $R^2 = 0.805$

Hall-Effect Thrusters Combined

Table C.4: Additional Hall-effect thruster data.

Thruster	**Propellant**	$\mathbf{T_{max}}$ **[mN]**	$\mathbf{p_{max}}$ **[W]**	$\mathbf{P_{in}}$ **[MPa]**	**m [kg]**	$\mathbf{I_{sp}}$ **[s]**	$\boldsymbol{\eta}$ **[%]**	**Ref.**
Busek BHT-200	Xenon	13	200	-	-	1390	-	[265]
Busek BHT-600	Xenon	39	600	-	-	1585	-	[265]
Busek BHT-1000	Xenon	58	1000	-	-	1750	-	[265]
Busek BHT-1500	Xenon	101	1500	-	-	1670	-	[266]
Busek BHT-8000	Xenon	507	8000	-	-	1880	-	[266]
Busek BHT-20k	Xenon	807	15000	-	-	2320	-	[266]
Alta-Space HT-100	Xenon	12	235	0.25	0.436	1300	40	[267]
Alta-Space HT-400	Xenon	35	600	-	0.9	1850	50	[267]
Alta-Space HT-15k	Xenon	250	5000	-	12.2	2250	60	[267]
Aerojet BPT-4000 2kW	Xenon	132	2000	-	12.3	1676	-	[264]
Aerojet BPT-4000 3kW	Xenon	195	3000	-	12.3	1700	-	[264]
Aerojet BPT-4000 4.5kW	Xenon	290	4500	-	12.3	1790	-	[264]

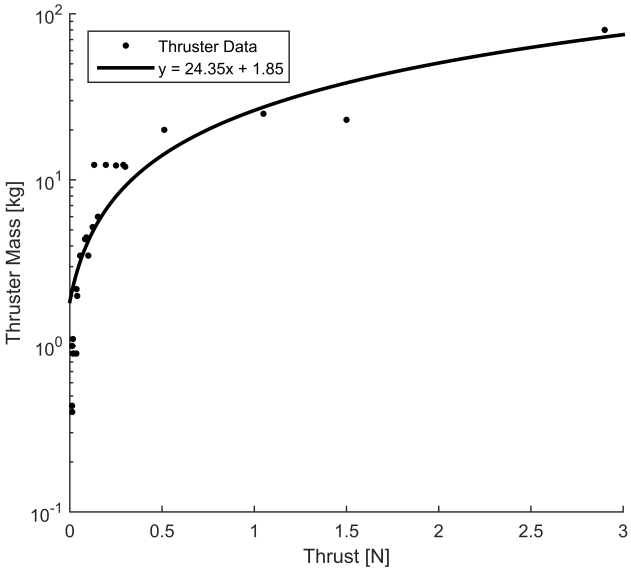

Figure C.13: Data and identified trend between thrust and thruster mass for Hall-effect propulsion systems. Trend $R^2 = 0.924$

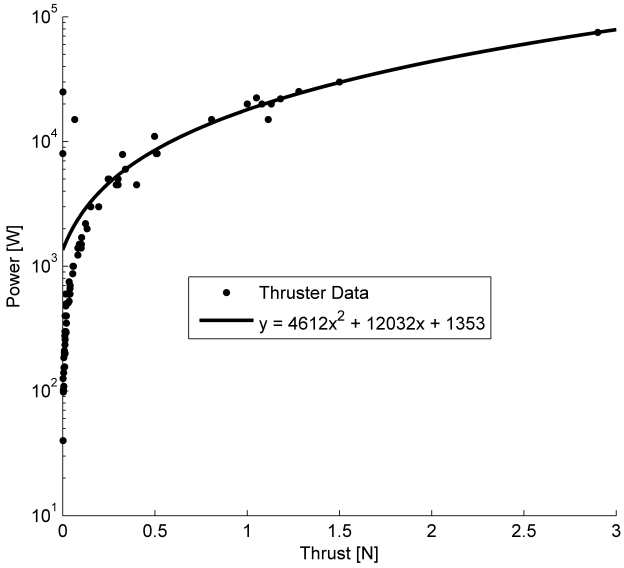

Figure C.14: Data and identified trend between thrust and power for Hall-effect propulsion systems. Trend $R^2 = 0.899$

Low-Power Hall-Effect Thrusters

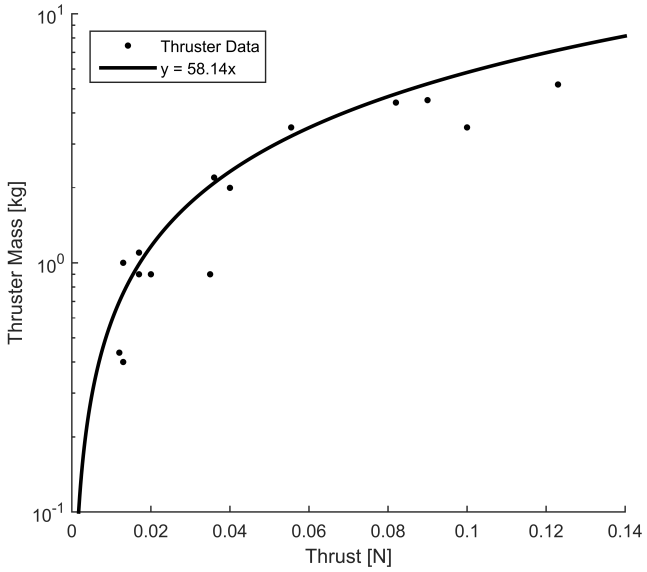

Figure C.15: Data and identified trend between thrust and thruster mass for low-power (<2.5 kW) Hall-effect propulsion systems. Trend $R^2 = 0.749$

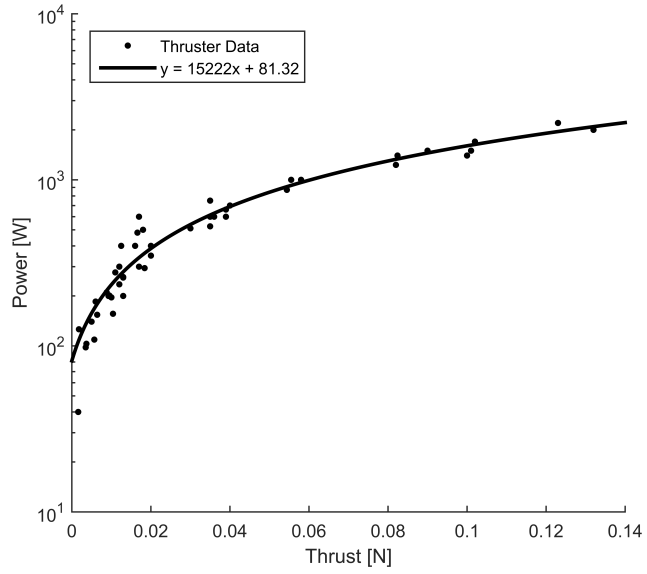

Figure C.16: Data and identified trend between thrust and power for low-power (<2.5 kW) Hall-effect propulsion systems. Trend $R^2 = 0.973$

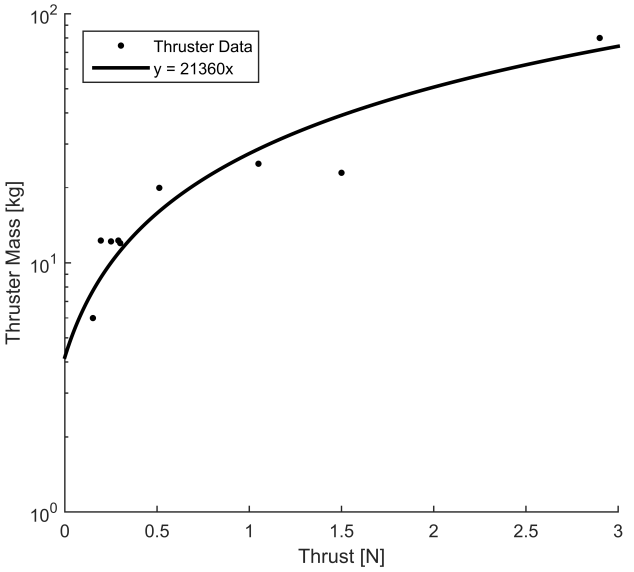

Figure C.17: Data and identified trend between thrust and thruster mass for high-power (>2.5 kW) Hall-effect propulsion systems. Trend $R^2 = 0.907$

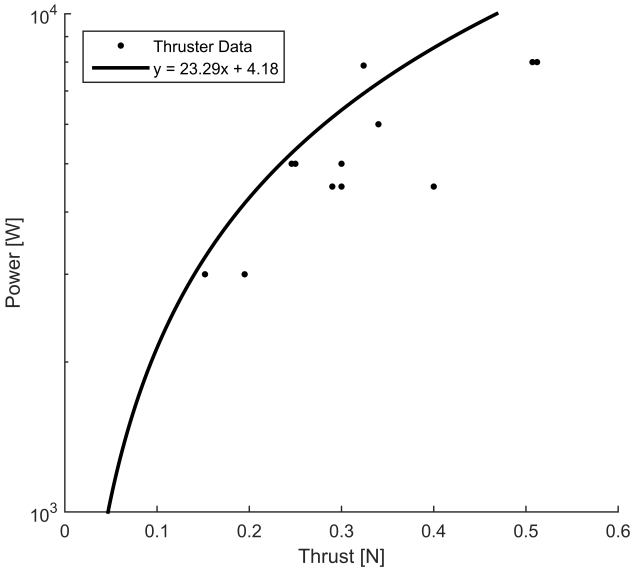

Figure C.18: Data and identified trend between thrust and power for high-power (>2.5 kW) Hall-effect propulsion systems. Trend $R^2 = 0.938$